Drift Capacity of Slab-Column Connections Reinforced with Headed Shear Studs and Subjected to Combined Gravity Load and Biaxial Lateral Displacements

By:

Eric M. Matzke

Rémy D. Lequesne

Carol K. Shield

Gustavo J. Parra-Montesinos

July 2013

ACKNOWLEDGEMENTS

Table of Contents

TABLE OF TABLES

TABLE OF FIGURES

1. INTRODUCTION

1.1. Slab-Column Connections in Flat Plate Frame Systems

In reinforced concrete construction, flat plate frame systems feature slabs supported directly by columns without the use of beams, drop panels, or column capitals. Flat plates are widely used and often preferred due to economical, functional, and architectural benefits. Some of these advantages include simplified formwork, which reduces installation time and material costs; reduced story heights, which decreases construction costs; and general aesthetic appearance.

When used in combination with a lateral force resisting system, such as a moment resisting frame or shear wall, flat plates are sometimes utilized in areas of medium to high seismicity. Although flat plate frames are not designed to contribute to lateral resistance, they still must exhibit sufficient ductility to support gravity loads while undergoing lateral displacements experienced by the structure during a seismic event.

There are two types of shear failures that must be accounted for in the design of flat-plate slabs: one-way (or 'beam') shear and two-way shear. A one-way shear failure is characterized by an inclined crack which extends the entire width of the slab. In general, however, the primary shear design concern for flat plate slabs is two-way shear, which occurs in slab regions where shear forces are transferred from the slab to supporting columns or where concentrated loads are applied on the slab. Slabs failing in two-way shear typically exhibit an inclined crack oriented at 20-45 degrees to the horizontal (slab plane) around the column, creating a failure surface that resembles a truncated pyramid. These failures are commonly referred to as "punching shear" failures, as the column appears to punch through the slab as the latter drops away from the failure surface around the column.

Punching shear failures result in a nearly complete and sudden loss of shear capacity, offering little warning to building occupants. To reduce the likelihood of partial or progressive collapse following a punching shear failure, continuous slab bottom reinforcement passing through the column is often required (ACI Committee 318 2008,

ACI-ASCE Joint Committee 352 2011). This reinforcement ensures the slab can continue to transfer gravity loads to the column through catenary action. However, due to the brittle nature of punching shear failures, and the potential for partial or total structural collapse, these failures must be prevented in flat plate structures.

1.2. Shear Reinforcement in Seismic Regions

Although slab-column frame systems are typically not assumed to contribute to the lateral strength and stiffness of a structure, slab-column connections must be designed to transfer shear from gravity loads as the structure undergoes earthquake-induced lateral displacements. In addition to imposing large deformations on slab-column connections, these lateral displacements lead to slab moments that need to be transferred to the columns. These moments cause an increase in connection shear stress which, combined with the presence of large deformations, further increases the potential for a punching failure.

Degradation of shear resistance attributed to concrete, V_c, (i.e., aggregate interlock, dowel action, and shear carried by the compression zone) in flexural members subjected to shear reversals is well known (Wight and Sozen 1975, Scribner and Wight 1980). Thus, the shear design of reinforced concrete beams is typically performed assuming the member resists shear only through truss action (i.e., $V_c = 0$). However, preventing shear failures in reinforced concrete flexural members subjected to large shear reversals not only requires the use of sufficient transverse reinforcement to resist the entire shear demand, but also of transverse reinforcement capable of maintaining the integrity of the concrete through confinement (Wight and Sozen 1975). Although the use of shear reinforcement in slab-column connections in earthquake-prone regions has become common practice in the past few years, most types of shear reinforcement offer little or no confinement to the slab concrete. This lack of confinement, combined with the fact that degradation of concrete shear resisting mechanisms in slab-column connections is typically not accounted for in design (ACI Committee 318 2008), increases the susceptibility of slab-column connections to punching shear failures during earthquakes.

Currently, the most popular form of shear reinforcement for slabs in the United States is headed shear stud reinforcement, also referred to as "stud rails." Installation of shear stud reinforcement is relatively simple; the base rails are nailed to the formwork prior to placing the slab flexural reinforcement. A typical stud rail assembly is shown in Figure 1-1 and consists of smooth thin rods, each with a head at one end and welded to a base rail at the other end. In the United States, stud rails are typically oriented perpendicularly to each column face in order to minimize interference with reinforcing bars or post-tensioning strands, as shown in Figure 1-2. In Europe, rails are more commonly placed in a radial pattern around the column face (Broms 2007a), which allows a more even distribution of reinforcement around the column compared to the orthogonal stud rail layout shown in Figure 1-2.

As illustrated in Figure 1-3, shear stud reinforcement is intended to prevent punching shear failures by intercepting inclined shear cracks as they form around the column. Because the stud shanks are generally smooth, load in the studs is developed entirely through mechanical anchorage provided by the head and the base rail. Testing has shown that in order to reach the full yield strength of the stud prior to crushing the concrete, the bearing area of the head must be at least 10 times the area of the vertical rod (Dilger and Ghali 1981). A minimum head area of ten times the shank area is specified in the ACI Building Code (ACI Committee 318 2008). Furthermore, shear stud reinforcement shall extend as close as possible to the top and bottom slab surfaces in order to increase its effectiveness in resisting shear.

Other forms of reinforcement have also been found to be effective at increasing punching shear strength and rotational capacity of slab-column connections (Robertson et al. 2002); however, shear stud reinforcement remains the most popular form, as the installation of other types of shear reinforcement such as stirrups and shearheads tends to be difficult and labor intensive.

1.3. Shear Design Provisions for Slab-Column Connections with Headed Shear Stud Reinforcement (2008 ACI Building Code)

Design provisions for headed shear stud reinforcement were first introduced to the ACI Building Code in 2008 (ACI Committee 318 2008). The nominal punching shear strength of slab-column connections, v_n, is taken equal to the summation of a concrete contribution, v_c, and a steel reinforcement contribution, v_s. In connections with headed shear stud reinforcement the concrete contribution to shear strength is taken equal to $3\sqrt{f_c'}$ (psi), which is 50% greater than the strength value used for connections with any other bar-type shear reinforcements. In the commentary for Section 11.11.5 in the 2008 ACI Code, the use of a greater strength value in connections with headed shear studs is attributed to a better reinforcement anchorage of shear studs compared to single leg stirrups, which leads to "smaller [reinforcement] slip" and "smaller shear crack widths." Similarly, the maximum nominal shear stress in connections with headed shear stud reinforcement is $8\sqrt{f_c'}$ (psi), 1/3 greater than that used for other bar-type shear reinforcements ($6\sqrt{f_c'}$ [psi]).

Contribution of shear stud reinforcement to shear strength is calculated as for other bar-type shear reinforcements as follows,

$$v_s = \frac{A_v f_y}{s b_o} \tag{1.1}$$

where A_v is the area of headed stud reinforcement in a single peripheral line of reinforcement, f_y is the yield strength of the headed stud reinforcement, s is the spacing between peripheral lines of reinforcement, and b_o is the perimeter of the critical section. The amount of shear reinforcement provided must be such that $v_s \geq 2\sqrt{f_c'}$ (psi), while the spacing is limited to $3d/4$ for connections with a shear stress of up to $6\sqrt{f_c'}$ (psi) and to $d/2$ for higher shear stresses. Also, a spacing limit of $2d$ is specified between studs in the first peripheral line of shear reinforcement.

For slab-column connections of structures located in areas designated as seismic design categories D, E, and F and not part of the seismic-force-resisting system, in addition to

gravity load design considerations, Chapter 21 of the 2008 ACI Building Code requires $v_s \geq 3.5\sqrt{f_c'}$ (psi) over at least four times the slab thickness from the column faces, unless either 1) the shear stress demand due to gravity shear and moment transferred in the connection at the design lateral displacement, calculated according to the eccentric shear stress model in Chapter 11, does not exceed the design shear strength of the connection, or 2) the design drift does not exceed the larger of 0.005 and [0.035-0.05$v_{ug}/(\phi v_c)$], where v_{ug} is the shear stress due to gravity load and ϕ = 0.75. ACI Committee 318 recently approved the elimination of the combined shear stress check for design of slab-column connections not part of the seismic-force-resisting system in seismic design categories D, E and F. Assuming this change is published as approved in the 2014 ACI Building Code, slab-column connections of these structures that do not satisfy item 2) above would be required to have shear reinforcement proportioned such that $v_s \geq 3.5\sqrt{f_c'}$ (psi).

Typical practice in the United States for connections with square or rectangular columns consists of laying studs in a cruciform pattern, with stud rails perpendicular to each column face. While the maximum spacing between studs within a peripheral line of reinforcement increases as the peripheral line is farther from the column (governed by distance between studs in rails framing into adjacent, perpendicular column faces), this layout is possible because in the 2008 ACI Code peripheral stud spacing is only required to be checked for the first stud peripheral line. In recently released recommendations by ACI Committee 352 (2011), however, the 2d peripheral spacing limit also applies to the second peripheral line. Further, the ACI Code spacing provisions contrast with those in the Eurocode (Comité Européen de Normalisation, 2004), where a maximum spacing limit of 1.5d is applied to several peripheral lines of studs, and a limit is also imposed to the width of the slab engaged by the shear studs. The result is thus a more uniform distribution of shear reinforcement around the column compared to that obtained following a cruciform pattern.

1.4. Research Motivation and Objectives

As reported in Cheng et al. (2010), three large-scale slab-column connection subassemblies were previously tested under combined gravity load and biaxial lateral displacements. The slab tensile reinforcement ratio in the column strip was 0.6% based on the slab overall thickness and 0.7% based on the slab average effective depth. Shear reinforcement for two of the specimens was provided in the form of discontinuous hooked steel fibers, whereas the connection of the third specimen was reinforced with shear stud reinforcement for comparison. The specimen reinforced with shear stud reinforcement, Specimen SB3, was designed according to ACI 318-08 (ACI Committee 318 2008) to resist shear stresses on the critical section due to concentric shear and moment transferred between the slab and column. A transfer moment of 1500 kip-in. was used to design the shear studs because that was approximately the transfer moment exhibited by the fiber reinforced concrete specimens at 2% drift. A gravity shear ratio of approximately 50% was maintained throughout the test. Gravity shear ratio is defined as the ratio of shear induced by gravity loads, calculated at a critical section at $d/2$ from the column faces, to the nominal punching shear strength of the connection, where d is the average slab effective depth. The shear reinforcement consisted of two shear stud rail assemblies placed perpendicular to each column face with eight 3/8 in. diameter shear studs on each rail spaced at $0.75d$ (3.5 in.). This connection detail is shown in Figure 1-4.

Specimen SB3 exhibited surprisingly poor performance. As shown in Figure 1-5, the connection failed in punching while being cycled at a drift of 1.15% in each principal loading direction (1.65% resultant drift due to biaxial displacements). This was an unexpectedly low inter-story drift that could reasonably be exceeded during a strong earthquake. As can be seen in Figure 1-6, which shows part of the failure surface in Specimen SB3, a steep crack that crossed the second peripheral row of studs led to the failure of the specimen. Once this diagonal crack developed, the studs were not capable of bridging this crack as a breakout failure of the concrete occurred. Peak shear stress due to direct shear and moment transfer between the slab and the column on the critical perimeter, calculated according to the ACI Building Code (ACI Committee 318 2008), was $3.97\sqrt{f_c'}$ (psi) and $4.29\sqrt{f_c'}$ (psi) in each principal lateral loading direction. These

stresses are similar to the nominal shear stress capacity in ACI 318-08 for connections with the geometry tested and no shear reinforcement ($4\sqrt{f_c'}$ [psi]). Based on the failure mode exhibited by Specimen SB3, it appears the provided shear stud reinforcement did not contribute to either shear strength or drift capacity of the connection.

The performance of Specimen SB3 reported in Cheng et al. (2010) has raised serious concerns about the effectiveness of shear stud reinforcement when used in amounts near the minimum specified in the 2008 and 2011 ACI Building Codes for cases in which a combined shear stress check is performed, and consequently the vulnerability of a large number of slab-column connections with headed shear reinforcement. To the writers' knowledge, prior to the research reported herein, Specimen SB3 was the first and only test of a slab-column connection with shear stud reinforcement subjected to combined gravity load and biaxial lateral displacements. The other connection tests with shear stud reinforcement under biaxial lateral displacements known to the writers, reported by Tan and Teng 2005, included a supporting element with an aspect ratio of 5, which corresponds more to a wall than a column. There is thus need for experimental data on the behavior of slab-column connections with various configurations of shear stud reinforcement in order to better evaluate the adequacy of the ACI Building Code requirements for the design of slab-column connections that are not part of the lateral-force-resisting system in structures assigned to Seismic Design Categories D, E, and F.

The objective of the research reported herein was therefore to investigate the effectiveness of various configurations of shear stud reinforcement at increasing the drift capacity of slab-column connections in structures subjected to ground motions. For this purpose, four large-scale slab-column connections were tested under combined gravity load and biaxial lateral displacements. With the exception of the shear reinforcement used in the slab-column connection region, each specimen was nominally identical to Specimen SB3 (Cheng et al. 2010) and tested using the same experimental set up and following the same loading protocol.

2. EXPERIMENTAL INVESTIGATION

2.1. Overall Specimen Configuration

Four nearly full-scale slab-column subassemblies with identical geometry were tested under combined gravity loading and biaxial lateral displacements. Specimen design was based on a previous experimental investigation (Cheng et al. 2010). Elevation views of the specimen are shown in Figure 2-1 and Figure 2-2. Each specimen consisted of a 17 ft square, 6 in. thick slab supported on top of a full-story 16 in. square column with a clear height of 10 ft-3 in. The column extended 5 ft above the slab. The column base was fixed to a 63 in. x 63 in. x 32 in. heavily reinforced concrete base block. A 42 in. x 42 in. x 16 in. top block was cast monolithically on top of the second half-story column for application of lateral displacements. A point of inflection was controlled at the top of the top block.

The clear span-to-depth ratio of the slab, 31.3, is close to 33, the limit defined in Table 9.5(c) of the 2008 ACI Building Code for two-way slabs not checked for deflections. Further, data obtained from Cary Kopcyznski & Company indicate that this ratio is consistent with typical clear span-to-depth ratios for slabs designed by that office. It is therefore believed the specimens are representative of typical reinforced concrete two-way slab construction. It should be mentioned, however, that the dimensions of the specimens were not intended to represent prestressed (e.g., post-tensioned) slabs, which are generally more slender.

The slab was vertically supported by hydraulic actuators at each corner. The connection detail between each vertical actuator and the slab is shown in Figure 2-3. In order to reduce slab edge vertical deflections and thus make the slab edge support conditions closer to a continuous roller support, steel tube sections were fastened to the slab along its perimeter with two rows of 3/4 in. threaded rods spaced at 12 in., as shown in Figure 2-4. Even though it was not possible to realistically simulate the boundary conditions along the slab perimeter, the slab dimensions were large enough (distance from inner edge of

steel tube to closest column face was equal to 12.7 slab thicknesses or 76 in.) to minimize any significant effect on connection behavior.

2.2. Specimen Design

The slab-column connection in the test specimens was designed assuming it is not part of the seismic-force-resisting system. The magnitudes of dead and live loads used in design were determined such that the average shear stress on the critical section of the connection (at $d/2$ from the column faces) was equal to $2\sqrt{f_c'}$ (psi) (gravity shear ratio of 0.50) for a ratio between dead and live load of 2. The load combination used for calculation of the gravity shear stress (and gravity shear ratio) was $1.2D+0.5L$, as specified in Section 21.13.6 of ACI 318-08 (ACI Committee 318 2008) for structures other than "garages, areas occupied as places of public assembly, and all areas where L is greater than 100 lb/ft^2." For design purposes, the compressive strength of concrete and yield strength of the reinforcement were assumed to be 5,000 psi and 60 ksi, respectively. Moments used in the slab design were determined based on the calculated dead and live load intensities using the Direct Design Method outlined in Section 13.6 of ACI 318-08 (ACI Committee 318 2008). The reinforcement layouts were nominally identical in each principal direction with an average effective depth, d, of 4.75 in. The reinforcement design resulted in No. 4 bars spaced at 6 in. in the column strip, which corresponded to a tensile reinforcement ratio of 0.6% based on the slab overall thickness and 0.7% based on the slab average effective depth. This is close to design data for reinforced concrete two-way slabs obtained from Cary Kopczynski & Company, in which tension reinforcement ratios ranging between 0.0065 and 0.0075, based on the slab thickness, have been used. An elevation view of the specimen reinforcement is shown in Figure 2-5 and the slab bottom and top reinforcement layouts are shown in Figure 2-6 and Figure 2-7, respectively.

Per Section 13.3.8.5 of ACI 318-08 (ACI Committee 318 2008), the slabs were provided with two continuous bottom bars in each direction that passed through the column core. These bars are referred to as "integrity steel" and are intended to transfer slab gravity

loads to the column after punching occurs at the connection to prevent partial or progressive collapse. As illustrated in Figure 2-8, after the slab drops, this reinforcement allows gravity loads to be resisted through catenary action.

The test specimens were nominally identical except for the shear reinforcement design at the slab-column connections. The reinforcement of each specimen, along with other slab properties, is summarized in Table 2-1.

All four connections were designed to resist shear stresses on the critical perimeter induced by gravity loads (corresponding to a 50% gravity shear ratio) and expected moment transferred into the column (so-called "unbalanced" moment), according to ACI 318-08 Section 21.13.6(a). A moment transfer of 1400 kip-in was assumed for design based on results from Specimen SB3 reported in Cheng et al. (2010), which was a reinforced concrete slab-column connection with the same flexural reinforcement layout.

The calculations for shear reinforcement design in Specimens B1 and B2 can be found in Appendix A. Stud rails for Specimens B1 and B2 were arranged in a cruciform pattern, with rails placed orthogonally to each column face. This is the arrangement typically used in the United States to minimize interference with slab flexural reinforcement. Both connections had twelve 3/8 in. diameter studs in each peripheral row of shear reinforcement (three rails per column face). On each column face, adjacent rails were equally spaced, with two placed at the outer edges of the column, and the remaining rail placed at the center of the column face. The design for Specimen B1 was based on the assumption of zero concrete contribution to shear capacity ($v_c = 0$), resulting in a shear stud spacing perpendicular to each column face of $0.5d$, or 2-3/8 in. It should be mentioned that at the time the test specimens were designed, recent changes to code design provisions had not yet been adopted (see Section 1.3). The connection and stud rail assembly details for Specimen B1 are shown Figure 2-9.

Specimen B2 was provided with shear reinforcement such that $v_s = 3.5\sqrt{f_c'}$ (psi) extending at least $4h$ (24 in.) away from the column face. This is the minimum amount of shear reinforcement that is required by Section 21.13.6 of the ACI Building Code (ACI Committee 318 2008) if no shear stress or drift capacity check is performed as outlined in

Section 21.13.6(a) and (b), respectively. This resulted in a shear stud spacing perpendicular to each column face of 0.75d, or 3-1/2 in. Complete connection details for Specimen B2 are shown in Figure 2-10.

Specimen B3 was reinforced with the same number of stud rails with the same stud spacing as Specimen B1 (twelve rails with 3/8 in. diameter studs spaced at 0.5d); however, four of the twelve stud rails were placed at the column corners, oriented at a 45 degree angle to the column faces. The other eight rails were placed perpendicular to the column faces (two per column face). This type of rail configuration is often utilized in European construction (Broms 2007a). The orthogonal rails on each column face were placed such that studs in the second peripheral row of shear reinforcement were spaced at approximately 1.5d around the perimeter of the column. The concept of this arrangement was to increase the size of the shear reinforced area in the connection region and limit the maximum stud spacing in each peripheral row of shear reinforcement. The maximum stud spacing was kept below 2d in the first three peripheral rows of shear studs. Full connection details for Specimen B3 are shown in Figure 2-11.

A total of 20 shear stud assemblies were used in the connection of Specimen B4 (Figure 2-12) with sixteen shear stud assemblies placed orthogonally to the column faces. Of those sixteen, eight were placed (two per column face) 6 in. apart, centered on each face of the column. The other eight orthogonally oriented rails (two per column face) were placed 15 in. apart, centered on the column face (1/2 in. away from the column corners). These rails were also placed such that the first stud on each assembly was in line with the second peripheral row of shear reinforcement. As in Specimen B3, one rail was placed at each column corner at a 45-degree angle to the faces of the column. In order to minimize interference with slab reinforcement, the stud spacing on these radially placed assemblies was increased by a factor of $\sqrt{2}$ so that the studs would lie on an orthogonal grid. The concept of this connection was to further decrease the maximum stud spacing in each peripheral row of studs compared to that in Specimen B3. In Specimen B4, the fourth peripheral row of shear studs was the last row to have a maximum stud spacing less than 2d.

Stud rails used in Specimens B1 and B2 were provided by the same supplier. During a post-test inspection of Specimen B2, several studs were found to have fractured from the base rail at the weld, which led to use of a different supplier for the stud rails used in Specimens B3 and B4. There were minor differences in the assemblies provided by each supplier. The cross sections of base rails from the first and second suppliers were 1/4 in. x 1-1/4 in. and 3/16 in. x 1 in., respectively, while the stud dimensions were identical.

The column was designed to resist all anticipated axial loads and bending moments. An axial load of approximately 200 kips was assumed throughout the test: 140 kips applied to the top of the specimen by the crosshead to simulate weight from the stories above for a first story column in a typical structure, and 60 kips of gravity shear being transferred from the slab to the column. The total applied axial load amounted to approximately $0.15A_g f_c'$, where A_g is the gross cross sectional area of the column. The flexural demands on the column were previously estimated (Cheng and Parra-Montesinos 2009) based on a 2-D slab-column frame model constructed following the recommendations in Hueste and Wight (1999). Flexural demands in this new series of tests, however, were obtained from the results of tests reported in Cheng et al. (2010).

The column was designed with Bressler's Reciprocal Load Method (Bresler 1960). The resulting longitudinal reinforcement consisted of twelve No. 6 bars with 90-degree hooks at each end (Figure 2-5). Transverse reinforcement consisted of No. 3 closed-hoop stirrups spaced at 3 in. in accordance with ACI 318-08 Section 21.6.4 (ACI Committee 318 2008). The longitudinal column reinforcement in each specimen was spliced using mechanical splices shown to satisfy Type 2 seismic splice requirements. In Specimens B1, B2, and B3, threaded screw-type mechanical splices were used to splice six column bars 3 ft below the bottom of the slab and the other six bars 5 ft below the bottom of the slab. In Specimen B4, six bars were spliced 6 ft below the bottom of the slab and six bars were spliced 7 ft below the bottom of the slab. Column reinforcement in Specimen B4 was spliced using bar-lock type mechanical couplers. Although it is unusual to splice column reinforcement below the slab, this was done to simplify specimen construction and was not expected to alter the behavior of the specimen.

There were problems with consolidation of the concrete in the first-story column of Specimen B4. To address the honeycombing evident after removal of the formwork, all of the concrete in the first story of the column was removed using hand tools and jackhammers. Special care was taken to avoid damaging the column reinforcement. The column concrete was then re-cast.

The base and top blocks were designed to resist loads corresponding to the specimen reaching its capacity. The reinforcement designs for the base and top blocks are shown in Figure 2-13 and Figure 2-14, respectively.

2.3. Specimen Instrumentation

2.3.1. Strain Gauges

A total of 74 strain gauges were applied to flexural reinforcing bars in the slab. Figure 2-15 and Figure 2-16 show the strain gauge layouts in the top and bottom mats of slab reinforcement. Gauges were labeled such that "T" refers to gauges on top mat reinforcement, and "B" refers to gauges on bottom mat reinforcement. The second character indicates the direction the bar is laid. Gauges with a second character "E" are on bars laid longitudinally in the East-West, or Y, direction; gauges with an "S" are on reinforcing bars laid longitudinally in the North-South, or X, direction. The specific locations of individual gauges on top and bottom mat reinforcement can be described by two distances, t and l (Figure 2-17). The variable t is the transverse distance (in the X direction for 'TE' and 'BE' gauges, and in the Y-direction for 'TS' and 'BS' gauges) of the individual bar from the center of the column, and l indicates the location of a gauge on an individual bar as measured from the center of the column in the direction parallel to the bar. Gauges were applied to several bars in both the top and bottom mat of reinforcement in one of five bar locations, l, equal to 0 in., $\pm(b+d)/2$ ($\pm$10-3/8 in.) and $\pm(b+5d)/2$ ($\pm$19-7/8 in.), where b is defined as the width of the column (16 in.). Top and bottom strain gauge layouts were identical in each principal direction. The coordinates, t and l (with subscripts indicating the direction of each measurement) for each gauge are listed in Table 2-2.

Strain gauges were also placed on the northwest and southwest corner longitudinal bars of each column 1 in. and 7 in. from the base (Figure 2-18). These gauges allowed for yielding of the reinforcement at the column base, which was expected to occur during the later cycles of the tests, to be monitored.

Strain gauges were placed on the shanks of several shear studs in each specimen. On instrumented studs, gauges were placed 2 in. from the top of the base rail (approximately mid-height on the stud) to measure the longitudinal strain in the stud. Each connection had a slightly different shear stud rail arrangement; therefore, the instrumentation plans for the rails were different as well. Instrumentation plans for Specimens B1, B2, B3, and B4 can be found, respectively, in Figure 2-19 to Figure 2-22, where instrumented studs are marked by black dots.

2.3.2. *Linear Variable Differential Transformers (LVDTs)*

Slab deformations across distances of $1d$ and $2d$ from the column face were measured by LVDTs located as shown in Figure 2-23. The slab rotation at each section, relative to the column rotation, was calculated in radians by taking the difference in displacement between top and bottom horizontal LVDTs, and dividing it by the vertical distance between the two instruments.

In Specimens B2, B3, and B4, an LVDT was mounted vertically in the corner of each face of the column on the underside of the slab. These LVDTs were used to monitor the vertical drop of the slab throughout the test. All locations of LVDTs in the slab region are shown in Figure 2-23. Specimen B1 did not have LVDTs labeled L-Z (i.e., LVDTs to measure slab drop).

Column base rotations 14 in. (approximately the effective depth of the column) from the top of the base block were calculated from data collected with LVDTs mounted on each face of the column, as shown in Figure 2-24. Column base rotations (in radians) were calculated by dividing the difference in displacement measured by LVDTs placed on opposite column faces by the distance between LVDTs.

For all specimens, two LVDTs were mounted to the strong floor to monitor slipping of the base block, as shown in Figure 2-25.

2.3.3. String Potentiometers

On the north and west faces of the laboratory's strong wall, four string potentiometers were mounted at mid-slab height and connected to the negative X and Y faces of the slab. String potentiometers were used to measure the lateral displacement of the slab edges in the X and Y directions, as shown in Figure 2-26.

2.3.4. Telepresence

Photographs of the top and bottom of the connection region were collected by four telepresence towers placed at the corners of the testing area. Photos were taken at corner points on the cloverleaf of each loading cycle (Figure 2-28) and also upon the completion of a drift cycle.

2.4. Material Properties

2.4.1. Concrete

Concrete for all specimens was supplied by a local ready mix supplier. The same mixture design was used throughout the project. The concrete was specified to have a compressive strength of 5000 psi, a slump of 6 in., and maximum aggregate size of 3/8 in. The resulting mixture proportions by weight of cement, water, sand, and 3/8 in. bedrock aggregate were 1:0.48:2.05:2.5, respectively.

The minimum slump of 6 in. was verified on site prior to placing the concrete to ensure sufficient workability and flow. The measured compressive strength of the concrete used on various locations of each specimen was taken as the average of three 4 in. x 8 in. concrete cylinders tested according to ASTM C39 (ASTM Standard C39 2012). The results are shown in Table 2-3. Three cylinders cast with concrete used in each slab were tested one day prior to the testing of each connection to determine the load required to induce a 50% gravity shear ratio in the connection. The other concrete cylinders were tested after the specimen test and approximately 90 days after the day of casting. All

cylinders were kept in their molds at room temperature next to the slab specimens until testing.

2.4.2. Reinforcing Steel

The reinforcing bars for each specimen, except for the longitudinal steel in the column, were purchased from a local supplier. The longitudinal steel in column was mechanically spliced within the first story, as discussed in Section 2.2. All reinforcing bars were uncoated Grade 60 steel compliant with ASTM A615, Type 2, requirements (ASTM Standard A615 2009). The yield and ultimate strengths of the reinforcing bars used in each specimen were determined through tests of three 2-ft long bars of each size in accordance with ASTM A370 (ASTM Standard A370 2012). Reinforcement coupons were tested without modification or removal of deformations. The average yield and ultimate strengths calculated from each set of three test bars are listed in Table 2-4. For Specimens B1 and B2, no additional pieces of No. 3 and No. 5 reinforcing bars were available for testing; therefore the yield and ultimate strengths are not listed in Table 2-4.

2.4.3. Shear Stud Reinforcement

For Specimens B1 and B2, shear stud reinforcement was provided by VSL Post-Tensioning. The studs were made with steel specified to have a minimum yield strength of 55 ksi. This value was not verified independently, but documentation provided by VSL indicated the yield and ultimate stress of the steel studs were 70.0 and 79.8 ksi, respectively. A different vendor, SRL Industries, donated shear stud reinforcement for Specimens B3 and B4 after failure of several of the stud welds in Specimen B2 were discovered. The steel used to manufacture the studs provided by SRL Industries, and used in Specimens B3 and B4, was specified to have a minimum yield strength of 55 ksi. This value was not verified.

2.5. Test Activities

2.5.1. Pretest Activities

Upon moving the test specimen to its final location on the laboratory strong floor, a 1/4 in. thick layer of grout was placed between the base block and strong floor to ensure an

even contact surface between the specimen and the strong floor prior to pretensioning the specimen down to the floor. After 24 hours, the specimen was anchored to the strong floor using twelve 1.5 in. diameter threaded rods posttensioned to 100 kips.

Approximately one week before testing, a 1/4 in. thick layer of grout was placed between the top block and crosshead. The grout was given 24 hours to cure before the specimen top block was fastened to the crosshead with sixteen 1.5 in. diameter threaded rods posttensioned to 75 kips.

One day prior to testing, all four ancillary actuators were connected to the specimen at each slab corner with four 0.75 in. threaded rods (Figure 2-3) tensioned with a spud wrench.

2.5.2. Loading Methods

Loads and displacements at the top of the column were applied by a "rigid" steel crosshead connected to the specimen top block (Figure 2-1 and Figure 2-2). The crosshead was driven by four horizontal actuators (two in each principal direction), and four vertical actuators. Vertical actuators attached to the crosshead are only shown in Figure 2-2. The system operates with a six degree-of-freedom control system, and is capable of applying up to 1320 kips of vertical force, and nearly 900 kip of horizontal force in each principal direction. In addition, four ancillary actuators were installed on the strong floor and connected to the underside of all four corners of the slab (Figure 2-1).

A constant slab gravity load (in addition to the self-weight of the slab) was simulated with four prestressing stands (1/2 in. diameter, Grade 270, 7-wire, low-relaxation strands) pulling down at mid-points on each side of the slab. Beneath the slab, strands were fastened with strand chucks bearing on the underside of brackets installed on the strong floor located directly below each strand. On top of the slab, each strand passed through a hydraulic jack and was fastened with a strand chuck bearing on the top of a load cell that rested on top of the jack. All hydraulic jacks were fed by the same pump to achieve a uniform pressure in each jack, thus an equal tension in each strand. Elevation and plan

views showing the location of all of the applied slab loads are shown in Figure 2-27. Ancillary actuators forces are labeled A1, A2, A3, and A4.

As in any test of a structural component, the test setup used in this study was not a perfect representation of structures found in practice. In particular, use of actuators to support the boundary of the slab prevented the sagging of the slab expected in a real structure as connection damage progresses. However, given the large distance between the center of the slab supports and the column face ($13.7h$, where h is the slab thickness), and because care was taken to impose realistic shear and moment demands on the connection, it is believed the effect of the slab edge support on connection deformation demands was minimal.

The method used for simulating gravity load in the test program reported herein was substantially different than those used in many previous test programs of slab-column connections, particularly those in slabs with shear stud reinforcement. For comparison, in most previous tests of slab connections reinforced with shear studs, the desired connection shear was generated by jacking the column while the slab boundary was restrained. While convenient, the jacking method has important drawbacks. These include an unrealistic moment-shear relationship in the slab and the need to further jack the column to maintain gravity shear, which could lead to connection deformations far from those expected in a structure subjected to earthquake-induced lateral displacements. Information on test setups used by various investigators can be found in Cheng and Parra-Montesinos (2009).

Maintaining a constant gravity shear force throughout the test was important; thus, the force in each strand was closely monitored using the following redundant measurements (listed in order of precision). 1) Load cells - At each strand location a load cell was fastened between the strand chuck and hydraulic jack. 2) Strain gauges - Prior to testing, three strain gauges were placed on separate wires of the strands approximately five feet from the bottom end of the strand. The load-strain relationship for each strain gauge was found by cycling each strand several times between 8 and 20 kips (the anticipated load range for testing). The strand force was taken to be the average force calculated from all

three gauges for each strand. 3.) Pressure gauge - While pumping the hydraulic jacks, the total applied gravity force was determined as a function of the pump pressure. The pump pressure reading was only accessible while pumping, and was lost after valves on the pump were closed. Cycling would only proceed if the load cells, strain gauges, and pressure gauge reported similar strand load values.

2.5.3. Loading Protocol

With the crosshead X and Y degrees of freedom locked in displacement control, an axial load of 140 kips (approximately $0.10A_g f'_c$) was applied to the column. This load was intended to simulate the weight of the stories above a typical first-story column. During the application of the column axial load, ancillary actuators located at the corners of the slab were held in load control at zero kips and were allowed to displace with the slab. After applying axial load to the column, ancillary actuators were switched to displacement control to maintain a constant elevation at the corners of the slab for the remainder of the test. Gravity load in addition to the slab self-weight was then applied to the slab such that an average shear stress of $2\sqrt{f'_c}$ (psi) (gravity shear ratio of 50%) was attained on the critical section of the connection (at $d/2$ from each column face). Equilibrium was used to calculate the concentric shear stress acting on the connection. The value of f'_c used for calculating the target shear stress was based on the average compressive strength of three 4 in. x 8 in. concrete cylinders broken on the day prior to slab testing, as discussed in Section 2.4.1. The required applied gravity loads for each specimen, corresponding to a 50% gravity shear ratio, are shown in Table 2-5. Prior to undergoing the first drift cycle, the moments at the top block about the X and Y axes were locked in load control at zero kip-ft for the remainder of the test to simulate an inflection point at the top of the column top block.

Lateral displacements were then applied at the top block through the crosshead. The displacement path for each drift cycle followed a clover leaf pattern as shown in Figure 2-28. Target drifts for each cycle are listed in Table 2-6 and plotted in Figure 2-28. Maximum resultant drifts due to biaxial effects occurred at corner points on the cloverleaf.

The lateral inter-story drift ratio is defined as the relative lateral displacement of floor slabs in consecutive stories in a building as a percentage of the height of the respective story. The ACI Building Code defines the design story drift ratio as the larger of the story drift ratios of adjacent stories above and below the slab-column connection (ACI Committee 318 2011). In this study, the primary measure of drift, δ, was taken as the drift of the entire 1.5 stories of the specimen. This was calculated as

$$\delta = \frac{Total\ Applied\ Displacement - Base\ Block\ Displacement}{Height\ of\ Specimen} \cdot 100\% \qquad (2.1)$$

where the height of the specimen was taken as 205 in., calculated as the total height of the subassembly (237 in.), minus the height of the foundation block (32 in.). For comparison, the drift experienced over the top half-story, δ_2, and bottom story, δ_B, were also calculated as follows:

$$\delta_2 = \frac{Total\ Applied\ Displacement - Slab\ Displacement}{Height\ of\ Second\ Half\ Story} \cdot 100\% \qquad (2.2)$$

$$\delta_B = \frac{Slab\ Displacement - Base\ Block\ Displacement}{Height\ of\ First\ Story} \cdot 100\% \qquad (2.3)$$

The total applied displacement was controlled by the movement of the crosshead. The slab displacement used for calculation in Eqn. (2.2) was taken as the average measurement of two string potentiometers monitoring lateral displacements at mid-height of the slab in each principal loading direction (see Section 2.3.3 and Figure 2-26). A value of 79 in. was used as the second half-story height, calculated as the sum of one half of the slab thickness (3 in.), the height of the second-story column (60 in.), and the height of the top block (16 in.). The height of the first story (126 in.) was taken as the sum of the height of the first story column (123 in.) and one half of the slab thickness (3 in.).

Throughout each drift cycle, a steady, but relatively small decrease in the applied gravity load was observed (due to specimen damage, slab settlement, and/or strand relaxation). At the end of each drift cycle, the strands were reloaded to forces corresponding to the

target gravity shear ratio. In the higher drift cycles, however, when a substantial amount of the gravity shear had diminished (approximately 20% of the target gravity shear) as the slab accumulated more damage throughout a cycle, the cycle was paused and loads in the strands were adjusted to reestablish the target gravity shear ratio before resuming the test. The test was terminated when significant damage had developed in the slab at the connection. In the case of Specimens B1 and B2, the test was terminated when the gravity load could no longer be transferred through the slab-column connection. The test of Specimen B3 was terminated when extensive connection damage led to significant twisting of the slab relative to the column. Testing of Specimen B4 was terminated after the slab had dropped considerably relative to the column and resulted in an unrealistic shift of applied gravity loads to the slab boundary supports.

3. EXPERIMENTAL RESULTS

Results from experiments performed on four large-scale slab-column subassemblies, Specimens B1, B2, B3, and B4, are discussed in this chapter. Each section is focused on a specific specimen response, described using data collected from instrumentation and photographs taken throughout the test.

In Section 3.1, a discussion of visual damage progression of each specimen throughout the test is provided. Visually observed failure surface of each specimen, and any other details uncovered after completion of testing that explained specimen behavior, are discussed in Section 3.2.

The following five sections (Sections 3.3 through 3.11) deal with interpretation and discussion of data collected from instrumentation, related in particular with specimen hysteresis behavior, gravity shear history, peak shear stress on connection critical section, and strains in shear studs and slab flexural bars.

3.1. Damage Progression

3.1.1. Specimen B1

Narrow flexural cracks were first observed on top of the slab during the 0.25% drift cycle, very close to the west face of the column. After completion of the 0.45% drift cycle, flexural cracks were visible near all sides of the column. Small cracks extending from the column corners towards the slab corners, approximately $2d$ in length, also formed during the 0.45% drift cycle. By the end of the 0.90% drift cycle, flexural cracks on each side of the connection had become much wider. Crack widths, however, could not be measured throughout the test because of safety concerns.

During the 1.15% drift cycle, small cracks began to form underneath the slab, extending orthogonally from the faces of the column. Through the 1.60% drift cycle, cracking on top of the slab became more widespread in regions farther away from the connection

(>2*d*), especially in the southwest corner of the connection. The first punching shear related crack was observed on the east face of the slab during the 1.85% drift cycle at Point 8 in the cloverleaf load pattern, as shown in Figure 3-1. At Point 5 of the 2.30% drift cycle, punching shear related damage had propagated along the west, south and east faces of the connection. After returning to zero lateral displacement, the test was terminated because the specimen could no longer support gravity loads. A photograph of the south-west side of the connection at this loading stage is shown in Figure 3-2. An approximately 1 in. vertical settlement of the slab was also observed. In the northeast and northwest corners of the connection, long cracks were observed in the slab that extended from the column corners approximately 36 in. toward their respective corners of the slab. The punching shear failure that developed around the west, south and east faces of the column did not develop in the north portion of the slab. North of the column, only the bottom cover of the slab dropped relative to the column (see Section 3.2.1 for further discussion). The inclined crack on the northeast corner of the face of the connection is shown in Figure 3-3.

3.1.2. Specimen B2

Flexural cracks in the slab of Specimen B2 were first observed near the slab-column interface during the 0.25% drift cycle. During the 0.70% drift cycle, cracks formed on top of the slab, emanating from the column corners and extending toward the corners of the slab. These cracks were approximately 2*d* in length. Damage on the bottom of the slab was first noticed during the 0.90% drift cycle, which consisted of narrow cracks extending orthogonally from the west face of the column. On the bottom surface of the slab, cover concrete at the slab-column interface also began to spall on all faces. After the 1.40% drift cycle had been completed, the bottom surface of the slab was observed to have dropped approximately 1/8 in. relative to the column. This estimation was based on the position of the slab relative to lines drawn on the column surface prior to testing at distances of 1/4, 1/2, 3/4, and 1" below the bottom surface of the slab (Figure 3-4). Cracks on the top of the slab had also become significantly wider during the 1.40% drift cycle.

The first cracks associated with punching developed during the 1.85% drift cycle at Point 8, and can be seen in Figure 3-5 on the north east face of the connection. By the end of the 1.85% drift cycle, the bottom of the slab had dropped approximately 0.25 in. down the column. The failure surface appeared to have formed around the entire perimeter of the connection.

While moving from Point 1 to Point 2 at the 2.30% drift cycle, the slab dropped abruptly. Upon reaching Point 2, the bottom of the slab had dropped approximately 3/4 in. on the south and west sides of the connection. The failure surface at this point is shown in Figure 3-6. There was a significant decrease in applied gravity load as a consequence of the slab dropping, releasing some of the force in the prestressing strands. At this point, an attempt was made to reload the prestressing strands to attain the target gravity shear into the connection prior to resuming lateral displacements. While loading the slab, the bottom of the slab began to drop in the north and east regions, resulting in a total drop of 3/4 in. around the entire perimeter of the connection. After returning the specimen to zero lateral displacement, the test was terminated.

3.1.3. Specimen B3

By the end of the 0.25% drift cycle imposed on Specimen B3, flexural cracks near the column were observed on all faces of the connection on the top side of the slab. During the 0.45% drift cycle, cracks approximately $3d$ in length developed in the slab, which emanated from each column corner and extended towards their respective slab corners. Cracking beneath the slab was first noticed while loading at the 0.90% drift cycle. Flexural cracks on the top of the slab had also begun to widen in this drift cycle.

During the 1.40% drift cycle, concrete cover began to spall from the bottom surface of the slab at the column interface. Punching shear related cracking first appeared on the west face of the connection, approximately $2d$ away from the column face after loading to Point 2 during the 1.85% drift cycle. Figure 3-7 shows the damage on the north-west corner of the connection at Point 5 of the loading cycle to 1.85% drift. During the cycle to 2.30% drift, punching shear-related damage was severe and extended nearly the entire connection perimeter (Figure 3-8) There was also a nearly 1/4 in. vertical drop of the slab

observed on the underside of the connection. The slab continued to slide down the column during the remainder of the cycle, resulting in a total drop of more than 1 in. by the end of the 2.30% drift cycle. Also during the 2.30% drift cycle, the slab began to twist around the axis of the column as damage accumulated in the connection. At the end of the 2.30% drift cycle, the slab had rotated 1.5 radians about the vertical axis, relative to the column. The cycle to 2.75% drift was initiated, but the test was terminated after reaching Point 4 due to excessive relative twisting between the slab and the column (approximately 11 radians at termination of the test).

3.1.4. Specimen B4

As observed during the tests of Specimens B1, B2, and B3, flexural cracking was first observed in Specimen B4 during the 0.25% drift cycle. Cracks approximately $3d$ in length, extending from each column corner toward its respective slab corner, formed in the 0.45% drift cycle. Underneath the slab, small cracks orthogonal to the column faces formed during the 0.90% drift cycle. At Point 11 of the 1.15% drift cycle, cover had begun to spall from the bottom of the slab on the north and west sides of the slab-column interface. Flexural cracks located within $2d$ of the column face began to widen during the 1.60% drift cycle.

The first punching shear-related cracks where observed when loading to Point 11 during the 1.85% drift cycle, located approximately $2d$ from the west and south column faces (Figure 3-9). As shown in Figure 3-10, after loading to Point 8 of the ensuing 2.30% drift cycle, punching shear-related damage had extended around the entire perimeter of the column. By the end of this cycle, the slab had dropped a total of approximately 1 in. from its original position. Specimen B4 was cycled at the 2.70% drift level to investigate the post-punching behavior of the connection. Throughout the cycle, the slab dropped approximately 1 additional inch (2 in. total).

3.2. Observations After Completion of Testing

After completion of each test, the loose concrete was removed from the connection in order to better inspect the condition of the connections. Observations made during the post-test inspection of each connection are discussed in the following sections.

3.2.1. Specimen B1

Failure of Specimen B1 was caused by a combination of severe concrete degradation in the region adjacent to the west, south and east column faces, and two long diagonal cracks that initiated at the north-west and north-east column corners and extended approximately 36 in. toward their respective corner of the slab, as illustrated in Figure 3-11. A photograph showing one of these inclined cracks is shown in Figure 3-3. Sectional slab views of the slab, also shown in Figure 3-11, show more details of the damage in the connection of Specimen B1. In Figure 3-11, section cuts A-A and B-B show how the inclined crack at the north-west corner of the connection penetrated through the depth of the slab and continued below the bottom flexural reinforcement along the north column face. As can be seen in Figure 3-11, the inclined cracks at the north-west and north-east corners of the column split the slab into two pieces. The entire slab piece south of the inclined cracks and the cover concrete from the north piece slid down the column, while the north slab piece did not. In Figure 3-12, it is shown that the stud rail orthogonal to the east face of the column dropped approximately 1 in., while the stud rail orthogonal to the north face did not drop to a measurable extent. Because only stud rails orthogonal to each column face were used in Specimen B1, shear studs on the north side of the connection were not engaged by the failure surface.

Severe concrete degradation was observed on the east, south and west regions of the connection. In Figure 3-13, the east face of the connection is shown after all loose concrete was removed following completion of the test. The north section of the connection, meanwhile, was relatively solid (Figure 3-14), as the inclined cracks emanating from the north-west and north-east corners of the column tended to "isolate" the portion of the slab framing directly into the north column face. The severe concrete degradation observed on the east, south and west sides of the connection indicates that the shear studs, while potentially being active in bridging diagonal cracks, did not

provide the confinement necessary to maintain the integrity of the concrete at the column faces to allow shear transfer through diagonal struts and the slab compression zone. As shown in Figure 3-13, the studs on the east side of the connection were only capable of maintaining the integrity of the concrete in between and immediately adjacent to the stud heads, while the concrete regions in between stud rails showed severe degradation. In cases where the head of the first stud in each orthogonal row rested directly on top of a slab bar (Figure 3-13), it was observed that the slab bar effectively anchored the stud and prevented significant drop of the slab at that particular location. Instead, significant bending of the supporting rail and shear stud was often observed as adjacent studs away from flexural bars dropped with the slab (in Figure 3-13, stud head rotation can be seen in the first stud visible on the south face of the column).

3.2.2. *Specimen B2*

A sketch of the damage distribution in the connection of Specimen B2 is shown in Figure 3-15. The region shaded in grey on the east and north faces of the connection represents an area where the slab concrete was found to be severely degraded during the post-test investigation. This concrete had a loose gravel-like consistency and was easily removed by hand after the test had been completed. Once all loose concrete was removed, what remained was a traditional punching shear failure surface on the west and south faces of the connection, and a completely void area within a distance d from the column face on the north and east faces of the connection (the region shaded in grey on Figure 3-15), as shown in Figure 3-16. As in Specimen B1, such degradation of concrete is indicative of the lack of adequate confinement provided by the shear studs.

Several studs were also found to have fractured from the base rail at the weld. These studs are indicted by black dots in Figure 3-15. In Figure 3-17, a view of the bottom slab surface on the west face of the connection highlights damage to several shear stud assemblies, including a severely bent base rail between the first and second shear studs on the center shear stud assembly, and a stud that fractured from its base rail due to a weld failure. The head of the first stud on the bent rail (shown in Figure 3-17) was located within 1 inch of a top mat reinforcing bar, but was not resting directly on it.

The severe concrete degradation in the connection of Specimen B2 at the end of the test did not allow an effective shear transfer mechanism between the slab and the column to develop, resulting in the column punching through the slab. As the slab dropped, all rail assemblies dropped with the slab with the exception of the center rail on the west face (also the rail with the only engaged stud in the first peripheral row of studs), where the rail dowelled between the first and second stud.

3.2.3. Specimen B3

The failure of Specimen B3 included severely degraded concrete in the slab within the first two rows of studs (d from the column face) surrounding the column perimeter. Similar to Specimens B1 and B2, the degraded concrete had a loose gravel-like consistency. After all loose concrete was removed, there was a void space between the slab and the column that penetrated through the entire depth of the slab. This void region encircled the entire connection. A corner of the connection that was cleaned out of loose concrete is shown in Figure 3-18. As can be seen in Figure 3-18, only the concrete within the diameter of the head of a few studs remained which, as in Specimens B1 and B2, is indicative of the poor confinement offered by the shear studs.

For the most part, rail assemblies dropped away from the connection along with the outer slab region. The exception was a rail assembly whose first stud was anchored by one of the slab bars passing through the column. In this particular case, the base rail dowelled between the first and second shear stud, as shown in Figure 3-19. Unlike the other shear stud assemblies, this rail likely contributed shear resistance even after the slab had begun to drop significantly.

3.2.4. Specimen B4

Similar to the other test specimens, the failure of Specimen B4 included loose gravel-like concrete in the slab surrounding the column perimeter. In Figure 3-20 and Figure 3-21, the north face of the connection is shown before and after all loose concrete had been cleaned out of the section. The removal of concrete around this connection was more difficult than in the three previous specimens, indicating more sound concrete at the end

of the test. This was likely due to the increased number and overall tighter spacing of shear studs, which provided superior confinement to the concrete.

At the end of the test of Specimen B4, the slab had dropped approximately 3 in. from its original position. All but one of the shear stud assemblies completely dropped away from the column with the outer portion of the slab. The stud rail that stayed in place was orthogonally placed to the south face of the column and is shown in Figure 3-22. This stud rail dowelled between the first and second shear stud much like the assembly from Specimen B3 shown in Figure 3-19. As in the other specimens, this was due to the first shear stud being anchored by top mat flexural reinforcement that passed through the column. It is again probable that unlike the other stud rails, this shear stud assembly contributed to shear resistance even after the slab had begun to drop significantly.

3.3. Load Drift Response and Gravity Shear History

The load versus drift response of each specimen is plotted for each perpendicular loading direction. Also plotted is the resultant force versus resultant drift due to biaxial loading. Resultant drift δ_R and resultant force F_R were calculated throughout the test as,

$$\delta_R = \sqrt{\delta_X^2 + \delta_Y^2} \tag{3.1}$$

$$F_R = \sqrt{F_X^2 + F_Y^2} \tag{3.2}$$

Principal loading directions, X and Y, are defined with positive and negative X corresponding with south and north, respectively, and positive and negative Y corresponding with east and west, respectively. The same coordinate system was used for each experiment.

As discussed in Section 2.5.3, the primary measure of drift used in this report is the drift that was imposed on the entire 1.5 stories of the specimen, which was calculated using Eqn. (2.1). For each specimen, the drift of the first story and second half-story of the specimen were also calculated, using Eqs. (2.2) and (2.3). The drift calculated for the first

and second half-stories of Specimen B2 are plotted in Figure 3-23 along with the drift calculated for the full 1.5 story specimen. The trends shown are typical of the four specimens tested. First story drift was approximately 20% less than the full specimen drift throughout the tests, whereas second half-story drift was approximately 20% greater. In an attempt to approximate interstory drift, defined as the drift between column inflection points, the location of the inflection point in the column was estimated using equilibrium of forces applied to the specimen. The column inflection point was estimated to be within ±20 inches of the bottom of the slab in all four specimens, but varied widely within and between loading cycles. Due to the high variation, the estimated interstory drift is not shown. However, given the approximate inflection point location, the calculated interstory drift was more similar to second half-story drift than the drift calculated for either the first story or full specimen. Load versus drift responses based on first story and second half-story drift are reported in Appendix B.

As described in Section 2.1, the reinforced concrete slabs in these specimens were relatively slender (clear span-to-depth ratio of 31.3, which is close to the limit defined in Table 9.5(c) of the 2008 ACI Building Code for two-way slabs not checked for deflections (33) and consistent with slenderness values used in design of reinforced concrete flat plates). Because the slenderness of the slabs is representative of typical reinforced concrete slab construction, and the columns are stiff relative to the slabs, it is believed that slab deformations in the connection region of the test specimens at a given drift level are similar to those expected in a structure at similar lateral displacements. It should be emphasized that the test specimens were not intended to represent prestressed (e.g., post-tensioned) slabs, which are typically more slender than reinforced concrete slabs.

3.3.1. Specimen B1

Specimen B1 was tested over a two-day period. After completion of the 1.15% drift cycle, the slab was fully unloaded and all but 25 kips of the axial load was removed from the column. At the beginning of the second day of testing, the column and slab were reloaded following the same procedure described in Section 2.5.3.

Hysteresis plots for loading in the X and Y directions for Specimen B1 are shown in Figure 3-24 and Figure 3-25, respectively. Hysteresis plots with resultant forces and drifts are plotted in Figure 3-26. Also, the relationship between the slab moments transferred into the column about the X- and Y-axes is plotted in Figure 3-27, with the portions of the response representing the drift cycles to 1.85% and 2.30% drift highlighted. As discussed in Chapter 3, a gravity shear ratio of 50% was targeted throughout each test. A time history of the gravity shear ratio and the imposed lateral drifts in the X and Y directions is plotted for the entire test in Figure 3-28. For reference, the target gravity shear ratio of 50% is also plotted in Figure 3-28 with a dashed line.

Hysteresis behavior in both the X and Y directions remained relatively linear through the end of the 0.90% drift cycle (Figure 3-24 and Figure 3-25). The peak force exhibited during the cycles to 1.15%, 1.40%, 1.60%, and 1.85% drift was nearly equal. The maximum lateral force for the entire test was achieved at Point 7 of the 1.15% drift cycle in the X-direction (Figure 3-24), and Point 2 of the 1.60% drift cycle in the Y-direction (Figure 3-25).

The plot of moment transferred between the slab and column for the X- and Y-axes shows some interdependency throughout the early drift cycles. For example, after the specimen was displaced to Point 1 in the cloverleaf loading pattern, where the moment about the X-axis was positive and the moment about the Y-axis was nearly zero, the specimen was displaced in the negative X-direction while the Y-displacement was held constant. This displacement along the X-axis caused a reduction in the moment about the X-axis that was relatively consistent throughout the early drift cycles. A similar relationship is evident between moment about the Y-axis and Y-axis drift. These relationships (slopes) were relatively constant until the specimen was displaced from Point 1 to Point 2 of the 2.30% drift cycle, where displacement in the negative X-direction caused a large decrease in moment about the X-axis. This increased interdependence between X- and Y-axis moments seems to indicate that membrane action played a significant role by the end of the test.

Moving from Point 1 to Point 2 during the 2.30% drift cycle, there was a steep decline in gravity shear ratio, as shown in Figure 3-28, and also a flattening in the hysteresis plots (Figure 3-24 and Figure 3-25). Through Point 4, the gravity shear ratio continued to drop rapidly to a value of 37%. This substantial decrease in gravity shear ratio was associated with extensive punching shear-related damage (Figure 3-2) and a large drop of the slab relative to the column. The vertical settlement of the slab resulted in a reduction in the tension in each prestressing strand, which led to a decrease in the applied vertical force on the slab. At Point 4, the target gravity shear in the connection was reestablished by reloading the slab. At Point 5, another substantial drop in gravity shear occurred. The Y direction hysteresis plot also showed a large decrease in lateral stiffness (Figure 3-25). Before moving to Point 6, the gravity shear ratio was again brought back to 50% by further tensioning of the prestressing strands. As the specimen was displaced to Point 6 during the cycle at 2.30% drift, the gravity shear ratio dropped significantly again; however, the attempt to reload to the target gravity shear ratio was unsuccessful as the slab continued to slide down the column with little increase in gravity shear (Figure 3-28).

3.3.2. Specimen B2

Specimen B2 was the only test to be completed in one day; thus, the slab and column were never fully unloaded for the duration of the test. Hysteresis plots from the X and Y loading directions for Specimen B2 are shown in Figure 3-29 and Figure 3-30, respectively. In Figure 3-31, the hysteresis response is plotted using resultant load and drift values.

The hysteresis plots show that peak force, limited by the flexural capacity of the slab, was relatively constant during the cycles to 1.15%, 1.40%, 1.60%, and 1.85% drift (Figure 3-29 and Figure 3-30). During the cycle to 2.30% drift, however, a substantial reduction in peak lateral force occurred for both loading directions as a punching shear failure developed in the specimen.

Similar to Specimen B1, results from Specimen B2 showed a consistent relationship between moments transferred between the slab and the column about the X- and Y-axes

throughout the early drift cycles (Figure 3-32). These relationships (slopes) were relatively constant until the specimen was displaced from Point 10 to Point 11 of the 1.85% cycle; at which point displacement in the negative Y-direction caused a large decrease in moment about the Y-axis. As mentioned earlier, the increase in the interdependence between moments about the X- and Y-axes is believed to be indicative of the membrane action in the slab. Shortly after this increased interdependence, the slab failed between Points 1 and 2 of the 2.30% drift cycle.

A time history of the gravity shear ratio and applied lateral drifts is plotted Figure 3-33. The gravity shear ratio remained within 10% of the target gravity shear during the cycles between 0.45% and 1.60% drift (Figure 3-33). The slightly higher drop in gravity shear throughout the first drift cycle (0.25% drift) was likely caused by initial cracking in the slab.

Throughout the 1.85% drift cycle, it was not possible to maintain a stable gravity shear ratio, especially beyond Point 7 on the load path, as a punching shear failure began to develop. As the slab began to drop down the column, tension dropped in the prestressing strands and loads were redistributed to the actuators supporting the slab corners.

When loading from Point 1 to Point 2 in the 2.30% drift cycle, there was a severe drop in the gravity shear (Figure 3-33). This event was associated with a slight but sudden drop in applied lateral load in the X direction and an overall decrease in lateral stiffness and strength during the ensuing lateral displacements (see portion of hysteresis response highlighted in black in Figure 3-29). The sudden drop in lateral force was likely caused by the fracture of several studs, as discussed in Section 3.2.2. These stud fractures, along with the severe concrete degradation in the connection region, led to a severe loss of stiffness and gravity load capacity of the specimen. As a result, the test was terminated.

3.3.3. Specimen B3

Testing of Specimen B3 was completed over two days. Day one of testing ended after the completion of the 1.60% drift cycle. Hysteresis plots in the X and Y directions for Specimen B3 are shown in Figure 3-34 and Figure 3-35, respectively, while the specimen hysteresis response using resultant load and drift values is shown in Figure 3-36. The

hysteresis behavior of Specimen B3 was stable throughout the cycles up to 1.85% drift, with a relatively constant peak force, limited by flexural yielding, during the cycles between 0.90% and 1.85% drift. During the cycle to 1.85% drift, however, an approximately 15% drop in gravity shear occurred. This led to a pause in the test at zero lateral displacement between Points 6 and 7 on the loading path to further tension the strands in order to restore the gravity shear in the connection (Figure 3-38).

During the 2.30% drift cycle, a large decrease in lateral stiffness from the previous 1.85% drift cycle was observed while the specimen was displaced from Point 1 to Point 2. The gravity shear ratio also became very unstable throughout the 2.30% drift cycle as punching related damage developed and the slab dropped down the column (Figure 3-8). As indicated in Figure 3-38, the slab was reloaded during the 2.30% drift cycle at zero displacement in X and Y directions, when loading from Point 3 to 4, Point 6 to Point 7, and Point 9 to Point 10 on the loading path. Each time, a gravity shear ratio of 50% was successfully reestablished in the connection. In contrast to the previous specimens, this connection was capable of supporting gravity loads and could be cycled after significant punching shear damage was observed.

A substantial loss of torsional stiffness in the connection was also observed during the 2.30% drift cycle, resulting in the slab rotating relative to the column about the column longitudinal axis. This was unrealistic behavior for a flat-slab frame system. The test was terminated after loading to Points 1 and 2 of the 2.75% drift cycle, when significant twisting about the column was observed and after the slab had dropped well over 1 in. down the column.

The relationship between the moments in the slab about the X- and Y-axes are plotted in Figure 3-37. Similar to Specimens B1 and B2, results from Specimen B3 showed a consistent relationship between X- and Y-axis slab moments throughout the early drift cycles, with a slightly increased interdependence during the 1.85% drift cycle. A sudden increase in this interdependence was observed when the specimen was displaced from Point 1 to Point 2 of the 2.30% cycle; at which point displacement in the negative X-direction caused a large decrease in moment about the X-axis. This increased

interdependence of moments in both directions was believed to be the result of membrane action in the slab in the connection region that developed as a consequence of the substantial deterioration of the slab concrete. Shortly after this change in slope, while loading to Points 5 and 6 of the 2.30% drift cycle, the flexural strength of the slab degraded to near zero.

3.3.4. Specimen B4

Testing of Specimen B4 was completed over two days. Day one of testing ended after the completion of the 1.60% drift cycle. Hysteresis plots in the X and Y loading directions for Specimen B4 are shown in Figure 3-39 and Figure 3-40 respectively. In Figure 3-41, the hysteresis response is plotted using resultant load and drift values.

Specimen B4 exhibited a stable response throughout the cycles up to 1.85% drift, with relatively constant peak force for the cycles between 0.90% and 1.85% drift. The peak force capacity of Specimen B4 was controlled by flexural yielding, as in the other specimens. At Point 5 in the 2.30% drift cycle, the first substantial decrease in peak lateral force relative to the previous cycle was observed (Figure 3-40). From this point forward in the test, the hysteresis loops showed a large decrease in specimen stiffness and strength. The connection gravity shear also became very unstable beyond this point, requiring the slab to be reloaded for the first time in the middle of a cycle. This was done at zero displacement while loading from Point 9 to Point 10, as indicated in Figure 3-43.

In Figure 3-42, the relationship between the moments in the slab about the X- and Y-axes is plotted. Similar to the previous specimens, results from Specimen B4 showed a consistent relationship between X- and Y-axis slab moments throughout the early drift cycles. These relationships were relatively consistent until the 2.30% drift cycle, where an increased interdependence was observed. This interdependence increased modestly while loading from Point 1 to Point 2. The moments became strongly correlated while loading from Point 4 to Point 5. By the time the specimen was loaded to Point 9 of the 2.30% cycle, the connection had exhibited a substantial loss of moment capacity.

Although the slab had dropped a substantial amount (more than 1 in.) by the end of the 2.30% drift cycle, the connection was still capable of holding the required gravity shear.

The specimen was subjected to a full cycle at 2.75% drift. During the 2.75% drift cycle, the slab was reloaded to the target gravity shear when it was at zero displacement prior to loading to Points 4, 7, and 10. When reloading the slab prior to Point 7, the slab corners were lowered to increase the amount of simulated gravity load attracted to the connection. After the last quarter cycle to 2.75% drift, the specimen was still capable of supporting the required gravity shear. However, the test was terminated because the slab had sustained severe damage and dropped more than 2 in.

3.4. Load versus Drift Envelope Response

Tabulated in Table 3-1 to Table 3-4 are the values of peak resultant lateral force that were recorded at each of the thirteen points on the cloverleaf loading path at each drift level. The maximum resultant lateral force achieved at each of the points in the cloverleaf loading pattern during the each test is marked on the table with an asterisk. Connections exhibiting ductile performance should exhibit a good strength and stiffness retention capacity through large drift levels. In Table 3-1 to Table 3-4, values exceeding at least 90% of the maximum lateral load recorded at the respective loading point, prior to and after reaching the peak force, are bolded. To facilitate specimen comparisons, the maximum resultant force (the value with an asterisk in each column in Table 3-1 to Table 3-4) and corresponding drift level for each respective loading point are recorded in Table 3-5.

Figure 3-44 to Figure 3-46 show load versus drift envelope curves corresponding to each of the thirteen points in the cloverleaf loading pattern shown in Figure 2-28 (the values for a particular curve are associated with a column from Table 3-1 to Table 3-4). The corner points on the loading path are plotted in Figure 3-44 and the points on the loading path associated with drifts in only the X or Y direction are plotted, respectively, in Figure 3-45 and Figure 3-46. Each plot contains curves corresponding to the four specimens tested in this investigation (Specimens B1 through B4), as well as Specimen SB3 (with shear stud reinforcement) tested in a previous study (Cheng et al. 2009). For comparison, the resultant lateral force and resultant drift values were used in each set of plots.

36

The slopes of the envelope plots in Figure 3-44 to Figure 3-46 show that the stiffness of each of the specimens tested in the current study and that of Cheng's shear stud reinforced specimen were nearly identical in the elastic range. The drift level at which the maximum lateral loads, governed by flexural yielding, were achieved generally varied from 1.15% to 1.60% for every loading point, while lateral forces exceeding at least 90% of the peak force at each respective loading point were often reached in the 0.90% to 1.85% drift cycles. Specimens B1, B3, and B4 shared a similar pattern of behavior, where a large decrease in peak lateral force was not observed until the 2.30% drift cycle (3.25% resultant drift). During this cycle, substantially lower lateral forces were reached at each loading point relative to the previous drift cycle (Figure 3-44 to Figure 3-46). The first significant drop in peak lateral force for Specimen B1 occurred at Point 2, where the peak resultant force dropped to 12.5 kips, approximately equal to 70% of the peak resultant lateral force of 17.4 kips reached at the 1.15% drift cycle. Similarly for Specimen B3, at Point 3 of the 2.30% drift cycle the peak resultant lateral force was approximately 70% of the maximum force that was reached at this point during the 1.40% drift level (Table 3-3, Figure 3-45). For Specimen B4, at Point 6, the peak force of 8.6 kips was 70% of the peak value of 12.3 kips reached at this point during the 1.40% drift cycle (Table 3-4, Figure 3-46). The decrease in peak force measured during the cycle to 2.30% drift in Specimens B1, B3 and B4 was due to a substantial loss of stiffness and strength caused by the formation of punching shear cracks around the column perimeter, as well as the severe degradation of slab concrete adjacent to the column faces.

Specimen B2 displayed nearly identical behavior to Specimens B1, B3, and B4, attaining lateral forces that were at least 90% of the maximum force recorded at each cloverleaf loading point in the 0.90% drift cycle, and maintaining relatively similar peak forces through the 1.85% drift cycle (Table 3-2). While loading to Point 1 of the 2.30% drift cycle, a reduction in Y-axis specimen stiffness was observed that led to a peak lateral force of 10.6 kip, 22% less than the peak force previously imposed at Point 1. The peak resultant force reached while loading to Point 2 of the 2.30% drift cycle was 7.1 kips, approximately 60% less than the maximum force reached at Point 2 in previous drift cycles. In contrast with the other test specimens, where no sudden drop in lateral force occurred, a small but sudden drop in the applied lateral force occurred when Specimen

B2 was displaced from Point 1 to Point 2, as highlighted in Figure 3-29. As mentioned earlier, this sudden load drop is believed to have been caused by the fracture of several shear studs in the connection. The response immediately after this load drop indicated a substantial decrease in lateral stiffness of the specimen.

There was a sharp contrast in behavior between the specimens tested in this investigation and Specimen SB3 reported in Cheng et al. (2010). All four test specimens in the current study behaved very similarly in regards to load versus drift response for drift levels up to 1.85%. The behavior throughout these loading cycles was stable, with only gradual decreases in stiffness and strength. Specimen SB3 (Cheng et al. 2010), designed to have the minimum amount of shear studs required by the ACI Building Code (ACI Committee 318 2008), showed a sudden and substantial drop in applied lateral force during the cycle to 1.15% drift (Figure 3-44 to Figure 3-46). The substantially lower drift capacity exhibited by this specimen can be explained by the fact that the shear stud reinforcement was not capable of bridging the critical diagonal punching shear crack once it formed, leading to a behavior similar to that expected for a connection unreinforced in shear. The much larger amount of shear studs provided in the four specimens tested in this investigation prevented a connection failure when diagonal cracking initiated, and forced other failure modes to develop. These other failure modes involved a substantial degradation of slab concrete adjacent to the column faces.

3.5. Vertical Drop of Slab at Column

The downward vertical displacement of the bottom of the slab relative to the column ("slab drop") can be taken as a measure of the degradation of shear transfer mechanisms between the slab and the column. These vertical displacements result from either diagonal punching shear cracking in the slab or sliding shear displacements near the face of the column if a traditional punching failure is prevented by reinforcement (a schematic of these mechanisms is shown in Figure 3-47). Slab drop in Specimens B2, B3 and B4 was measured by eight Linear Variable Differential Transformers (LVDTs) fixed to the column below the slab, as shown in Figure 2-23. The average slab drop measured by the

two LVDTs closest to each column corner is plotted in Figure 3-48 through Figure 3-50 for these three specimens. Slab drop around the perimeter of the column was not recorded for Specimen B1.

In Specimens B2 through B4, slab drop was shown to exhibit two trends: 1) the average drop of the slab gradually increased as the number of cycles and drift level increased, and 2) within each drift cycle, the slab drop at each of the column corners varied as the direction and magnitude of drifts imposed on the specimen varied. The first of these observations is evidence that cracking and deterioration of the slab concrete gradually reduced the shear stiffness of the connection, as expected. The second observation, that slab drop varied among the cloverleaf pattern corners within a drift cycle, demonstrates the ability of the slab to partially recover the slab drop when unloaded (and loaded in the opposite direction). These trends appeared stable until, in later cycles, the slab drop approached 1/4 in. Once the average slab drop reached approximately 1/4 in. in each of the specimens, the slab drop began to increase rapidly with continued cycling. This rapid increase in the average slab drop began during the 1.85%, 1.85%, and 2.3% drift cycles for Specimens B2, B3, and B4, respectively.

3.6. Maximum Shear Stress Based on Eccentric Shear Model

The nominal shear stress, v_n, on each face of the critical perimeter due to direct gravity shear, V, and moment transferred to the column, typically referred to as "unbalanced" moment, M_{ub}, in each principal direction was calculated using the "eccentric shear model" specified in the ACI Building Code, Section 11.11.7 (ACI Committee 318 2008). The direct gravity shear was calculated as the net sum of all vertical forces on the slab outside of the critical perimeter, i.e., weight of the slab and perimeter steel tubes, forces applied by prestressing strands, and forces applied by vertical ancillary actuators at the slab corners. The moment transferred between the slab and the column in each principal direction was calculated as the resultant of all moments about the slab critical section centroid caused by external loads applied directly to the slab. All applied slab forces and their respective moment arms to the connection centroid are shown in the plan view of

Figure 2-27. Forces A1 – A4 represent loads applied by ancillary actuators; their sign convention is taken such that positive loads represent an upward force on the slab. Strand loads are labeled north, south, east, and west according to their location relative to the connection. The sign convention of strand loads is taken such that positive loads represent a downward force on the slab. Using the labels and moment arms shown in Figure 2-27, the following equations were used to calculate unbalanced moment in each principal direction, where the forces are expressed in kips and the moments about the X- and Y-axes, M_{ubx} and M_{uby}, have units of kip-inches.

$$M_{ubx} = (A_3 + A_2 - A_1 - A_4)90in + (Strand_{West} - Strand_{East})45in \tag{3.3}$$

$$M_{uby} = (A_3 + A_4 - A_1 - A_2)90in + (Strand_{South} - Strand_{North})45in \tag{3.4}$$

Following Commentary Section R11.11.7.2 of the ACI Building Code (ACI Committee 318 2008), for square interior columns the shear stress distribution due to gravity shear is assumed to be uniform on the critical section, as shown in Figure 3-51A. The shear stress distribution due to moment transferred through eccentric shear is assumed to vary linearly about the critical section, as shown in Figure 3-51B. With V and the corresponding M_{ubx} and M_{uby}, the maximum shear stresses v_{ux} and v_{uy} were taken as the largest value calculated by,

$$v_{ux} = \frac{V}{A_c} \pm \frac{\gamma_v M_{uby} c_x}{J_c} \tag{3.5}$$

$$v_{uy} = \frac{V}{A_c} \pm \frac{\gamma_v M_{ubx} c_y}{J_c} \tag{3.6}$$

In Eqns. (3.5) and (3.6), A_c is defined as the area of the critical section at $d/2$ from the column faces, equal to $d \cdot b_o$, where d is the average slab effective depth (4.75 in.) and b_o is the length of the critical perimeter (83 in.). The area of the critical section A_c for the connection of each specimen was calculated as 394.25 in.^{2}. The term γ_v is an empirical constant that represents the fraction of moment transferred to the column through eccentric shear about the critical section. This value is calculated as,

$$\gamma_v = 1 - \gamma_f \tag{3.7}$$

$$\gamma_f = \frac{1}{1 + (2/3)\sqrt{b_1/b_2}} \tag{3.8}$$

In Eqn. (3.7), γ_f is the fraction of moment to be transferred through flexure over the effective width. For a rectangular column, the dimension b_1 is the width of the column faces parallel to the direction about which moment is being transferred, while b_2 is the width of the perpendicular column faces. For the square columns used in this study $b = b_1 = b_2 = 16$ in.; therefore, according to this model, $\gamma_f = 0.60$ and the corresponding fraction of moment transferred through eccentric shear γ_v was 0.40.

The c_x and c_y variables represent the distance from the geometric centroid of the column to the failure plane oriented parallel to the X- and Y-axes, respectively, and were calculated using Eq. 3.9. Because the columns in each test were square, $c_x = c_y = 10.375$ in.

$$c_x = c_y = \frac{b + d}{2} \tag{3.9}$$

The property J_c is analogous to the polar moment of inertia of the critical section about its centroid. For interior columns, it is taken as,

$$J_c = \frac{d(b_1 + d)^3}{6} + \frac{(b_1 + d)d^3}{6} + \frac{d(b_2 + d)(b_1 + d)^2}{2} \tag{3.10}$$

The 16 inch square column used in this study had a calculated value of J_c for moment transfer about both axes of the connection equal to 28,662 in^4.

Using the properties listed above, the maximum shear stress for moment transfer about either the X or Y axis was calculated for each point on the cloverleaf for each drift level using Eqns. (3.5) and (3.6). The maximum shear stress at a corner point on the critical perimeter was also calculated, even though this check is not explicitly required in the ACI Building Code. This was calculated by taking the maximum value obtained when using the following equation,

$$v_{xy} = \frac{V}{A_c} + \frac{\gamma_v M_{ubx} c_y}{J_c} + \frac{\gamma_v M_{uby} c_x}{J_c} \tag{3.11}$$

For each specimen, the maximum shear stresses on the critical section in each direction at each loading point throughout the test can be found in Table 3-6 to Table 3-9, where maximum values attained throughout the test are bolded. The maximum values of shear stress v_x, v_y, and v_{xy} recorded throughout each test for Specimens B1 through B4, and Specimen SB3 reported in Cheng et al. (2010), are shown in Table 3-10. Shear stresses are normalized by $\sqrt{f_c'}$ (psi) taking f_c' as the compressive strength of cylinders made from the slab concrete tested on the day prior to the test of each respective specimen.

The strength of each specimen, and therefore the shear stress imposed on the critical section in the slabs, was limited by the flexural strength of the slab (Sections 3.3 and 3.9). The peak shear stress on the critical section in each principal loading direction was similar in the four specimens of the current study, with values that ranged from $4.1\sqrt{f_c'}$ (psi) to $4.4\sqrt{f_c'}$ (psi) in either principal loading direction (Table 3-10). These values are also very similar to the peak shear stresses reached by Specimen SB3 (specimen with stud rails reported in Cheng et al. 2010) of $4.0\sqrt{f_c'}$ (psi) and $4.3\sqrt{f_c'}$ (psi) in the X and Y loading directions, respectively (Cheng and Parra-Montesinos 2009). The peak shear stress at any point on the critical section due to biaxial bending, v_{xy}, was also nearly identical with values ranging from $5.8\sqrt{f_c'}$ (psi) to $6.2\sqrt{f_c'}$ (psi). These values again were comparable with the peak shear stress reported in Cheng et al. (2009) of $5.7\sqrt{f_c'}$ (psi).

As discussed in Section 3.3, the main difference between each of the specimens was the drift level at which a substantial loss of lateral strength and stiffness, and more importantly a loss of gravity shear transfer capacity between the slab and the column, occurred. The decline in peak shear stress for Cheng's Specimen SB3 occurred in the 1.15% drift cycle, whereas the specimens in the current study did not experience significant drops in critical perimeter shear stresses until the 1.85% to 2.30% drift cycles. The same drift levels were associated with a loss of gravity shear transfer capacity between the slab and the column for Specimens B1 and B2, whereas Specimens B3 and

B4 continued to transfer gravity shear after losing the ability to transfer moments between the slab and column.

Using the f_c' measured on the day prior to specimen testing and the specified yield stress of the studs of 55 ksi, Specimens B1 and B2 had nominal shear stress capacities of $6.8\sqrt{f_c'}$ (psi) and $5.6\sqrt{f_c'}$ (psi), respectively, calculated according to ACI Building Code Section 11.11.5 (ACI Committee 318 2008). Although a different shear stud layout was used in Specimen B3, with one stud rail at each column corner oriented at 45 degrees from each column face, the same number of shear studs is assumed to contribute to punching shear capacity as in Specimen B1. The nominal shear stress capacity for Specimen B3 was $6.9\sqrt{f_c'}$ (psi). The nominal shear stress capacity of the connection of Specimen B4 was governed by the upper shear stress limit of $8\sqrt{f_c'}$ (psi) for sections provided with shear stud reinforcement per Section 11.11.5 of ACI 318 (ACI Committee 318 2008).

The nominal shear stress capacities of all four connections were considerably greater than the peak shear stress attained during the tests for moment transfer in either the X or Y direction because flexural yielding controlled the strength of the specimens. When biaxial moment transfer is considered, the peak shear stresses calculated using Eq. (3.11) were lower than or equal to the nominal shear stress capacity for Specimens B1, B3, and B4 (Table 3-11). Furthermore, the nominal shear stress capacity attributed to the shear stud reinforcement (v_s) in these specimens was greater than the calculated stress demand for moment transfer in either the X or Y direction. In the case of Specimen B4, the nominal shear stress capacity attributed to the shear stud reinforcement was approximately 30% greater than the peak shear stress calculated for biaxial moment transfer. In the test of Specimen B2, although the nominal shear stress capacity exceeded the peak shear stress in either the X or Y loading directions by approximately 25% ($5.6\sqrt{f_c'}$ [psi] compared to $4.4\sqrt{f_c'}$ [psi]), the peak biaxial shear stress of $6.2\sqrt{f_c'}$ (psi) exceeded the calculated nominal shear stress capacity of $5.6\sqrt{f_c'}$ (psi). Recall that several studs in Specimen B2 fractured from the base rail at the weld before yielding of the instrumented studs

occurred. Thus, the potential stress capacity of the fractured studs was likely less than the design yield stress.

3.7. Slab-Column Flexural Rotations

LVDTs were fixed to the top and bottom of the slab at both d and $2d$ from each column face so that flexural rotations in the slab could be calculated (see Section 2.3.2 and Figure 2-23). In general, all four specimens exhibited a similar behavior in terms of connection flexural rotations. Prior to evidence of slab punching becoming visually apparent during testing, peak calculated flexural rotations were between 0.005 and 0.01 radians in the positive direction and -0.03 and -0.04 radians in the negative direction (where negative rotation indicates larger tension strains at the extreme top fibers of the slab). These calculated rotations are believed to be representative of the rotations that develop in connections of typical reinforced concrete two-way slab systems at similar lateral displacement levels because of the slenderness ratio and scale of the slabs tested.

Figure 3-52 shows the slab moment about the Y-axis plotted versus rotations calculated d and $2d$ from the north column face of Specimen B2. The similarity between the two plots in terms of peak rotations calculated for each loading cycle and the shape of the hysteresis indicates that very little change in rotation was exhibited by the slab beyond d from the column face. This observation is typical of all four column faces in all four specimens and indicates that most or all inelastic flexural deformations concentrated within d from the column faces. See Appendix B for plots of slab moment versus rotation for all of the specimens.

3.8. Shear Stud Strains

3.8.1. Stud Rail Strain Profile

The axial strain in the stud shanks was monitored in several shear studs in each specimen. Due to varying shear reinforcement details between specimens, the instrumentation plan differed accordingly for each test (Figure 2-19 to Figure 2-22). In Figure 3-53 to Figure

3-60 strain profiles of individual stud rails are plotted throughout the test. Each data point represents the maximum strain observed in a given stud during the drift cycle plotted versus the stud distance to the column face. For studs connected to rails placed at a 45 degree angle with respect to the column faces, strains are plotted versus the distance from the column corner to the respective stud.

Several shear stud strain gauges were damaged in the late stages of the test as wide cracks opened up and gauge wires were severed. Data were therefore not available for all instrumented studs through the end of each test. Data points with hollow markers indicate that either the gauge was not functional for the entire cycle or the entire cycle was not completed.

3.8.2. *Specimen B1*

The first five shear studs were instrumented on the center stud rails placed orthogonal to the south and east faces of the column (Figure 2-19). The strain profile of these rails is shown in Figure 3-53. Beyond $1.5d$ (7-1/8 in.) from the column periphery, strain readings were relatively low in all instrumented shear studs throughout the test. This agrees with photographs of the specimen showing a majority of the cracking to be within a distance d (4-3/4 in.) of the column face.

In the 0.90% drift cycle, there was a relatively large increase in strain in the second and third studs of the instrumented stud rail on the east column face. A similar strain increase was observed in the second stud of the instrumented rail on the south column face during the 1.15% drift cycle. At this stage of the test the peak shear stress on the critical perimeter was approximately $4\sqrt{f_c'}$ (psi) (Table 3-6). Based on these observations, it is likely two-way shear cracks initiated during the 0.90% and 1.15% drift cycles.

In the 1.40% through the 1.85% drift cycles, the peak strains in the first three rows of shear studs on the south and east face of the connection steadily increased in each subsequent drift cycle; however, the corresponding moment transferred into the column remained relatively constant. This suggests a shift in connection shear resistance from the so-called concrete shear mechanisms to the shear resistance mechanism associated with the shear stud reinforcement. Maximum measured stud strain was slightly lower than

0.003 in the second stud of the instrumented rail on the east column face. This strain was measured during the cycle at 1.85% drift.

3.8.3. Specimen B2

The first five shear studs on the center stud rails placed orthogonally to each face of the column of Specimen B2 were instrumented (Figure 2-20). The strain profile of these rails is shown in Figure 3-54. Similar to Specimen B1, strain values remained relatively low throughout the entire test beyond $1.5d$ (beyond the third row of shear studs) from the column periphery.

Two-way shear cracks likely formed during the 0.90% and 1.15% drift cycles, as large increases in strain were observed in the first and second rows of studs on the north, south, and east faces of the connection. Following the formation of diagonal shear cracks, strains increased steadily throughout the remainder of the test. At the time of failure during the 2.30% drift cycle, where it is likely that studs fractured from the base rail, readings from many of the gauges were lost; however, in several studs near the connection, strain readings decreased significantly. As in Specimen B1, peak measured stud strain was slightly below 0.003. The first stud closest to the south face of the column on the center rail was the only stud instrumented with a strain gauge that also fractured from its base rail due to a weld failure. The maximum strain recorded in this stud was approximately 0.0027, and occurred in the 1.85% drift cycle (Figure 3-54).

3.8.4. Specimen B3

The strain profiles of stud rails placed orthogonally on each face of the column of Specimen B3 are plotted in Figure 3-55. Strain profiles for stud rails placed at the corners of the column and oriented 45 degrees from the column faces are plotted in Figure 3-57. A number of strain readings for Specimen B3 were omitted for the 1.40% drift cycle due to a malfunction of the data acquisition system (DAQ), which led to unreliable data recorded in several of the DAQ channels. The DAQ was restarted after the completion of the 1.40% drift cycle and it functioned properly thereafter.

As observed in the other tests, shear stud strain readings were only large within a distance of $1.5d$ from the column face. The substantial increase in stud strain between the 0.90%

and 1.60% drift levels indicated the formation of diagonal shear cracks during these stages of the test. In general, strain data from studs on the rails placed at the corners of the column were lower than those of studs on orthogonally placed rails during the cycles to 1.85% drift and higher. An explanation for this behavior may be related to biaxial bending at the connection. The highest stress levels on the critical perimeter due to biaxial bending occur near the column corners. The higher stresses in these areas may have contributed to a more rapid degradation of concrete, resulting in a less efficient engagement of the shear studs.

In the 2.30% drift cycle, significant punching shear-related damage developed in the connection of Specimen B3 as the slab concrete degraded. Many of the studs lost anchorage and dropped with the slab. However, a large increase in strain was observed in the second shear stud on the south face of the column in the 2.30% drift cycle, reaching a strain of approximately 0.0065 (Figure 3-55 and Figure 3-56). After the test, a kink was found in this rail between the first and second stud (Figure 3-19). It was also found that the head of the first shear stud was anchored by top mat flexural reinforcement that passed through the column. The strain readings and the kink in the rail show that the bar provided anchorage to the shear stud after the concrete had become loose and the slab dropped. In the ensuing 2.75% drift cycle, the maximum recorded strain level in this stud was significantly less than in the 2.30% drift cycle. After the test, the stud was not found to be anchored by any flexural reinforcement. Thus, it is likely that this decrease in strain was due to the stud slipping off the bar and losing anchorage at some point between the 2.30% and 2.75% drift cycles.

3.8.5. Specimen B4

The strain profiles of orthogonally placed stud rails on each face of the column of Specimen B4 are plotted in Figure 3-58 and Figure 3-59. Strain profiles of stud rails oriented at 45 degrees from each column face are plotted in Figure 3-60. The data for the rail profiles in Figure 3-58 are labeled "inner orthogonal," and were constructed with strain readings from stud rails that were placed closer to the center of the column face (Figure 2-22). Similarly, the data for the rail profiles in Figure 3-59 are labeled "outer orthogonal," and were constructed with strain readings from rails placed between inner

orthogonal rails and rails at the column corners oriented at 45 degrees from the column faces (Figure 2-22).

As in Specimens B1, B2 and B3, the increase in the strain of several studs in the 0.90% and 1.15% drift cycles indicated the development of diagonal shear cracks at the connection. Specimen B4 contained eight more rails than the other specimens. Due to the greater number of shear studs, less load was required to be resisted per stud after diagonal cracks had formed, resulting in lower strains per stud as well. Peak strains in the first and second rows of studs in Specimen B4 ranged mostly from 0.001 to 0.0015 (Figure 3-58 and Figure 3-59), in contrast to the other specimens, where measured peak strains were approximately 0.003 for Specimens B1 and B2, and 0.005 for Specimen B3.

3.9. Slab Flexural Reinforcement Strain Readings

3.9.1. Specimen B1

The strain gauge layout for slab flexural reinforcement is shown in Figure 2-15 and Figure 2-16. The strain gauge locations were defined by coordinates l (parallel) and t (transverse) with respect to the column center (Figure 2-17). Strain gauges were applied to flexural reinforcement placed at several distances t from the column center and at five distances l, equal to $\pm(b+d)/2$ (±10.375 in.), $\pm(b+5d)/2$ (±19.875 in.), and 0 in. from the center of the column. Coordinates l and t for each strain gauge are listed in Table 2-2.

Strain profiles of flexural reinforcement laid along the X and Y axes of the slab were plotted for each specimen of the current study, and are shown for Specimen B1 in Figure 3-61 and Figure 3-62, respectively. The strain profile for bars laid in the X-direction shows the strains recorded by gauges TS3, TS7, TS9, TS11, TS12, and TS13 at Point 4 of each drift cycle (it was found that strains were generally maximum in these gauges at Point 4). These gauges were located at the same position, $l=-(b+d)/2$ in the X-direction, on separate bars placed at distances, t, of -3 in., -15 in., -27 in., -39 in., -57 in., and -81 in. from the center of the column in the Y-direction (Figure 2-16). Similarly, the strain profile for bars laid along the Y-direction is shown for strains recorded at Point 7 for each drift cycle by gauges TE2, TE6, TE10, TE11, TE12, and TE13. These gauges were

located in the same position in the Y-direction, $l=(b+d)/2$, on separate bars placed at distances, t, of -3 in., -15 in., -27 in., -39 in., -57 in., and -81 in. from the center of the slab in the X-direction (Figure 2-16).

In Specimen B1, two gauges in the top mat of reinforcement (gauges TS1 and TS2 shown in Figure 2-16) were damaged during the casting of the slab and did not provide reliable data.

The yield strain of 0.00233, determined from coupon tests, was exceeded in instrumented bars at $l=\pm(b+d)/2$ within a 30 in. (5h) slab section centered on both the X and Y faces of the column, as shown in the strain profiles in Figure 3-61 and Figure 3-62. Strains remained below yielding in all of the gauges located on the top reinforcement at $l = \pm(b + 5d)/2$ in either direction.

Figure 3-63 and Figure 3-64 show plots of the applied lateral load in the Y-direction versus the strain in gauges TE2 and TE3, respectively, throughout the entire test. The onset of yielding is highlighted in each plot by a sudden jump in strain in the 0.90% drift cycle. In the X-direction, yielding was observed at the 1.15% drift level in gauge TS3, as highlighted in Figure 3-65. This yielding coincides with a change in the slope of the load-drift plots discussed in Section 3.4.

The bottom mat of reinforcement remained elastic prior to punching in the 2.30% drift cycle. As the south slab region began to drop relative to the column, large increases in strain occurred in bottom slab reinforcement. In particular, this occurred in bars that passed through the column support and served as integrity steel. This is highlighted in the strain history for gauges BS2 and BS3 shown in Figure 3-66 and Figure 3-67, respectively. Large strain increases were also observed in gauges BS6, BS7, and BE7, as shown in Figure 3-68 to Figure 3-70. These gauges were placed in the region where the inclined cracks formed in the northwest slab region, as illustrated in Figure 3-11. It is likely that bars in this location acted as hangers similar to integrity steel passing through the column support (Figure 2-8) as the south piece of slab began to drop relative to the north piece, as described in Section 3.2.1.

3.9.2. Specimen B2

For Specimen B2, strain gauges BS4 and TS10 were broken during specimen construction and strain data could not be collected at either location. Strain profile plots in the X and Y directions are shown in Figure 3-71 and Figure 3-72.

Flexural yielding was concentrated within the central 30 in. (5h) of the slab for loading in the X direction, as shown by the strain profile across the slab width for gauges located at d/2 from the column face on bars parallel to the Y axis (Figure 3-71). Yielding for loading in the Y direction concentrated over a somewhat narrower region, as indicated by the strain profile shown in Figure 3-72, obtained from strain gauges located at d/2 from the column face on bars parallel to the X axis (loading in the Y direction).

Strain gauges TE2 and TE3 indicated flexural yielding for loading in the Y direction during the 0.70% drift cycle, as highlighted in Figure 3-73 and Figure 3-74, respectively. Flexural yielding for loading in the X direction also occurred during this cycle, as indicated by the strains measured through strain gauge TS2. On the opposite side of the connection, however, strains greater than the yield strain were measured by gauge TS3 during the 0.90% drift cycle (Figure 3-76). All of these strain gauges were placed on bars at $l = \pm (b + d)/2$. During the 1.85% drift cycle, yielding was indicated by readings from gauges TE4, TS1, and TS4. These were placed on reinforcing bars $l = \pm (b + 5d)/2$ from the column center, as highlighted in Figure 3-77 to Figure 3-79, respectively. Specimen B2 was the only specimen to show yielding in any flexural bar at $l = \pm (b + 5d)/2$.

Bottom reinforcement remained elastic throughout the entire test prior to punching in the 2.30% drift cycle. After the column punched, large strain increases in bottom bars passing through the column occurred, as shown by the strain histories of gauges BE2, BE3, and BS3 (Figure 3-80 to Figure 3-82).

3.9.3. Specimen B3

Strain profile plots in the X and Y directions for Specimen B3 are shown in Figure 3-83 and Figure 3-84. Flexural reinforcement in the slab remained elastic until the 0.70% drift cycle, when reinforcement laid in the X-direction at t=3 in, and $l=\pm(b+d)/2$ indicated

yielding, as shown by the lateral load versus strain plots for gauges TS2 and TS3 in Figure 3-85 and Figure 3-86, respectively. During the ensuing 0.90% drift cycle, bars placed in the Y-direction showed signs of yielding at $l=\pm(b+d)/2$, as indicated by the strain history of gauges TE2 and TE3 shown in Figure 3-87 and Figure 3-88, respectively.

In profile plots Figure 3-83 and Figure 3-84, it is shown that the yield strain of 0.00223, determined from coupon tests, was exceeded by measurements taken on flexural reinforcement at a distance of $d/2$ from the column face. None of the lateral force versus drift plots of gauges placed at $2.5d$ from the column face indicated yielding throughout the test.

In the bottom mat of reinforcement, strain gauge BS6 was damaged during specimen construction. Behavior of bottom reinforcement was mostly elastic through the end of the 1.85% drift cycle, although yielding was spreading in the top mat of reinforcement (Figure 3-89). As in the previous specimens, increases in bottom bar strains were observed during the 2.30% drift cycle as a punching shear failure developed and the slab dropped significantly with respect to the column (Figure 3-90). These increased strains indicate that these bars had begun to act as integrity reinforcement through the column.

3.9.4. Specimen B4

Strain profile plots in the X and Y directions for Specimen B4 are shown in Figure 3-91 and Figure 3-92. In the top mat of reinforcing bars, strain gauge TE3 was damaged during specimen construction and TS3 was damaged after the cycle to 1.85% drift. The initial yield of flexural reinforcement at $t = -3$ in. and $l = \pm(b+d)/2$ occurred at much higher drift levels than in the other three specimens. For loading in the Y direction, gauge TE2 recorded yielding during the 1.40% drift cycle, as shown in Figure 3-93. For loading in the X-direction, strain gauges TS2 and TS3 initially showed yielding during the 0.90% and 1.85% drift cycles, respectively (Figure 3-94 and Figure 3-95). In the previous specimens, gauges in these locations indicated yielding during the cycles at 0.70% to 1.15% drift. The reason for this different yielding pattern is unclear. Strain gauge TS5,

located at t = -15 in. (2.5h) and $l = \pm (b + d)/2$, showed inelastic behavior during the 1.85% drift cycle (Figure 3-96).

In the strain profile plots shown in Figure 3-91 and Figure 3-92, it can be seen that peak reinforcing bar strains at the latter drift cycles were greater than or approximately equal to the yield strain of 0.00232, determined from coupon tests, within a 30 in. (5h) slab section centered on both the X and Y faces of the column. Yield strains were exceeded on flexural reinforcement at a distance $l = \pm (b + 5d)/2$; however, none of the lateral force versus strain plots of gauges at this distance indicated inelastic behavior at any point throughout the test.

In the bottom mat of reinforcement, strain gauge BS2 was damaged during specimen construction. During the 2.30% drift cycle, strain gauges on bars passing through the column recorded a change in behavior and inelastic deformations in some cases, which was likely associated with the slab beginning to drop relative to the column. Lateral load versus strain histories for gauges BE2, BE3, and BS3, shown in Figure 3-97 to Figure 3-99, respectively, highlight this behavior. Strain readings on all other bottom mat reinforcement showed elastic behavior throughout the entire test.

3.10. Column Base Rotations

The base of the first story column was expected to undergo inelastic flexural deformations right above the specimen base block (see Figure 2-5 for specimen layout). As shown in Figure 2-24, LVDTs were fixed to each face of the column 14 in. from the base block so that column "hinge" rotations could be calculated (the assumed hinge length of 14 in. is equal to the effective flexural depth of the 16 in. square column). The relationship between moment at the base of the column and calculated flexural hinge rotations is plotted in Figure 3-100 through Figure 3-107. The moments in the base of the column about the X- and Y-axes, M_X and M_Y, were calculated using Eq. (3.12), where F_X, F_Y, and F_Z are the forces applied to the top block along the X-, Y-, and Z-axes, H is the height of the specimen (205 in.), M_{slab-X} and M_{slab-Y} are the moments transferred from the slab to the column about the X- and Y-axes, V is the net vertical force transferred

from the slab to the column, and Δ and Δ_{slab} are the horizontal displacements measured at the top of the specimen and at the slab, respectively. Both Δ and Δ_{slab} were adjusted to account for slip of the base block.

$$M_X = F_Y H + M_{slab-X} + V\Delta_{slab} + F_Z\Delta$$

$$M_Y = F_X H + M_{slab-Y} + V\Delta_{slab} + F_Z\Delta \qquad (3.12)$$

In Eq. (3.12), a positive direction for M_{slab} corresponds to the same direction of the moment generated by a positive lateral force (either $F_Y H$ or $F_x H$). In general, however, the direction of M_{slab} is opposite to the direction of the moment caused by the lateral force. Positive direction for M_X and M_Y, on the other hand, is opposite to the positive direction for the moment generated by the lateral force.

The columns were subjected to axial forces of approximately 200 kip, or $0.1 A_g f_c'$, and shear stresses of approximately $0.9\sqrt{f_c'}$ (psi), where A_g is the cross-sectional area of the column and f_c' is the cylinder compressive strength of the concrete. The hysteresis relationships of the columns were similar for the four specimens and both loading directions. All of the curves show evidence of yielding at a rotation of approximately 0.005 rad. Peak moment at the column base occurred at a column rotation of approximately 0.007 rad. The greatest difference between the hysteresis responses was the maximum calculated rotation in each of the specimens, which ranged approximately from 0.008 to 0.016 rad. Peak rotations were similar for Specimens B1 through B3 (between 0.008 and 0.011 rad), while the column base of Specimen B4 underwent the largest rotations (approximately 0.016 rad), as this specimen was subjected to the largest lateral displacement. No major damage was observed in the columns by the end of the tests.

3.11. Twist of Slab Relative to Column

As shown in Figure 2-26, four LVDTs were placed in the plane of the slab to measure relative displacements between the slab and the reaction wall along both the X- and Y-

axes. Data from these LVDTs were also used to calculate rotation of the slab about the (vertical) Z-axis. Because column rotations about the Z-axis were restrained at the bottom and top of the column, the measured slab rotation about the Z-axis can be considered to be the same as the twist of the slab relative to the column. As discussed in Section 3.3, such twisting of the slab is not representative of typical slab-column deformations and should be minimized during tests of slab-column connections. Figure 3-108 through Figure 3-111 show the twist of the slab calculated for Specimens B1 through B4. Except for very small twists calculated near the end of the tests, the slab of Specimens B1, B2, and B4 essentially did not twist relative to the column. The slab in Specimen B3, however, did twist relative to the column starting during the cycle at 2.30% drift. Z-axis rotations exceeded 0.10 rad by the end of the test of Specimen B3. The pre-punching behavior of Specimen B3 was not affected by this twisting, however, as it began once a punching shear failure started to develop. As discussed previously, the connection of Specimen B3 substantially degraded during the cycles to 1.85% and 2.3% drift, yet slab twists remained below 0.015 rad up to the end of the 2.30% drift cycle. Significant twisting of the slab and unrealistic deformation demands did develop during the cycle to 2.75% drift.

4. DISCUSSION OF FAILURE MECHANISMS AND RECOMMENDATIONS FOR DESIGN

4.1. Specimen Performance

The results from the test of each specimen were closely examined in an effort to identify the mechanisms controlling their behavior and failure. In particular, the degradation of slab moment capacity, vertical (downward) displacement of the slab relative to the column face, and the relationships between reinforcement strain and imposed specimen drift were examined. The findings for each specimen and discussion of the implications for reinforced concrete (non-prestressed) flat-plate slab design are presented in the following sections.

4.1.1. General

The performances of the four specimens to initial application of gravity loads and to lateral displacements up to approximately 1% drift were very similar. As shown in Figure 4-1, data from LVDTs indicate that initial application of the gravity load caused compression on the bottom surface of the slab adjacent to the column. The data plotted in Figure 4-1, taken from Specimen B1, are typical of the four specimens. Measurements taken on top of the slab near the column faces indicate that gravity load application caused top surface tension strains to develop, as expected. Gravity load application resulted in strains of approximately 0.0005, 0.0004, 0.0004, and 0.00035 on the top mat of reinforcement approximately 2 in. from the column faces in Specimens B1 through B4, respectively. Lateral displacements caused the slab strains to vary with enough magnitude that tension strains sufficient to cause cracking were measured on the bottom of the slab starting in the first drift cycle (to 0.25% drift). It should be mentioned that initial strains resulting from the self-weight of the slab were not measured.

Tensile strains exceeding the reinforcement yield strain were first measured in the top mat reinforcement near the face of the column at approximately 0.7% drift. In all four specimens, strain gauges placed on the top mat of reinforcement at the column face had developed strains exceeding 0.005, with results from one gauge in Specimen B2 reaching

0.0085 before the 0.90% drift cycle had been completed. By 1% drift, extensive yielding in the top mat of reinforcement (with the associated wide cracks) and tensile strains large enough to crack the compression zone on the bottom of the slab had been observed. This yielding of the top mat of reinforcement controlled the strength capacity of each of the specimens, whereas shear-related concrete degradation and punching controlled the drift capacities.

4.1.2. *Specimen B1*

Discussion of the performance of Specimen B1 is more limited than that of the other specimens for two reasons: 1) vertical drop of the slab, an indicator of punching, was not measured on all four column faces in this specimen, and 2) several of the strain gauges failed to record strains through to the end of the test (including 13 out of 16 strain gauges mounted on studs). Damage such as debonding of strain gauges and severing of strain gauge wires, particularly if it developed in a pattern consistent with expected cracking, could be an indicator of new cracking or increased crack width. Where it may be informative, the occurrence of new damage to gauges is included in the following discussion.

Specimen B1 was reinforced with studs designed to satisfy the ACI Building Code requirements neglecting the concrete contribution to shear strength (see Figure 2-19 for the layout of studs and location of instrumented studs) and arranged so that the maximum stud spacing in the first three peripheral rows of studs was 1.6*d*, 1.6*d*, and 2*d*, respectively. Specimen B1 performed in a stable flexurally-dominated manner for several cycles beyond 1% drift. This finding is supported by strain gauge data, which showed no indication of diagonal shear cracking until late in the 1.6% drift cycle, and hysteresis behavior, which showed relatively wide loops with a nearly constant moment capacity, controlled by flexural yielding, until early in the 2.30% drift cycle (Figure 3-27).

There is some indication that diagonal cracking in the connection began late in the 1.60% drift cycle. Data from gauge R-E1, located on a stud 1.5 in. from the center of the east column face, showed a change in slope in the relationship between strain and drift and an increase in strain from 0.0008 to 0.0015 while loading to Point 8, the south-west corner

of the loading sequence (Figure 4-2). Given the stud strain of 0.0008 at Point 7, it is likely that at this point this particular stud was crossed by a nearly vertical (flexural crack) and that the gradual rather than sudden increase in strain to 0.0015 when loading to Point 8 was caused by the turning of this crack into a flexural shear crack.

As Specimen B1 was subsequently loaded to Points 10 and 11 in the cycle to 1.60% drift, the north-west corner of the loading sequence, three gauges on studs were damaged (R-S3, R-S5, and R-W3). Two of the three damaged gauges were located south of the column where shear stresses were expected to be greatest. It is possible these damaged gauges indicate that diagonal cracking began to spread towards the south of the column as the direction of loading changed.

During the cycle to 1.85% drift, several strain gauges were damaged. Nearly all of the damaged gauges were located where shear stresses according to the eccentric shear model were highest at the time of gauge failure. Gauge R-W4, located west of the column, failed while loading to Point 2, the north-east corner of the loading sequence. Gauges R-N2 and R-N3, located north of the column, failed while loading to Point 5, the south-east corner of the loading sequence. While loading to Point 7, west of the column, gauge BS-E1, located approximately 9 in. (1.9d) east of the column on the bottom mat of reinforcement, failed. As discussed in Section 3.1.1, visual evidence of a punching failure developing was first noted on the east side of the connection when loading to Point 8. Finally, while displacing the specimen to Points 10, 11, and 12, located north-west in the loading sequence, gauges R-E2, R-E3, R-E5, R-S4, and BS-S3, located south and east of the column, were all damaged.

The timing and location of each of the gauge failures are consistent with, but not clear evidence of, punching shear-induced diagonal cracking developing and extending around the column as the location of maximum shear stresses changed with the direction of loading. The increase in strain from 0.0016 to 0.0028 in gauge R-E2, mounted on a stud located 4 in. (approximately 0.8d) from the center of the east column face, does suggest the development of diagonal cracking as the specimen was loaded towards Point 11 of the 1.85% drift cycle (Figure 4-3). Despite the evidence that punching shear-related damage

57

began to develop during this loading cycle, hysteresis plots (Figure 3-24 and Figure 3-25) show that the specimen performance remained stable through the end of the 1.85% drift cycle. This is an indication that the shear studs were effectively delaying punching shear failure of the slab.

The connection of Specimen B1 failed early in the cycle to 2.3% drift. While loading towards Point 2, located north-east in the loading sequence, strain data from gauge R-S1, which was mounted on a stud 1.5 in. from the south face of the column, indicated a sudden change in behavior with a strain increase from 0.002 to 0.0029 followed by a decrease to 0.0023 (Figure 4-4). Simultaneously, data from gauge BS-S2, mounted on the bottom mat of reinforcement at the south column face, showed a shift from a compression strain of 0.0009 to a tension strain of 0.0017 (Figure 4-5). This seems to indicate that the bottom mat of reinforcement started to act as integrity reinforcement through the column as the slab began to drop significantly due to the development of a punching shear failure. Figure 3-24 and Figure 3-25 show that while loading to Point 2, the lateral capacity of the specimen decreased to less than 50% of its peak capacity. This lateral strength loss was accompanied by a significant reduction in gravity shear, as can be seen in Figure 3-28.

After punching had developed in the slab, subsequent loading was attempted but the connection proved unable to transfer the required gravity shear.

4.1.3. Specimen B2

Specimen B2 had shear stud reinforcement designed to satisfy the minimum amount in Section 21.13.6 of the 2008 ACI Building Code when a shear stress or drift capacity check is not performed. These studs were arranged in a cruciform layout with a maximum stud spacing of 1.6d, 1.8d, and 2.9d in the first three peripheral rows, respectively (see Figure 2-20 for stud layout and location of instrumented studs).

Specimen B2 behaved in a stable flexurally-dominated manner up to the cycle at 1.60% drift (inclusive). After initiation of flexural yielding in the slab and up to this drift level, lateral load capacity remained relatively constant (Figure 3-32), none of the data from strain gauges placed on flexural reinforcement exhibited uncharacteristic changes in

slope, and the slab had dropped, on average, less than approximately 1/8 in. (Figure 3-48). Furthermore, of the nineteen shear studs instrumented with strain gauges, eighteen studs showed strains below 0.0015 with most studs showing strains below 0.001. The only exception was the stud located 2 in. ($0.4d$) from the east face of the column, which developed strains exceeding 0.002 during the 1.60% drift cycle (Figure 4-6).

The performance of the connection in Specimen B2 degraded during the cycle to 1.85% drift, as indicated by both the slab drop and the interaction between X- and Y-axis slab moments. During this drift cycle, the average slab drop increased approximately from 1/8 in. to 1/3 in., an increase of nearly threefold (Figure 3-48). Also, the X- and Y-axis moments transferred into the column became more interdependent during the cycle to 1.85% drift, a sign that membrane action became more dominant as the slab concrete degraded.

Data from strain gauges show that diagonal cracking of the slab initiated when the specimen was loaded from Point 4 to Point 5 in the cycle to 1.85% drift (where Point 5 is the second of four corners in the loading pattern and oriented south-east of the column). The three instrumented studs closest to the north and west column faces (within two slab depths of the column face), showed significant increases in strain between Points 4 and 5 and while holding the specimen at Point 5. This includes gauge R-W1, located on the stud 2 in. ($0.4d$) from the center of the west face of the column, which showed an increase in strain from 0.0008 to 0.002 (Figure 4-7). Furthermore, data from a strain gauge placed on one of the bottom slab bars passing through the column showed a change from a compression strain of 0.001 to a tension strain of 0.0005 between Points 4 and 5 (Figure 4-8). This bar transitioned from flexure-induced compression to the tension strains expected in a bar engaged as integrity reinforcement after punching has occurred.

Despite stable specimen performance during the next quarter-cycle at 1.85% drift (points 7, 8 and 9), as evidenced by plots of moment transferred into the column, there are indications that diagonal cracking spread towards the north-east after it initiated north-west of the connection. The strain history measured by gauge BS-E2, placed on a bottom slab bar at the east face of the column, showed a sudden change in trend with a strain

59

decrease of approximately 0.0006 as the slab was loaded from Point 7 to Point 8 (Figure 4-9). Also, data from three strain gauges placed on top slab reinforcement located between 3 and 5 slab depths away from the north-east corner of the column (strain gauges TS-E9, TS-E10, and TS-E11) showed a change in slope in the relationship between strain and drift (see Figure 4-10 for a plot of strain and drift for gauge TS-E9). Although vertical slab displacement associated with punching would be expected to increase tension in the flexural bars at the diagonal crack instead of the observed decreases, it is possible that bending of the flexural bars at the crack caused the reduced strains. Regardless, these data signal a change in the deformation mechanism north-east of the column.

The locations of the observed changes are consistent with diagonal cracks intersecting the bottom reinforcement close to the column face and the top reinforcement farther away from the column. Also, during this quarter-cycle to Points 7, 8, and 9, the average vertical drop of the slab exceeded 1/4 in., and visual evidence of punching shear-induced damage on the north east side of the connection was first noted (Section 3.1.2). Data from strain gauges placed on studs located to the north and east of the column, however, did not show notable changes in strain while the specimen was loaded to Point 8.

As Specimen B2 was loaded from Point 10 to Point 11 during the 1.85% drift cycle (the north-west corner of the loading pattern), punching-related damage spread to the south-east corner of the connection and compromised the integrity of the slab. Sudden increases in the strain data from gauges on studs 2 and 5.5 in. ($0.4d$ and $1.2d$, respectively) from the south face of the column, followed by large increases in strain up to near yield, showed that diagonal cracking had extended to the south of the slab (Figure 4-11). Once punching-related damage extended from the north-west corner around to the south-east corner of the connection, stressing the studs to near their yield capacity, the shear studs were unable to maintain the integrity of the slab. At this point in the test, average drop of the slab had increased to more than 0.3 in. and X- and Y-axis slab moments transferred into the column became strongly correlated.

Loading to the first point of the 2.30% drift cycle caused the slab drop to increase rapidly and showed that the slab had lost significant flexural capacity. The test was terminated shortly thereafter. It was later determined that as the specimen was displaced towards Point 2 of the 2.30% drift cycle, several stud-to-base rail welds fractured (after the punching failure had developed, as discussed in Section 3.2.2).

4.1.4. Specimen B3

As in Specimen B1, Specimen B3 was reinforced with shear studs proportioned to resist the applied shear stresses assuming no shear strength contribution from the concrete. Four of the twelve stud rails were located at the column corners and oriented at 45 degrees from the principal column axes (see Figure 2-21 for stud layout and location of instrumented studs). This layout resulted in a maximum stud spacing of 1.5d, 1.6d, and 2.0d in the first three peripheral rows of studs, respectively. Specimen B3 generally performed in a stable manner, dominated by flexural deformations, up to the 1.60% drift cycle (inclusive). This observation is supported by stable hysteresis loops (Figure 3-37) and relationships between flexural reinforcement strains and imposed drift, and average slab drop below approximately 1/8 in. prior to the 1.85% drift cycle (Figure 3-49).

There is evidence that some studs were crossed by cracks beginning in the cycle to 1.15% drift. While loading to Point 2 of the 1.15% drift cycle (the corner north-east of the column), there was a definite but gradual change in the slope between measured strains and imposed drift for three studs grouped near the south-west corner of the column. These studs were located where shear stresses calculated according to the eccentric shear model were greatest at this stage in the loading. Figure 4-12 shows the relationship between strain and drift for one of these studs, stud RO-SW2. As discussed in Section 4.1.2, it is likely that the gradual rather than sudden increase in stud strains was due to the propagation and opening of a flexural shear crack as opposed to the formation of a new diagonal crack.

Of the other thirty six instrumented studs, four studs showed strains larger than 0.0015 (up to 0.0021) prior to the cycle to 1.85% drift. The four studs exhibiting strains greater than 0.0015 (RO-EN2, RO-ES2, RO-WS2, and RR-NW1) were located either 0.4d or

0.9d from the face of the column at each of the four column corners. Although these strains indicate the studs were crossed by cracks, the role some of these studs played in resisting shear is difficult to evaluate given the gradual increase in strain with cycles. Such gradual increase in strain without a noticeable change in pattern suggests that these studs were primarily engaged by slightly inclined flexural cracks. The relationship between strain and drift for one of these four studs is shown in Figure 4-13 (gauge RR-NW1). Increases in strains measured by gauge RR-NW1 to 0.00035 and 0.0005, which are consistent with cracking at the stud, occurred in the drift cycles to 0.70% and 0.90% - the same drift cycles in which the first indication of yielding was identified in strain gauges TS-S3 and TS-E3 located on the top-mat reinforcement at the north and west column faces, respectively. That strains consistent with cracking were first recorded by gauge RR-NW1 when yielding was first recorded in flexural reinforcement at the column faces supports the interpretation that cracks crossing the stud at the northwest corner of the column were associated with widening of flexural cracks at the faces of the column.

Measurements indicate that slab performance began to deteriorate during the cycle to 1.85% drift, although not as rapidly as in Specimen B2. Visual evidence of slab punching was first noted while loading to Point 2 of the 1.85% drift cycle. While loading to Point 5, the south-east corner of the loading sequence, the relationship between drift and strain in stud RR-NW6 showed a sudden change in slope (Figure 4-14). Stud RR-NW6 was located almost 14 in., approximately 3d, from the north-west corner of the column. This change in behavior of stud RR-NW6 suggests that, by delaying concentration of damage near the column face, the radially arranged studs led to a better spread of deformations in the connection away from the column face.

When loading to Point 8 in the 1.85% drift cycle, south-west in the loading sequence, strains measured on studs extending from the north-east corner of the column 45 degrees from the column principal axes showed evidence of a shifting of stresses in the shear studs. As shear stresses increased north-east of the column, strains measured in studs close to the column decreased while strains in studs further from the column increased. Strains measured in studs RR-NE1 and NE-2, located 2 and 4-3/8 in. (0.4d and 0.9d, respectively) from the column, decreased (Figure 4-15), strains measured in stud RR-

NE4, located 9-1/8 in. ($2d$) from the corner of the column, remained relatively constant, and strains measured in stud RR-NE6, located 13-7/8 in. ($2.9d$) from the column, increased, although they remained less than 0.0002.

As the specimen was loaded towards Point 11, north-west of the column, a change in trend in the strain history from several strain gauges was observed. Studs RO-EN1, RO-EN2, RO-ES2, RO-SE1, RO-SE2 and RO-SE4, all located east and south of the column, showed a change in slope and/or marked increases in strain (Figure 4-16 is typical). These changes suggest that punching-related cracking developed in the south-east corner of the connection when the slab was displaced to Point 11. Despite this evidence of punching-related damage, and an increase in vertical slab drop to approximately 1/4 in., the specimen lateral load capacity remained stable near 80% of its peak capacity at the end of the cycle to 1.85% drift.

The integrity of the specimen was compromised in the first quarter-cycle to 2.30% drift. As shown in Figure 3-37 and Figure 3-49, while the quarter-cycle to Points 1-2-3 of the 2.30% drift cycle was performed, the specimen lost much of its flexural capacity and the average vertical drop of the slab increased from approximately 1/4 to 1/2 in. While loading to Point 2 (north-east of the column), stud RO-WS1, located 2 in. ($0.4d$) from the west column face, yielded (Figure 4-17). Also while loading to Point 2, several strain gauges located on top mat reinforcement within d of the south and west faces of the column showed either strains exceeding 0.01, erratic strains, or were damaged completely. Strains recorded by Gauge BS-S3, located on the bottom mat reinforcement at the west face of the column, which had become negative (compression) during the 1.85% drift cycle, decreased further to -0.0015 during this first quarter cycle. These bottom mat compressive strains may indicate bending of the bar near the column caused by the vertical drop of the slab.

Subsequent loading towards Points 4 and 5 of the 2.30% drift cycle spread the damage around a greater percentage of the perimeter of the column, leading to a nearly total loss of lateral load capacity. At this point in the test, several studs near the column exhibited a constant strain independent of imposed drifts, indicating a loss of anchorage consistent

with severe concrete degradation (Figure 4-15). This damage rendered the slab unable to hold a steady vertical load (Figure 3-38). As subsequent displacements were imposed on the specimen, the slab began to rotate (twist) about the vertical Z-axis (Section 3.11). Z-axis rotations exceeded 0.015 radians after the 2.30% drift cycle and 0.10 radians prior to termination of the test, evidencing degradation of the slab concrete around the perimeter of the column.

4.1.5. Specimen B4

Specimen B4 was reinforced with a large number of shear studs arranged in a pattern designed to minimize the spacing between studs within the same peripheral row (see Figure 2-22 for stud layout and location of instrumented studs). This layout resulted in a maximum stud spacing of 1.3d, 1.3d, and 1.4d in the first three peripheral rows of studs, respectively. The area of studs within 2d of the column face exceeded by 50% the area of studs in Specimens B1 and B3, which had been designed to satisfy strength requirements assuming that $v_c = 0$.

Specimen B4 exhibited a behavior dominated by flexural deformations for several cycles beyond 1% drift. As in previous specimens, this observation is supported by relationships between flexural reinforcement strains and imposed drift, nearly constant specimen capacity after flexural yielding until the 2.30% drift cycle (Figure 3-42), and average slab drop slightly larger than 1/8 in. prior to the 2.30% drift cycle (Figure 3-50).

Although the global performance of the specimen continued to be stable throughout the cycle to 1.85% drift, there was evidence of diagonal cracking and localized shifting of stresses in a larger number of studs located around the perimeter of the column. The first evidence in the strain gauge data of a significant change in the slab condition occurred while loading to Point 11, located north-west in the loading sequence, during the cycle to 1.85% drift. Strains measured in studs OO-SE2, OO-ES2, and R-SE3, all located south and east of the column, decreased (Figure 4-19), while nearby stud OI-SW2 exhibited a steep increase in strain from 0.0009 to 0.0018 (Figure 4-20). It was at this point, while loading to Point 11 of the 1.85% drift cycle, that visual evidence of slab punching was

first noted on the west and south sides of the connection. Global performance, however, remained stable throughout the 1.85% cycle.

Early in the cycle to 2.30% drift, results from several strain gauges indicated that diagonal cracks were spreading within the slab and engaging the studs. While loading to Point 2, located north-east of the column, studs OI-WN2 and OI-WS2, located west of the column, exhibited strains of 0.0025 and 0.0032, nearly doubling the previous maximum strain in these studs (see Figure 4-21 for a plot of the data from stud OI-WN2). As the specimen was pushed towards Point 4, south of the column, strains recorded in studs north-west of the column indicated that diagonal cracking had extended to that area of the slab. Also, as shown in Figure 3-50, the average vertical drop of the slab surpassed 1/4 in. while the specimen was loaded to Points 4 and 5. During the load step to Point 5, south-east of the column, strains recorded in stud OI-WN2 increased to 0.007 (Figure 4-21); the first significant yielding of an instrumented shear stud in this series of tests. Also while loading to Point 5, Gauge BS-S3, located on the bottom mat reinforcement at the north face of the column, showed an increase in strain from 0.0016 to 0.008 (Figure 4-22). This large increase while loading to Points 4 and 5 is consistent with the bottom mat reinforcement being engaged as integrity reinforcement as the drop of the slab increased.

Figure 3-42 and Figure 3-50 show that by the time Point 9 of the 2.30% drift cycle was reached, the lateral capacity of Specimen B4 had decreased to less than 1/3 of its peak capacity and the slab had dropped more than 1/2 in. vertically relative to the column. However, the 2.30% drift cycle was completed and a cycle to 2.75% drift was conducted because, although the flexural capacity of the slab had degraded to near zero, the slab connection continued to support the target gravity shear forces until the end of the 2.75% drift cycle (Figure 3-43). The shear stiffness of the connection, however, had degraded such that the test needed to be paused after each quarter cycle, beginning with the third quarter-cycle of the 2.3% drift cycle, to adjust the specimen and reapply the target gravity loads.

4.2. Summary of Failure Evolution

Descriptions provided herein of the connection damage uncovered after completion of testing suggest that there are at least three potential mechanisms that contribute to shear failures in two-way slab-column connections subjected to combined gravity shear and lateral displacement reversals. These mechanisms are: 1) traditional punching dominated by diagonal cracking that tends to form a "cone" around the column, 2) shear sliding along flexural cracks near the column face, and 3) degradation of unconfined concrete in the connection region. In each of the specimens tested, the observed failure surface tended to show the influence of all three mechanisms to varying extents.

A schematic of the traditionally assumed cracking at punching failure in a slab-column connection subjected to monotonic direct punching shear is shown in Figure 4-27. Connection damage includes flexural cracks near the column face, and flexural-shear cracks or diagonal cracks within $1d$ to $2d$ of the face of the column. There is evidence that diagonal cracking in the specimens tested herein began to develop at approximately 1.15-1.40% drift. The shear stud reinforcement in the tested slabs, however, was effective at constraining the growth of these cracks and delaying the occurrence of a traditional punching failure. This is in contrast to Specimen SB3 reported in Cheng et al. (2009), which had shear stud reinforcement designed to resist the expected combined shear stress based on a concrete contribution to shear strength, v_c, equal to $3\sqrt{f_c'}$ (psi). This specimen failed during the cycle to 1.15% drift when diagonal cracking first developed.

Results from tests of Specimens B1 through B4 show that the shear studs, in the amounts used, were able to bridge diagonal cracks once they formed. This led to a ductile connection behavior dominated by flexural yielding during the cycles up to 1.60% drift. As the connections underwent several cycles of inelastic deformation reversals, however, extensive flexural cracking and concrete degradation due to lack of adequate concrete confinement were observed. Prior to severe degradation of concrete, flexural cracks that did not fully close upon unloading led to sliding along some vertical cracks, specifically between the column face and the first row of studs or between the first and second rows of studs. Further deformation reversals led to severe degradation of the concrete and its

inability to transfer diagonal compression, and thus, shear failure (see Figure 4-23, Figure 4-24, Figure 4-25, and Figure 4-26).

All possible shear failure surfaces must be considered and addressed for a reinforcement scheme to successfully improve the drift capacity of flat-plate specimens. In addition to restraining diagonal shear cracks, reinforcement for flat-plate slabs, particularly in connections subjected to large gravity shear and inelastic deformation reversals induced by earthquakes, must confine the core of the slab in order to maintain the integrity of the concrete and ensure adequate drift capacity. Test data indicate that shear studs do not provide the necessary confinement to ensure adequate drift capacity in connections subjected to gravity shear ratios of approximately 50% or higher, as discussed next.

4.3. Shear Studs and Concrete Confinement

It has been argued (ACI-ASCE Joint Committee 421 1999) that due to their "almost slip-free" headed anchorages, headed shear studs provide beneficial confinement to the concrete in the connection region in flat-plate slabs. Such confinement would be expected to: 1) enhance the contribution of concrete to shear capacity, and 2) maintain the integrity of the concrete in the connection region such that specimen drift capacity is improved. The presumption that headed shear studs provide this confinement is cited by ACI Committee 421 (and indirectly by Committee 318) as justification for using a concrete shear stress contribution of $3\sqrt{f_c'}$ (psi) and a maximum shear stress of $8\sqrt{f_c'}$ (psi) in design of slabs with headed shear studs (compared with $2\sqrt{f_c'}$ and $6\sqrt{f_c'}$ (psi), respectively, in slabs reinforced with other forms of shear reinforcement). The performance of the specimens described in this report, however, does not support the assertion that headed studs effectively confine concrete subjected to large deformation reversals.

It is evident from visual observations during and after testing that the slab concrete in the tested specimens was not confined. Rather than finding a well confined core of concrete between the top and bottom mats of reinforcement, large, loose pieces of concrete and

crushed "gravel-like" debris were found after the tests were completed (Section 3.2). As shown in Figure 4-23 through Figure 4-26, the concrete in the connection region of all four specimens was destroyed after testing. In cases where shear studs were located in the failure region, the concrete in the immediate vicinity of the headed studs was also not well confined. In some cases, a cylinder of concrete around the stud rod with a diameter smaller than the stud head remained intact after testing (Figure 4-24), indicating that it was either confined by or bonded to the stud. In other cases, the rod of the stud was exposed after testing, indicating that no concrete was effectively confined by the shear stud (Figure 4-23 and Figure 4-26).

Transfer of stresses within a slab-column connection ultimately relies on the ability of the concrete to resist diagonal compression. In the connection tests reported herein, the headed studs, while able to bridge diagonal cracks through several displacement cycles, could not prevent significant degradation of the concrete in the connection region. Once substantial degradation of concrete had occurred, the required diagonal thrust in the connection could not develop and the connection lost its ability to resist shear. Had the headed stud reinforcement been able to effectively confine the concrete, concrete degradation would have been delayed and a larger drift capacity would have likely been observed.

In connections subjected to low levels of shear stress and lateral displacements, it is possible that only limited degradation in the connection concrete with no significant impact on drift capacity would occur. However, as the test results show, concrete degradation in connections with shear studs subjected to gravity shear ratios of approximately 50% could be significant during large displacement reversals. In this case, limiting lateral displacements to 1.5% drift for loading in a single direction or to 2% resultant drift when accounting for simultaneous biaxial lateral displacements seems adequate.

4.4. Recommendations for Design

4.4.1. Contribution of Concrete to Shear Capacity

As mentioned previously, ACI Committee 318 recently approved the elimination, for the 2014 Building Code, of Section 21.13.6(a) of the 2011 Code. This change occurred during the course of this investigation. Section 21.13.6(a) allows the design of slab-column connections not part of the seismic-force-resisting system to be performed based on the calculation of a combined shear stress due to gravity shear and moment transfer at the design lateral displacement. If such a design is to be performed (while the provisions of the 2011 Building Code are still in effect or as allowed by other building codes), it is recommended that the contribution of concrete to shear strength be neglected (i.e., $v_c = 0$) when designing shear stud reinforced slab-column connections with gravity shear ratios comparable to those applied in this study (50%) and in which large drift capacity is required (e.g., greater than 1.5% drift).

A previously tested flat-plate slab (Cheng et al. 2009) with shear studs provided according to the 2008 ACI Code provisions, such that $v_s = 2\sqrt{f_c'}$ (psi) and $v_c + v_s = 5\sqrt{f_c'}$ (psi) $> v_u = 4.29\sqrt{f_c'}$ (psi) (where v_u is the largest applied shear stress calculated from the test results) failed during the cycle at 1.15% lateral drift (1.60% resultant drift) shortly after the flexural reinforcement in the slab began to yield. Specimen B2 (of this study), on the other hand, was designed with shear studs such that $v_s = 3.5\sqrt{f_c'}$ (psi). Based on the maximum calculated shear stresses of $v_u = 4.41\sqrt{f_c'}$ (psi), the maximum theoretical concrete contribution to shear strength was approximately $0.9\sqrt{f_c'}$ (psi). This specimen was able to sustain a cycle to 1.85% lateral drift (2.60% resultant drift) prior to failure. This level of drift, which is comparable with drift demands expected during a large seismic event, was therefore achieved when less than $1\sqrt{f_c'}$ (psi) of shear stress was theoretically required of the concrete.

In Specimens B1, B3, and B4, shear stud reinforcement was designed to provide sufficient shear strength to resist the shear demand expected after the flexural capacity of the slab was reached (such that $v_c = 0$). Specimens B1 and B3, with shear studs proportioned such that $v_s = 5.2\sqrt{f_c'}$ (psi), showed a slightly larger deformation capacity

as these two specimens were able to maintain their gravity load through part or the totality of the cycle at 2.30% drift. On the other hand, Specimen B4, with $v_s = 7.8\sqrt{f_c'}$ (psi) and significantly reduced stud spacing within the first three peripheral lines, was able to maintain its gravity load capacity up through the cycle at 2.75% drift.

4.4.2. *Minimum Shear Stud Reinforcement and Maximum Peripheral Shear Stud Spacing*

Specimen B2 was reinforced with shear reinforcement such that $v_s = 3.5\sqrt{f_c'}$ (psi). As discussed earlier, this specimen exhibited the first signs of punching shear failure during the cycle to 1.85% drift (2.60% resultant drift), but gravity load capacity was maintained throughout the cycle to this drift level. This suggests that the minimum shear reinforcement amount required in Section 21.13.6 of the 2008 and 2011 ACI Building Codes when neither a drift nor a combined shear stress check is performed is adequate for connections subjected to a gravity shear ratio of up to 50% and resultant drifts from biaxial displacements of 2.0%. For larger drifts, as indicated by the behavior of Specimen B2, significant shear related damage and possibly loss of gravity load capacity could be expected. The behavior of Specimens B3 and B4 indicate that a more stringent spacing requirement for shear studs within each of the first three peripheral lines, and possibly a larger amount of shear stud reinforcement, should be used in order to further increase drift capacity for connections subjected to gravity shear ratios approximately equal to or greater than 50%.

ACI 318-08 provisions require that the maximum spacing between studs in the first peripheral line does not exceed 2d. Specimens B1, B2, and B3, which were able to maintain their gravity load capacity through at least the full cycle at 1.85% drift, had maximum stud spacing of approximately 1.5d in the first peripheral line and 2.0d, 2.9d, and 2.0d in the third peripheral line, respectively. The maximum stud spacing in the third peripheral line of Specimen B4, on the other hand, was 1.4d. Specimen B4 was able to maintain its gravity load capacity throughout the entire cycle at 2.75% drift. Although the amount of shear stud reinforcement provided in Specimen B4 was substantially greater than that provided in the other three specimens, the closer stud spacing within the first three peripheral lines, which helped delay concrete degradation through cycling, rather

70

than the increased theoretical shear capacity, is believed to be responsible for the increased drift capacity exhibited by this specimen. Thus, it seems sensible, based on the limited data, to limit stud spacing within the first three peripheral lines to $1.5d$ for resultant drifts, from biaxial displacements, greater than 2.0%.

4.4.3. Maximum Connection Shear Capacity

If a combined shear stress check due to gravity shear and moment transfer is used for shear design of slab-column connections (while the provisions of the 2011 Building Code are still in effect or as allowed by other building codes), the maximum shear stress for slab-column connections reinforced with headed shear studs is recommended to be reduced from $8\sqrt{f_c'}$ to $6\sqrt{f_c'}$ (psi), as used for other types of shear reinforcement. Although the specimens tested in this investigation were not subjected to such large shear stresses, because the flexural strength of the slab limited the peak combined shear stress to approximately $4.5\sqrt{f_c'}$ (psi), the test results provide evidence of the inability of shear studs to provide confinement to the concrete in connections subjected to large deformation reversals. The fact that severe concrete deterioration in the test connections started to occur during the cycle at 1.85% drift, and the calculated peak combined shear stress did not exceed $4.5\sqrt{f_c'}$ (psi), suggests that a more severe (and likely earlier) concrete degradation could be expected in connections with shear stresses close to the current shear stress limit of $8\sqrt{f_c'}$ (psi).

4.5. Drift and Gravity-Shear Ratio

Figure 4-28 shows a plot of drift capacity versus gravity shear ratio for previous slab-column tests reported in the literature (listed in Table 4-1 and Table 4-2). The results of the four specimens in the current study are included in this figure for comparison. Drift capacities of Specimens B1, B2, B3, and B4 were taken as the maximum resultant drift achieved prior to loss of gravity load capacity. The gravity shear ratio used for the specimens was calculated using the applied gravity load at the time of failure. Drift capacity versus gravity shear ratio interaction for slab-column connections without shear

reinforcement in the 2008 ACI Code (ACI Committee 318-08) and in Hueste and Wight (1999) are also plotted in Figure 4-28.

As can be seen in Figure 4-28, the ultimate drift capacity of the specimens tested in this investigation, while greater than that of specimens without shear reinforcement, was substantially lower than the drift capacity of other test connections with shear stud reinforcement. This lower drift capacity is likely the result of the following two factors that apply to the specimens tested in this investigation: 1) the relatively low, but realistic, flexural reinforcement ratio of 0.7% used in the column strip (as discussed in Section 2.2, the flexural reinforcement ratio used is consistent with reinforcement amounts used in reinforced concrete two-way slabs), and 2) the application of biaxial rather than uni-axial displacements.

5. SUMMARY AND CONCLUSIONS

An experimental study was conducted on four subassemblies of non-prestressed concrete flat-plate slab-column connections reinforced with headed shear studs, loaded to a gravity-shear ratio of 50%, and subjected to biaxial lateral displacements. The intent of these tests was to investigate the effectiveness of shear stud reinforcement as a means to increase the shear resistance and deformation capacity of reinforced concrete slab-column connections. This study was motivated by results from a test of a similar specimen (Cheng et al. 2010) that showed the current (2008 and 2011) ACI 318 Code provisions for headed shear stud reinforcement may be non-conservative when used to design non-prestressed slab-column frames that are not part of the seismic-force-resisting system. The results reported by Cheng et al. showed limited drift capacity when using minimum shear stud reinforcement required by the 2008 and 2011 ACI Building Codes when combined shear stresses due to gravity shear and moment transfer are used for design; the specimen failed in punching shear during the cycle at 1.15% drift in each perpendicular loading direction.

The slabs in the specimens described herein had a clear span-to-thickness ratio of 31.3, which is close to the upper limit defined in the 2008 ACI Building Code for slabs not checked for deflections and consistent with ratios found in design practice. The tension reinforcement ratio of 0.6% based on the slab thickness and 0.7% based on the slab average effective depth is also consistent with reinforcement amounts used in design practice. The slabs were nominally identical aside from the layout of shear stud reinforcement. Specimens B1 and B2 were reinforced with twelve stud rails placed in a cruciform pattern, with studs spaced at $0.5d$ and $0.75d$ perpendicular to the column faces, respectively. The area of studs in Specimen B1 satisfied the strength requirements of ACI 318-08 neglecting the concrete contribution to shear capacity. Specimen B2 was designed to satisfy the minimum area of shear studs required when a shear stress or drift check is not performed in design ($v_s \geq 3.5\sqrt{f_c'}$ [psi]). Specimen B3 was designed with the same area of shear studs as Specimen B1, but one stud rail was located at each corner of the column and oriented at a 45-degree angle to the column principal axes. In Specimen B4,

additional rails were placed orthogonally to the column to achieve a closer and more uniform stud spacing within the first three stud peripheral lines. The maximum stud spacing in the first peripheral row was 1.5d in Specimens B1, B2 and B3, and 1.25d in Specimen B4. In the third peripheral row of studs, the maximum spacing was 2d, 2.9d, 2d, and 1.3d in Specimens B1, B2, B3, and B4, respectively. In each specimen, flexural yielding limited the lateral strength of the test specimens. Shear-related cracking and degradation of the concrete in the slab limited the drift capacity of the specimens.

The following conclusions were drawn based on the results of these tests. As the tests were not intended to represent prestressed (e.g., post-tensioned) slabs, caution should be exercised when evaluating the implications of these conclusions for the design of connections between prestressed concrete slabs and columns.

- Compared to previously tested slab-column connections with shear stud reinforcement reported in the literature, the four specimens tested in this investigation exhibited substantially lower drift capacities. This lower drift capacity is believed to be due to: 1) the lower, but realistic, flexural reinforcement ratio of 0.7% (based on the average slab effective depth) used in the slab column strip of the test specimens, and 2) the application of biaxial rather than uni-axial lateral displacements. The first sign of punching shear-related damage in the test specimens was observed during the cycle at 1.85% drift (2.60% resultant drift). Loss of gravity load carrying capacity in Specimens B1 and B2 occurred during the cycle at 2.30% drift (3.20% resultant drift). Specimens B3 and B4 continued to carry imposed gravity loads until the tests were terminated, at 2.30% and 2.75% drift (3.20% and 3.90% resultant drift), respectively.

- Visual observations indicate that shear studs did not provide adequate confinement to the concrete in the connection region. Severe concrete degradation of connection concrete in Specimens B1, B2 and B3 occurred during the cycles at 1.85% drift and higher. In Specimen B4, with a maximum stud spacing of 1.4d within the first three peripheral lines, concrete degradation was slightly delayed

compared to the other three specimens, allowing the performance of one additional drift cycle.

- In the test of Specimen B2, in which shear stud reinforcement was provided such that $v_s = 3.5\sqrt{f_c'}$ (psi), the first signs of punching shear failure were observed during the cycle at 1.85% drift in each perpendicular direction (2.6% resultant drift). This suggests that the minimum shear reinforcement amount required in Section 21.13.6 of the 2008 and 2011 ACI Building Codes when neither a drift nor a combined shear stress check is performed is adequate for connections subjected to a gravity shear ratio of up to 50% and resultant drifts from biaxial displacements of up to 2.0%. The behavior of Specimens B3 and B4 indicate that a more stringent spacing requirement for shear studs within each of the first three peripheral lines (approximately 2 slab thicknesses), and possibly an increase in the amount of shear stud reinforcement, is necessary to further increase drift capacity for connections subjected to gravity shear ratios approximately equal to or greater than 50%.

- Based on the better performance exhibited by Specimen B4 compared to the other three test specimens, particularly with regard to a delay in concrete degradation, it seems sensible to limit stud spacing within the first three peripheral lines to $1.5d$ for connections subjected to gravity shear ratios similar to those applied in this study (50%) and resultant drifts, from biaxial displacements, greater than 2%.

- If a combined shear stress check due to gravity load and unbalanced moment is used for shear design of slab-column connections with shear stud reinforcement (while the provisions of the 2011 Building Code are still in effect or as allowed by other building codes), the concrete contribution to shear strength is recommended to be neglected (i.e., $v_c = 0$) and the maximum shear stress reduced from $8\sqrt{f_c'}$ to $6\sqrt{f_c'}$ (psi), as used for other types of shear reinforcement. This recommendation is based on the severe concrete degradation observed in the test specimens attributed to lack of confinement in the connection.

- Placement of stud heads on top of flexural slab reinforcement substantially improved shear stud anchorage. Severe double curvature bending at failure was typical in base rails supporting studs anchored by top slab reinforcement as the bar anchorage prevented any significant downward movement of the stud.

- When yielding of the shear stud reinforcement was detected, failure of the slab followed shortly after. Although a slab can fail in shear without yielding of the shear stud reinforcement, test results indicate that once a single stud yields, diagonal cracks are no longer effectively restrained and punching is likely to develop.

- In the three specimens where vertical displacement of the slab was measured around the perimeter of the column, an average drop of approximately 1/4 in. coincided with imminent failure of the slab in punching.

- After punching in Specimen B2 occurred, several studs fractured at their base connection with the rails. Stringent quality control is thus required to prevent fracture of studs at their bases.

REFERENCES

ACI Committee 318. "Building Code Requirements for Structural Concrete and Commentary (ACI 318-08)." American Concrete Institute, Farmington Hills, Michigan, 2008.

ACI Committee 318. "Building Code Requirements for Structural Concrete and Commentary (ACI 318-11)." American Concrete Institute, Farmington Hills, MI, 2011.

ACI-ASCE Joint Committee 352. *Guide for Design of Slab-Column Connections in Monolithic Concrete Structures, ACI 352.1R-11.* American Concrete Institute, Farmington Hills, 2011.

ACI-ASCE Joint Committee 421. *Shear Reinforcement for Slabs (ACI 421.1R-99).* American Concrete Institute, Farmington Hills, Michigan, 1999.

ASTM Standard A370. *Standard Test Methods and Definitions for Mechanical Testing of Steel Products.* DOI: 10.1520/A0370-12A , West Conshohocken, PA: ASTM International, 2012.

ASTM Standard A615. *Standard Specification for Deformed and Plain Carbon-Steel Bars for Concrete Reinforcement.* DOI: 10.1520/A0615_A0615M-09B , West Conshohocken, PA: ASTM International, 2009.

ASTM Standard C39. *Standard Test Method for Compressive Strength of Cylindrical Concrete Specimens.* DOI: 10.1520/C0039_C0039M-12A, West Conshohocken, PA: ASTM International, 2012.

Bresler, B. "Design Criteria for Reinforced Columns Under Axial Load and Biaxial Bending." *Journal of the American Concrete Institute*, 1960: 481-490.

Broms, Carl Erik. "Ductility of Flat Plates: Comparison of Shear Reinforcement Systems." *ACI Structural Journal* 104, no. 66 (Nov-Dec 2007a): 703-711.

Broms, Carl Erik. "Flat Plates in Seismic Areas: Comparison of Shear Reinforcement Systems." *ACI Structural Journal* 104, no. 64 (Nov.-Dec. 2007b): 712-721.

Cheng, Min-Yuan, and Gustavo J. Parra-Montesinos. "Punching Shear Strength and Deformation Capacity of Fiber Reinforced Concrete Slab-Column Connections Under Earthquake-Type Loading." Report No. UMCEE 09-01, Ann Arbor, Michigan, 2009, 334.

Cheng, Min-Yuan, J. Gustavo Parra-Montesinos, and Carol Shield. "Shear Strength and Drift Capacity of Fiber-Reinforced Concrete Slab-Column Connections Subjected to Biaxial Displacements." *Journal of Structural Engineering* 136, no. 9 (September 2010): 1078-1088.

Comité Européen de Normalisation. "Eurocode 2: Design of Concrete Structures — Part 1-1: General Rules and Rules for Buildings." English Version, EN 1992-1-1:2004: E, Brussels, Belgium, 225 pp.

Dilger, Walter H., and H. Cao. "Behavior of Slab-Column Connections Under Renersed Cyclic Loading." *Proceedings of the 2nd international conference of High-Rise Bulidings.* China, 1991.

Dilger, Walter H., and S. J. Brown. "Earthquake Resistance of Slab-Column Connections." *Proceedings of Canadian Society of Civil Engineering Conference.* Winnipeg, Canada, 1994. 388-397.

Dilger, Walter, and Amin Ghali. "Shear Reinforcement for Concrete Slabs." *Journal of the Structural Division* 107, no. 12 (1981): 2403-2420.

Durrani, Ahmad J., Y Du, and Y. H. Luo. "Seismic Resistance of Nonductile Slab-Column Connections in Existing Flat-Slab Buildings." *ACI Structural Journal* 92, no. 46 (July-Aug. 1995): 476-487.

Farhey, Daniel N., Moshe A. Adin, and David Z. Yankelevsky. "RC Flat Slab-Column Subassemblages Under Lateral Loading." *Journal of the Structural Division* 119, no. 6 (June 1993): 1903-1916.

Ghali, Amin, M. Z. Elmasri, and Walter Dilger. "Punching of Flat Plates under Static and Dynamic Horizontal Forces." *ACI Journal* 73, no. 10 (Oct. 1976): 566-572.

Hawkins, Neil M, D. Mitchell, and M. S. Sheu. "Cyclic Behavior of Six Reinforced Concrete Slab-Column Specimens Transfering Moment and Shear." Progress Report, University of Washington, Seattle, Washington, 1974.

Hueste, Mary Beth D., and James K. Wight. "Nonlinear Punching Shear Failure Model for Interior Slab-Column Connections." *Journal of Structural Engineering*, September 1999: 997-1008.

Islam, Shafiqul, and Robert Park. "Tests on Slab-Column Connections with Shear and Unbalanced Flexure." *Journal of the Structural Division* 1012, no. ST3 (March 1976): 549-568.

Megally, Sami H. "Punching Shear Resistance of Concrete Slabs to Gravity and Earthquake Forces." PhD Dissertation, Department of Civil Engineering, University of Calgary, Calgary, Alberta, Canada, 1998, 468.

Megally, Sami, and Amin Ghali. "Seismic Behavior of Edge Column-Slab Connections with Stud Shear Reinforcement." *ACI Structural Journal* 97, no. 6 (Jan.-Feb. 2000): 53-60.

Morrison, Denby G, and Mete A. Sozen. "Response of Reinforced Concrete Plate-Column Connections to Dynamic and Static Horizontal Loads." PFR-78-16318, University of Illinois at Urbana-Champaign, 1981, 272.

Pan, Austin, and Jack P. Moehle. "Lateral Displacement Ductility of Reinforced Concrete Flat Plates." *ACI Structural Journal* 86, no. 3 (May-June 1989): 250-258.

Robertson, Ian N., and Gaur Johnson. "Cyclic Lateral Loading of Nonductile Slab-Column Connections." *ACI Structural Journal* 103, no. 37 (May-June 2006): 356-364.

Robertson, Ian N., Kawai Tadashi, James Lee, and Brian Enomoto. "Cyclic Testing of Slab-Column Connections with Shear Reinforcement." *ACI Structural Journal* 99, no. 62 (Sept.-Oct. 2002): 605-613.

Robertson, Ian Nicol, and Ahmad J. Duranni. "Seismic Response of Connections in Indeterminate Flat-Slab Subassemblies." Thesis, Department of Civil Engineering, Rice University, 1990, 284.

Scribner, C.F., and J.K. Wight. "Strength Decay in R/C Beams under Load Reversals." *ASCE Journal of the Structural Division*, 1980: 861-876.

Tan, Y., and S. Teng. "Interiar Slab-Rectangular Column Connections Under Biaxial Lateral Loadings." *ACI Special Publication* 232, no. 09 (October 2005): 147-174.

Wey, Eric H., and Ahmad J. Durrani. "Seismic Response of Interior Slab-Column Connections with Shear Capitals." *ACI Structural Journal* 89, no. 65 (Nov.-Dec. 1992): 682-691.

Wight, James K., and Mete A Sozen. "Strength Decay of RC Columns under Shear Reversals." *Journal of the Structural Division*, 1975: 1053-1065.

Zee, H. L., and Jack P Moehle. "Behavior of Interior and Exterior Flat Plate Connections Subjected to Inelastic Load Reversals." Report No. UCB/EERC-84/07, Earthquake Engineering Research Center, University of California-Berkley, Berkley, California, 1984, 130.

Table 2-1: Slab and Connection Details for Each Specimen

Specimen	Dimensions	Reinforcement Ratio in Effective Width	Effective Depth (d)	Number of Orthogonal Rails per Column Face	Stud Spacing on Orthogonal Rails	Radial Rails?	Stud Spacing on Radial Rails
B1	17 ft x 17 ft x 6 in.	0.006	4.75 in.	3	0.50d (2-3/8")	N	N/A
B2	17 ft x 17 ft x 6 in.	0.006	4.75 in	3	0.75d (3-1/2")	N	N/A
B3	17 ft x 17 ft x 6 in.	0.006	4.75 in.	2	0.50d (2-3/8")	Y	0.50d (2-3/8")
B4	17 ft x 17 ft x 6 in.	0.006	4.75 in.	4	0.50d (2-3/8")	Y	0.70d (3-3/8")

Table 2-2: Strain Gauge Locations

Bottom Mat Reinforcement					
X-Direction			Y-Direction		
Gauge	t_y [in]	l_x [in]	Gauge	t_x [in]	l_y [in]
BS1	-4	19-7/8	BE1	-4	19-7/8
BS2	-4	10-3/8	BE2	-4	10-3/8
BS3	-4	-10-3/8	BE3	-4	-10-3/8
BS4	-4	-19-7/8	BE4	-4	-19-7/8
BS5	-16	10-3/8	BE5	-16	19-7/8
BS6	-16	-10-3/8	BE6	-16	10-3/8
BS7	-16	-19-7/8	BE7	-16	-10-3/8
BS8	-40	10-3/8	BE8	-40	10-3/8
BS9	-40	-10-3/8	BE9	-40	-10-3/8
BS10	-64	10-3/8	BE10	-64	10-3/8
BS11	-64	-10-3/8	BE11	-64	-10-3/8

Top Mat Reinforcement					
X-Direction			Y-Direction		
Gauge	t_y [in]	l_x [in]	Gauge	t_x [in]	l_y [in]
TS1	-3	19-7/8	TE1	-3	19-7/8
TS2	-3	10-3/8	TE2	-3	10-3/8
TS3	-3	-10-3/8	TE3	-3	-10-3/8
TS4	-3	-19-7/8	TE4	-3	-19-7/8
TS5	-15	10-3/8	TE5	-15	19-7/8
TS6	-15	0	TE6	-15	10-3/8
TS7	-15	-10-3/8	TE7	-15	0
TS8	-15	-19-7/8	TE8	-15	-10-3/8
TS9	-27	-10-3/8	TE9	-27	19-7/8
TS10	-27	-19-7/8	TE10	-27	10-3/8
TS11	-39	-10-3/8	TE11	-39	10-3/8
TS12	-57	-10-3/8	TE12	-57	10-3/8
TS13	-81	-10-3/8	TE13	-81	10-3/8

Table 2-3: Average Concrete Cylinder Strengths [psi]

Specimen	Base Block[1]	Bottom Column[1]	Slab[2]	Top Column/Block[1]
B1	6700	6800	5800	7300
	7500	5600	6100	7000
	7300	6600	5800	6900
Average	7200	6300	5900	7100
B2	6800	7200	5100	4800
	5600	6500	4700	4800
	6600	6600	5000	4800
Average	6300	6800	4900	4800
B3	7200	7700	5500	7200
	7900	7500	5600	6600
	7500	8500	5900	7200
Average	7500	7900	5700	7000
B4	7500	7200	6500	6900
	7000	7500	5800	7300
	7500	6900	5900	7000
Average	7300	7200	6100	7100

1) Tested after test had been completed (~90 days from casting)
2) Tested on the day prior to specimen testing

Table 2-4: Strength of Steel Reinforcement [ksi]

Specimen	Bar Size							
	#3		#4		#5		#6	
	Yield	Ultimate	Yield	Ultimate	Yield	Ultimate	Yield	Ultimate
B1	NA	NA	67.6	110.4	NA	NA	65.9	94.1
	NA	NA	68.1	110.3	NA	NA	59.7	99.1
	NA	NA	67.1	110.1	NA	NA	63.6	95.0
Average	NA	NA	67.6	110.3	NA	NA	63.1	96.1
B2	NA	NA	70.1	111.6	NA	NA	65.9	94.1
	NA	NA	69.8	112	NA	NA	59.7	99.1
	NA	NA	70.0	111.8	NA	NA	63.3	95.0
Average	NA	NA	70.0	111.8	NA	NA	63.1	96.1
B3	73.3	110.9	64.7	100.0	67.6	111.9	66.9	104.6
	71.4	109.7	65.0	100.3	66.3	110.3	66.0	104.9
	72.1	110.3	64.5	100.0	67	111.5	65.9	104.7
Average	72.3	110.3	64.7	100.1	67.0	111.2	66.3	104.7
B4	67.9	101.6	66.8	108.2	66.1	108.9	65.1*	101.8*
							67.9*	103.7*
	70.1	104.8	66.7	108.2	65.0	108.7	65.7*	101.3*
							65.8†	101.9†
	70.3	106.3	68.6	111.0	66.2	109.2	66.8†	106.3†
							67.2†	106.4†
Average	69.4	104.2	67.4	109.1	66.2	108.9	66.2*	102.3*
							66.6†	104.9†

*Column vertical reinforcing bars below the splice (first 4 ft of column)
†Column vertical reinforcing bars above the splice

Table 2-5: Applied Gravity Shear to Connection

Specimen	Concrete Compressive Strength [psi]	Required Shear [kips]	Slab Weight[1] [kips]	Weight of Steel Tubes, Threaded Rods and Instrumentation[2] [kips]	Total Dead Weight [kips]	Target Applied Force [kips]
B1	5900	60.7	21	4	25	35.7
B2	4900	54.8	21	4	25	29.8
B3	5700	59.4	21	4	25	34.4
B4	6100	61.5	21	4	25	36.5

1) This value includes the following: 204" x 204" x 6" concrete slab, minus concrete within the critical perimeter (20-3/4" x 20-3/4" x 6"). The assumed density of concrete was 150 lb/ft^3

2) This value included four 6" x 12" x 3/16" steel tubes (two of 160" and two of 192" in length respectively); and four 6" x 12" x 1/4" steel tubes (two of 160" and two of 192" in length respectively). The assumed density of steel was 480 lb/ft^3. Assumed weight of threaded rods and instrumentation was 500 lbs.

Table 2-6: Lateral Story Drift at Each Cycle

Cycle	Target Unidirectional Drift[1] [%]	Maximum Resultant (Biaxial) Drift[1] [%]
1	0.25	0.35
2	0.45	0.64
3	0.70	0.99
4	0.90	1.27
5	1.15	1.63
6	1.40	1.98
7	1.60	2.26
8	1.85	2.62
9	2.30	3.25
10	2.75	3.89
11	3.70	5.23

1) Refers to the total specimen drift (1.5 stories)

Table 3-1: Specimen B1 - Peak Resultant Lateral Forces (in kips) Achieved throughout Test

Drift Cycle [%]	Point on Cloverleaf (Figure 2-28)											
	1	2	3	4	5	6	7	8	9	10	11	12
0.25	6.4	8.0	5.4	7.5	7.9	5.2	7.4	9.1	4.6	6.2	8.2	6.3
0.45	10.1	12.2	8.3	10.5	11.4	7.4	11.5	12.6	6.6	9.6	12.3	8.6
0.70	**12.2**	15.0	9.9	12.1	13.7	8.7	**13.6**	15.5	8.0	11.7	15.0	9.8
0.90	**13.0**	**16.6**	**10.7**	**13.0**	**15.1**	**9.9**	**14.0**	**16.8**	**8.9**	**12.7**	**17.0**	**11.1**
1.15	**13.5***	**17.4**	**11.3***	**13.5**	**15.7***	**10.3***	**14.9***	**17.8***	**9.2***	**13.3***	**17.4***	**11.5***
1.40	**13.2**	**17.5***	**11.0**	**13.7***	**15.4**	**10.0**	**14.7**	**17.8***	**8.9**	**13.1**	**17.3**	**11.2**
1.60	**13.1**	**16.8**	**10.7**	**13.6**	**14.5**	**9.5**	**14.4**	**17.6**	**8.5**	**12.9**	**17.3**	**10.5**
1.85	**12.8**	**16.0**	**10.5**	**12.9**	13.8	8.9	**14.1**	**16.4**	7.7	**12.9**	**16.4**	9.7
2.30	**12.5**	12.5	8.5	11.2	8.4	6.2	-	-	-	-	-	-

* Peak value for point for entire test
Bolded – At least 90% of peak force recorded at point

Table 3-2: Specimen B2 - Peak Resultant Lateral Forces (in kips) Achieved throughout Test

Drift Cycle [%]	Point on Cloverleaf (Figure 2-28)											
	1	**2**	**3**	**4**	**5**	**6**	**7**	**8**	**9**	**10**	**11**	**12**
0.25	6.7	7.3	4.8	7.8	8.4	4.6	6.7	8.7	5.2	6.0	7.7	5.4
0.45	10.4	11.0	7.6	11.1	12.1	7.0	9.8	12.0	7.1	9.1	11.2	7.5
0.70	**12.1**	13.7	8.7	**12.5**	14.2	8.6	11.6	14.4	8.3	10.5	13.4	8.9
0.90	**13.2**	**15.5**	**9.5**	**13.3**	**15.8**	**9.6**	**12.5**	**15.7**	**9.4**	**11.1**	**14.9**	**9.7**
1.15	**13.4**	**16.2**	**9.9**	**13.6**	**16.8**	**10.0**	**13.4**	**16.9**	**9.8**	**11.6**	**15.8**	**10.0**
1.40	**13.4**	**16.8***	**10.2**	**14.0***	**17.0***	**10.1***	**13.3**	**17.1***	**10.0***	**12.1**	**16.2***	**10.0**
1.60	**13.5***	**16.0**	**10.2***	**14.0***	16.5	9.5	**13.6***	16.7	9.9	**12.1***	16.0	**10.1***
1.85	**13.0**	**15.0**	**9.8**	**14.0***	15.3	8.0	**13.1**	15.2	8.1	**11.5**	13.4	8.2
2.30	10.6	7.1	6.5	-	-	-	-	-	-	-	-	-

* Peak value for point for entire test
Bolded – At least 90% of peak force recorded at point

Table 3-3: Specimen B3 - Peak Resultant Lateral Forces (in kips) Achieved throughout Test

Drift Cycle [%]	Point on Cloverleaf (Figure 2-28)											
	1	2	3	4	5	6	7	8	9	10	11	12
0.25	9.8	10.4	5.7	7.7	10.3	7.0	6.8	9.5	6.6	7.6	8.1	5.3
0.45	12.6	14.3	8.1	11.2	13.9	9.4	10.2	12.5	7.8	10.6	11.7	7.4
0.70	**14.5**	16.8	**9.7**	12.7	16.0	10.9	11.8	14.7	9.1	12.2	14.2	8.6
0.90	**15.6**	**18.2**	**10.6**	**13.6**	**17.5**	**12.0**	**12.9**	**16.3**	**10.2**	**13.3**	**15.7**	**9.5**
1.15	**16.0**	**19.3**	**11.2***	**14.4**	**18.6**	**12.5***	**13.3**	**17.1**	**10.6***	**13.7**	**16.3**	**9.8***
1.40	**16.2***	**19.6***	**11.2***	**14.6***	**18.9***	**12.4**	**13.4***	**17.4***	**10.6***	**14.0**	**16.7***	**9.7**
1.60	**16.2***	**19.3**	**11.2***	**14.4**	**18.9***	**12.2**	**13.3**	**16.9**	**10.6***	**14.1***	**16.5**	**9.5**
1.85	**15.2**	**18.1**	**10.3**	**14.2**	**17.6**	11.0	**12.5**	**15.4**	**9.9**	**13.4**	13.8	8.0
2.30	**15.2**	14.7	7.7	12.0	11.0	7.7	7.9	8.6	6.9	9.5	8.1	4.8

* Peak value for point for entire test
Bolded – At least 90% of peak force recorded at point

Table 3-4: Specimen B4 - Peak Resultant Lateral Forces (in kips) Achieved throughout Test

Drift Cycle [%]	Point on Cloverleaf (Figure 2-28)											
	1	**2**	**3**	**4**	**5**	**6**	**7**	**8**	**9**	**10**	**11**	**12**
0.25	8.3	9.2	5.8	7.7	9.4	5.9	7.5	9.5	5.6	6.8	8.8	6.2
0.45	11.1	12.9	8.0	11.1	12.6	8.0	11.1	13.2	7.5	9.7	12.0	8.3
0.70	13.2	15.4	9.5	12.8	15.3	9.7	12.9	15.7	9.0	11.4	14.6	9.7
0.90	14.1	17.6	**10.5**	**14.4**	17.1	10.8	13.5	**17.3**	**10.3**	**12.6**	**16.3**	**10.6**
1.15	**15.1**	**18.8**	**11.2**	**15.1**	**18.4**	**11.7**	**14.6**	**18.6**	**11.2**	**13.6**	**17.6**	**11.4**
1.40	**15.6**	**19.9**	**11.6**	**15.5**	**19.3**	**12.3***	**15.1**	**19.3***	**11.4**	**13.9**	**18.2***	**11.8**
1.60	**16.0**	**20.1***	**11.7***	**15.8***	**19.4***	**12.2**	**15.2***	**19.3***	**11.5***	**14.0***	**18.1**	**11.3**
1.85	**15.5**	**18.8**	**11.1**	**15.4**	**18.4**	**11.0**	**14.8**	**18.2**	**10.5**	**13.5**	**16.5**	10.2
2.30	**16.1***	16.5	9.9	**15.6**	14.7	8.6	**13.6**	12.8	7.4	10.1	10.0	6.6
2.75	10.0	10.0	6.8	9.9	8.9	5.8	9.0	8.9	5.9	9.2	8.1	6.0

* Peak value for point for entire test
Bolded – At least 90% of peak force recorded at point

Table 3-5: Peak Lateral Forces Achieved throughout Tests

Point on cloverleaf pattern		B1	B2	B3	B4
1	Maximum Resultant Force [kip]	13.51	13.50	16.20	16.11
	Drift Level [%]	1.15	1.60	1.60	2.30
2	Maximum Resultant Force [kip]	17.46	16.81	19.56	20.13
	Drift Level [%]	1.40	1.40	1.40	1.60
3	Maximum Resultant Force [kip]	11.35	10.24	11.23	11.69
	Drift Level [%]	1.15	1.40	1.40	1.60
4	Maximum Resultant Force [kip]	13.71	14.02	14.61	15.81
	Drift Level [%]	1.40	1.85	1.40	1.60
5	Maximum Resultant Force [kip]	15.75	16.99	18.89	19.41
	Drift Level [%]	1.15	1.40	1.60	1.60
6	Maximum Resultant Force [kip]	10.34	10.08	12.46	12.28
	Drift Level [%]	1.15	1.40	1.40	1.60
7	Maximum Resultant Force [kip]	14.90	13.60	13.40	15.21
	Drift Level [%]	1.15	1.60	1.40	1.60
8	Maximum Resultant Force [kip]	17.77	17.10	17.36	19.35
	Drift Level [%]	1.40	1.40	1.40	1.60
9	Maximum Resultant Force [kip]	9.16	10.02	10.64	11.46
	Drift Level [%]	1.15	1.40	1.60	1.60
10	Maximum Resultant Force [kip]	13.30	12.12	14.06	14.01
	Drift Level [%]	1.15	1.60	1.60	1.60
11	Maximum Resultant Force [kip]	17.40	16.24	16.66	18.18
	Drift Level [%]	1.60	1.40	1.40	1.60
12	Maximum Resultant Force [kip]	11.46	10.08	9.84	11.78
	Drift Level [%]	1.15	1.60	1.15	1.40

Table 3-6: Shear Stress at Critical Section for Specimen B1

Drift Level		Point	Peak Lateral Force [kip]		Gravity Shear		Unbalanced Moment [kip-in]		Normalized Shear Stress [psi]		
%			[kip]		Force	Ratio	[kip-in]		$\dfrac{V}{A_c\sqrt{f_c'}}+\dfrac{\gamma_v M_{uby}c_x}{J_c\sqrt{f_c'}}$	$\dfrac{V}{A_c\sqrt{f_c'}}+\dfrac{\gamma_v M_{ubx}c_y}{J_c\sqrt{f_c'}}$	$\dfrac{V}{A_c\sqrt{f_c'}}+\dfrac{\gamma_v M_{ubx}c_y}{J_c\sqrt{f_c'}}+\dfrac{\gamma_v M_{uby}c_x}{J_c\sqrt{f_c'}}$
δ_T	δ_2		x	y	[kip]	[%]	M_{ubY}	M_{ubX}			
	0.30	1	-0.1	6.4	58.7	48.4	-11	504	1.96	2.89	2.91
	0.45	2	-6.1	5.3	57.5	47.4	486	330	2.81	2.52	3.43
	0.30	3	-4.6	-2.9	57.2	47.1	351	-271	2.55	2.39	3.06
	0.30	4	7.4	-1.5	56.1	46.3	-604	-113	2.98	2.06	3.20
	0.45	5	5.1	6.0	55.5	45.7	-458	447	2.69	2.67	3.54
0.25	0.30	6	-1.0	5.1	55.8	46	121	324	2.06	2.44	2.67
	0.30	7	0.0	-7.4	55.3	45.5	0	-657	1.82	3.06	3.06
	0.45	8	6.6	-6.3	54.4	44.9	-541	-539	2.81	2.81	3.83
	0.30	9	4.5	1.2	54.7	45.1	-387	61	2.54	1.92	2.65
	0.30	10	-6.2	0.5	55.2	45.5	508	-60	2.78	1.93	2.89
	0.45	11	-4.8	-6.6	54.8	45.1	398	-578	2.56	2.89	3.64
	0.30	12	1.8	-6.0	54.6	45	-161	-459	2.10	2.66	2.96
	0.60	1	-0.1	10.1	58.9	48.6	-26	841	1.99	3.52	3.57
	0.90	2	-9.5	7.6	58.6	48.3	773	580	3.39	3.03	4.48
	0.65	3	-7.2	-4.2	58.6	48.3	544	-350	2.96	2.60	3.62
	0.65	4	10.4	-1.6	57.4	47.3	-901	-126	3.59	2.13	3.83
	0.90	5	7.2	8.9	56.6	46.6	-658	738	3.11	3.26	4.50
0.45	0.65	6	-2.3	7.0	57.3	47.2	186	478	2.23	2.78	3.13
	0.65	7	-0.1	-11.5	56.5	46.6	11.1	-1020	1.88	3.78	3.80
	0.90	8	9.0	-8.8	55.2	45.5	-774	-754	3.28	3.24	4.70
	0.65	9	6.5	1.4	55.8	46	-511	101	2.81	2.04	3.00
	0.65	10	-9.6	0.2	56.3	46.4	782	-84	3.33	2.02	3.49
	0.90	11	-7.3	-10.0	55.5	45.8	611	-887	2.98	3.50	4.65

	0.65	12	2.4	-8.3	55.6	45.9	-202	-636	2.21	3.03	3.41
	0.95	1	-0.4	12.2	59	48.7	-5	1060	1.96	3.94	3.95
	1.35	2	-11.7	9.5	58.5	48.2	981	742	3.77	3.32	5.17
	0.95	3	-9.0	-4.1	58.7	48.4	690	-364	3.24	2.62	3.92
	0.95	4	12.0	-1.7	57.2	47.2	-1040	-105	3.84	2.08	4.04
	1.30	5	8.4	10.8	56.8	46.8	-765	937	3.31	3.64	5.07
0.70	0.95	6	-3.0	8.1	57.8	47.6	236	618	2.35	3.07	3.52
	0.95	7	0.0	-13.6	57.2	47.2	18	-1190	1.92	4.12	4.16
	1.35	8	11.2	-10.7	56.2	46.3	-953	-900	3.64	3.54	5.33
	0.95	9	7.7	2.0	56.6	46.7	-612	142	3.02	2.14	3.29
	0.95	10	-11.7	-0.1	57.1	47.1	954	-86	3.68	2.05	3.84
	1.30	11	-9.0	-12.0	56.2	46.3	733	-1070	3.23	3.86	5.24
	0.95	12	2.4	-9.5	56	46.1	-229	-749	2.28	3.26	3.69
	1.25	1	-0.5	13.0	60	49.4	5	1150	1.98	4.14	4.15
	1.80	2	-13.0	10.3	59.6	49.1	1110	837	4.05	3.54	5.63
	1.25	3	-9.8	-4.3	59.4	49	751	-381	3.38	2.68	4.09
	1.25	4	12.9	-1.7	57.9	47.8	-1120	-93	4.02	2.08	4.19
	1.75	5	9.3	11.9	57.5	47.4	-835	1050	3.47	3.87	5.45
0.90	1.25	6	-3.1	9.5	58.3	48	254	707	2.40	3.25	3.73
	1.25	7	0.0	-14.0	57.9	47.7	6.75	-1250	1.92	4.26	4.28
	1.80	8	12.3	-11.5	56.9	46.9	-1060	-963	3.87	3.68	5.68
	1.25	9	8.6	2.3	57.1	47.1	-684	176	3.17	2.22	3.50
	1.25	10	-12.7	-0.1	57.6	47.5	1040	-82	3.86	2.05	4.01
	1.75	11	-10.0	-13.8	57	47	806	-1180	3.40	4.11	5.62
	1.25	12	3.0	-10.7	56.6	46.7	-274	-819	2.39	3.41	3.93
	1.55	1	-0.6	13.5	60.4	49.8	7	1170	2.00	4.19	4.20
	2.25	2	-13.7	10.8	59.5	49	1160	866	**4.15**	3.59	5.78
1.15	1.55	3	-10.5	-4.3	59.6	49.1	795	-386	3.46	2.69	4.19
	1.55	4	13.4	-1.6	58.3	48.1	-1160	-82	4.11	2.08	4.26
	2.15	5	9.6	12.5	57.7	47.5	-857	1100	3.51	3.97	5.58
	1.55	6	-3.4	9.8	58.3	48.1	291	718	2.47	3.28	3.82

	1.55	7	0.1	**-14.9**	58.4	48.1	8	-1270	1.94	**4.31**	4.33
	2.25	8	13.1	-12.0	57	47	-1100	-980	3.95	3.73	**5.80**
	1.55	9	8.8	2.5	56.9	46.9	-690	196	3.17	2.24	3.54
	1.55	10	-13.3	-0.1	57.5	47.4	1060	-64	3.89	2.02	4.01
	2.15	11	-10.6	-13.8	57.3	47.2	808	-1200	3.41	4.14	5.66
	1.55	12	2.8	-11.1	56.9	46.9	-279	-825	2.40	3.42	3.95
	1.90	1	-0.6	13.2	59.8	49.3	10.1	1070	1.99	3.99	4.01
	2.65	2	**-13.8**	10.7	57.7	47.5	1120	795	4.01	3.39	5.50
	1.85	3	-10.1	-4.2	57.5	47.4	703	-394	3.22	2.64	3.96
	1.85	4	13.6	-1.7	55.8	46	-1090	-106	3.88	2.03	4.08
	2.55	5	9.3	12.2	54.3	44.8	-786	1030	3.27	3.73	5.21
1.40	1.85	6	-3.6	9.3	55.2	45.5	272	642	2.33	3.03	3.54
	1.85	7	0.1	-14.7	55.5	45.7	6.38	-1180	1.84	4.05	4.07
	2.65	8	13.0	-12.1	53.1	43.8	-1060	-926	3.75	3.50	5.49
	1.85	9	8.6	2.4	52.9	43.6	-641	196	2.95	2.11	3.32
	1.85	10	-13.1	-0.2	53.9	44.5	981	-60	3.63	1.89	3.74
	2.60	11	-10.5	-13.8	52.9	43.6	757	-1140	3.17	3.89	5.31
	1.85	12	3.1	-10.8	52.6	43.4	-272	-753	2.24	3.15	3.66
	2.15	1	-0.7	13.1	60.7	50	10	1020	2.02	3.92	3.94
	3.05	2	-13.2	10.4	59.8	49.3	1060	765	3.97	3.42	5.41
	2.15	3	-9.8	-4.5	59.7	49.2	659	-355	3.20	2.63	3.87
	2.15	4	13.5	-1.8	57.6	47.5	-1050	-91	3.87	2.07	4.05
	2.90	5	8.7	11.6	56.9	46.9	-764	1010	3.31	3.77	5.21
	2.10	6	-4.1	8.6	58.2	48	281	618	2.45	3.09	3.62
1.60	2.20	7	0.0	-14.4	57.9	47.7	4	-1130	1.92	4.04	4.04
	3.10	8	12.9	-11.9	55.6	45.8	-1020	-876	3.75	3.48	5.40
	2.15	9	8.2	2.2	55.7	45.9	-612	226	2.98	2.26	3.41
	2.15	10	-12.9	-0.2	56.7	46.7	953	-42	3.67	1.95	3.74
	3.05	11	-10.5	-13.8	55.6	45.8	728	-1070	3.20	3.85	5.22
	2.15	12	3.0	-10.1	55.4	45.7	-256	-681	2.31	3.11	3.60
1.85	2.45	1	-0.9	12.8	61.1	50.3	14	990	2.04	3.88	3.90

94

	3.45	2	-12.8	9.6	60.3	49.7	1000	705	3.87	3.32	5.20
	2.40	3	-9.2	-5.1	59.7	49.2	623	-351	3.14	2.62	3.80
	2.45	4	12.8	-1.9	56.8	46.8	-993	-48	3.74	1.96	3.83
	3.25	5	8.1	11.2	56.5	46.5	-716	955	3.21	3.66	5.00
	2.35	6	-4.4	7.8	58.1	47.9	293	567	2.46	2.98	3.53
	2.50	7	-0.1	-14.1	57.6	47.5	27	-1010	1.95	3.80	3.85
	3.50	8	12.3	-10.9	54.9	45.3	-944	-743	3.58	3.21	4.98
	2.35	9	7.3	2.4	54.4	44.9	-560	255	2.85	2.27	3.33
	2.40	10	-12.9	-0.1	55.8	46	907	-9	3.55	1.86	3.57
	3.40	11	-9.9	-13.1	54.6	45	656	-907	3.03	3.50	4.74
	2.45	12	3.1	-9.1	54	44.5	-243	-546	2.24	2.81	3.27
2.30	3.00	1	-0.9	12.5	61	50.2	6	919	2.03	3.74	3.75
	4.15	2	-10.4	6.9	56.1	46.2	661	392	3.09	2.58	3.83
	2.90	3	-6.0	-6.0	51.3	42.3	227	-294	2.12	2.24	2.67
	3.00	4*	11.0	-1.9	44.3	36.5	-724	0	2.82	1.46	2.82
	4.00	5*	4.6	7.0	55	45.3	-222	362	2.22	2.49	2.91
	2.85	6*	-4.5	4.3	51.2	42.2	160	107	1.99	1.89	2.19

* Reloaded strands at point on cloverleaf

Table 3-7: Shear Stress at Critical Section for Specimen B2

Drift Level	Point	Peak Lateral Force		Gravity Shear		Unbalanced Moment		Normalized Shear Stress [psi]		
%		[kip]		Force	Ratio	[kip-in]		$\dfrac{V}{A_c\sqrt{f_c'}}+\dfrac{\gamma_v M_{uby}c_x}{J_c\sqrt{f_c'}}$	$\dfrac{V}{A_c\sqrt{f_c'}}+\dfrac{\gamma_v M_{ubx}c_y}{J_c\sqrt{f_c'}}$	$\dfrac{V}{A_c\sqrt{f_c'}}+\dfrac{\gamma_v M_{ubx}c_y}{J_c\sqrt{f_c'}}+\dfrac{\gamma_v M_{uby}c_x}{J_c\sqrt{f_c'}}$
δ		X	Y	[kip]	[%]	M_{ubY}	M_{ubX}			
0.25	1	0.5	6.7	52.5	48	-18	486	1.95	2.93	2.97
	2	-5.6	4.8	51.1	46.7	482	323	2.88	2.55	3.55
	3	-4.0	-2.6	50.4	46.1	349	-252	2.57	2.37	3.10
	4	7.7	-1.2	49.8	45.5	-584	-81	3.03	1.98	3.20
	5	5.7	6.2	48.9	44.7	-446	462	2.72	2.75	3.68
	6	-1.4	4.4	49.3	45	132	304	2.08	2.43	2.71
	7	0.1	-6.7	48.9	44.7	6.57	-606	1.80	3.05	3.06
	8	6.6	-5.6	48	43.9	-519	-474	2.84	2.75	3.83
	9	5.0	1.4	48.2	44	-371	68	2.53	1.90	2.67
	10	-6.0	0.1	48.4	44.2	508	-48	2.83	1.87	2.93
	11	-4.5	-6.3	47.8	43.6	404	-559	2.59	2.91	3.75
	12	2.2	-4.9	47.6	43.5	-140	-398	2.03	2.57	2.86
0.45	1	0.5	10.4	53.6	49	-8	848	1.98	3.73	3.74
	2	-8.3	7.1	52.3	47.7	791	549	3.57	3.06	4.71
	3	-6.7	-3.6	52.4	47.8	568	-355	3.10	2.66	3.84
	4	11.0	-1.3	51.9	47.4	-889	-79	3.76	2.06	3.92
	5	7.9	9.1	51.2	46.8	-643	753	3.21	3.44	4.78
	6	-1.7	6.8	51.7	47.2	200	469	2.30	2.86	3.28
	7	-0.1	-9.8	51	46.5	28	-924	1.92	3.78	3.84
	8	9.3	-7.7	50.2	45.8	-763	-674	3.42	3.23	4.83
	9	6.9	1.9	50.7	46.3	-518	135	2.94	2.14	3.22

	10	-9.1	0.0	50.3	46	800	-90	3.51	2.03	3.70
	11	-7.0	-8.8	49.9	45.6	620	-828	3.12	3.56	4.85
	12	2.8	-6.9	50.4	46	-177	-557	2.21	3.01	3.37
	1	0.4	12.1	53.4	48.8	-3	1040	1.97	4.13	4.13
	2	-10.3	9.1	52.7	48.1	975	717	3.96	3.43	5.46
	3	-8.0	-3.6	52.7	48.1	694	-357	3.38	2.67	4.12
	4	12.5	-0.9	52.6	48	-1020	-46.5	4.04	2.01	4.14
	5	9.1	10.9	51.6	47.1	-747	949	3.44	3.87	5.42
0.70	6	-2.1	8.3	52	47.5	234	620	2.39	3.19	3.68
	7	-0.1	-11.6	51.5	47.1	37	-1060	1.96	4.10	4.17
	8	11.2	-9.1	50.9	46.5	-935	-782	3.81	3.49	5.44
	9	8.1	2.0	51.2	46.8	-626	177	3.18	2.24	3.55
	10	-10.5	-0.3	50.9	46.5	935	-76	3.81	2.02	3.97
	11	-8.2	-10.6	50.5	46.1	710	-966	3.32	3.86	5.34
	12	3.1	-8.3	50.6	46.2	-215	-666	2.29	3.23	3.68
	1	0.4	13.2	54	49.3	6	1130	1.99	4.33	4.34
	2	-11.7	10.2	53.2	48.6	1090	809	4.22	3.63	5.90
	3	-8.7	-3.8	53.1	48.5	736	-355	3.48	2.68	4.22
	4	13.3	-0.8	53	48.4	-1110	-35	4.24	2.00	4.32
	5	10.1	12.2	52.2	47.7	-833	1070	3.64	4.13	5.87
0.90	6	-2.3	9.3	52.1	47.6	246	702	2.41	3.37	3.88
	7	0.0	-12.5	52.5	48	8	-1120	1.93	4.25	4.27
	8	12.3	-9.8	51.8	47.3	-1030	-830	4.03	3.62	5.77
	9	9.1	2.5	51.7	47.2	-685	211	3.32	2.33	3.76
	10	-11.1	-0.5	51.5	47	999	-85	3.97	2.06	4.15
	11	-9.1	-11.8	51.2	46.8	759	-1070	3.46	4.10	5.69
	12	3.4	-9.1	51.2	46.7	-246	-730	2.39	3.39	3.91
1.15	1	0.4	13.4	54.3	49.6	0	1150	1.99	**4.39**	4.39

	2	-12.2	10.7	53.5	48.9	1150	841	4.36	3.71	6.11
	3	-9.2	-3.8	53.4	48.8	784	-374	3.58	2.72	4.36
	4	13.6	-0.9	53.6	48.9	-1140	-28	4.34	2.02	4.40
	5	10.6	13.0	52.6	48.1	-866	1130	3.74	4.29	6.09
	6	-2.6	9.6	52.3	47.8	273	717	2.48	3.41	3.98
	7	0.0	-13.4	53.1	48.5	17	-1160	1.98	4.36	4.40
	8	13.2	-10.5	52.3	47.7	-1080	-879	4.17	3.75	6.00
	9	9.5	2.6	51.9	47.4	-715	233	3.39	2.39	3.88
	10	-11.6	-0.6	51.8	47.3	1020	-90	4.01	2.07	4.20
	11	-9.5	-12.6	51.6	47.1	775	-1120	3.50	4.22	5.84
	12	3.5	-9.3	51.4	47	-256	-758	2.41	3.45	3.99
	1	0.4	13.4	54.9	50.1	11	1140	2.02	4.38	4.40
	2	-12.8	10.9	53.8	49.2	1170	836	**4.41**	3.72	**6.16**
	3	-9.2	-4.5	53.8	49.1	765	-391	3.55	2.77	4.37
	4	14.0	-0.8	54	49.3	-1140	-33	4.35	2.04	4.42
	5	10.7	13.2	53.3	48.7	-862	1130	3.74	4.30	6.10
1.40	6	-2.8	9.7	52.7	48.1	282	712	2.52	3.41	4.00
	7	0.1	-13.3	53.6	48.9	-1.88	-1130	1.96	4.32	4.32
	8	13.5	-10.5	52.6	48	-1090	-853	4.19	3.69	5.97
	9	9.5	3.3	52.1	47.6	-711	250	3.38	2.42	3.91
	10	-12.1	-0.7	52	47.5	1030	-75	4.05	2.06	4.20
	11	-9.9	-12.9	51.8	47.3	769	-1100	3.49	4.18	5.78
	12	3.7	-9.3	51.6	47.2	-268	-711	2.45	3.37	3.93
	1	0.3	13.5	55.2	50.4	9	1120	2.03	4.35	4.37
	2	-12.2	10.4	53.9	49.2	1150	819	4.37	3.68	6.08
1.60	3	-8.8	-5.1	53.7	49	730	-373	3.48	2.74	4.26
	4	**14.0**	-0.7	54.2	49.5	-1090	-22.3	4.25	2.02	4.29
	5	10.6	12.7	53.5	48.9	-840	1110	3.71	4.27	6.03

	6	-2.7	9.1	52.7	48.1	282	687	2.52	3.36	3.95
	7	0.1	**-13.6**	53.6	49	-3.45	-1080	1.97	4.21	4.22
	8	13.3	-10.1	52.7	48.1	-1070	-800	4.16	3.60	5.83
	9	9.3	3.5	52	47.5	-691	278	3.34	2.48	3.92
	10	-12.1	-0.8	52	47.5	1000	-51	3.99	2.01	4.09
	11	-9.7	-12.8	51.8	47.3	751	-1070	3.45	4.12	5.68
	12	4.1	-9.2	51.5	47.1	-269	-677	2.45	3.30	3.86
	1	0.7	13.0	55.5	50.7	3	1070	2.04	4.26	4.27
	2	-11.7	9.3	54.3	49.6	1110	776	4.30	3.61	5.92
	3	-8.2	-5.4	53.7	49	702	-364	3.42	2.72	4.18
	4	13.9	-1.3	54.2	49.5	-1070	-8	4.22	2.00	4.23
	5	10.0	11.6	53.1	48.5	-746	967	3.50	3.96	5.52
1.85	6	-3.1	7.4	51.1	46.7	358	517	2.62	2.95	3.70
	7	0.0	-13.1	52.8	48.2	26.7	-1030	1.99	4.08	4.13
	8	11.8	-9.6	50.1	45.8	-821	-715	3.54	3.32	5.03
	9	7.4	3.4	48.3	44.1	-440	198	2.69	2.18	3.10
	10	-11.5	-0.7	50.8	46.4	937	-43	3.81	1.95	3.90
	11	-8.2	-10.6	48.2	44	546	-703	2.90	3.22	4.36
	12	4.1	-7.1	46	42.1	-233	-400	2.17	2.52	3.01
	1	0.4	10.6	53.4	48.7	128	640	2.21	3.28	3.55
2.30	2	-6.0	3.7	36	32.9	215	4	1.76	1.32	1.77
	3	-3.9	-5.2	41.4	37.8	11.2	-260	1.54	2.05	2.08

Table 3-8: Shear Stress at Critical Section for Specimen B3

Drift Level	Point	Peak Lateral Force		Gravity Shear		Unbalanced Moment		Normalized Shear Stress [psi]		
%		[kip]		Force	Ratio	[kip-in]		$\dfrac{V}{A_c\sqrt{f_c'}}+\dfrac{\gamma_v M_{uby}c_x}{J_c\sqrt{f_c'}}$	$\dfrac{V}{A_c\sqrt{f_c'}}+\dfrac{\gamma_v M_{ubx}c_y}{J_c\sqrt{f_c'}}$	$\dfrac{V}{A_c\sqrt{f_c'}}+\dfrac{\gamma_v M_{ubx}c_y}{J_c\sqrt{f_c'}}+\dfrac{\gamma_v M_{uby}c_x}{J_c\sqrt{f_c'}}$
δ		X	Y	[kip]	[%]	M_{ubY}	M_{ubX}			
0.25	1	0.1	9.8	57.3	48.2	-33	538	1.95	2.90	3.03
	2	-7.9	6.8	56.2	47.3	492	382	2.78	2.57	3.57
	3	-5.0	-2.8	56.3	47.4	320	-260	2.46	2.35	3.01
	4	7.7	-0.2	55.5	46.7	-615	-101	2.99	2.02	3.24
	5	5.3	8.8	54.8	46.1	-478	493	2.71	2.73	3.71
	6	-2.2	6.7	55.1	46.4	96.3	351	2.00	2.48	2.71
	7	0.2	-6.8	54.9	46.2	-45	-655	1.89	3.04	3.19
	8	8.1	-4.9	54.2	45.6	-583	-518	2.88	2.76	3.94
	9	5.2	4.1	54.6	45.9	-407	109	2.57	2.01	2.83
	10	-7.4	1.7	54.7	46	499	-18	2.74	1.84	2.83
	11	-4.8	-6.6	54.3	45.7	355	-556	2.46	2.84	3.58
	12	2.7	-4.6	54.2	45.6	-172	-434	2.11	2.60	2.99
0.45	1	0.0	12.6	57.6	48.5	-12	943	1.92	3.67	3.77
	2	-10.5	9.8	56.6	47.6	796	658	3.36	3.10	4.70
	3	-7.8	-2.3	56.9	47.9	527	-305	2.87	2.45	3.51
	4	11.2	-0.1	56.5	47.6	-930	-77	3.61	2.01	3.84
	5	7.9	11.4	54.8	46.1	-679	817	3.08	3.34	4.72
	6	-2.5	9.1	55.6	46.8	188	539	2.19	2.85	3.27
	7	0.0	-10.2	55.6	46.8	-21	-980	1.87	3.68	3.79
	8	9.8	-7.7	54.8	46.1	-801	-735	3.31	3.19	4.80
	9	7.1	3.2	54.9	46.2	-536	145	2.82	2.08	3.16

	10	-10.5	1.4	54.6	45.9	775	-61	3.26	1.91	3.44
	11	-7.6	-8.9	54.6	46	586	-867	2.90	3.43	4.63
	12	2.7	-6.9	54.7	46	-207	-616	2.19	2.96	3.42
	1	-0.1	14.5	57.7	48.6	-10	1110	1.92	3.99	4.09
	2	-12.3	11.4	57.6	48.5	994	789	3.77	3.38	5.36
	3	-9.4	-2.3	58.1	48.9	682	-333	3.20	2.54	3.91
	4	12.7	0.3	57	48	-1050	-54	3.86	1.98	4.04
	5	9.3	13.0	55.9	47	-771	985	3.29	3.70	5.25
0.70	6	-2.7	10.6	56.5	47.5	225	668	2.29	3.12	3.62
	7	-0.1	-11.8	57	48	-7	-1120	1.89	3.99	4.08
	8	11.6	-9.1	55.9	47.1	-959	-863	3.65	3.47	5.38
	9	8.4	3.7	55.6	46.8	-635	173	3.03	2.16	3.42
	10	-12.1	1.3	55.7	46.9	926	-64	3.58	1.96	3.78
	11	-9.2	-10.8	55.8	47	720	-1030	3.19	3.78	5.24
	12	2.7	-8.2	55.7	46.9	-241	-709	2.29	3.17	3.70
	1	-0.1	15.6	58.7	49.4	-9	1200	1.95	4.19	4.30
	2	-13.6	12.1	58	48.8	1110	863	4.00	3.54	5.74
	3	-10.3	-2.3	58.2	49	779	-364	3.38	2.60	4.15
	4	13.6	0.4	57.6	48.4	-1120	-53	4.01	2.00	4.19
	5	10.2	14.2	56.6	47.6	-844	1110	3.45	3.96	5.66
0.90	6	-3.2	11.6	56.9	47.9	244	750	2.34	3.29	3.82
	7	0.0	-12.9	57.8	48.7	0.653	-1200	1.91	4.16	4.25
	8	12.9	-9.9	56.5	47.5	-1070	-923	3.88	3.60	5.73
	9	9.4	4.1	55.9	47	-708	210	3.18	2.24	3.64
	10	-13.2	1.3	56.2	47.3	1030	-73	3.79	1.99	4.01
	11	-10.2	-12.0	56.3	47.4	789	-1130	3.34	3.98	5.58
	12	3.0	-9.0	55.9	47	-252	-780	2.32	3.31	3.86
1.15	1	-0.2	16.0	59.4	50	-6	1230	1.97	**4.27**	4.37

	2	-14.4	12.8	58.8	49.5	1150	897	**4.10**	3.63	**5.91**
	3	-10.9	-2.6	58.7	49.4	796	-372	3.43	2.64	4.22
	4	14.4	0.5	58.2	49	-1150	-45	4.08	2.00	4.25
	5	10.8	15.1	56.9	47.9	-863	1140	3.50	4.02	5.76
	6	-3.4	12.0	57.1	48.1	270	756	2.39	3.31	3.89
	7	0.0	-13.3	58.2	48.9	-17	-1210	1.95	4.20	4.32
	8	13.6	-10.4	56.9	47.9	-1100	-928	3.95	3.62	5.81
	9	9.7	4.2	56.1	47.2	-711	228	3.19	2.28	3.69
	10	-13.6	1.3	56.6	47.7	1030	-59	3.80	1.98	4.00
	11	-10.6	-12.4	56.2	47.3	774	-1130	3.31	3.98	5.55
	12	3.4	-9.3	55.9	47.1	-281	-753	2.37	3.26	3.87
	1	-0.2	16.2	59.4	50	-5	1160	1.97	4.14	4.24
	2	**-14.7**	12.9	58.5	49.3	1130	847	4.06	3.52	5.77
	3	-10.9	-2.7	58.5	49.3	743	-365	3.33	2.62	4.10
	4	14.6	0.5	58.5	49.2	-1110	-51	4.02	2.03	4.20
	5	10.8	15.5	57.1	48.1	-827	1110	3.44	3.97	5.64
1.40	6	-3.2	12.0	57	47.9	250	718	2.35	3.23	3.78
	7	0.0	-13.4	58.3	49	-16.8	-1170	1.95	4.12	4.24
	8	13.9	-10.4	57.3	48.2	-1110	-894	3.98	3.57	5.78
	9	9.5	4.6	55.9	47.1	-688	243	3.14	2.30	3.67
	10	-13.9	1.4	56.4	47.4	995	-67	3.73	1.99	3.94
	11	-10.9	-12.6	56.5	47.6	761	-1110	3.29	3.95	5.50
	12	3.2	-9.1	56.2	47.3	-276	-718	2.37	3.20	3.80
	1	-0.2	**16.2**	59.6	50.2	-6	1120	1.98	4.07	4.17
	2	-14.5	12.8	58.6	49.3	1100	808	4.00	3.45	5.64
1.60	3	-10.8	-2.8	58.7	49.4	722	-364	3.29	2.62	4.06
	4	14.4	0.7	58.7	49.4	-1090	-49	3.99	2.03	4.16
	5	10.9	15.4	57.6	48.5	-810	1070	3.42	3.91	5.55

	6	-3.5	11.7	57	48	262	681	2.37	3.16	3.73
	7	-0.2	-13.3	58.4	49.2	-10	-1130	1.94	4.05	4.16
	8	13.5	-10.1	57.5	48.4	-1070	-857	3.91	3.51	5.64
	9	9.5	4.8	56.4	47.5	-687	247	3.15	2.32	3.69
	10	-14.0	1.3	56.7	47.7	976	-67	3.71	1.99	3.91
	11	-10.9	-12.4	57.3	48.2	719	-1070	3.24	3.90	5.37
	12	3.7	-8.8	56.3	47.4	-302	-686	2.42	3.15	3.79
1.85	1	-0.2	15.2	59.1	49.7	10	933	1.97	3.70	3.80
	2	-13.6	11.9	56.2	47.3	1000	659	3.73	3.09	5.08
	3	-9.8	-3.0	56.3	47.4	626	-375	3.03	2.56	3.82
	4	14.2	0.3	55.4	46.7	-980	-102	3.67	2.02	3.94
	5	10.2	14.3	53.8	45.3	-691	901	3.07	3.47	4.87
	6*	-3.5	10.4	53	44.6	258	513	2.23	2.71	3.26
	7	0.0	-12.5	60.6	51	21	-1010	2.04	3.90	4.02
	8	12.6	-8.9	58.5	49.2	-885	-740	3.59	3.32	5.09
	9	8.5	5.1	57.3	48.2	-529	231	2.88	2.32	3.39
	10	-13.3	1.4	57	48	880	-56	3.54	1.99	3.72
	11	-9.2	-10.3	56.7	47.7	578	-813	2.96	3.40	4.58
	12	3.7	-7.1	54.7	46	-282	-499	2.33	2.74	3.34
2.30	1	0.0	15.2	59.4	50	-16	893	1.99	3.64	3.75
	2	-11.0	9.7	54.9	46.2	601	426	2.94	2.61	3.82
	3*	-6.7	-3.8	52.8	44.4	246	-346	2.20	2.39	2.91
	4	12.0	0.5	53.80	45.30	-612	-71	2.93	1.91	3.12
	5	6.4	9.0	48.9	41.1	-280	325	2.14	2.22	2.81
	6*	-4.5	6.3	44.6	37.5	239	100	1.92	1.66	2.15
	7	0.0	-7.9	53.9	45.3	-25	-204	1.82	2.16	2.25
	8	7.6	-3.9	48.4	40.7	-265	-54	2.09	1.70	2.24
	9*	4.2	5.5	44.6	37.5	-64.2	201	1.59	1.85	2.01

10	-9.4	1.4	55.7	46.9	247	-7	2.30	1.85	2.36
11	-5.5	-5.9	53	44.6	75	-178	1.89	2.08	2.27
12	3.7	-3.1	46.9	39.4	-174	-27.1	1.87	1.60	1.96

* Reloaded strands at point before reaching next loading point zero x-displacement and zero y-displacement

Table 3-9: Shear Stress at Critical Section for Specimen B4

Drift Level	Point	Peak Lateral Force		Gravity Shear		Unbalanced Moment		Normalized Shear Stress [psi]		
%		[kip]		Force	Ratio	[kip-in]		$\dfrac{V}{A_c\sqrt{f'_c}}+\dfrac{\gamma_v M_{uby}c_x}{J_c\sqrt{f'_c}}$	$\dfrac{V}{A_c\sqrt{f'_c}}+\dfrac{\gamma_v M_{ubx}c_y}{J_c\sqrt{f'_c}}$	$\dfrac{V}{A_c\sqrt{f'_c}}+\dfrac{\gamma_v M_{ubx}c_y}{J_c\sqrt{f'_c}}+\dfrac{\gamma_v M_{uby}c_x}{J_c\sqrt{f'_c}}$
δ		x	y	[kip]	[%]	M_{ubY}	M_{ubX}			
	1	0.3	8.3	59.6	48.5	-28	517	2.02	2.94	2.95
	2	-7.5	5.3	58.3	47.4	500	329	2.86	2.54	3.44
	3	-4.6	-3.6	58.0	47.2	329	-240	2.53	2.36	2.94
	4	7.6	-1.2	57.4	46.7	-580	-69	2.98	2.02	3.07
	5	5.4	7.7	56.9	46.3	-441	478	2.71	2.78	3.56
0.25	6	-2.7	5.2	56.9	46.3	124	314	2.11	2.47	2.67
	7	0.0	-7.5	56.1	45.7	6	-616	1.86	3.01	2.98
	8	7.5	-5.9	55.9	45.5	-534	-454	2.85	2.70	3.66
	9	5.0	2.5	56.0	45.5	-379	95	2.56	2.02	2.70
	10	-6.7	0.6	55.9	45.5	502	-48	2.79	1.93	2.84
	11	-4.5	-7.6	55.4	45.1	386	-570	2.55	2.90	3.58
	12	3.3	-5.3	55.5	45.2	-165	-405	2.14	2.59	2.87
	1	0.4	11.1	60.7	49.4	-50	867	2.09	3.63	3.68
	2	-9.8	8.4	59.7	48.6	769	569	3.42	3.04	4.43
	3	-7.3	-3.4	59.6	48.5	527	-331	2.96	2.59	3.53
	4	11.0	-1.1	59.1	48.1	-884	-69	3.61	2.08	3.69
0.45	5	8.1	9.6	57.6	46.8	-655	756	3.13	3.32	4.50
	6	-2.2	7.7	58.1	47.3	167	476	2.23	2.81	3.09
	7	0.0	-11.1	56.9	46.3	-6	-951	1.89	3.67	3.63
	8	9.9	-8.7	56.6	46.0	-796	-715	3.36	3.21	4.65
	9	7.2	2.1	57.1	46.5	-525	125	2.87	2.12	3.07

	10	-9.7	0.3	56.7	46.2	747	-86	3.28	2.03	3.39
	11	-7.2	-9.6	55.8	45.4	584	-861	2.94	3.46	4.50
	12	2.9	-7.8	56.4	45.9	-208	-580	2.25	2.95	3.30
	1	0.2	13.2	60.9	49.6	-31	1040	2.07	3.97	3.97
	2	-11.6	10.2	60.4	49.1	957	737	3.79	3.38	5.11
	3	-8.9	-3.6	60.0	48.8	661	-340	3.22	2.62	3.81
	4	12.8	-0.9	59.4	48.4	-1040	-59	3.92	2.07	3.98
	5	9.7	11.9	58.7	47.8	-793	957	3.43	3.74	5.16
0.70	6	-2.3	9.4	59.3	48.2	194	624	2.32	3.13	3.45
	7	0.3	-12.9	58.1	47.3	-6	-1110	1.93	4.00	3.96
	8	12.0	-10.2	57.7	47.0	-964	-840	3.72	3.48	5.23
	9	8.8	2.3	57.8	47.1	-638	151	3.11	2.19	3.35
	10	-11.4	0.2	57.6	46.9	907	-83	3.61	2.06	3.71
	11	-8.8	-11.7	57.1	46.5	708	-1020	3.21	3.80	5.07
	12	2.9	-9.3	57.2	46.6	-238	-715	2.33	3.23	3.63
	1	0.2	14.1	61.7	50.2	-41	1110	2.11	4.12	4.15
	2	-13.3	11.5	60.9	49.6	1090	817	4.06	3.55	5.53
	3	-9.9	-3.5	60.2	49.0	755	-346	3.41	2.64	4.01
	4	14.4	-0.8	59.9	48.7	-1160	-40	4.16	2.05	4.18
	5	10.9	13.2	59.4	48.4	-883	1080	3.62	3.99	5.58
	6	-2.7	10.5	59.5	48.4	218	717	2.37	3.31	3.67
0.90	7	0.4	-13.5	58.8	47.9	-20	-1200	1.98	4.20	4.18
	8	13.3	-11.1	58.3	47.5	-1100	-925	3.99	3.66	5.66
	9	9.9	2.9	58.2	47.3	-742	188	3.32	2.27	3.62
	10	-12.6	0.3	58.2	47.4	997	-82	3.80	2.07	3.90
	11	-9.9	-13.0	57.8	47.0	773	-1130	3.36	4.03	5.42
	12	3.2	-10.1	57.5	46.8	-273	-792	2.41	3.39	3.85
1.15	1	0.2	15.1	62.3	50.7	-27	1170	2.10	4.26	4.25

	2	-14.2	12.3	61.6	50.1	1160	866	4.21	3.66	5.77
	3	-10.6	-3.6	60.6	49.3	789	-353	3.48	2.66	4.09
	4	15.1	-0.6	60.4	49.2	-1220	-48	4.29	2.08	4.32
	5	11.7	14.2	60.3	49.1	-935	1150	3.75	4.15	5.84
	6	-2.8	11.3	60.3	49.0	233	773	2.43	3.44	3.83
	7	0.5	-14.6	59.9	48.8	-30	-1250	2.03	4.33	4.33
	8	14.4	-11.7	59.4	48.4	-1180	-961	4.18	3.77	5.91
	9	10.7	3.2	58.9	47.9	-800	213	3.45	2.34	3.80
	10	-13.6	0.3	59.1	48.1	1040	-90	3.91	2.12	4.02
	11	-10.7	-14.0	59.1	48.1	810	-1220	3.47	4.24	5.70
	12	3.4	-10.9	58.5	47.6	-290	-832	2.47	3.49	3.99
	1	0.2	15.6	62.9	51.2	-28	1210	2.13	4.35	4.35
	2	-15.1	13.0	62.2	50.6	1220	911	4.35	3.77	5.98
	3	-11.0	-3.6	61.3	49.9	820	-360	3.56	2.70	4.19
	4	15.5	-0.6	61.1	49.8	-1230	-36	4.33	2.08	4.34
	5	12.2	15.0	61.1	49.7	-962	1210	3.82	4.29	6.02
1.40	6	-3.0	11.9	60.7	49.4	256	822	2.48	3.55	3.98
	7	0.4	-15.1	60.6	49.3	-33	-1280	2.06	**4.41**	4.41
	8	15.1	-12.1	59.6	48.5	-1220	-987	4.26	3.82	6.04
	9	11.0	3.1	58.9	47.9	-813	226	3.47	2.37	3.85
	10	-13.9	0.3	59.3	48.3	1070	-89	3.97	2.12	4.08
	11	-11.1	-14.4	59.3	48.3	827	-1250	3.51	4.31	5.79
	12	4.0	-11.1	58.5	47.6	-301	-847	2.50	3.52	4.04
	1	0.1	16.0	63.5	51.7	-24	1220	2.14	4.39	4.38
	2	-15.2	13.2	62.8	51.1	1220	912	**4.37**	3.79	6.01
1.60	3	-10.9	-4.2	61.3	49.9	794	-397	3.52	2.77	4.21
	4	**15.8**	-0.6	61.3	49.9	-1230	-27	4.34	2.07	4.33
	5	12.2	15.1	61.6	50.1	-963	1220	3.84	4.33	**6.06**

	6	-3.3	11.8	61.1	49.7	271	805	2.52	3.53	3.99
	7	0.5	-15.2	60.9	49.6	-41	-1250	2.09	4.36	4.38
	8	15.1	-12.0	60.1	48.9	-1210	-975	4.26	3.82	6.02
	9	10.9	3.6	59.0	48.0	-796	249	3.44	2.41	3.86
	10	-14.0	0.4	59.9	48.7	1040	-78	3.93	2.12	4.03
	11	-11.1	-14.3	59.7	48.5	795	-1220	3.46	4.26	5.69
	12	4.0	-10.5	58.7	47.8	-331	-810	2.56	3.46	4.03
	1	0.1	15.5	62.3	50.7	-35	1110	2.12	4.14	4.16
	2	-14.4	12.1	59.3	48.2	1130	805	4.08	3.47	5.53
	3	-10.1	-4.7	57.8	47.0	693	-438	3.21	2.73	3.98
	4	15.4	-0.9	57.8	47.0	-1160	-68	4.09	2.03	4.16
	5	11.7	14.2	57.4	46.7	-883	1090	3.55	3.94	5.53
1.85	6	-3.3	10.5	56.5	46.0	227	676	2.29	3.13	3.52
	7	0.4	-14.8	55.5	45.1	-58	-1190	1.94	4.07	4.13
	8	14.4	-11.1	54.5	44.3	-1140	-877	3.94	3.45	5.52
	9	9.9	3.7	53.5	43.6	-709	248	3.10	2.23	3.52
	10	-13.5	0.2	53.5	43.5	965	-78	3.58	1.91	3.68
	11	-10.0	-13.1	52.9	43.1	677	-1080	3.02	3.78	4.99
	12	4.3	-9.3	52.0	42.3	-360	-672	2.39	2.98	3.61
	1	0.4	**16.1**	63.3	51.5	-68	1140	2.21	4.23	4.30
	2	-12.7	10.5	61.3	49.9	963	714	3.83	3.36	5.11
	3	-8.0	-5.8	59.0	48.0	494	-415	2.87	2.73	3.61
	4	15.6	-0.8	60.0	48.8	-1120	-41	4.09	2.06	4.11
2.30	5	9.4	11.3	57.2	46.5	-651	714	3.11	3.23	4.40
	6	-4.2	7.5	54.9	44.7	249	364	2.28	2.50	2.93
	7	0.4	-13.6	55.2	45.0	-52	-929	1.92	3.57	3.62
	8	10.1	-7.8	50.7	41.2	-508	-466	2.63	2.55	3.46
	9	6.1	4.2	47.0	38.2	-227	193	1.98	1.91	2.31

	10*	-10.1	0.2	55.4	45.1	315	-24	2.42	1.87	2.43
	11	-5.8	-8.1	51.9	42.2	76	-330	1.85	2.33	2.44
	12	4.3	-5.0	45.7	37.2	-238	-93	1.95	1.68	2.10
	1	0.4	10.0	60.7	49.4	-54	297	2.10	2.56	2.63
	2	-8.3	5.6	58.2	47.4	276	80	2.44	2.07	2.55
	3	-4.2	-5.3	51.0	41.5	26	-213	1.73	2.08	2.10
	4*	9.9	-1.0	60.1	48.9	-262	-32	2.47	2.04	2.50
	5	5.2	7.3	58.7	47.7	-131	220	2.18	2.35	2.56
2.75	6	-4.4	3.9	52.6	42.8	159	20	2.03	1.77	2.04
	7†	-0.1	-9.0	60.0	48.8	-1	-266	1.98	2.48	2.45
	8	7.7	-4.4	57.1	46.5	-226	-84	2.31	2.04	2.43
	9	3.5	4.8	51.2	41.6	-42	121	1.77	1.92	1.97
	10	-9.2	0.5	50.5	41.1	275	-14	2.18	1.69	2.18
	11	-4.6	-6.7	49.6	40.4	71	-213	1.77	2.04	2.14
	12	4.9	-3.4	43.6	35.5	-176	-68	1.77	1.57	1.87

* Stopped at zero x-displacement and zero y-displacement while loading to subsequent point on loading path, reloaded strands before continuing drift cycle

† Stopped at zero x-displacement and zero y-displacement while loading to subsequent point on loading path unloaded the slab completely, lowered slab perimeter, then reloaded slab before continuing drift cycle

Table 3-10: Peak Shear Stresses on Critical Section

Specimen	Normalized Maximum Shear Stress in X-Direction			Normalized Maximum Shear Stress in Y-Direction			Normalized Maximum Shear Stress at Corner		
	v_x [psi]	Drift Level [%]	Point	v_y [psi]	Drift Level [%]	Point	v_{xy} [psi]	Drift Level [%]	Point
SB3 (Cheng 2009)	3.97	0.9	4	4.29	0.9	1	5.68	0.9	2
B1	4.15	1.15	2	4.31	1.15	7	5.80	1.15	9
B2	4.41	1.40	2	4.39	1.15	1	6.16	1.40	2
B3	4.10	1.15	2	4.27	1.15	1	5.91	1.15	2
B4	4.37	1.60	2	4.39	1.40	1	6.06	1.60	5

Table 3-11: Design and Calculated Shear Capacity of Slabs and Peak Shear Stresses

Specimen	Design Nominal Shear Capacity* [psi]		Calculated Nominal Shear Capacity† [psi]		Peak Shear Stresses† [psi]		
	v_c	v_s^	v_c	v_s^	v_x	v_y	v_{xy}
B1	0	5.2	2	4.8	4.15	4.31	5.80
B2	0	3.6	2	3.6	4.41	4.39	6.16
B3	0	5.2	2	4.9	4.10	4.27	5.91
B4	0	8.0°	2	7.9°	4.37	4.41	6.06

* Normalized by the square root of the specified concrete strength
† Normalized by the square root of the concrete compressive strength measured one day prior to specimen testing
^ The specified yield stress of 55 ksi is assumed for the studs
° The maximum design shear stress capacity of $8\sqrt{f_c'}$ (psi) permitted by the ACI Building Code (ACI Committee 318 2008) governs

Table 4-1: Drift Capacity of Slab-Column Connections without Shear Reinforcement

Researcher	Label	h [in.]	ρ_t [%]	Setup[1]	V_g/V_c target	V_g/V_c Peak Load	Ultimate drift [%] (at punching)	Drift at peak load [%]	Failure mode[2]
Hawkins et al. (1974)	S1	6	1.20	B, D	0.34	0.34	4.0	4.0	P
	S2	6	0.84		0.45	0.45	1.4	1.4	P
	S3	6	0.55		0.42	0.43	1.4	1.4	P
	S4	6	1.20		0.37	0.42	2.1	2.1	P
Symonds et al.	S6	6	1.81	B, D	0.89	0.88	1.2	1.2	P
	S7	6	0.84		0.83	0.80	0.5	0.5	P
Ghali et al. (1976)	SM 0.5	6	0.50	A, C	0.31	NA	6.5	4.3	P
	SM 10.	6	1.00		0.33	NA	2.7	2.7	F-P
	SM 1.5	6	1.50		0.30	NA	2.0	2.0	F-P
Islam and Park (1976)	1	3.5	0.53*	B, D	0.25	0.25	4.4	3.7	P
	2	3.5	0.53*		0.23	0.23	5.0	4.1	P
	3C	3.5	0.53*		0.23	0.23	5.2	2.0	P
Morrison and Sozen (1981)	S4	3	0.98	B, C	0.078	NA	4.5	3.5	F-P
	S5	3	0.98		0.166	NA	4.8	3.3	F-P
Zee and Moehle (1984)	INT	2.4	0.80	B, C	0.29	0.29	3.5	3.5	P
Pan and Moehle (1989)	AP1	4.8	0.86	A, B, C	0.37	0.37	1.6	1.6	F-P
	AP2**	4.8	0.86		0.36	0.36	1.5	1.5	F-P
	AP3	4.8	0.86		0.18	0.18	4.8	3.7	F-P
	AP4**	4.8	0.86		0.19	0.19	3.5	3.5	F-P
Robertson and Durrani (1990)	3SE	4.5	0.73	B, C	0.19	0.15	4.0	3.5	F-P
	5SO	4.5	0.73		0.21	0.17	3.5	3.5	F-P
	6LL	4.5	0.73		0.54	0.54	1.0	1.0	P
	7L	4.5	0.73		0.37	0.37	1.5	1.5	P
Dilger and Cao (1991)	CD1	5	0.73	A, C	0.85	0.85	0.9	0.9	P
	CD2	5	0.49		0.65	0.65	1.2	1.2	P

	CD8	5	0.49		0.52	0.52	1.4	1.4	P
Wey and Durrani (1992)	SC0	4.5	1.0	B, C	0.18	.23	3.5	3.5	P
Farhey et al. (1993)	1	3.15	1.0	A, C	0.00	NA	5.5	5.5	F-P
	2	3.15	1.0		0.00	NA	5.0	3.9	F-P
	3	3.15	1.0		0.26	NA	3.7	3.2	P
	4	3.15	0.68		0.30	NA	2.5	2.5	P
Durrani et al. (1995)	DNY_2	4.5	0.42	B, C	0.37	0.37	2.0	2.0	P
	DNY_4	4.5	0.42		0.27	0.27	4.7	2.6	P
Robertson et al. (2002)	C1	4.5	0.42	B, C	0.25	0.17	3.5	3.5	P
Robertson and Johnson (2006)	ND1C	4.5	0.73	B, C	0.25	0.23	8.0	3.0	F-P
	ND4LL	4.5	0.31		0.37	0.28	4.0	3.0	F-P
	ND5XL	4.5	1.20		0.48	0.47	2.0	1.5	P
	ND6HR	4.5	0.84		0.30	0.29	5.0	3.0	P
	ND7LR	4.5	0.55		0.36	0.26	5.0	3.0	F-P

1) A – Jacked column at base; B – Hung weights from slab; C – Applied lateral force at column tip; D – Applied force couple at slab edges
2) F – Flexural yielding preceded punching; P – Primary failure mode was punching shear
*Grade 40 steel used, value multiplied by 2/3
**Biaxially loaded

Table 4-2: Drift Capacity of Slab-Column Connections with Headed Shear Stud Reinforcement

Researcher	Label	h [in.]	ρ_t [%]	s/d	Setup*	V_g/V_c Target	V_g/V_c Peak Load	Ultimate Drift [%] (Punching)	Drift at Peak Lateral Load [%]	Failure Mode**
Dilger and Cao (1991)	CD3	5	1.1	0.79	A, C	0.91	NA	3.5	NA	F-P
	CD4	5	1.1	0.79		0.62	NA	4.8	NA	F-P
	CD6	5	1.1	0.39		0.64	NA	5.4	NA	F-P
	CD7	5	1.1	0.79		0.51	NA	5.6	NA	F-P
Dilger and Brown (1994)	SJB-1	5.9	1.1	0.57	A, C	0.50	0.48	5.5	2.5	P
	SJB-2	5.9	1.1	0.57		0.50	0.47	5.7	3.8	P
	SJB-3	5.9	1.1	0.57		0.50	0.48	5.0	3.2	P
	SJB-4	5.9	1.1	0.57		0.50	0.43	6.4	5.5	P
	SJB-5	5.9	1.5	0.57		0.50	0.47	7.6	3.3	P
	SJB-8	5.9	1.1	0.57		0.50	0.46	5.7	4.3	P
	SJB-9	5.9	1.5	0.57		0.50	0.49	7.1	4.3	P
Megally (1998)	MG-10	10	1.6	0.75	A, C	0.59	NA	5.2	NA	NA
Megally and Ghali (2000)	MG-3	10	1.6	0.79	A, C	0.58	NA	5.4	3.2	NA
	MG-4	10	1.6	0.75		0.56	NA	4.6	2.0	F-P
	MG-5	10	1.6	0.75		0.86	NA	6.5	3.0	F-P
	MG-6	10	1.6	0.44		0.31	NA	6.0	3.5	F-P
Robertson et al. (2002)	4HS	4.5	0.68	0.68	B, C	0.24	0.15	8.0	5.0	N-A
Broms (2007b)	18c	7.1	1.2	0.50	A, C	0.67	0.67	4.0	2.5	P
	18d	7.1	0.67	0.50		0.67	0.67	4.0	2.0	P
Cheng et al. (2009)	SB3**	6	0.60	0.75	O	0.50	0.43	1.63	1.63	F-P

1) A – Jacked column at base; B – Hung weights from slab; C – Applied lateral force at column tip; D – Applied force couple at slab edges; O – Pulled down on slab with prestressing strands

2) F – Flexural yielding preceded punching; P – Primary failure mode was punching shear

**Biaxially loaded

FIGURES

Figure 1-1: Stud Rail Assembly

Figure 1-2: Orthogonal Stud Rail Arrangement
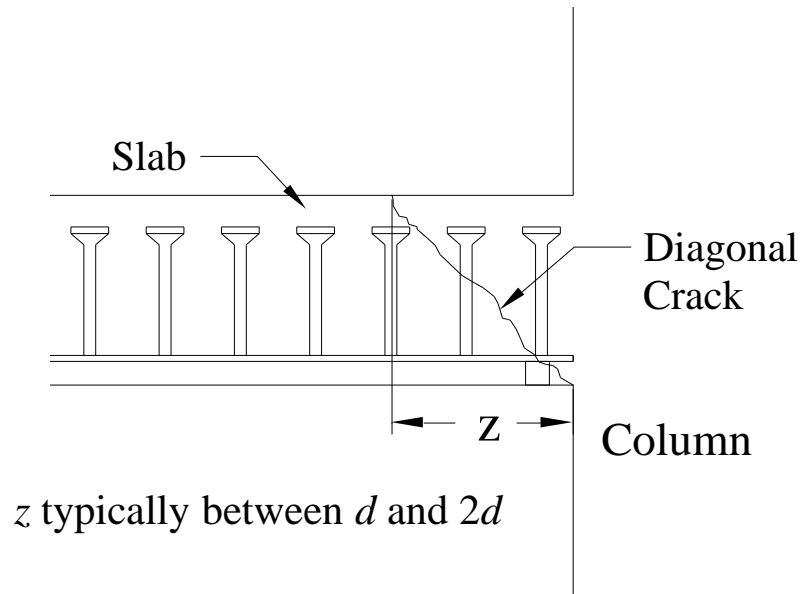
Figure 1-3: Shear Stud Reinforcement Shear Transfer Mechanism
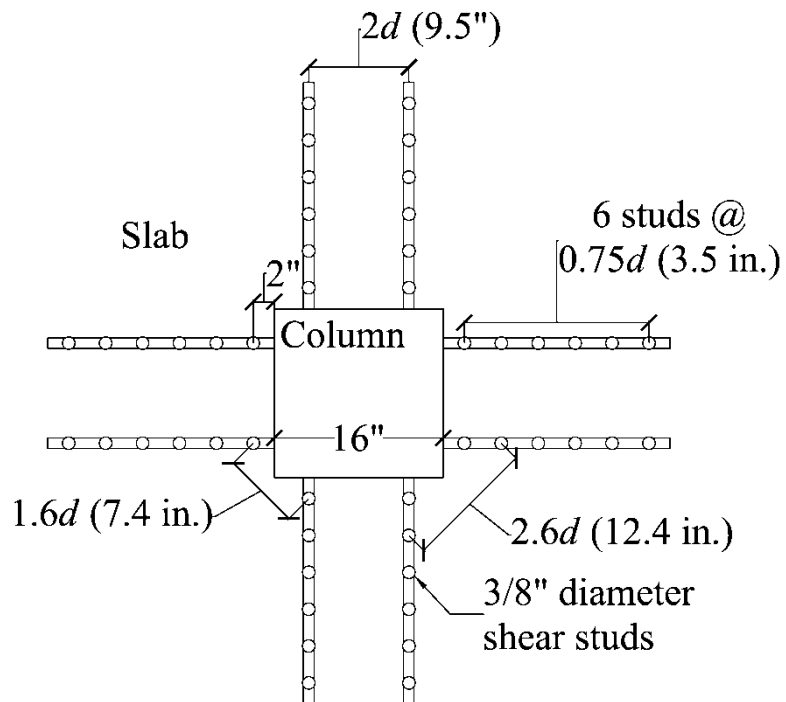
Figure 1-4: Shear Reinforcement Provided in a Previously Reported Shear Stud Reinforced Specimen
(Cheng et al. 2009)
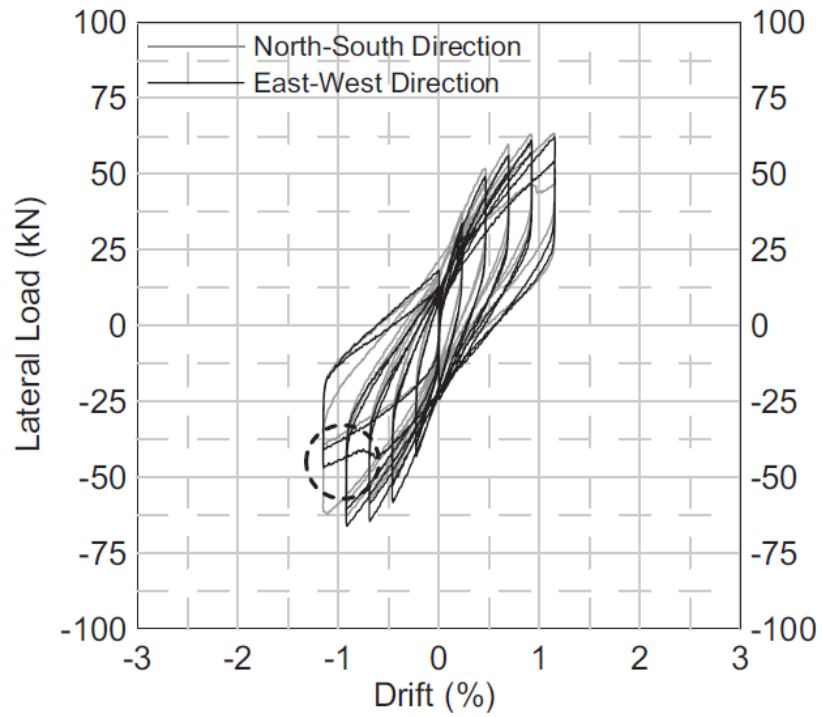
Figure 1-5: Lateral Load Versus Drift Response of Specimen with Shear Stud Reinforcement Reported in Cheng et al. (2010), with Circle Indicating Development of a Punching Shear Failure

Figure 1-6: Punching Shear Crack between First and Second Row of Shear Stud from Specimen SB3 (Cheng et al. 2010)

116
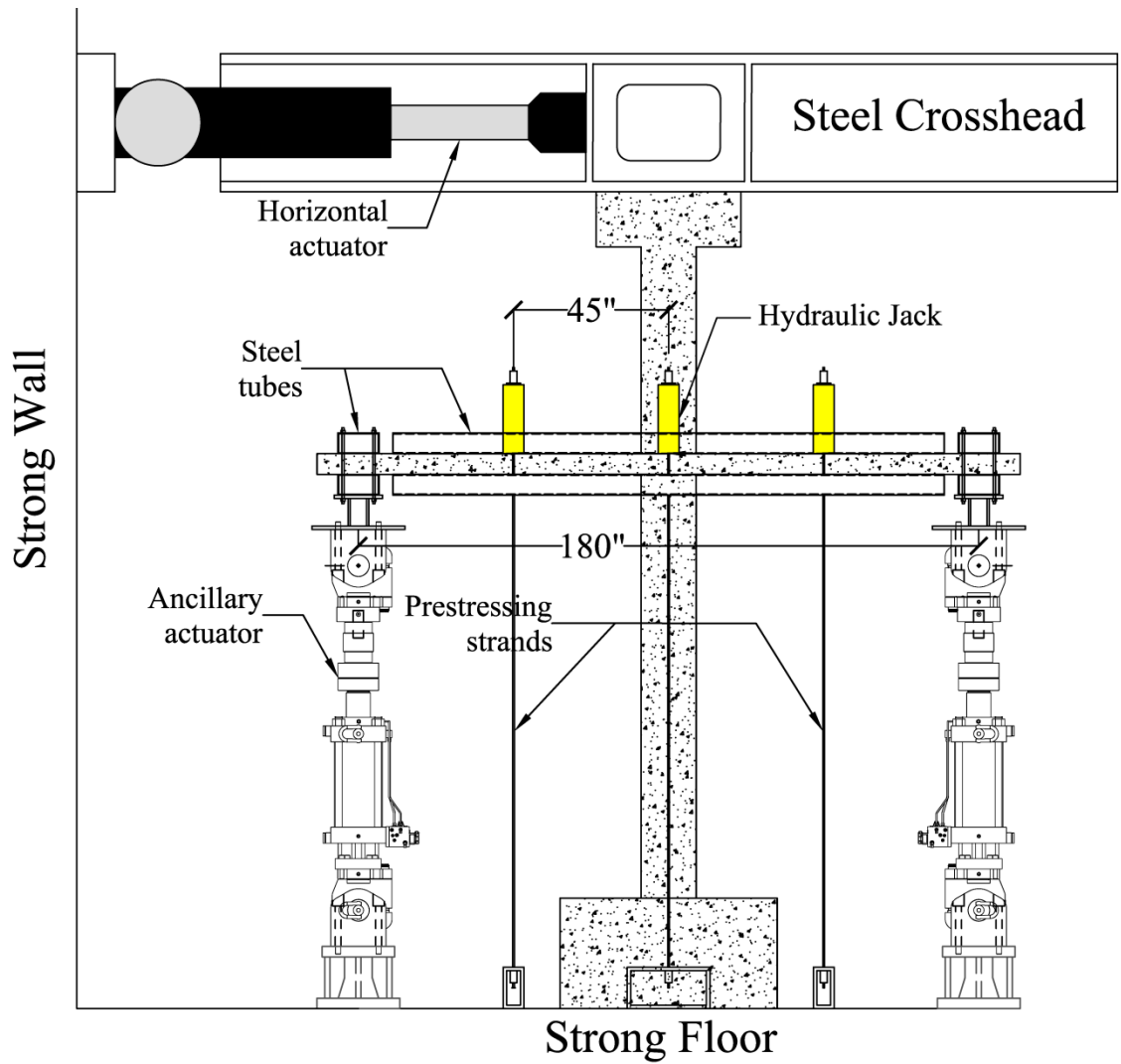
Figure 2-1: Elevation View of Setup
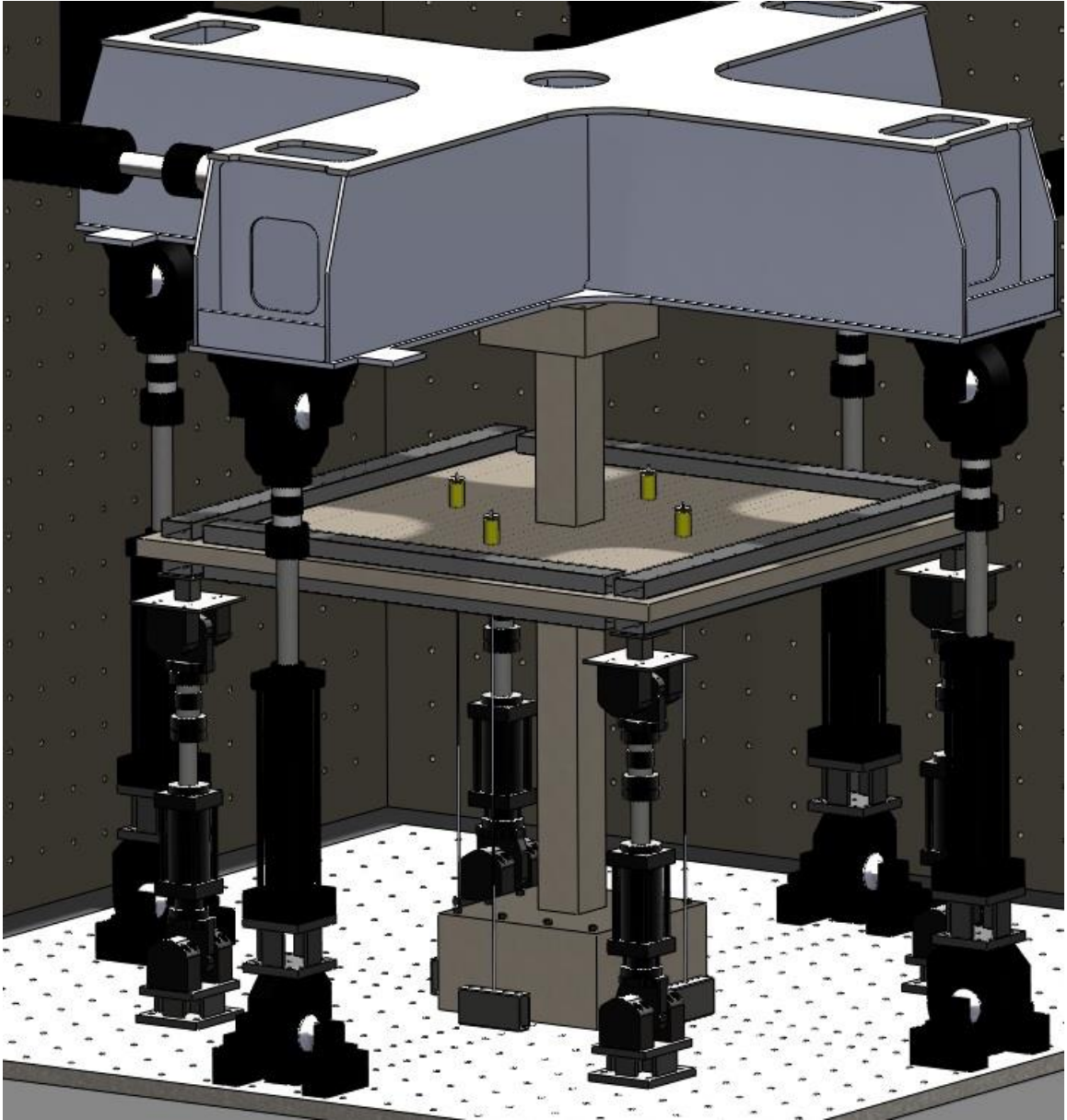
Figure 2-2: 3D Model of Test Configuration
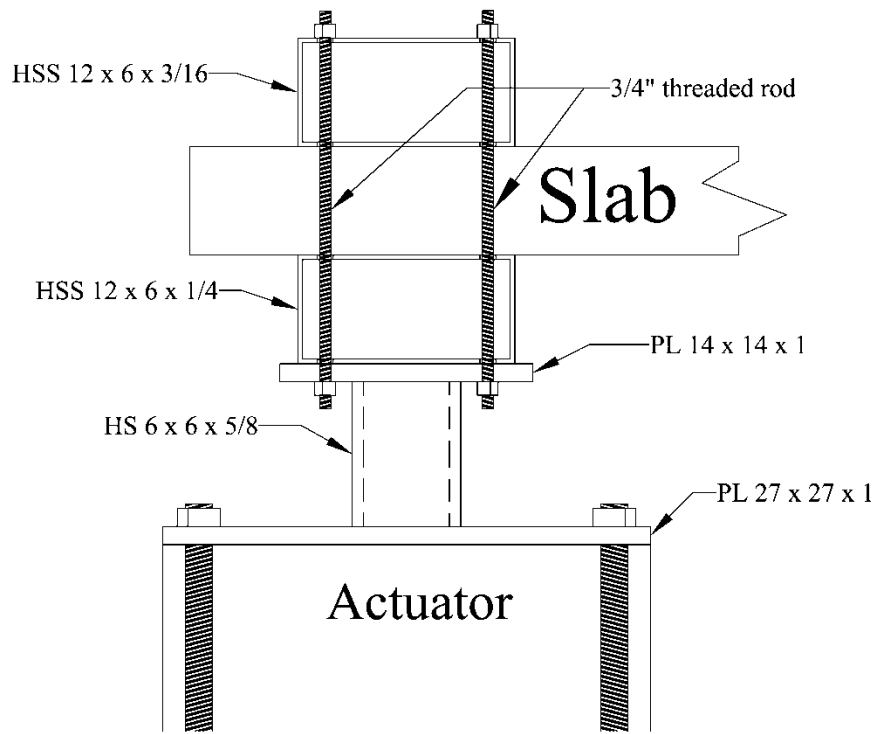
Figure 2-3: Detail of Ancillary Actuator-to-Slab Connection
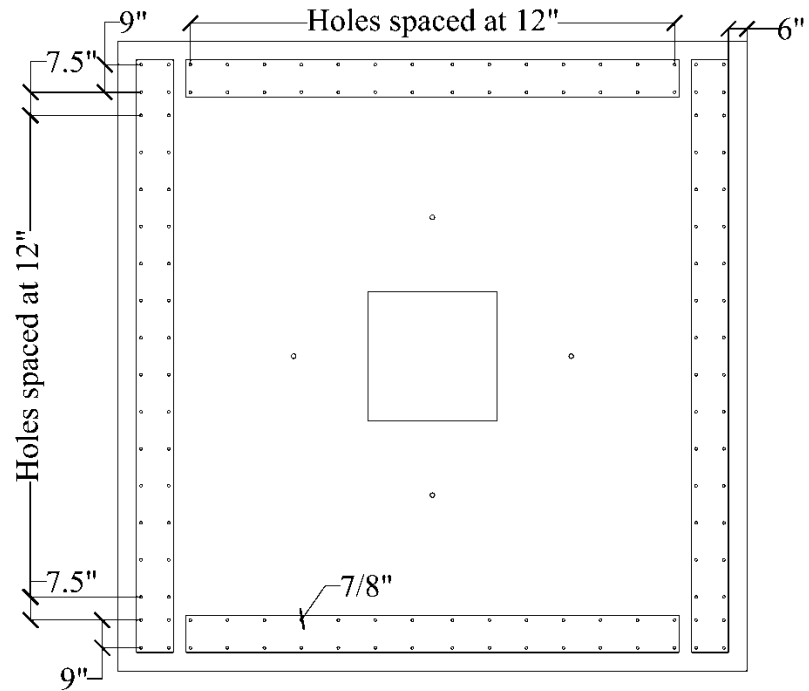
Figure 2-4: Steel Tube Layout on Slab Perimeter

All Reinforcing Bars: Grade 60
Column Longitudinal Bars: No. 6
Column Hoops: No. 3 @ 3" o.c.
Effective Flexural Slab Depth: 4.75"

Section A-A
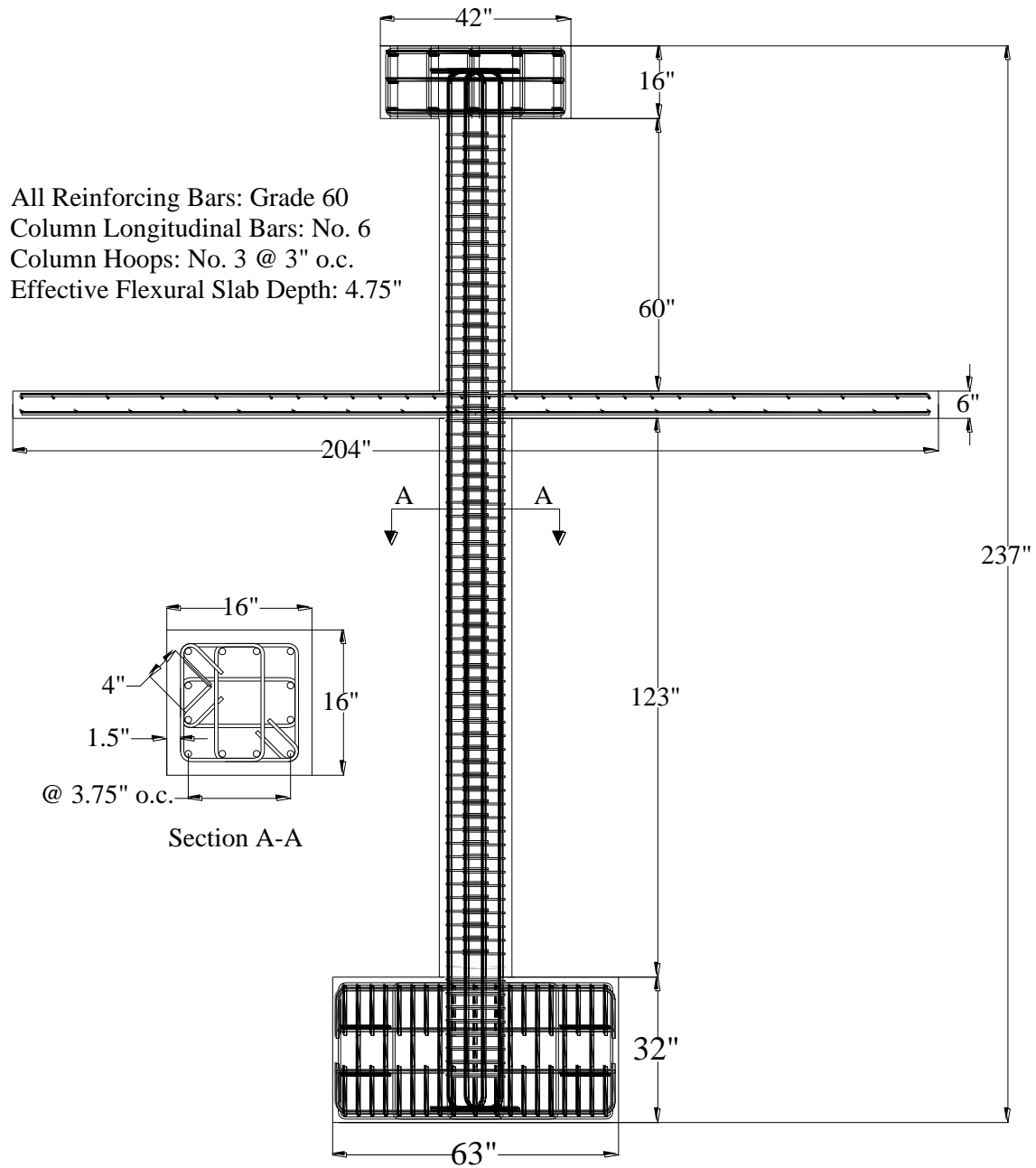
Figure 2-5: Specimen Elevation and Column Reinforcement Details
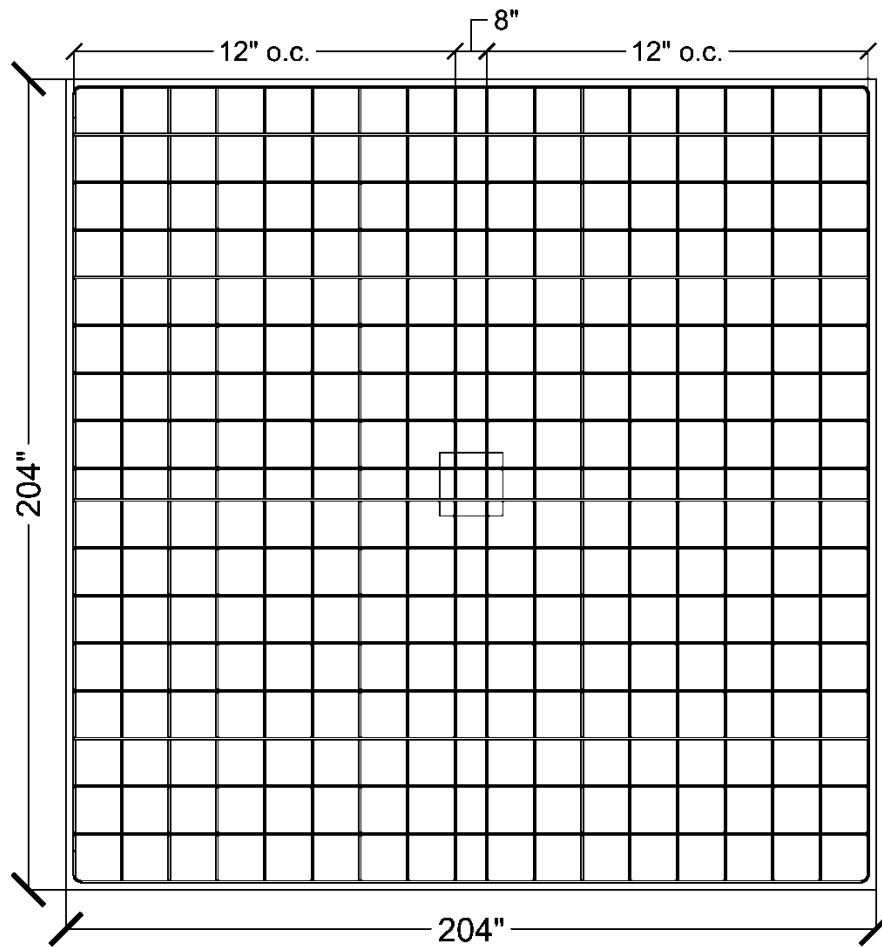
All Reinforcement: No. 4, Grade 60

Figure 2-6: Bottom Slab Reinforcement Layout
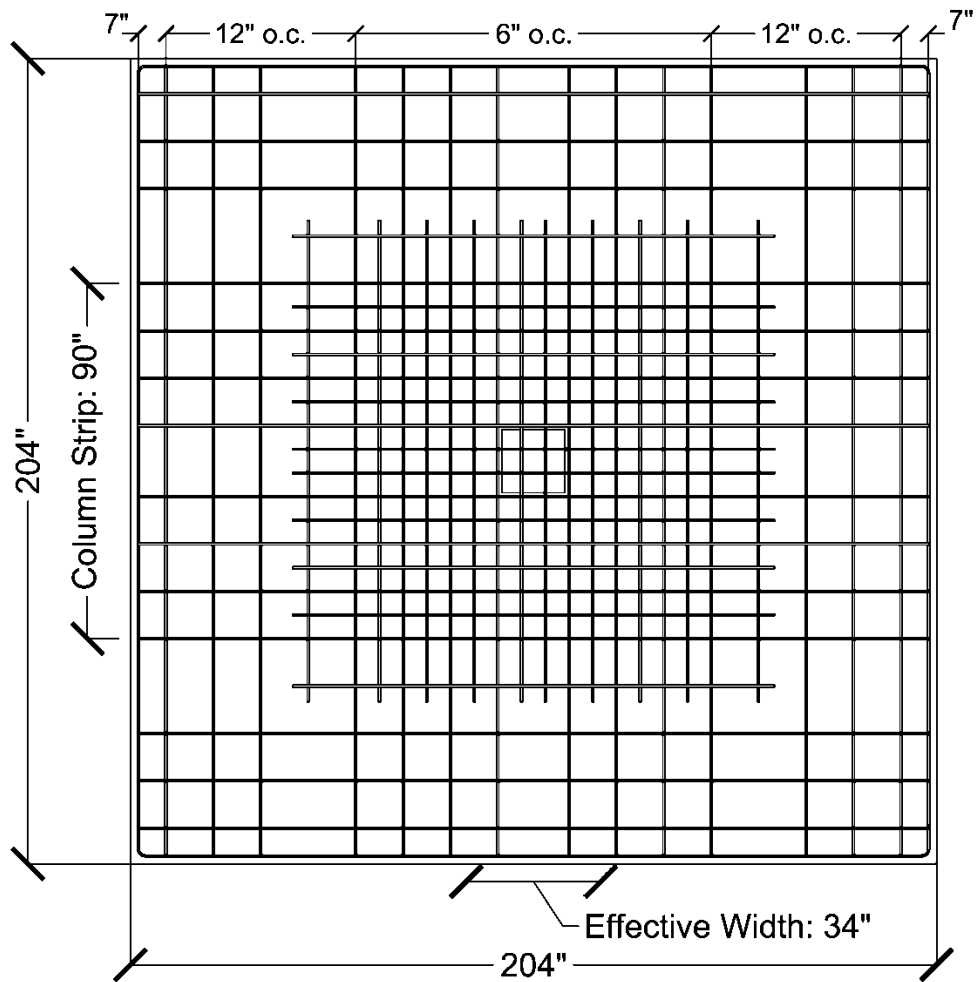
All Reinforcement: No. 4, Grade 60

Figure 2-7: Top Slab Reinforcement Layout
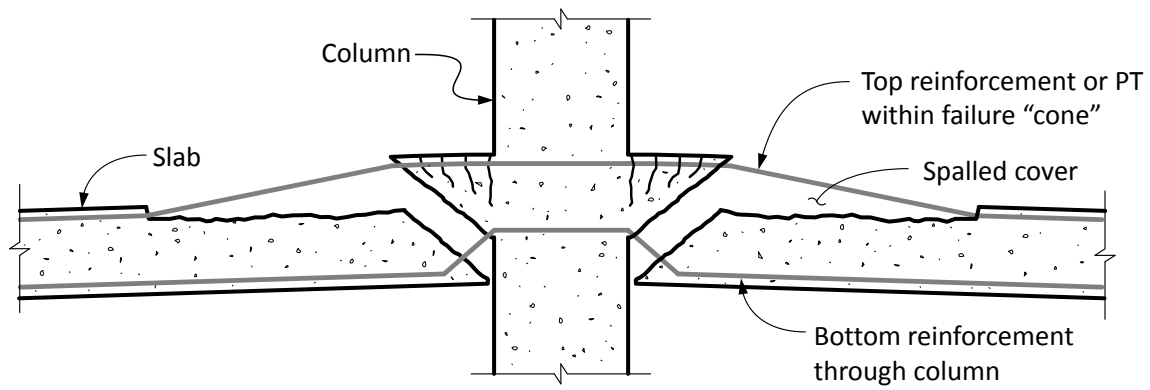
Figure 2-8: Bottom Mat Reinforcement Serving as Integrity Steel (courtesy of Jack P. Moehle)

Slab

Column

1-½" (0.3d)

A

A

9.7"
(2.0d)

20-½"
(4.3d)

9 studs @ 2-⅜" (0.5d)

1.19"

0.21"

4.25"

1.5"   0.375"   ¾" chairs   1.5"

Section A-A

7-⅜" (1.6d)
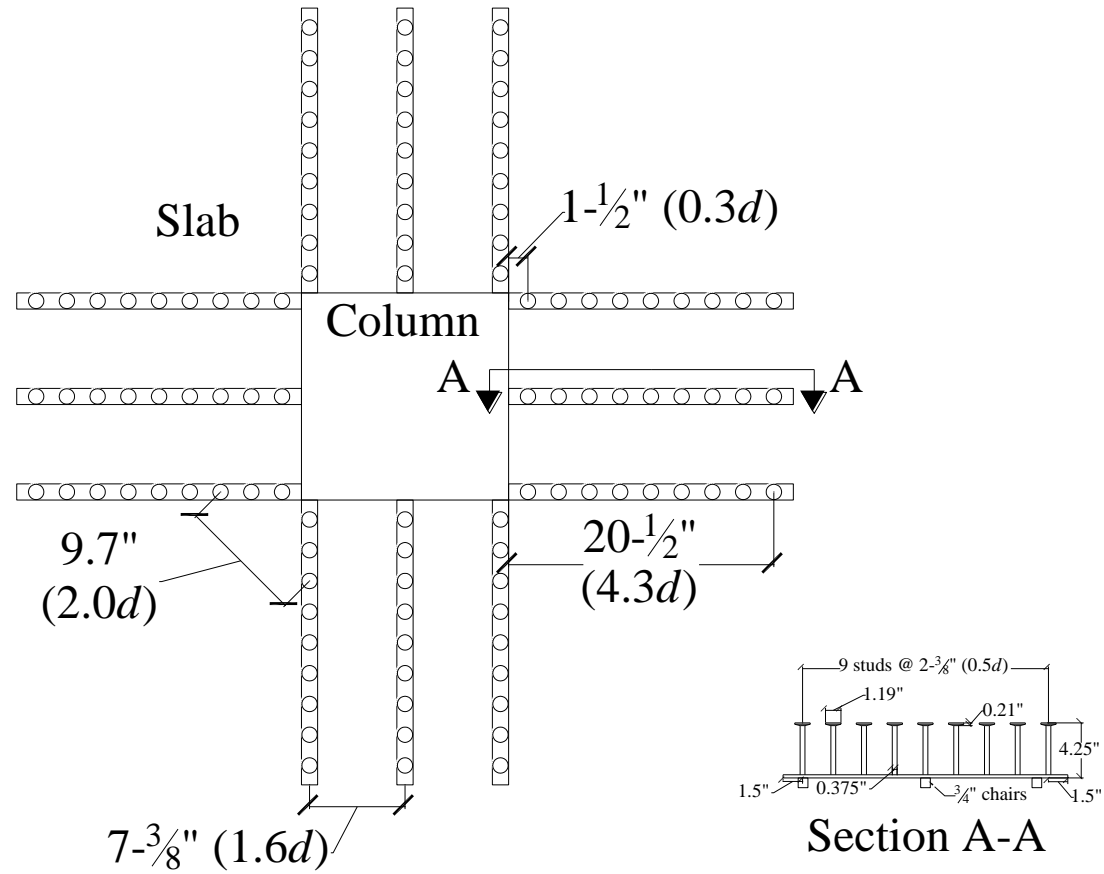
Rail Cross-Section 1-¼" x ¼"
Specified Minimum Yield Stress: 55 ksi

Figure 2-9: Shear Reinforcement Details for Specimen B1

Slab

2" (0.4d)

Column

A

A

A

26-½"
(5.6d)

13.6"
(2.9d)

7-³⁄₈" (1.6d)

8 studs @ 3-½" (0.75d)

1.19"

0.21"

4.25"

2"   0.375"   ¾" chairs   2"
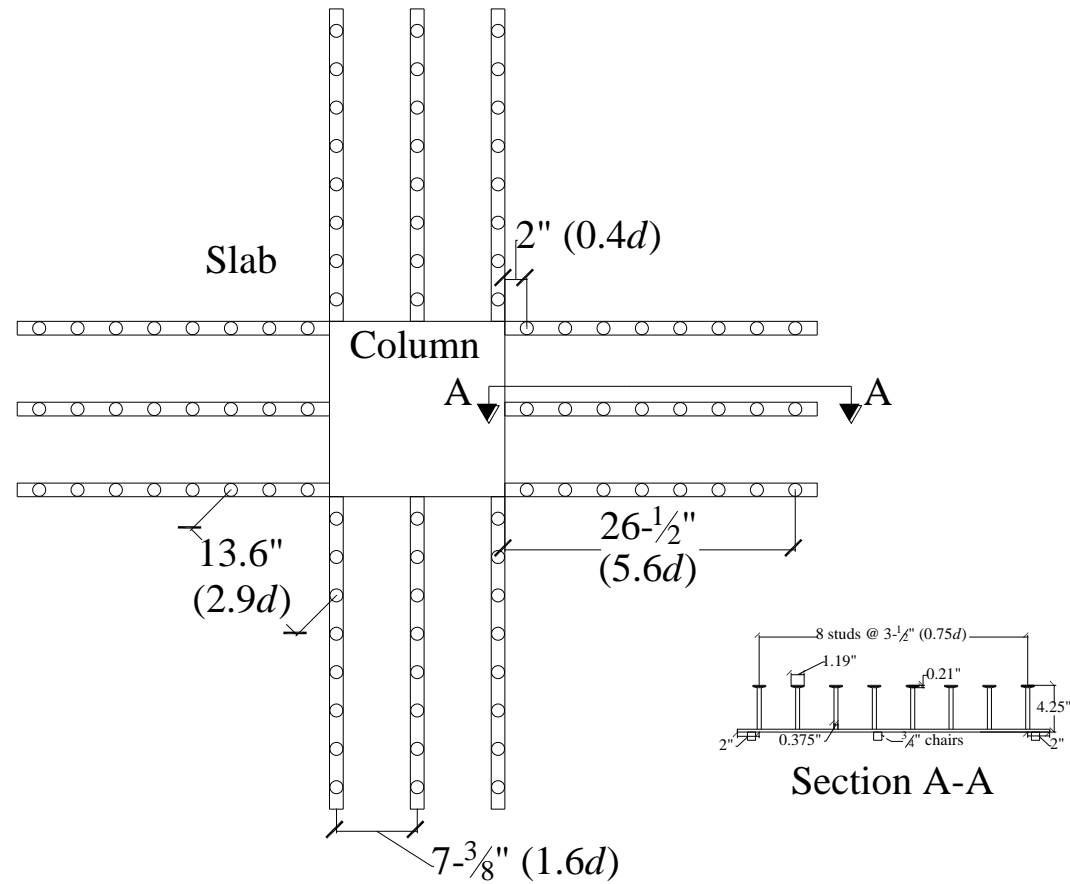
Section A-A

Rail Cross-Section 1-¼" x ¼"
Specified Minimum Yield Stress: 55 ksi

Figure 2-10: Shear Reinforcement Details for Specimen B2

125

7.6"
(1.6d)

Slab

2" (0.4d)

Column

25-¾" (5.4d)

A

A

B

9.4"
(2.0d)

45°

B

7-⅛" (1.5d)

11 studs @ 2-⅜" (0.5d)
1.19"
0.21"
4.25"
2"
0.375"
3/4" chairs
2"

Section A-A

15 studs @ 2-⅜" (0.5d)
1.19"
0.21"
4.25"
2"
0.375"
3/4" chairs
2"

Section B-B

Rail Cross-Section 1" x ³⁄₁₆ "
Specified Minimum Yield Stress: 55 ksi
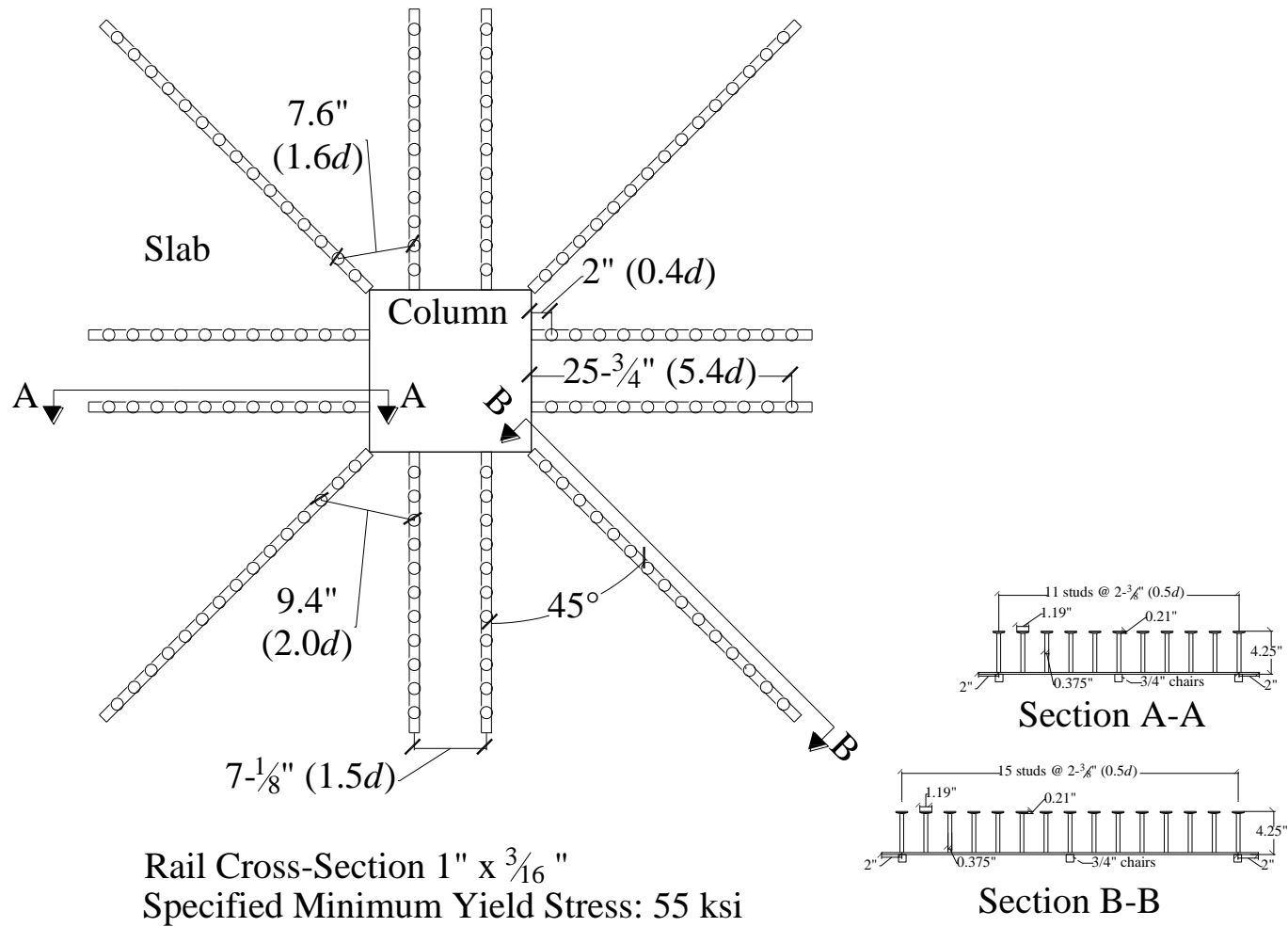
Figure 2-11: Shear Reinforcement Details for Specimen B3

15" (3.2*d*)

Slab

1-¼" (0.3*d*)

Column

25" (5.3*d*)

A

A

B

B

45°

6.5"
(1.4*d*)

6"
(1.3*d*)

Rail Cross-Section 1" x ³⁄₁₆ "
Specified Minimum Yield Stress: 55 ksi

11 studs @ 2-¾" (0.5*d*)
1.19"
0.21"
4.25"
1.25"
0.375"
¾" chairs
1.25"
Section A-A

11 studs @ 3-¾" (0.7*d*)
1.19"
0.21"
4.25"
2.25"
0.375"
¾" chairs
2.25"
Section B-B
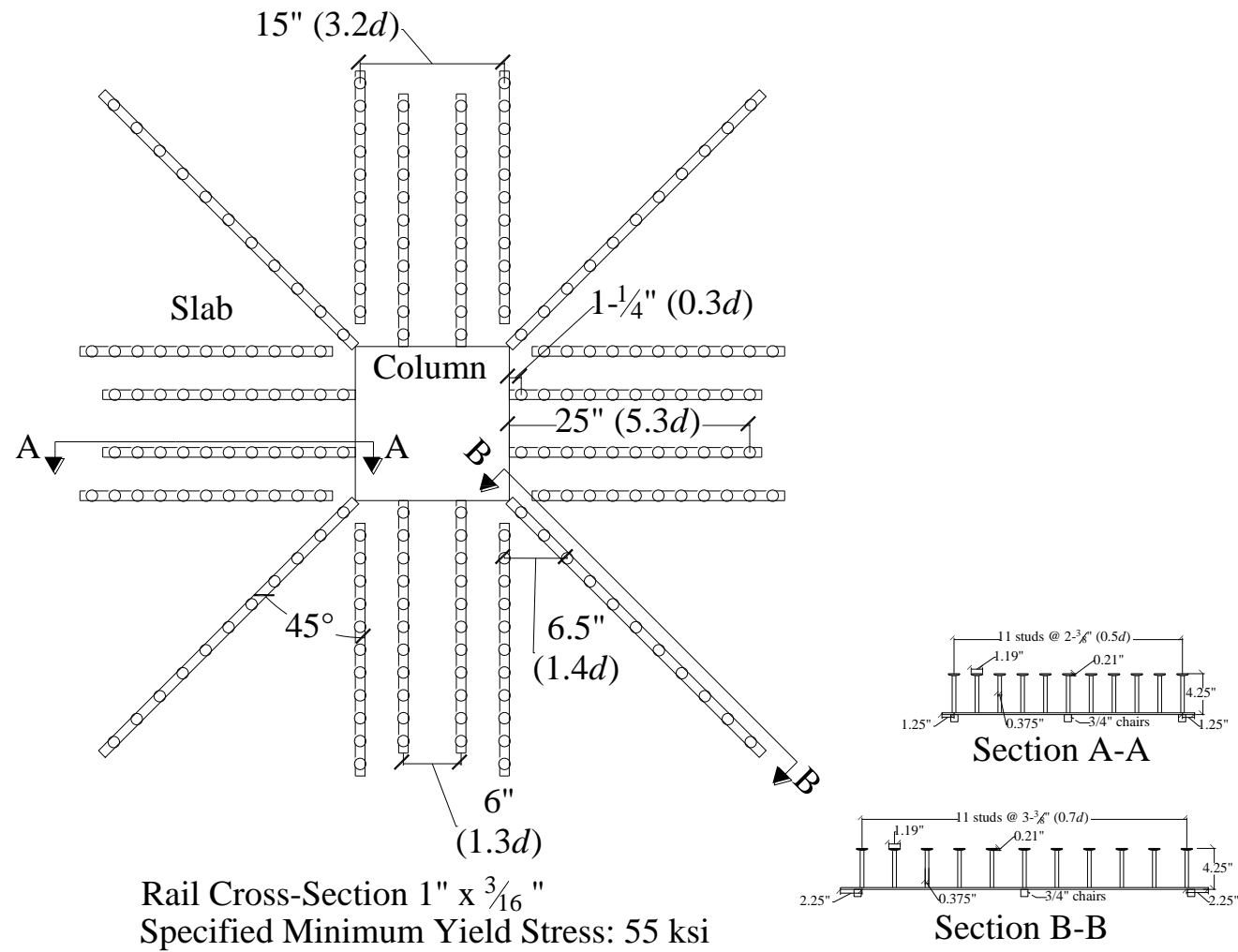
Figure 2-12: Shear Reinforcement Details for Specimen B4

127
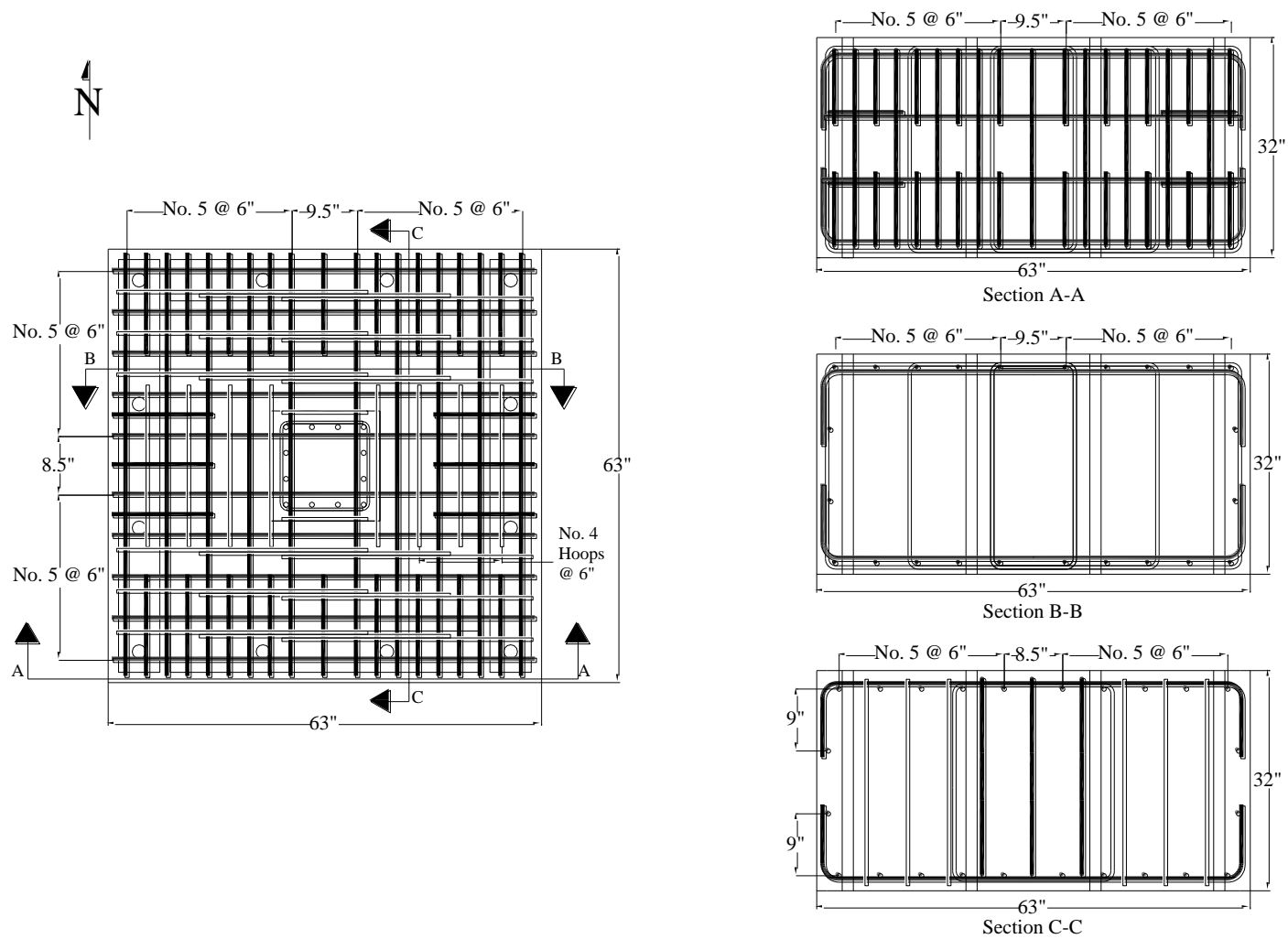
Figure 2-13: Base Block Dimensions and Reinforcement Details

42"

42"

6"

14"

6"

9" o.c.

N

A   A
B   B

1.75"

7.75"

14.25"

16"

Section A-A

1.75"

7.75"

14.25"

Section B-B
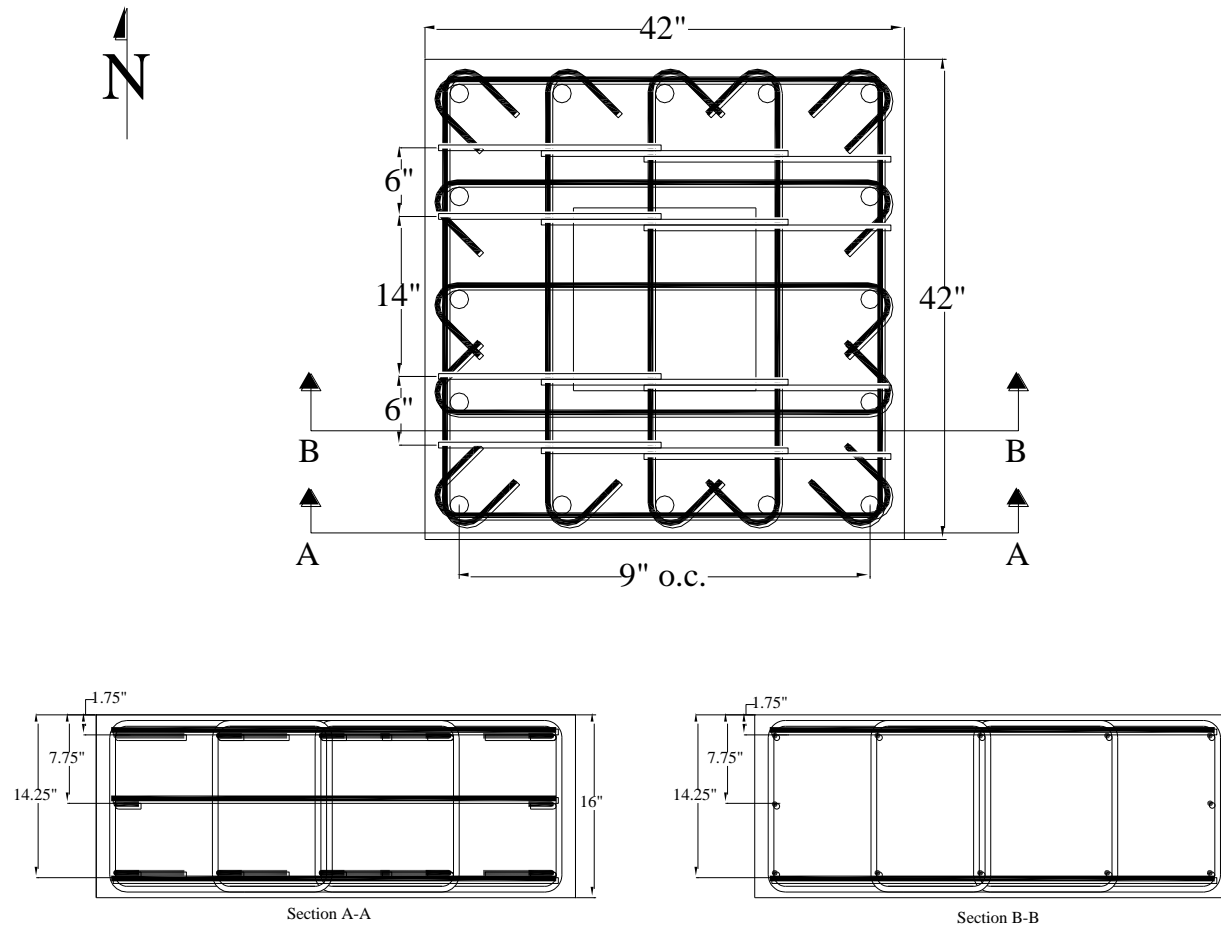
All Reinforcing Bars: No. 4, Grade 60

Figure 2-14: Top Block Dimensions and Reinforcement Details
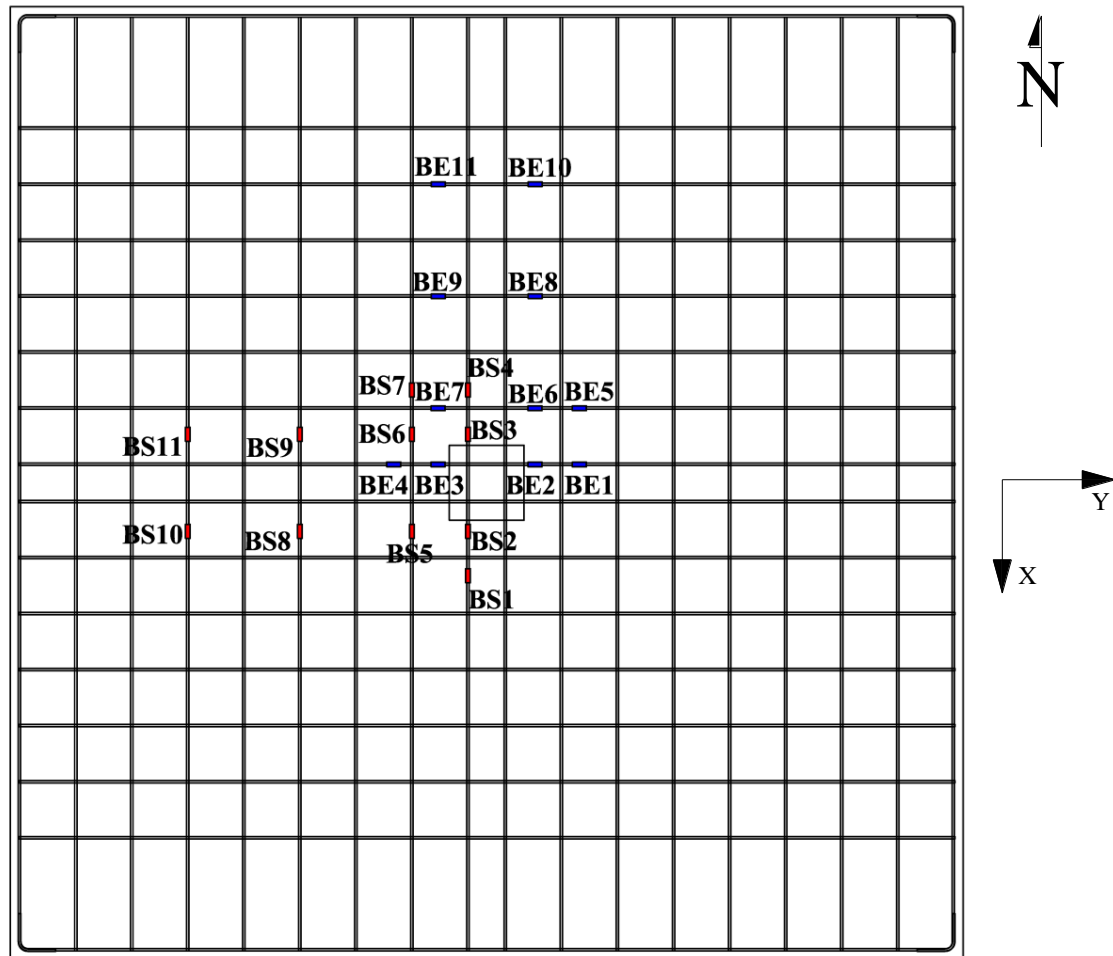
Figure 2-15: Strain Gauge Locations on Bottom Slab Reinforcing Bars
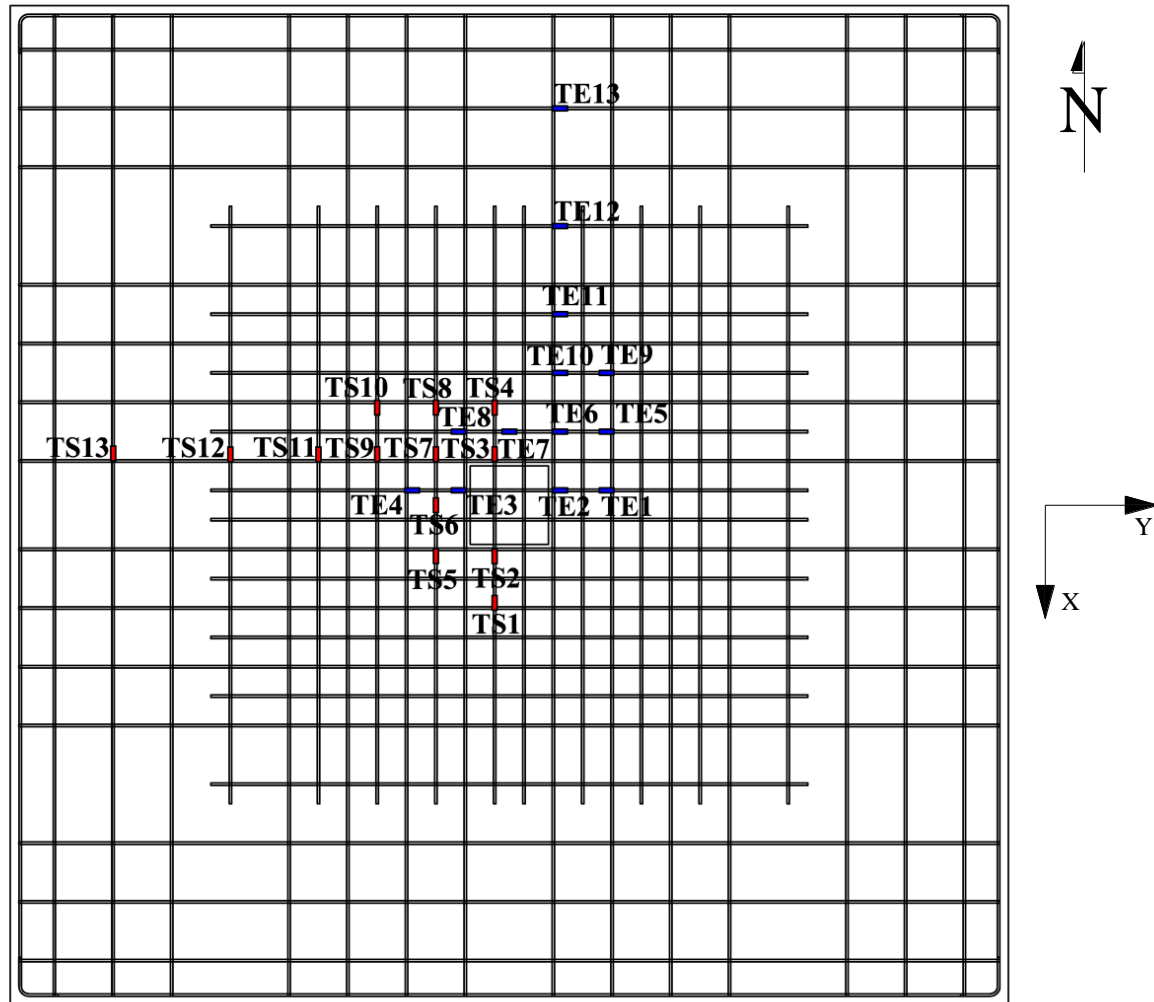
Figure 2-16: Strain Gauge Locations on Top Slab Reinforcing Bars
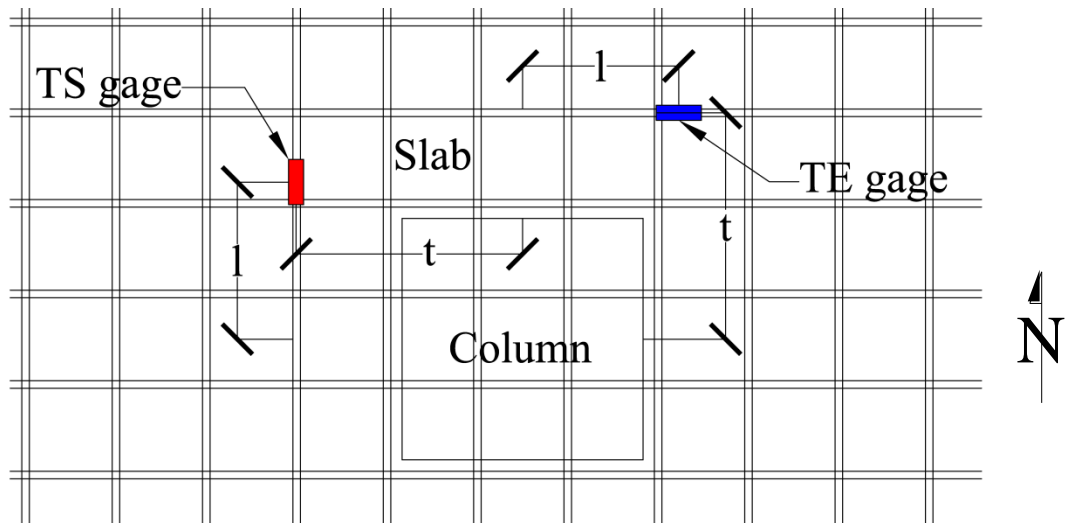
Figure 2-17: Strain Gauge Location Key
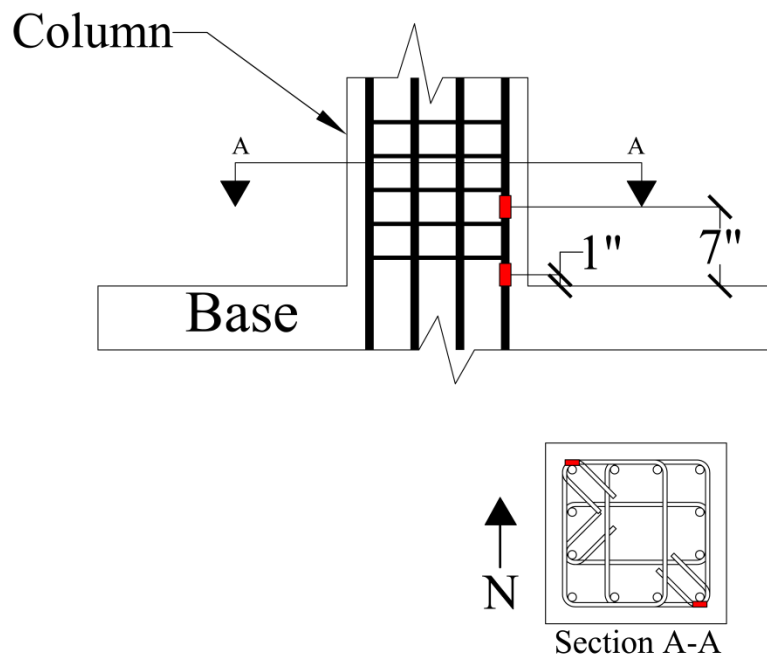
Figure 2-18: Location of Strain Gauges on Longitudinal Column Steel
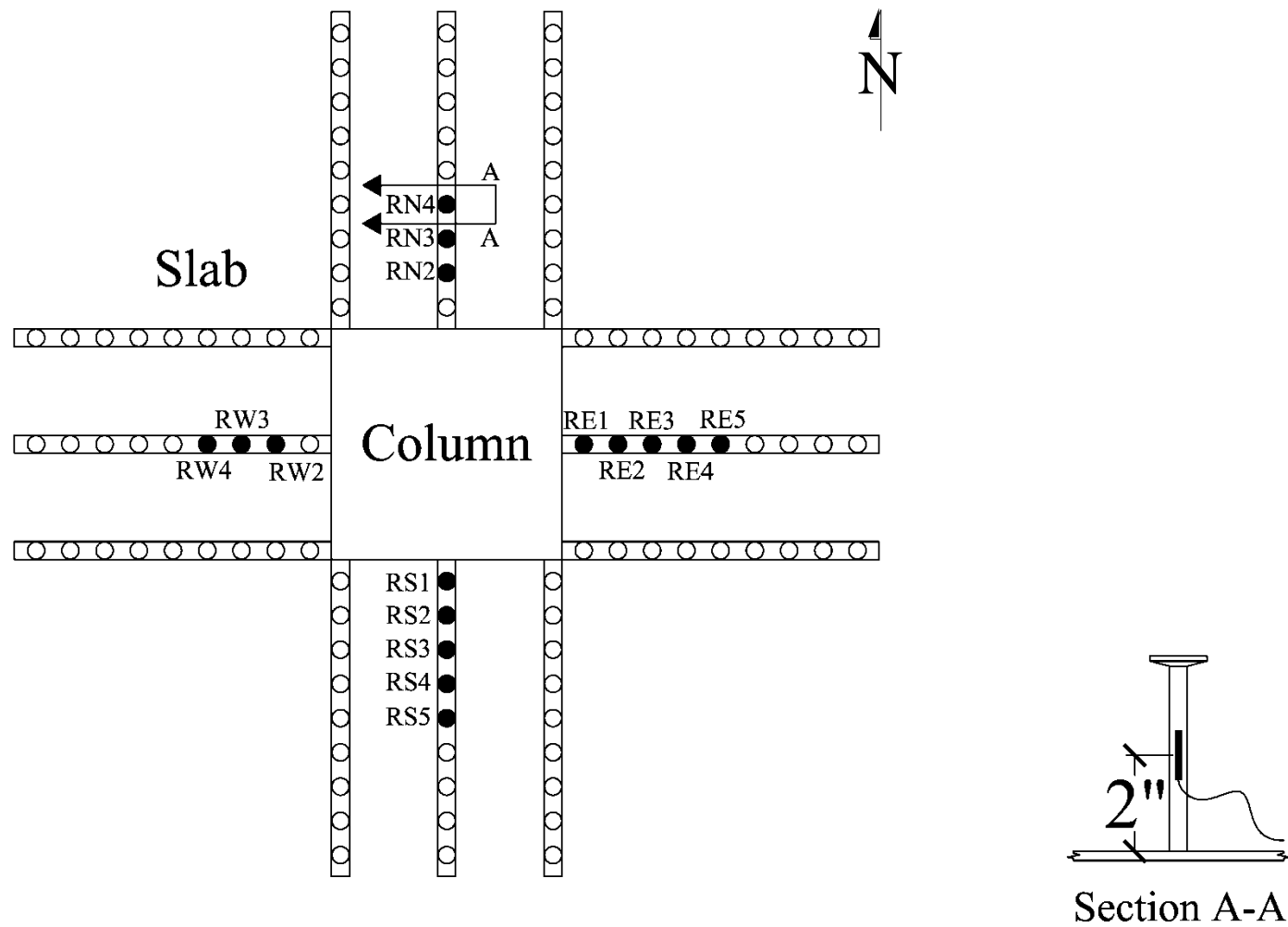
Figure 2-19: Specimen B1 Strain Gauge Layout for Shear Studs

133
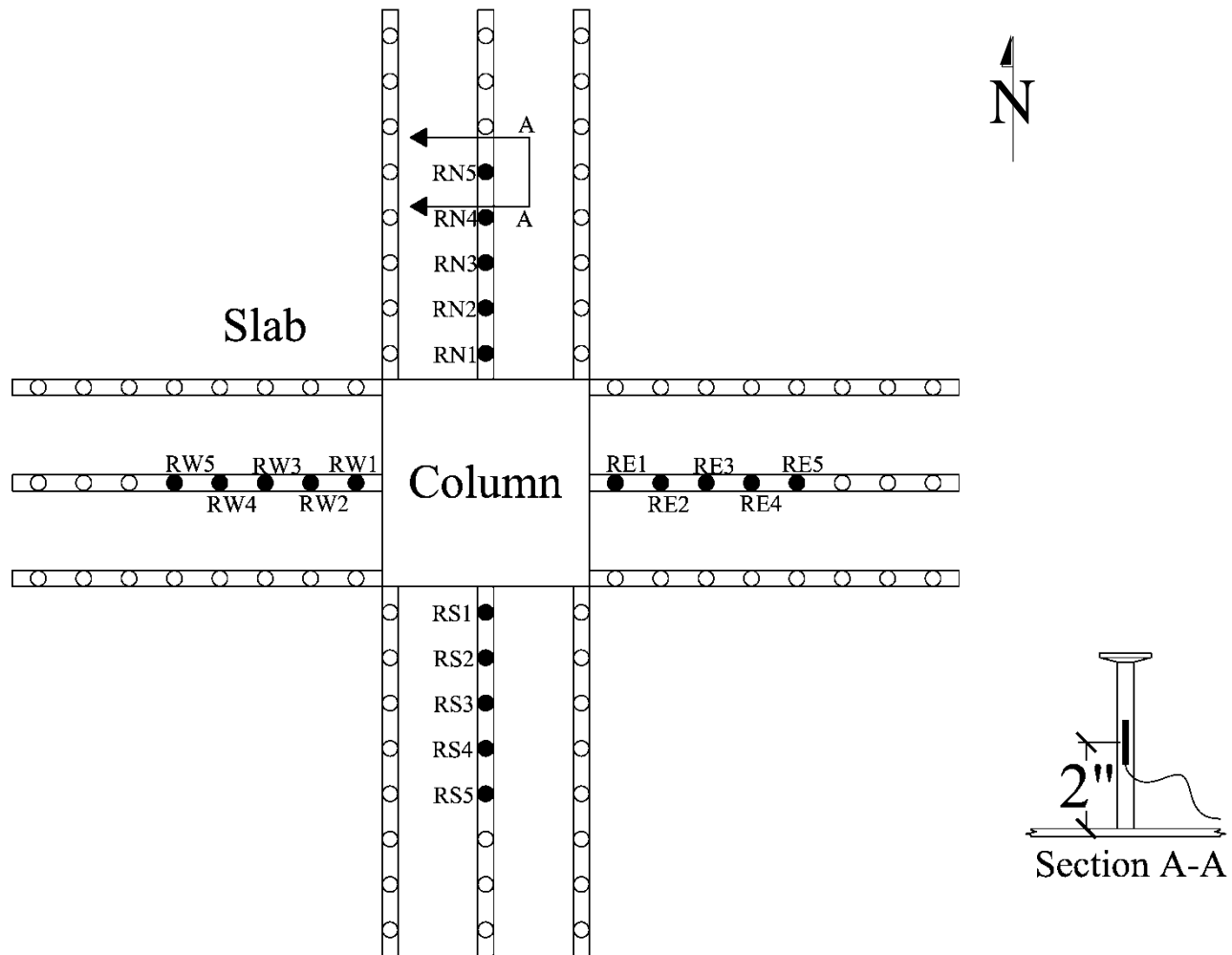
Figure 2-20: Specimen B2 Strain Gauge Layout for Shear Studs
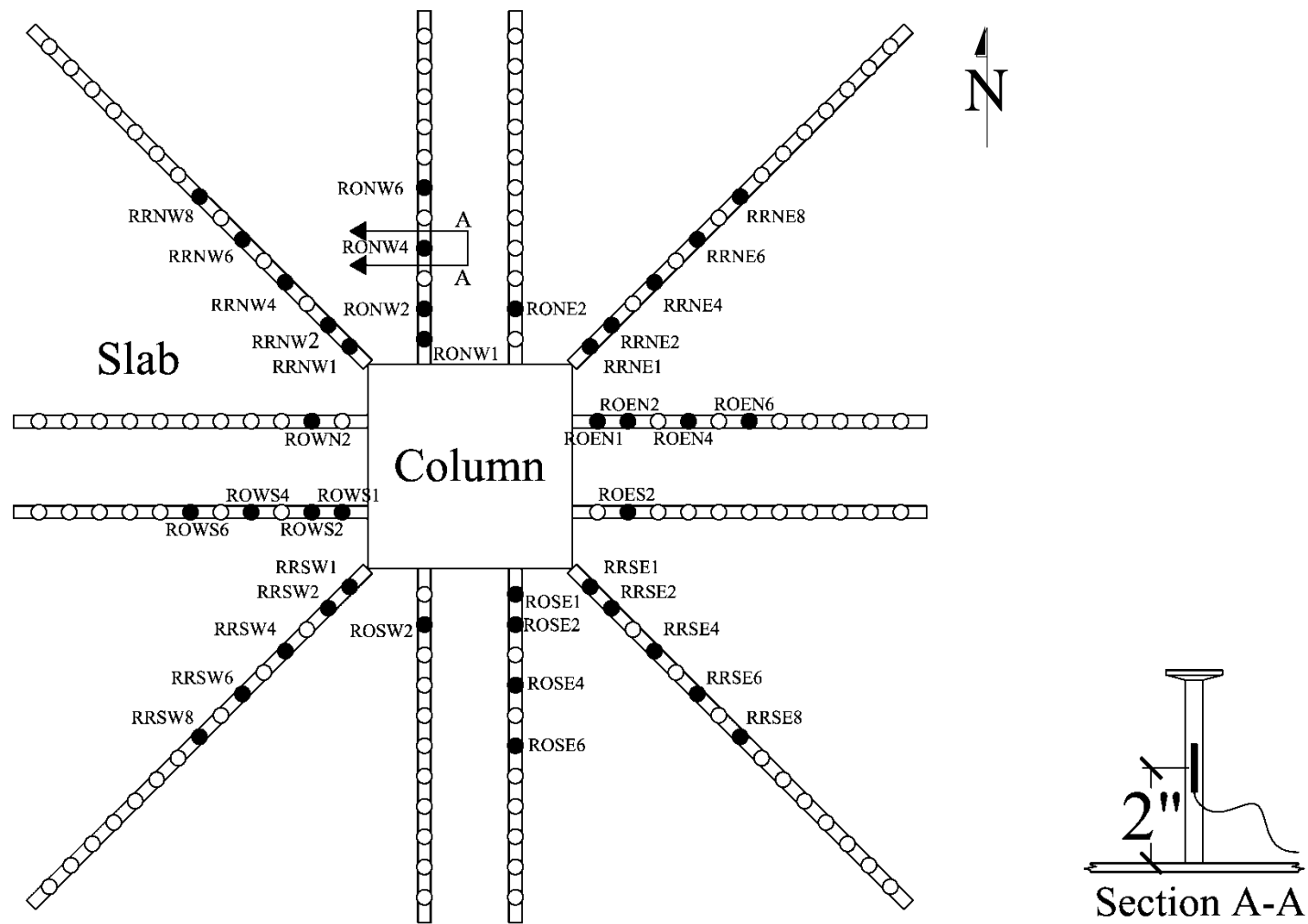
Figure 2-21: Specimen B3 Strain Gauge Layout for Shear Studs

135
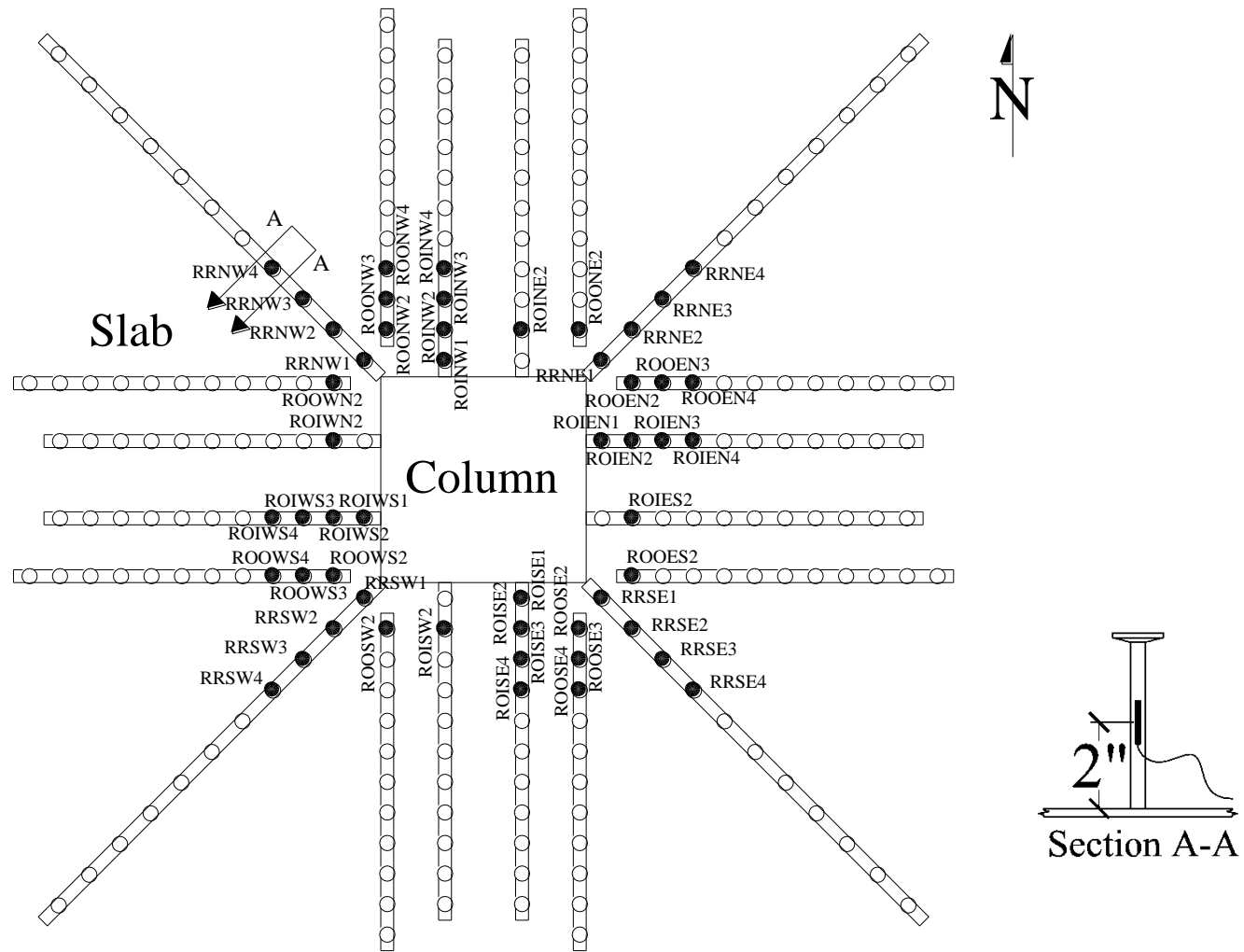
Figure 2-22: Specimen B4 Strain Gauge Layout for Shear Studs

LVDTs for Measuring
Slab Deformations

A

Column

A

5.5 in.

9.5 in.
(2.0d)

Slab

4.75 in. (1.0d)

3.0 in.

LVDTs for Measuring
Vertical Slab Settlement

B

B

a) Elevation View

Figure 2-23: LVDT Locations in Slab Region

137
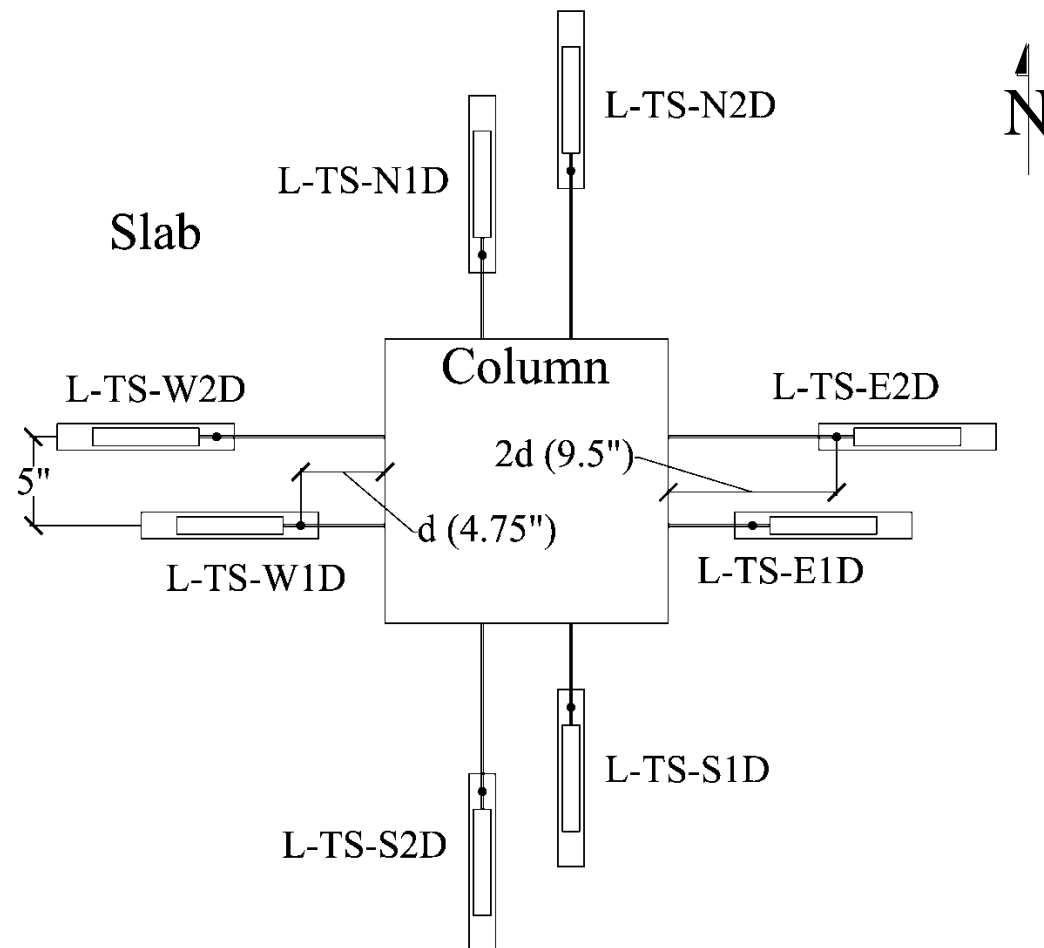
b) Section A-A

Figure 3-24: LVDT Locations in Slab Region
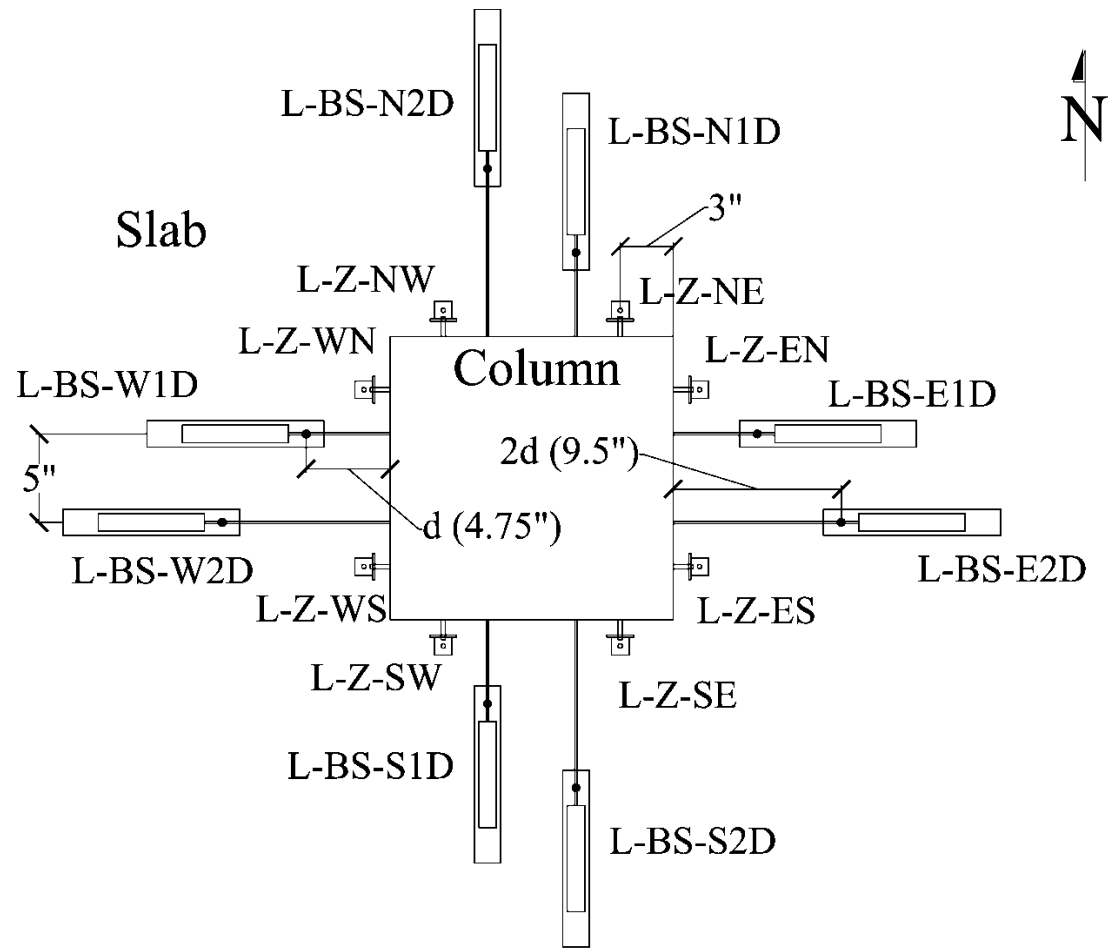
c) Section B-B

Figure 3-24: LVDT Locations in Slab Region
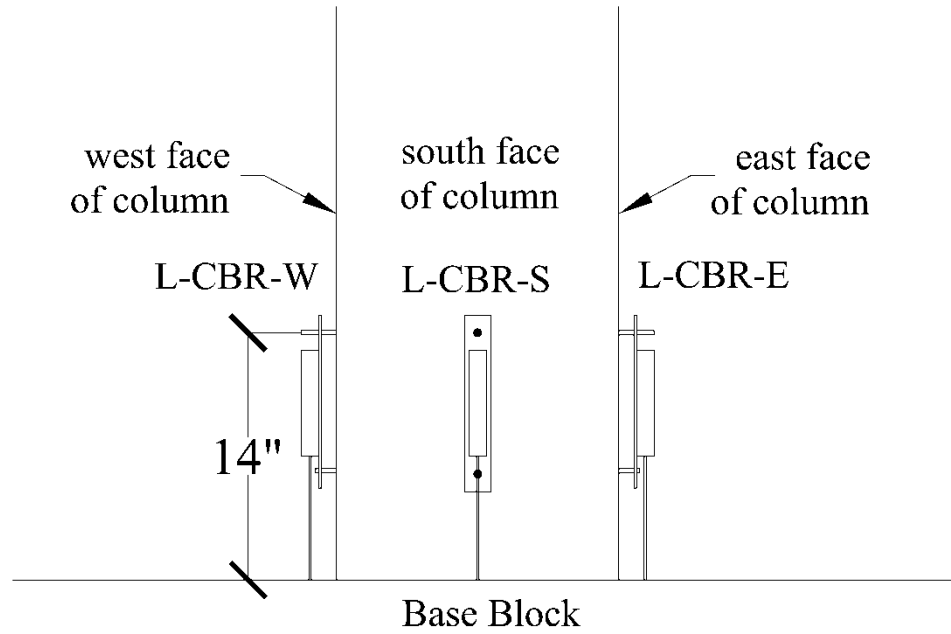
- L-CBR-N located on north face of column in the same location.

Figure 2-24: Column/Base LVDT Locations
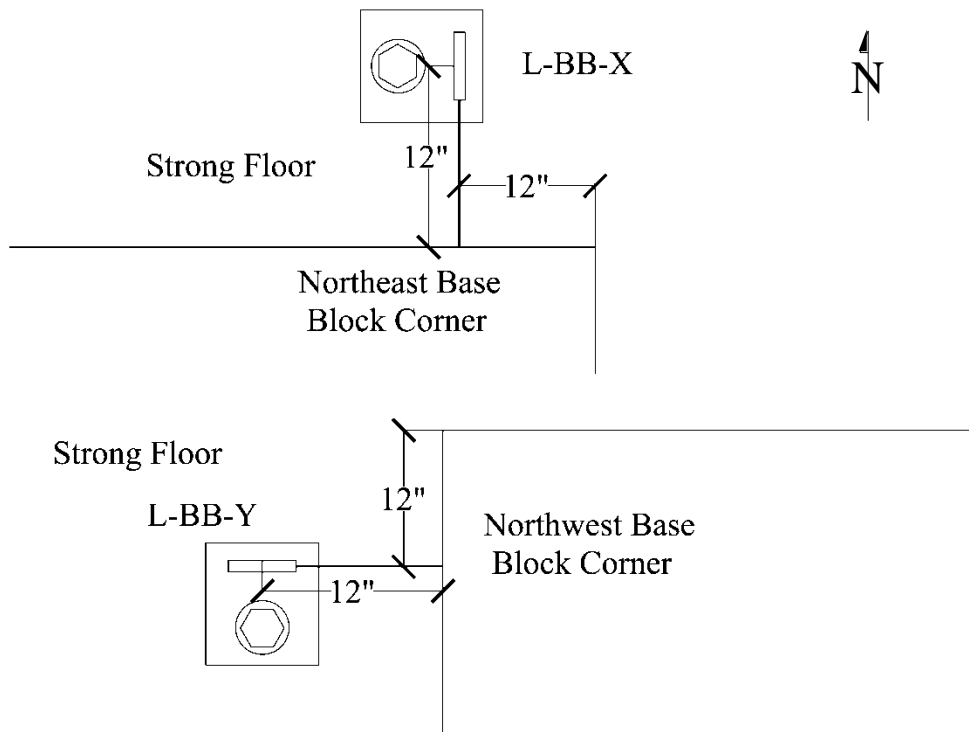
Figure 2-25: Location of LVDTs Measuring Base Block Slippage (As Viewed From Above)

A   A

Strong Wall

3"

String Potentiometer

158"

Strong Wall

Y

X

SPX1   SPX2

N

SPY1

Slab

SPY2
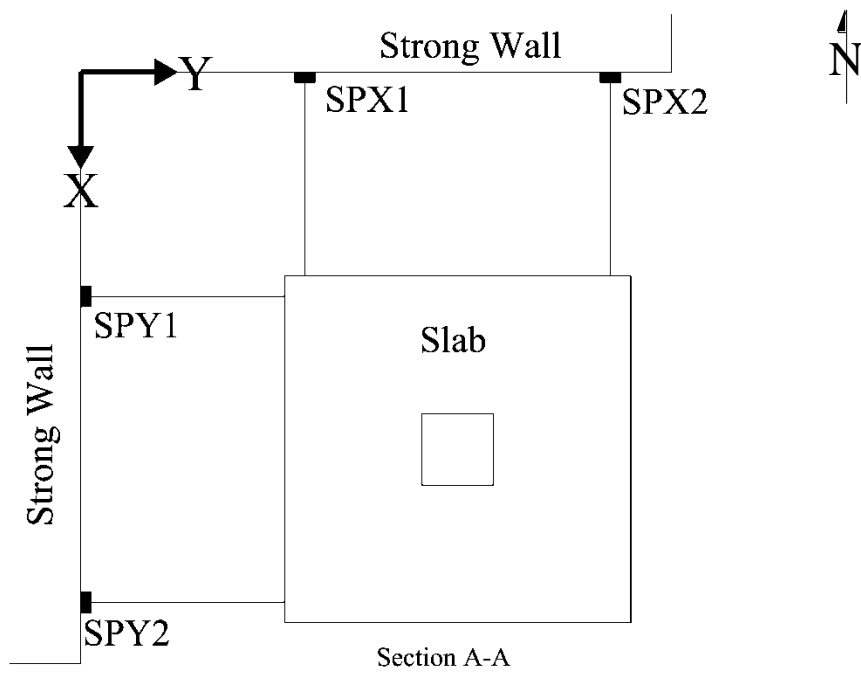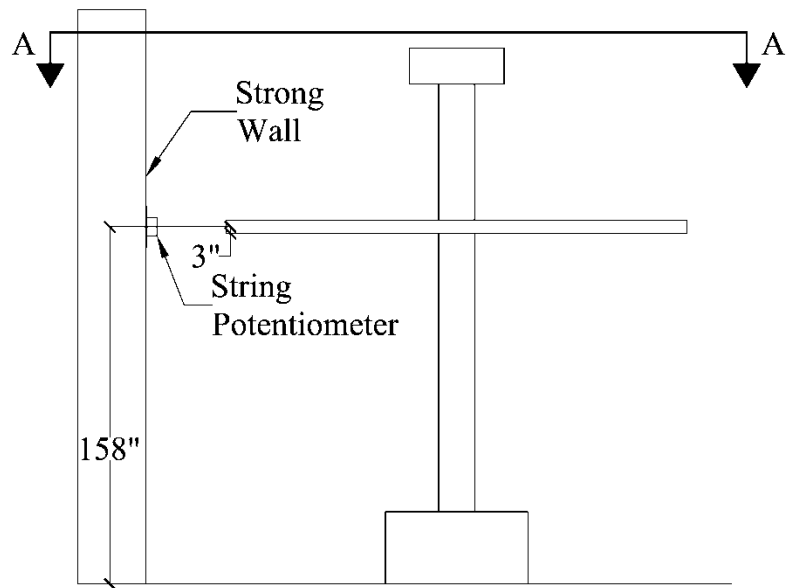
Section A-A

String Potentiometers Were Connected To Slab Edge 12" From Nearest Corner

Figure 2-26: String Potentiometer Locations
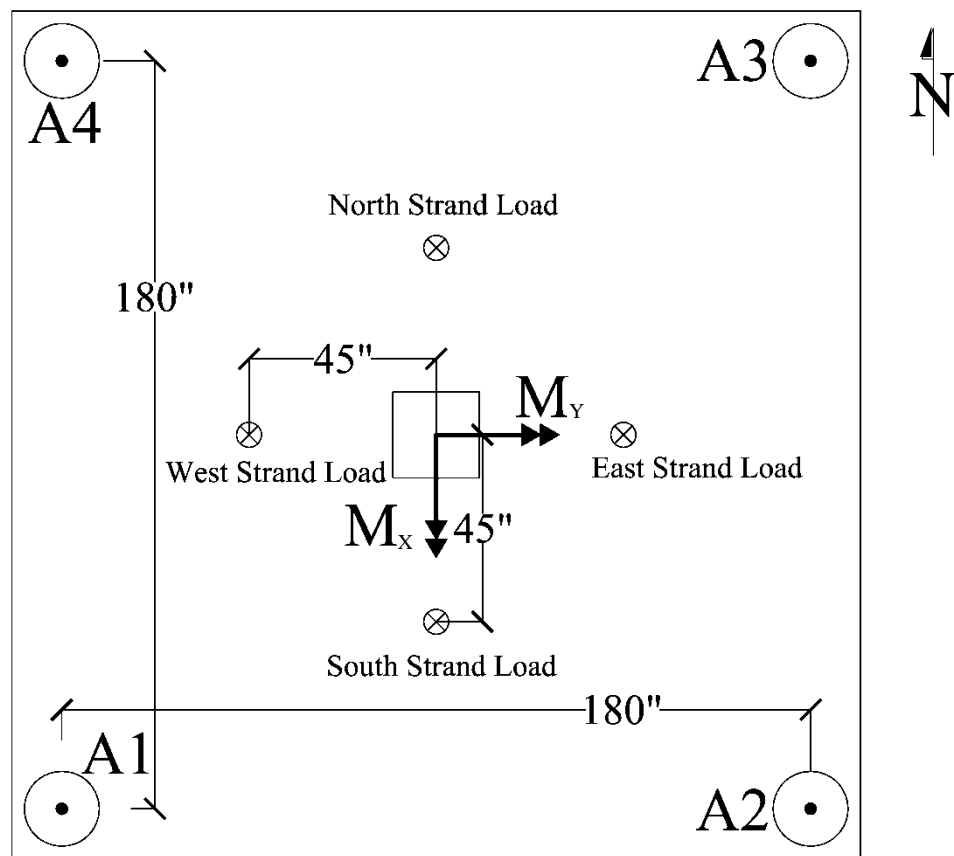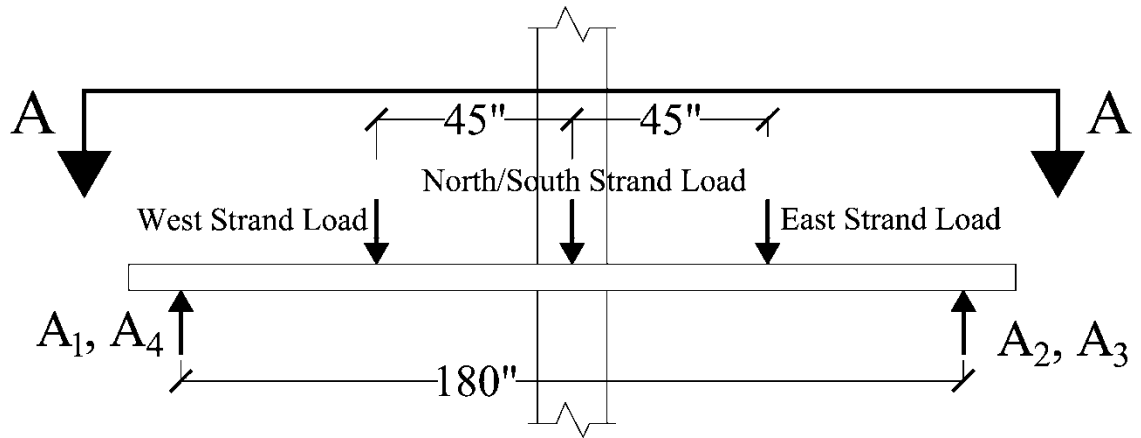
Section A-A

Figure 2-27: External Forces Applied to Slab
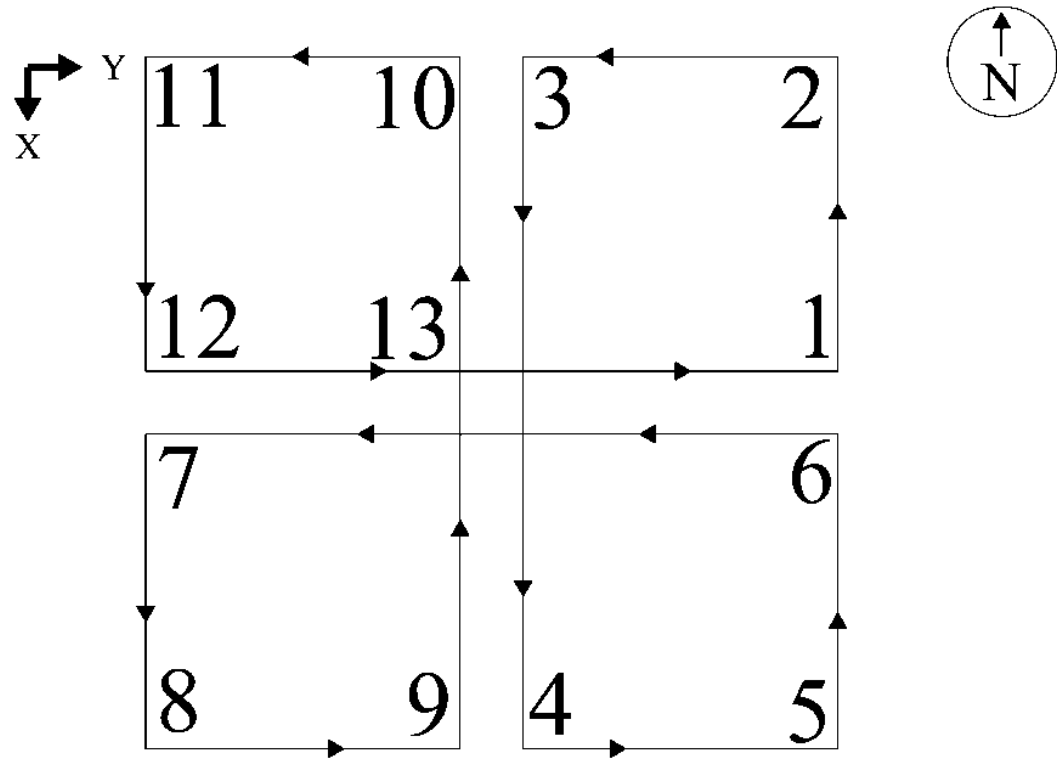
a) Cloverleaf Loading Pattern
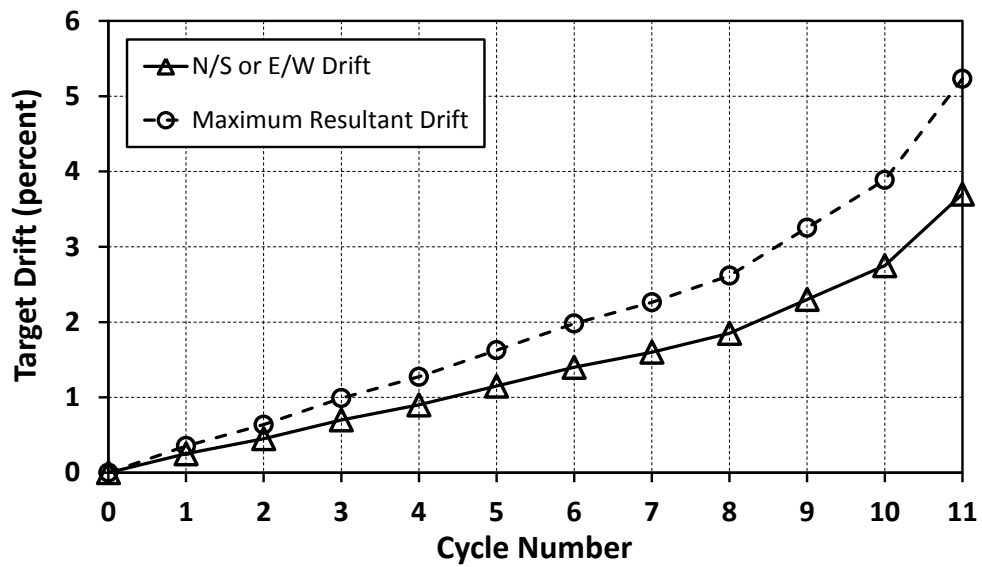
b) Target Drift Level Versus Cycle Number

Figure 2-28: Intended Loading Sequence
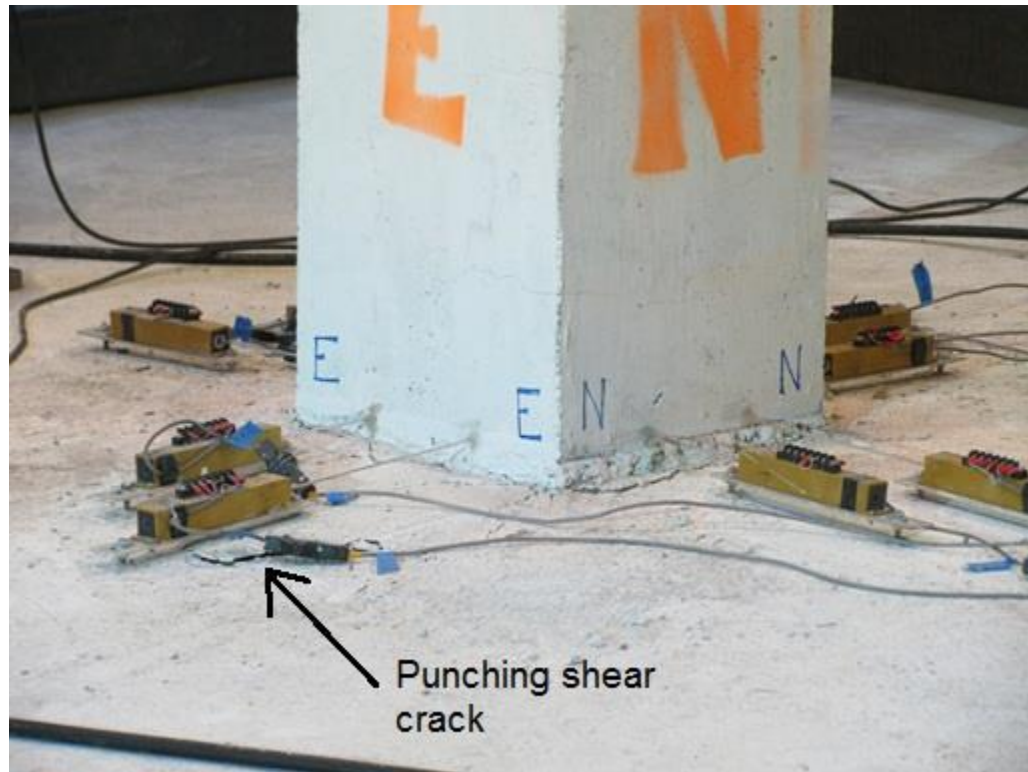
Figure 3-1: Specimen B1 – Initiation of Punching Shear Damage at 1.85% Drift, Point 8
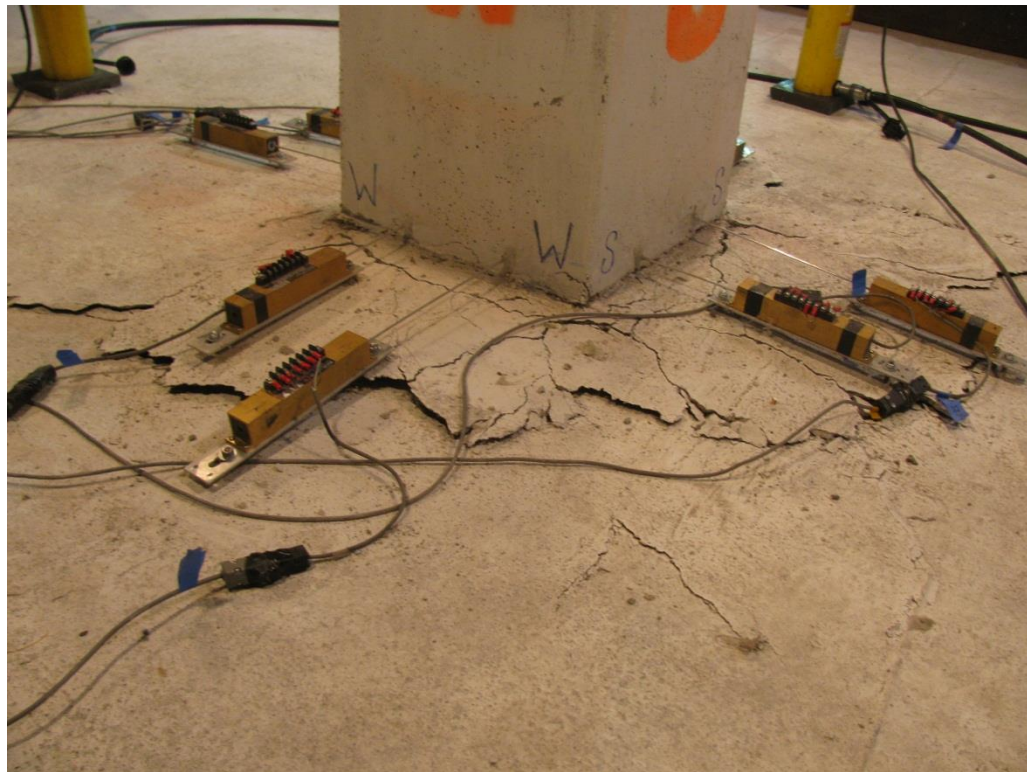
Figure 3-2: Specimen B1 – Connection Damage at 2.30% Drift, Point 4-5

144

Figure 3-3: Specimen B1 – Diagonal, Radial Crack at Northeast Column Corner

Figure 3-4: Specimen B2 – Bottom Surface of Slab-Column Connection Prior to Testing
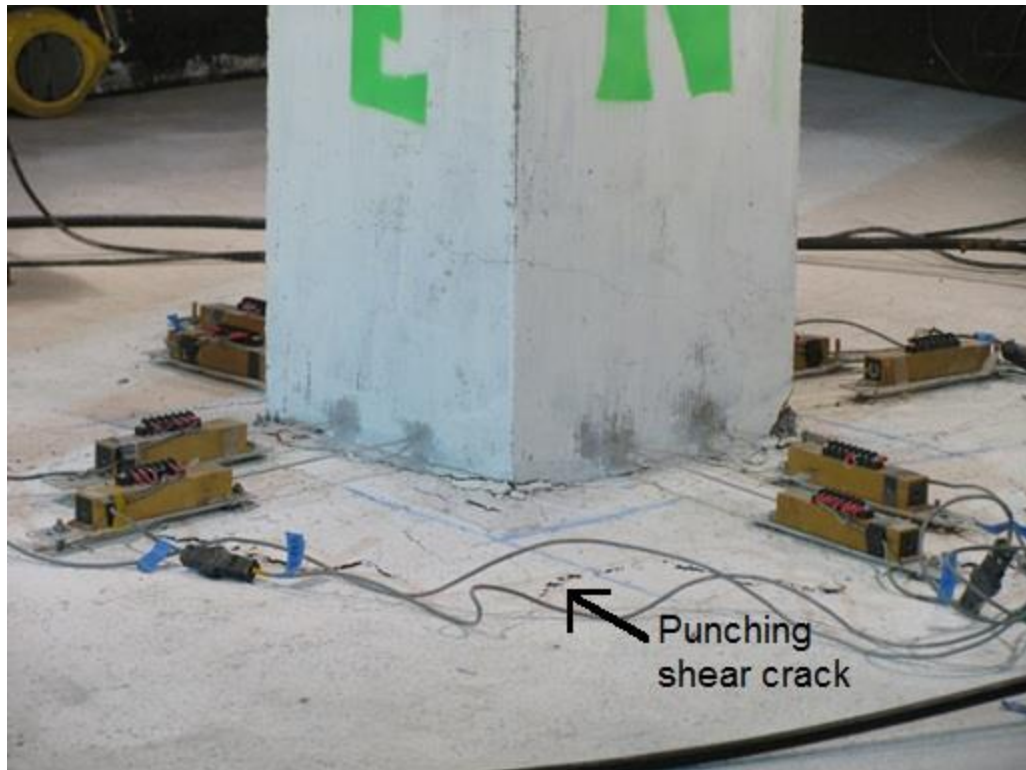
Figure 3-5: Specimen B2 – Initiation of Punching Shear Damage at 1.85% Drift, Point 5
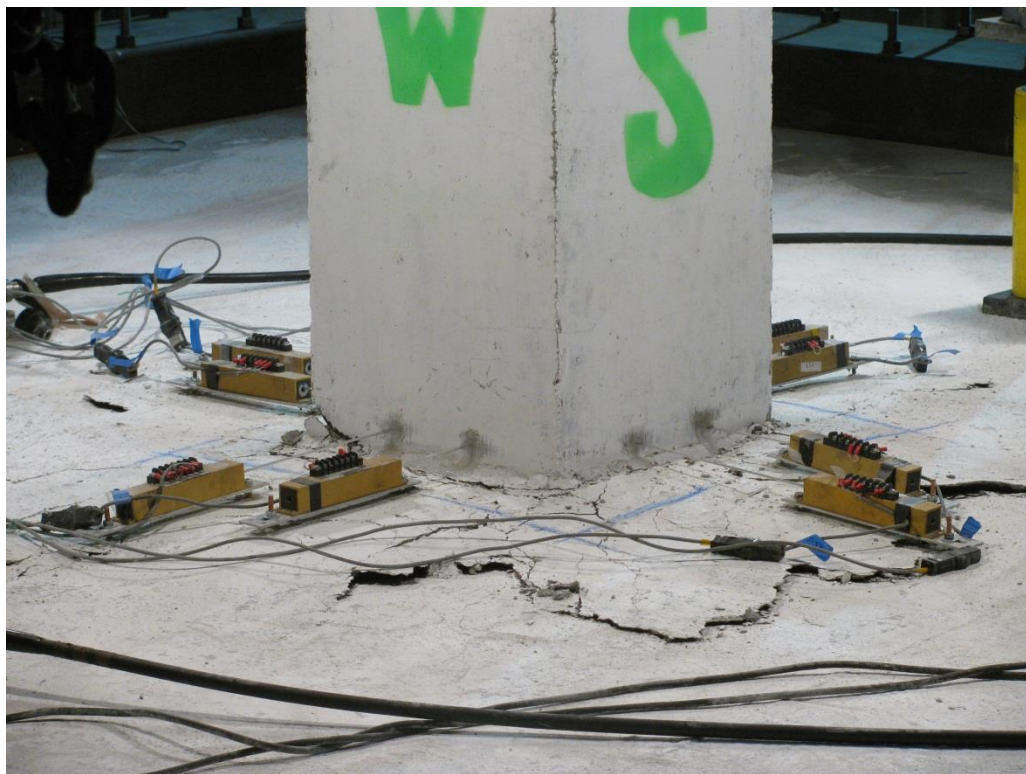
Figure 3-6: Specimen B2 – Connection Damage at 2.30% Drift, Point 1-2
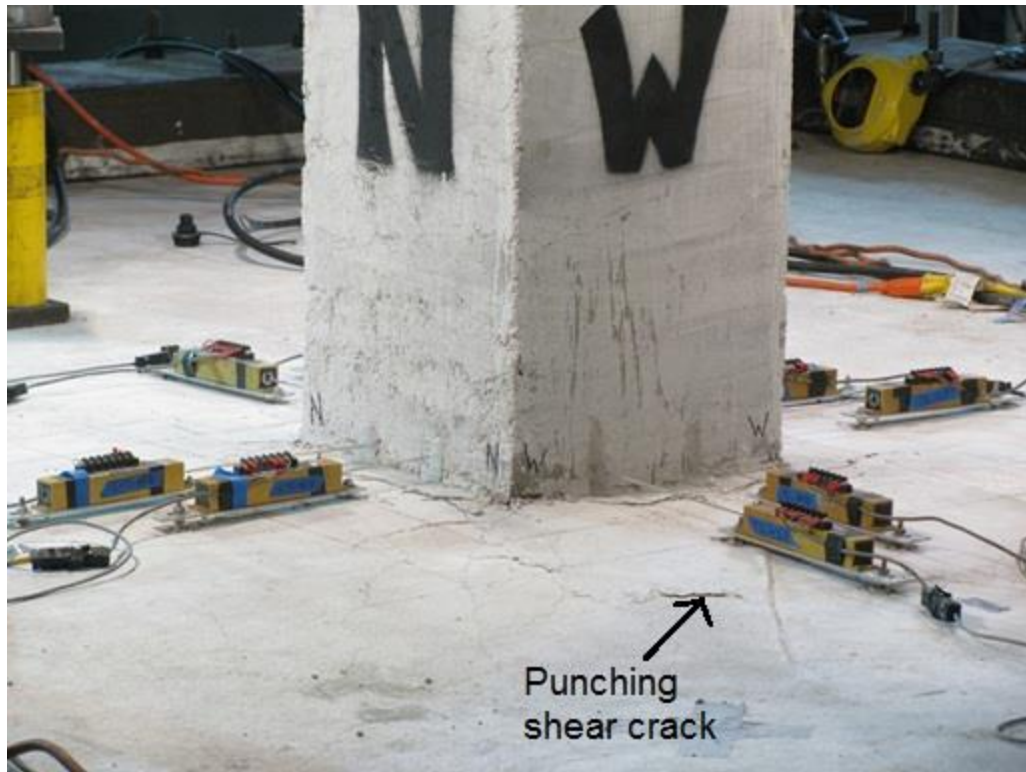
Figure 3-7: Specimen B3 – Initiation of Punching Shear Damage at 1.85% Drift, Point 5

Figure 3-8: Specimen B3 – Connection Damage at 2.30% Drift, Point 1-2
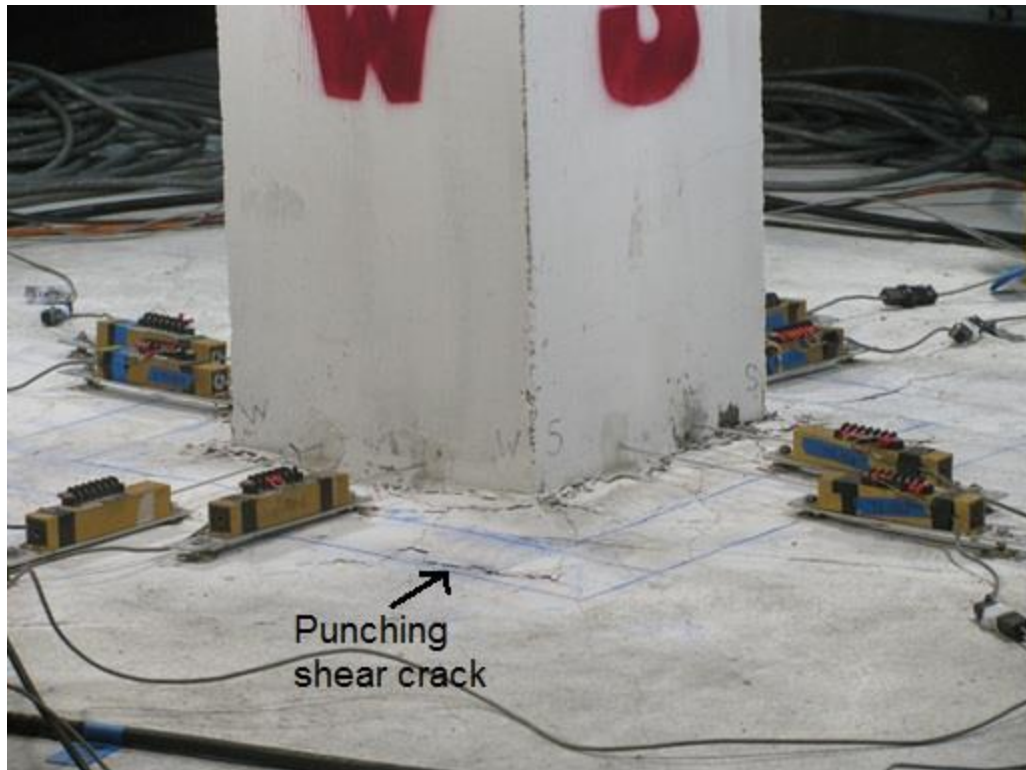
Figure 3-9: Specimen B4 – Initiation of Punching Shear Damage at 1.85% Drift, Point 11

Figure 3-10: Specimen B4 – Connection Damage at 2.30% Drift, Point 8

Gravity Load

A

A

Stiffest Connection Region

B

B

Gravity Load

Gravity Load

Column

Degraded Concrete

Gravity Load

Inclined Crack

North Slab
Piece

45°

Slab Piece
to the South

Cover
Concrete

Section A-A

Degraded Concrete

Solid Concrete in
North Piece of Slab

Degraded Concrete

Slab Piece to
the South

Column

Integrity Steel

Slab Piece to
the South
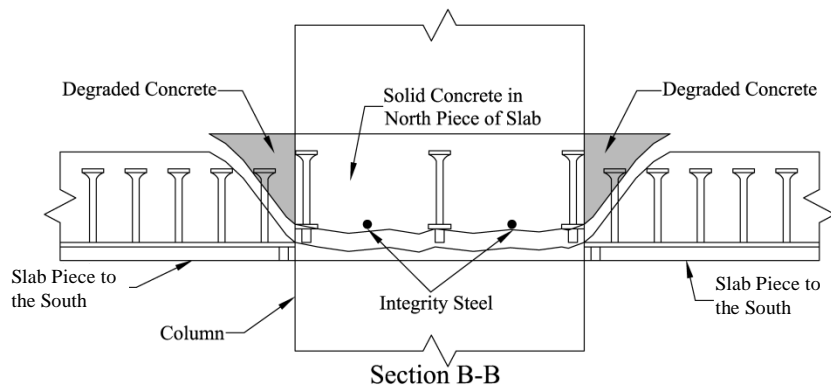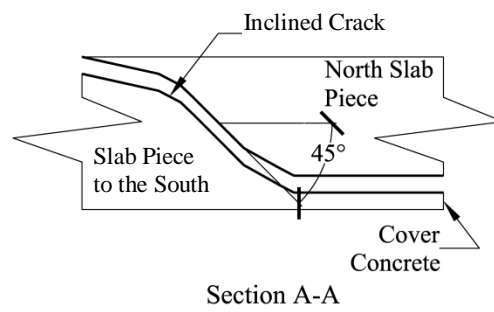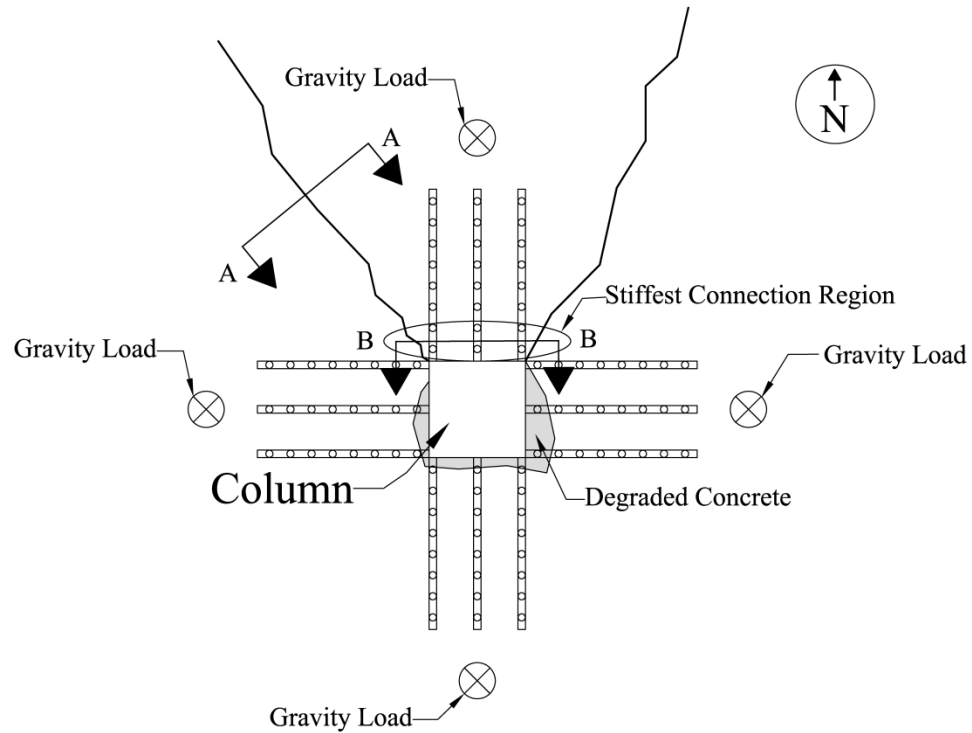
Section B-B

Figure 3-11: Failure Surface of Connection B1

Figure 3-12: Specimen B1 – Bottom View of North-East Corner of Slab-Column Connection After Test

Figure 3-13: Specimen B1 – Void in Connection Region on East and South Faces of Connection After Test

Figure 3-14: Specimen B1 – Sound Concrete on North Face of Connection After Test
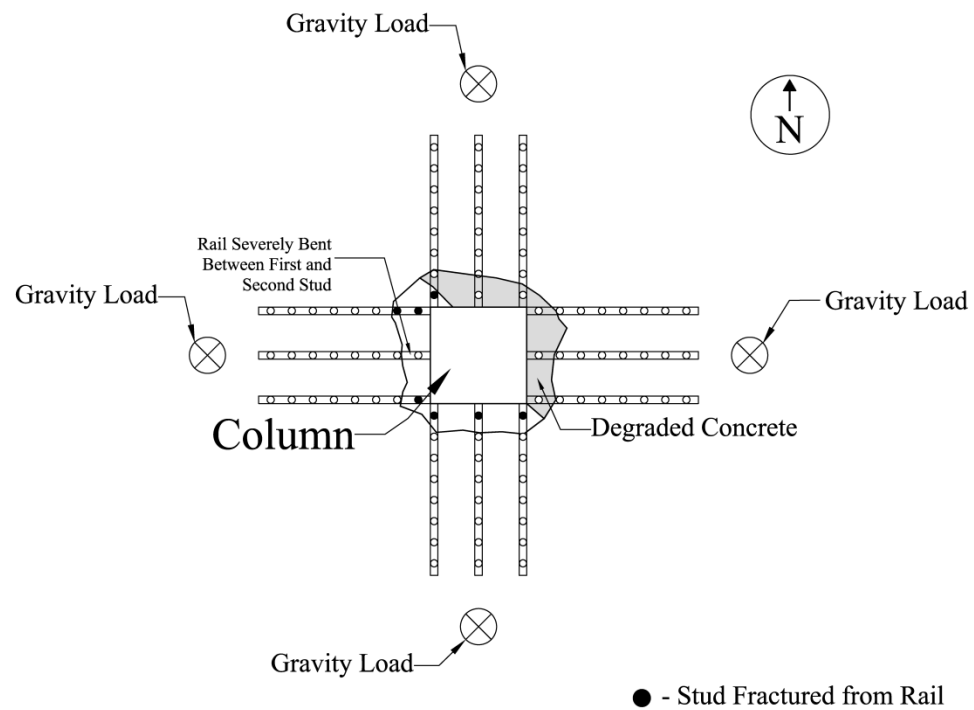
Figure 3-15: Schematic of Specimen B2 Failure Surface

151

Figure 3-16: Specimen B2 – Connection Region where Severely Degraded Concrete was Removed by Hand After Test

Studs fractured from base rail at weld

Rails dowel between first and second row of studs
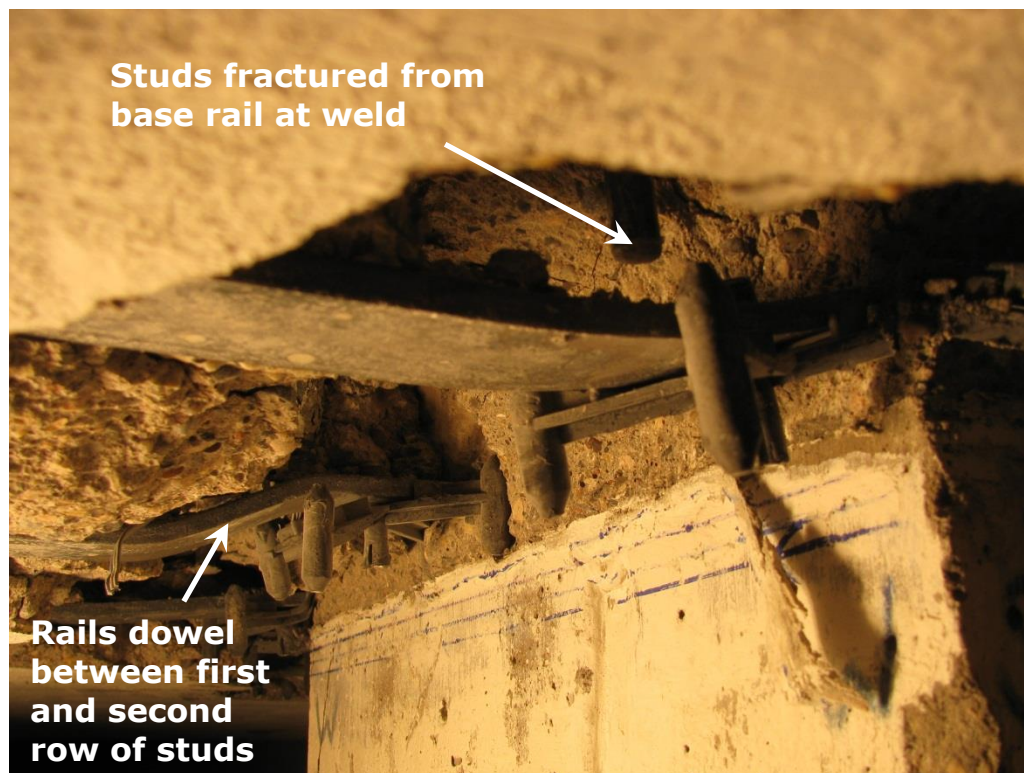
Figure 3-17: Specimen B2 – Stud Weld Fracture and Dowel Action in Rails

Figure 3-18: Specimen B3 – Void in Connection Region after Loose Concrete was Removed After Test

Figure 3-19: Specimen B3 – Bending of Base Rail between First and Second Shear Stud

Figure 3-20: Specimen B4 – Gravel-Like Concrete within Connection Region

Figure 3-21: Specimen B4 – Void in Connection Region after Loose Concrete was Removed After Test

Figure 3-22: Specimen B4 – Bending of Base Rail on South-East Face of Column After Test
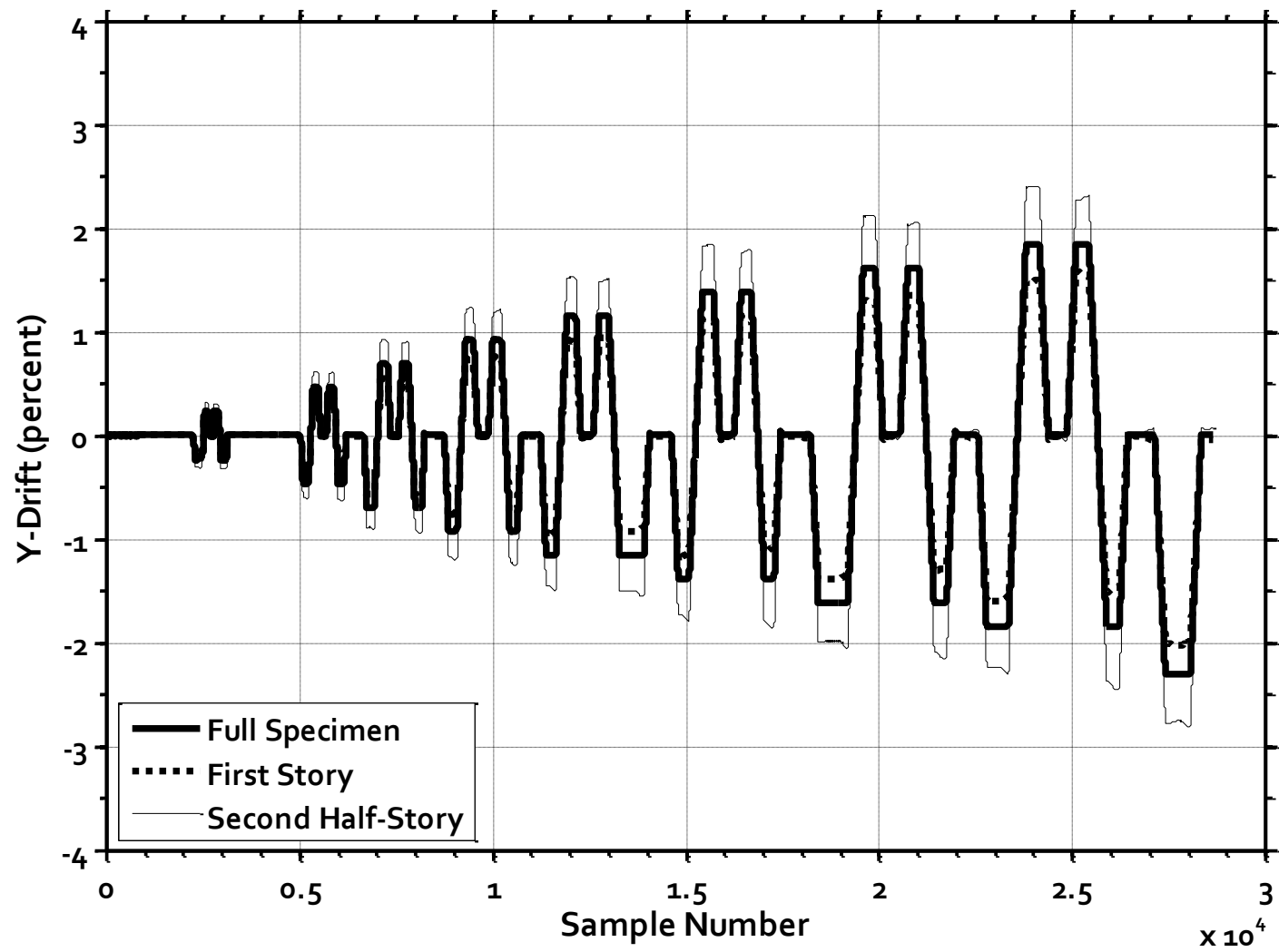
Figure 3-23: Y-Axis Drift for the First Story, Second Half-Story, and Full Specimen of Specimen B2
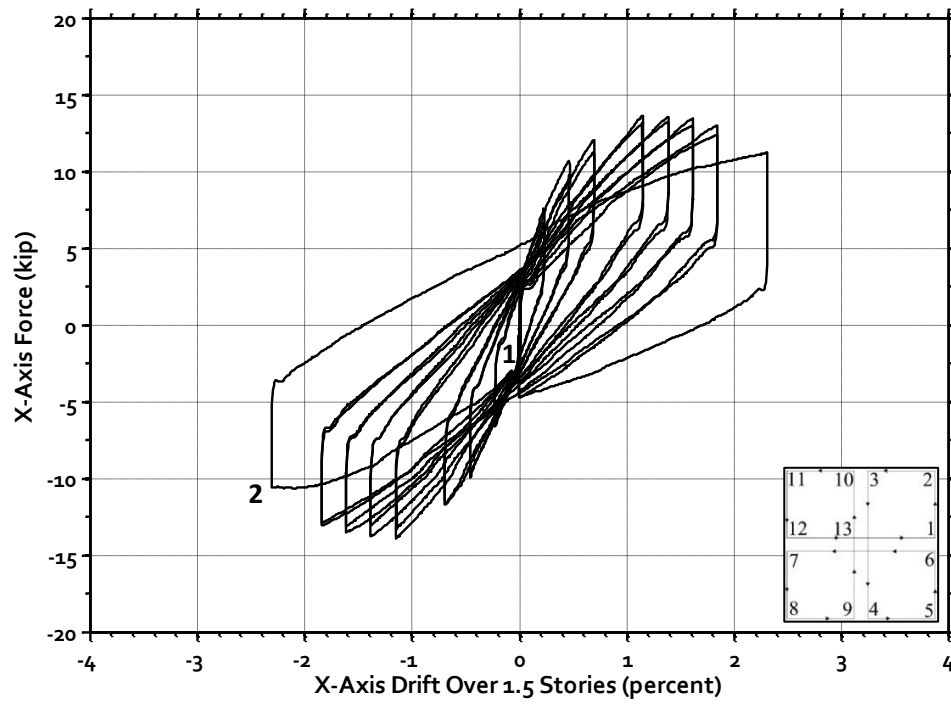
Figure 3-24: Specimen B1 – Load versus Drift Response (X-Direction)
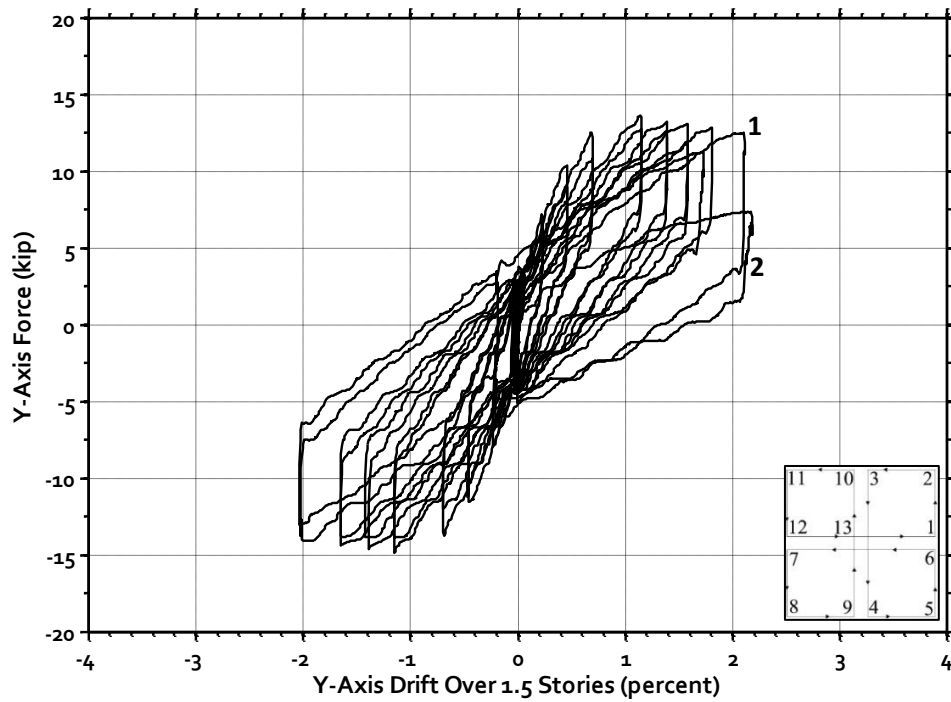
Figure 3-25: Specimen B1 – Load versus Drift Response (Y-Direction)
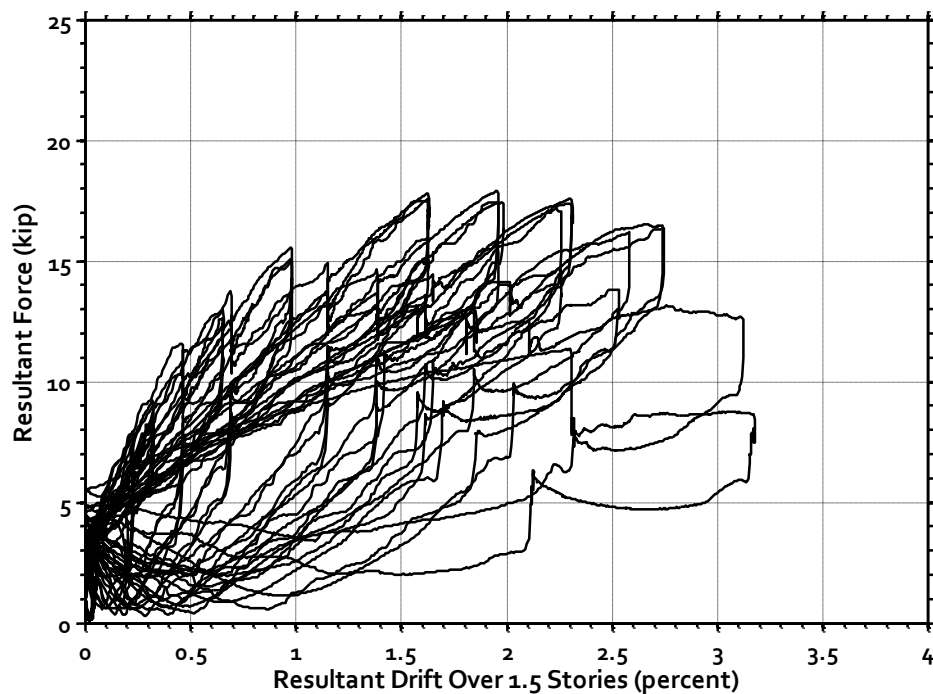
Figure 3-26: Specimen B1 – Resultant Load versus Drift Response
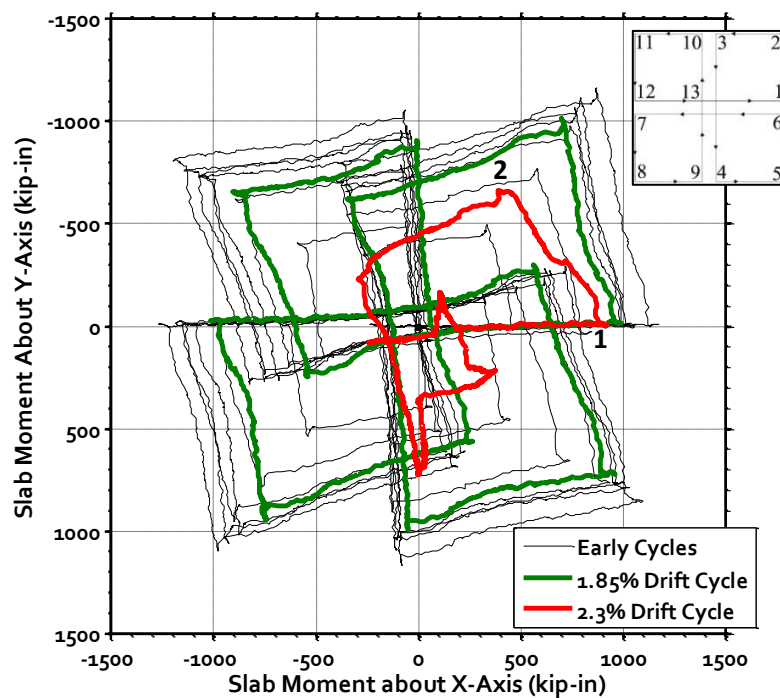
Figure 3-27: Specimen B1 – Relationship Between Moments Transferred into the Column About the X-
and Y-Axes
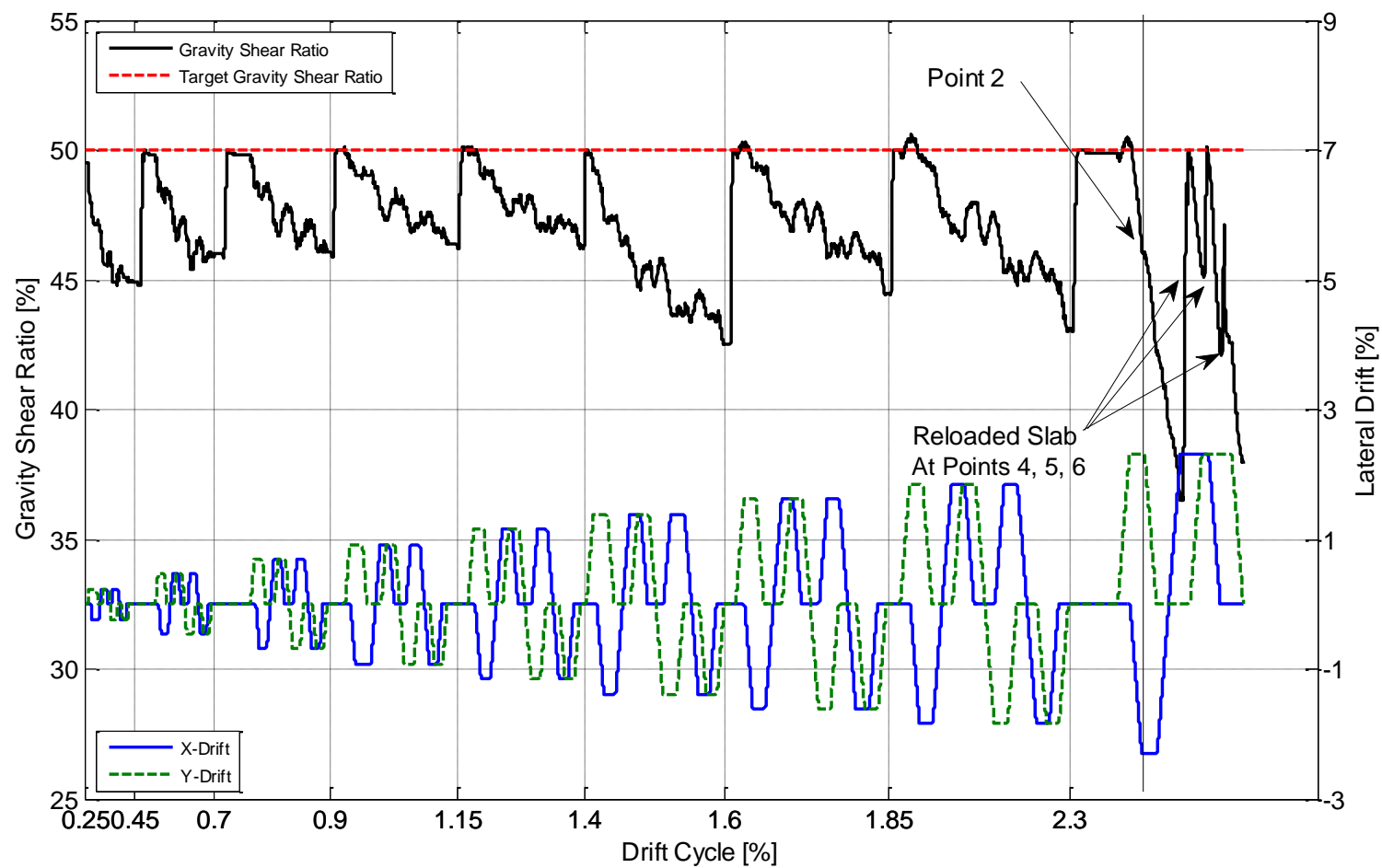
Figure 3-28: Specimen B1 – Gravity Shear History

159
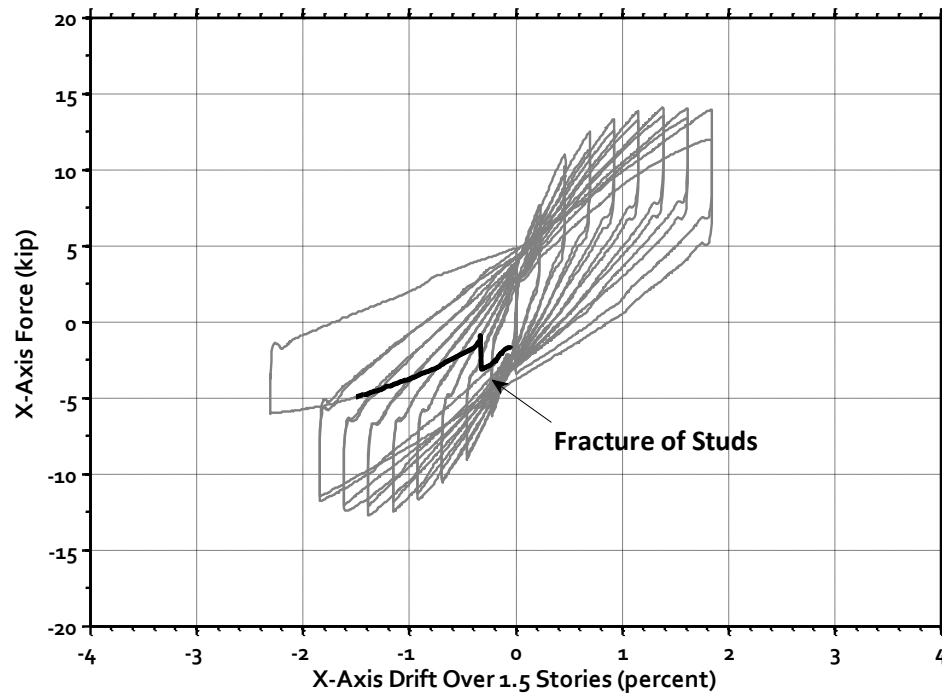
Figure 3-29: Specimen B2 – Load versus Drift Response (X-Direction)
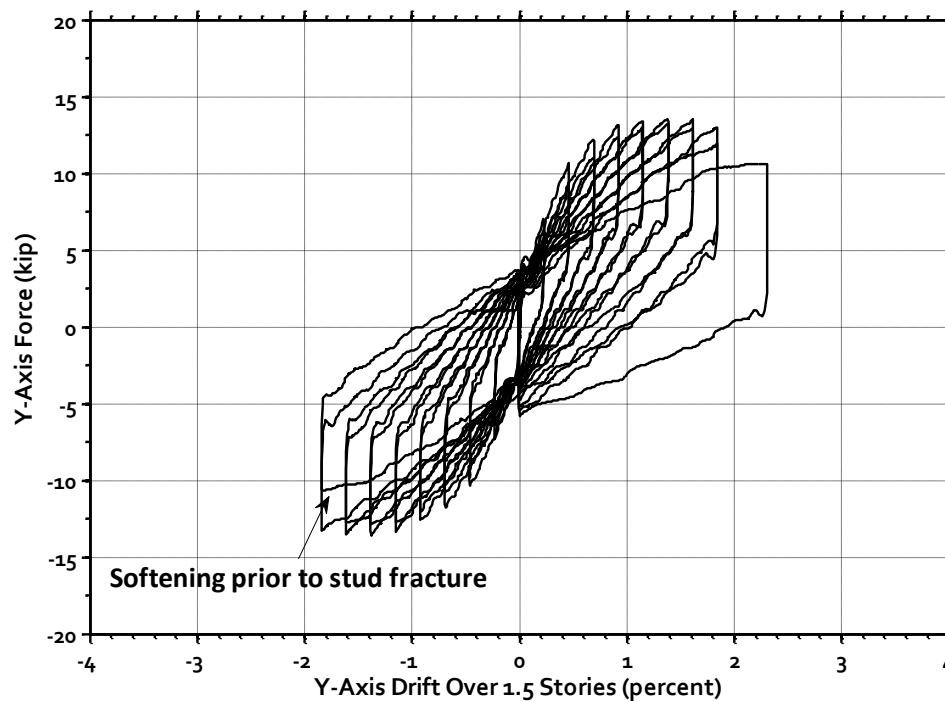
Figure 3-30: Specimen B2 – Load versus Drift Response (Y-Direction)

160
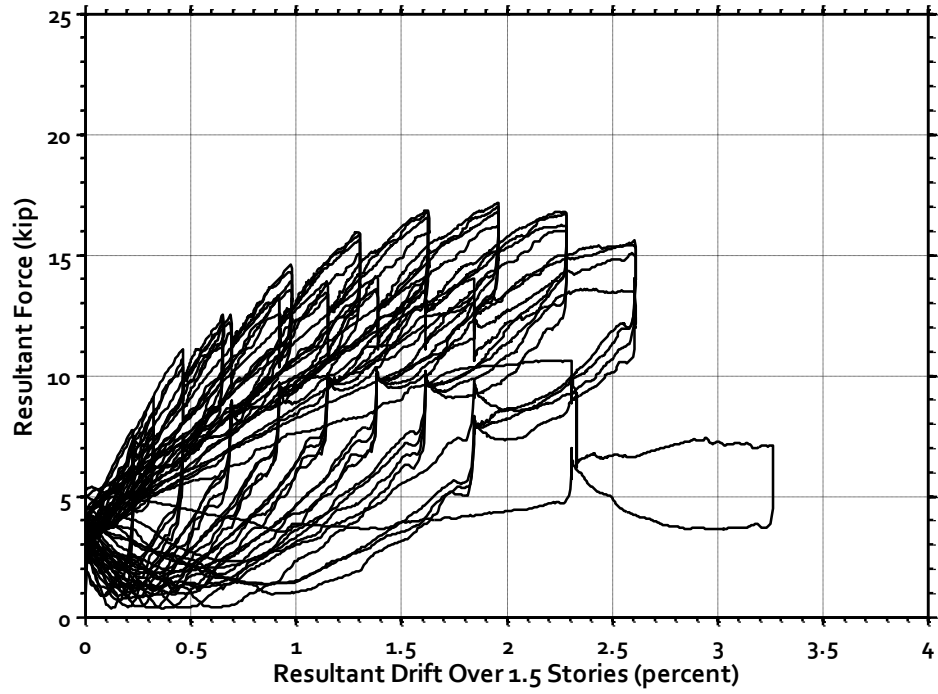
Figure 3-31: Specimen B2 – Resultant Load versus Drift Response
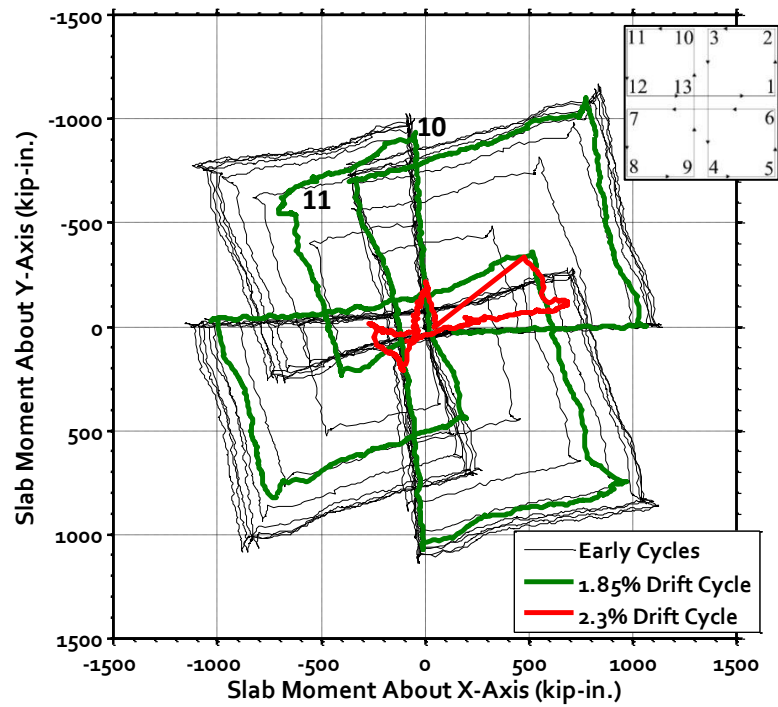
Figure 3-32: Specimen B2 – Relationship Between Moments Transferred into the Column About the X- and Y-Axes

161
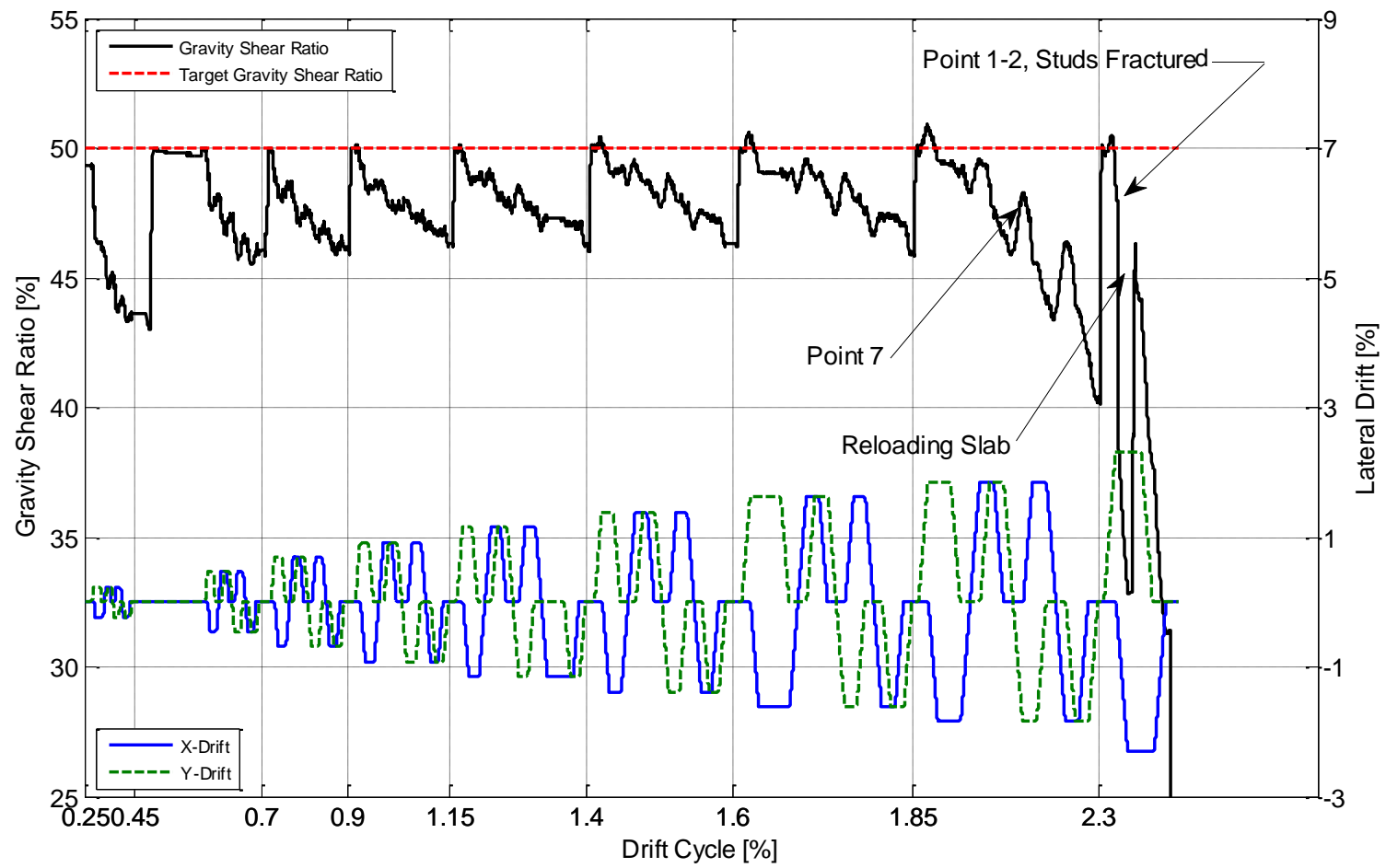
Figure 3-33: Specimen B2 – Gravity Shear History

162
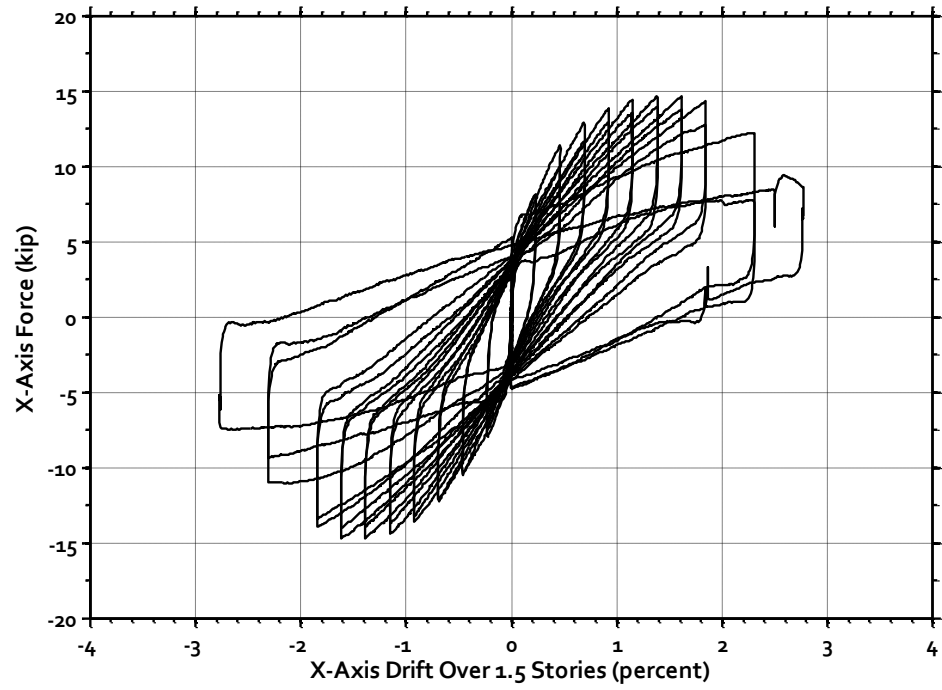
Figure 3-34: Specimen B3 – Load versus Drift Response (X-Direction)
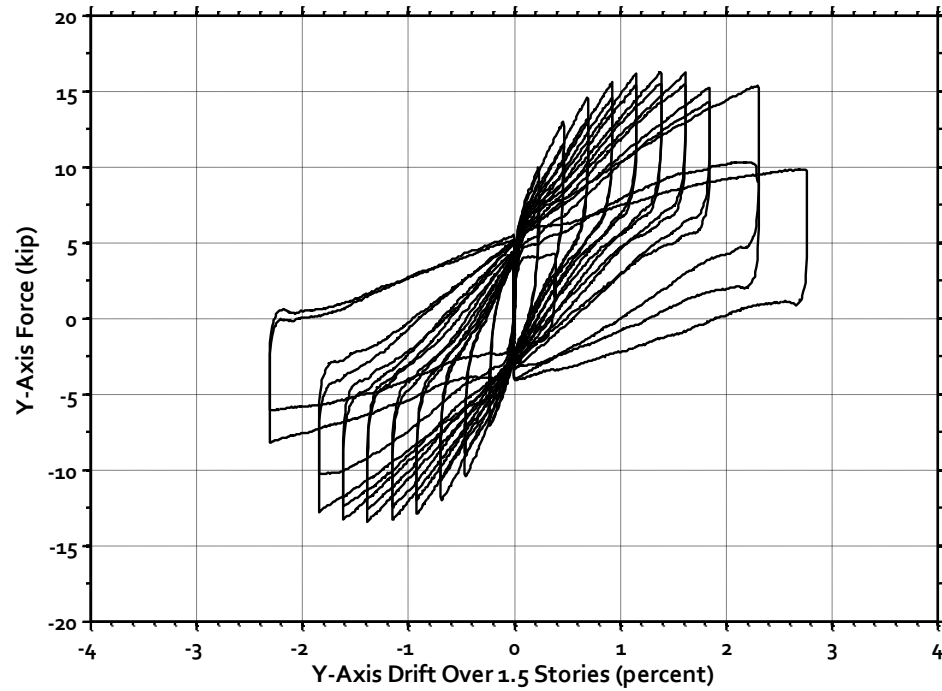
Figure 3-35: Specimen B3 – Load versus Drift Response (Y-Direction)
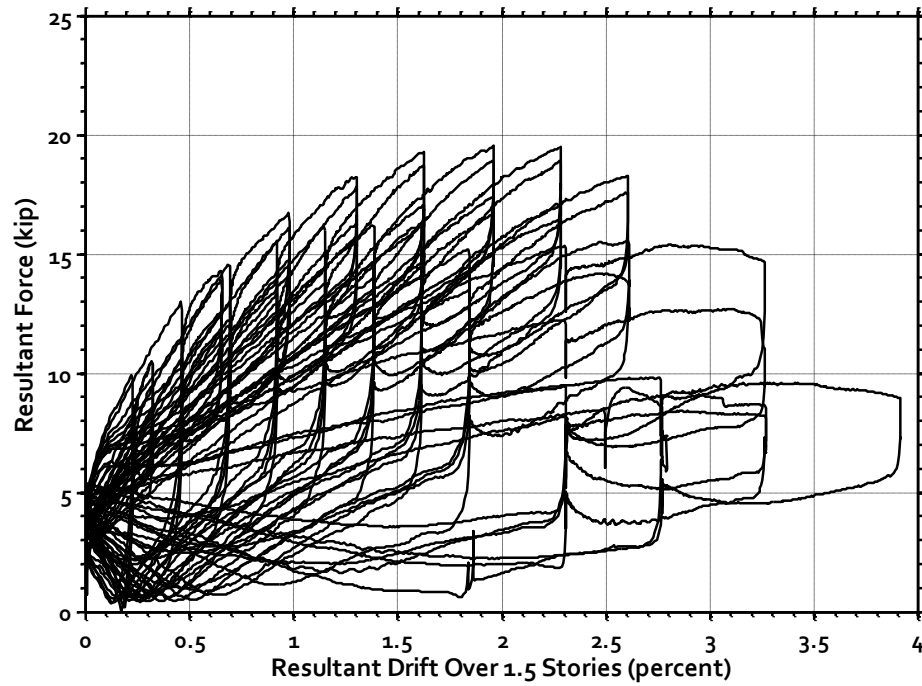
Figure 3-36: Specimen B3 – Resultant Load versus Drift Response
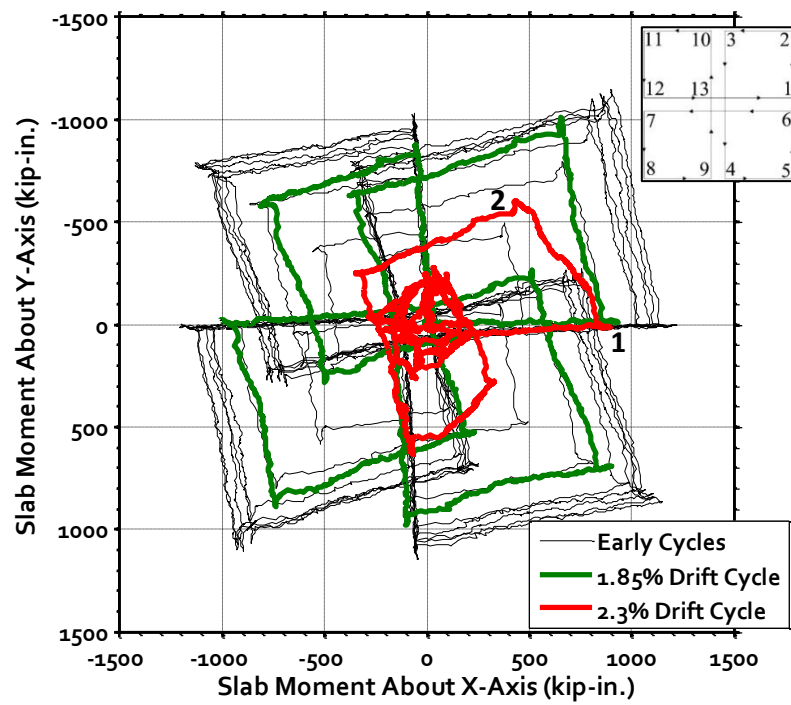
Figure 3-37: Specimen B3 – Relationship Between Moments Transferred into the Column About the X- and Y-Axes
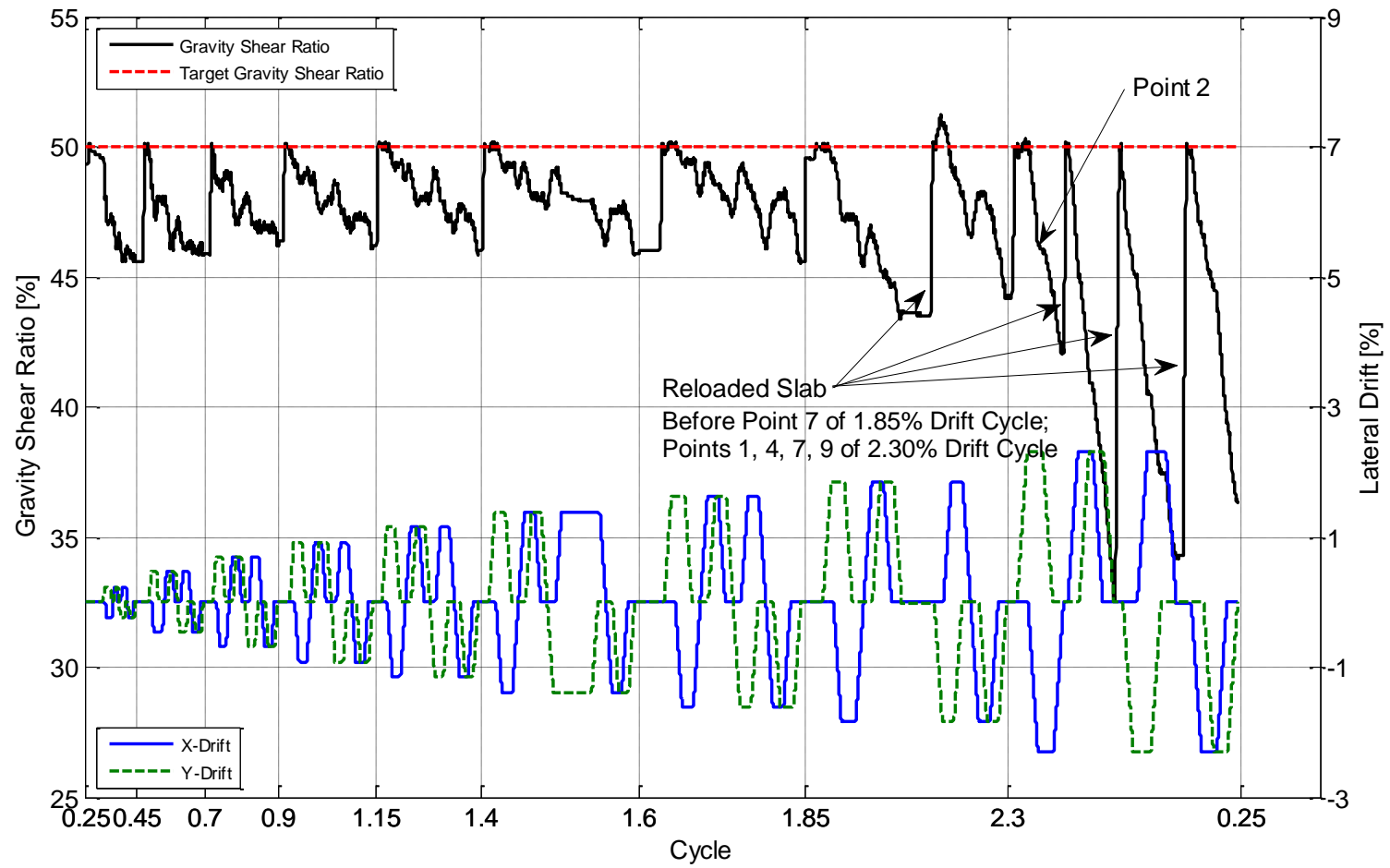
Figure 3-38: Specimen B3 – Gravity Shear History

165
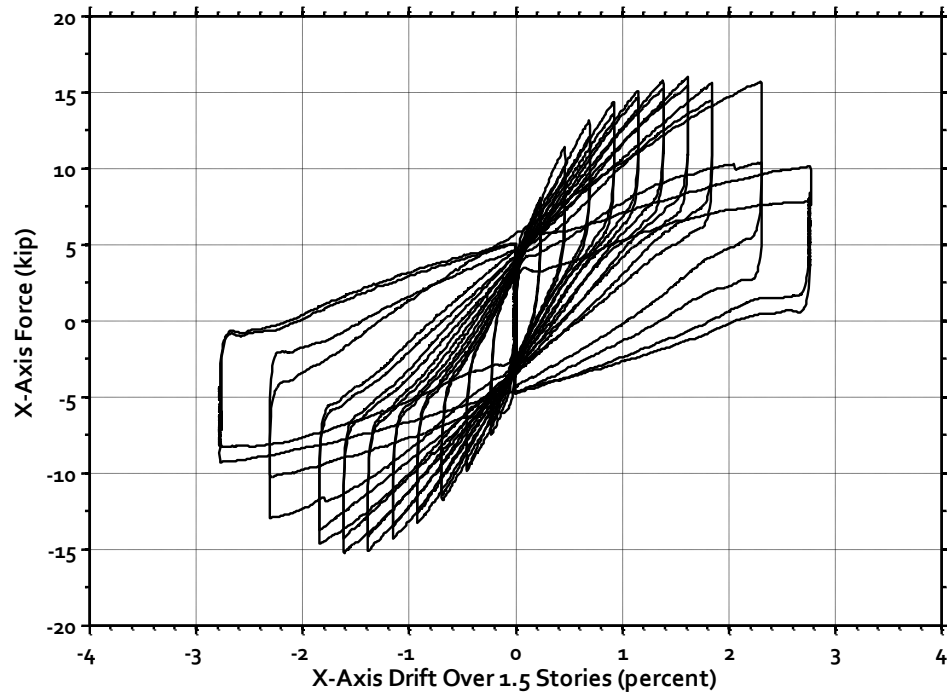
Figure 3-39: Specimen B4 – Load versus Drift Response (X-Direction)
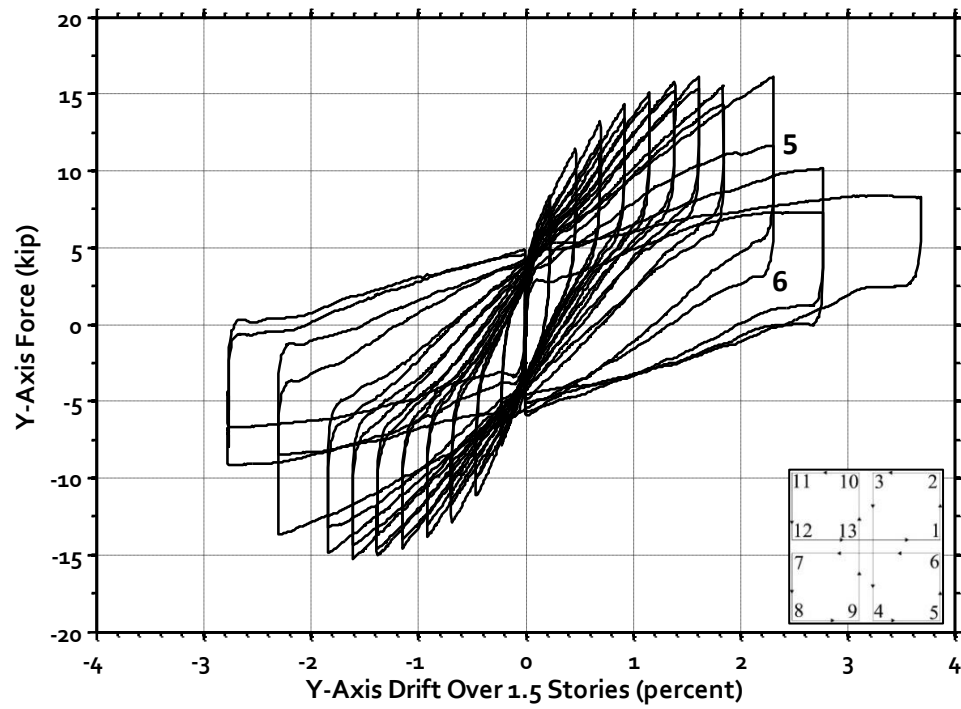
Figure 3-40: Specimen B4 – Load versus Drift Response (Y-Direction)

166
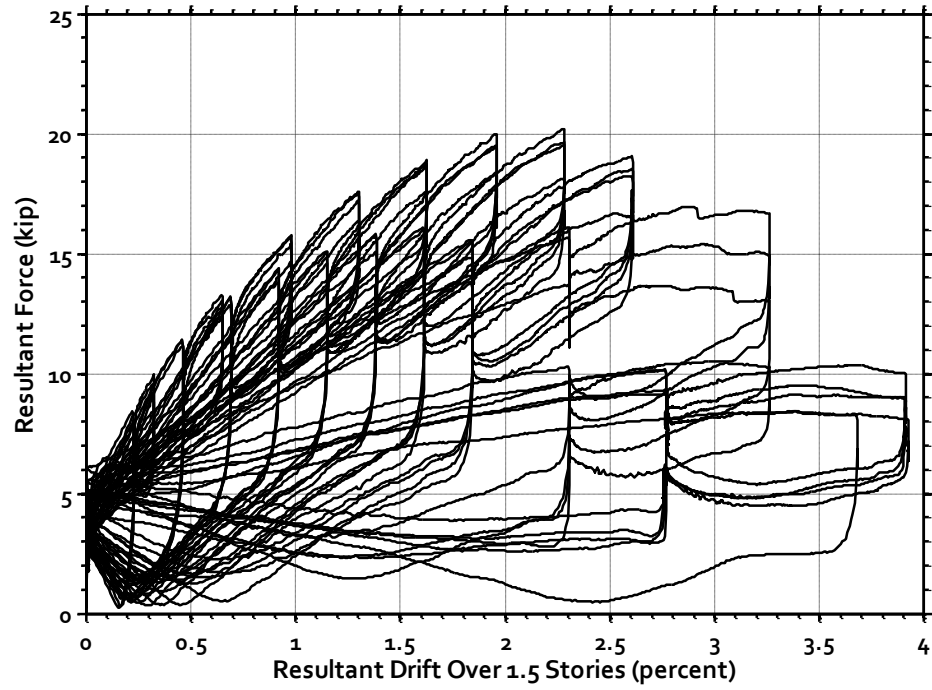
Figure 3-41: Specimen B4 – Resultant Load versus Drift Response
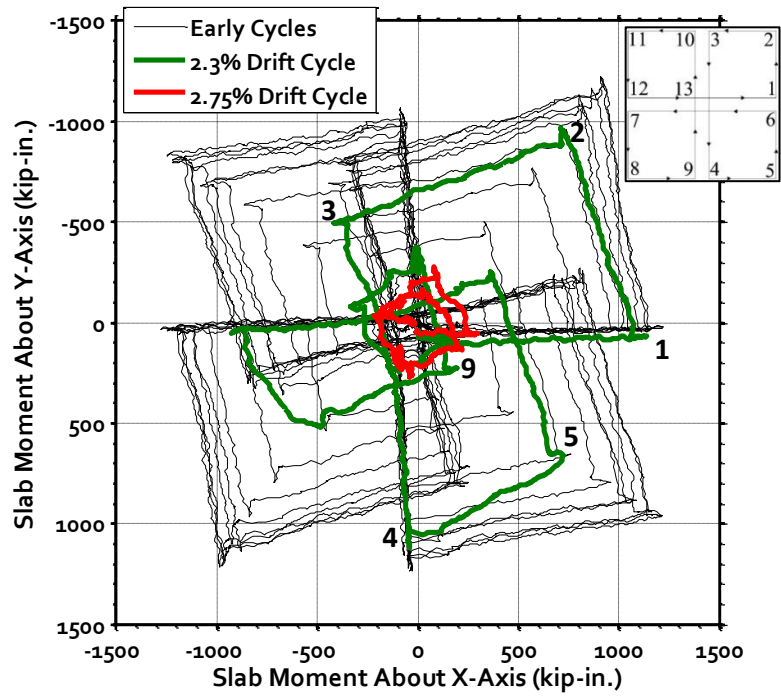
Figure 3-42: Specimen B4 – Relationship Between Moments Transferred into the Column About the X- and Y-Axes

167
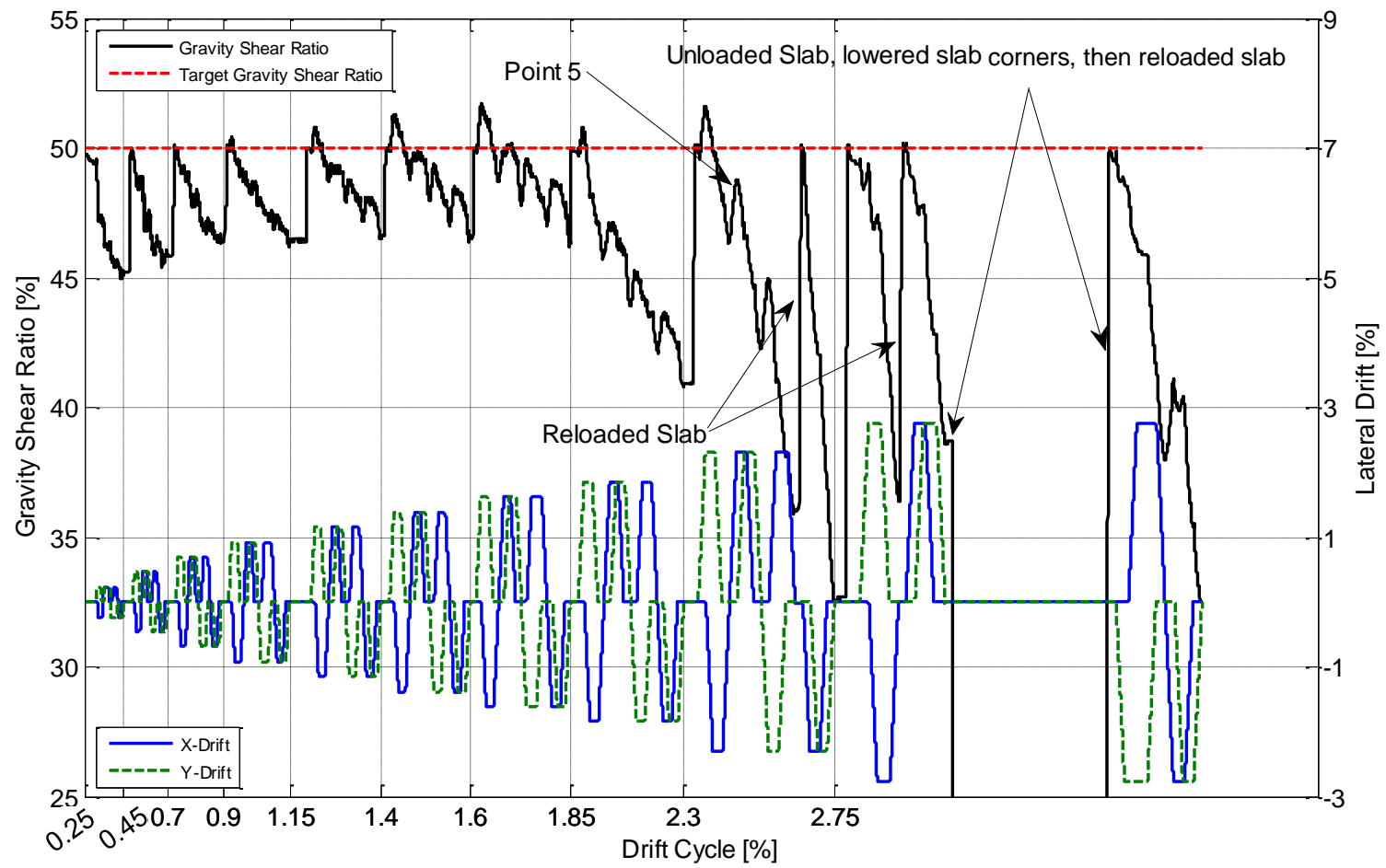
Figure 3-43: Specimen B4 – Gravity Shear History
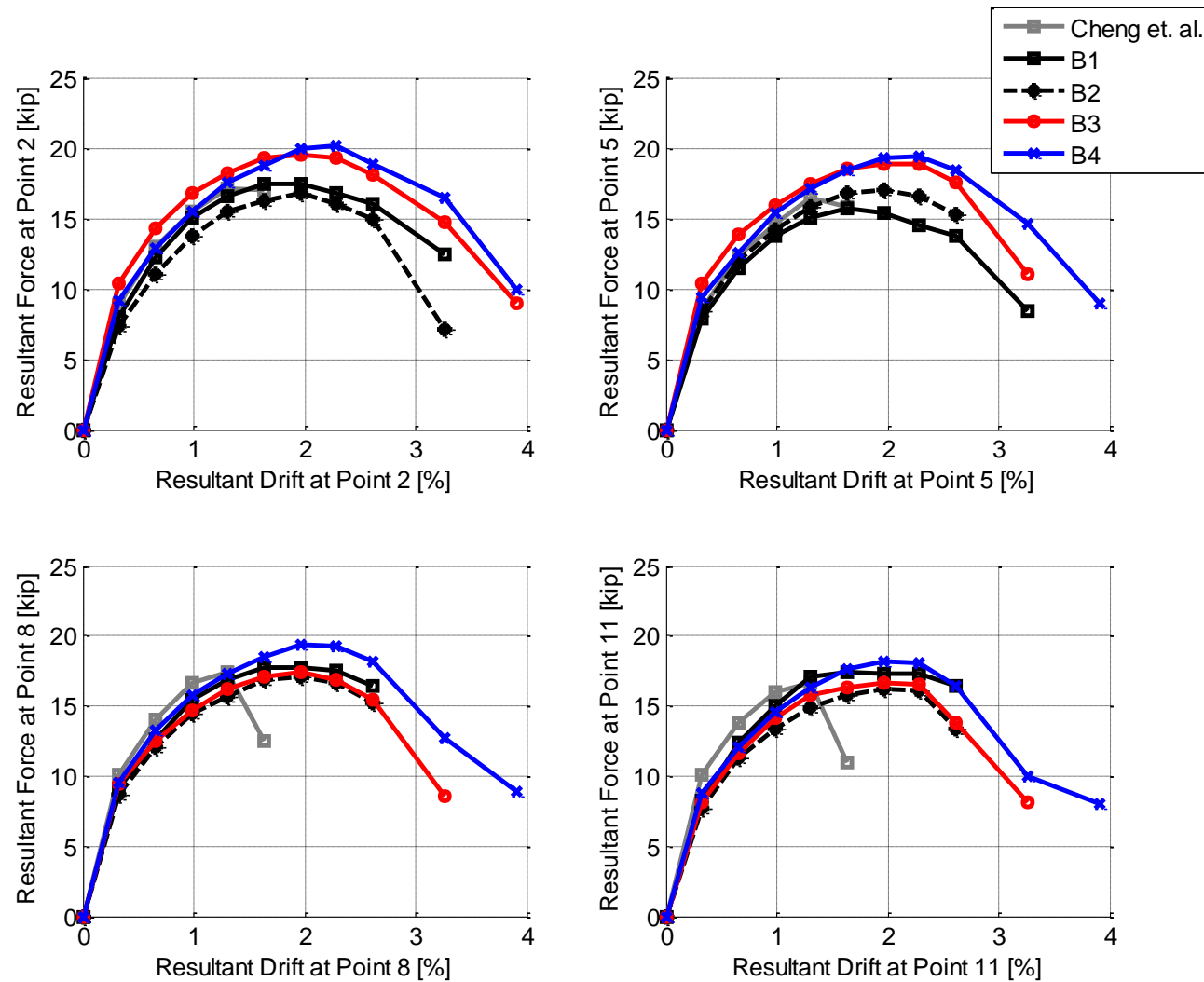
Figure 3-44: Resultant Lateral Load versus Resultant Drift Envelopes at Corner Points on Cloverleaf Cycle (Drift was Not Corrected For Base Slip)

169
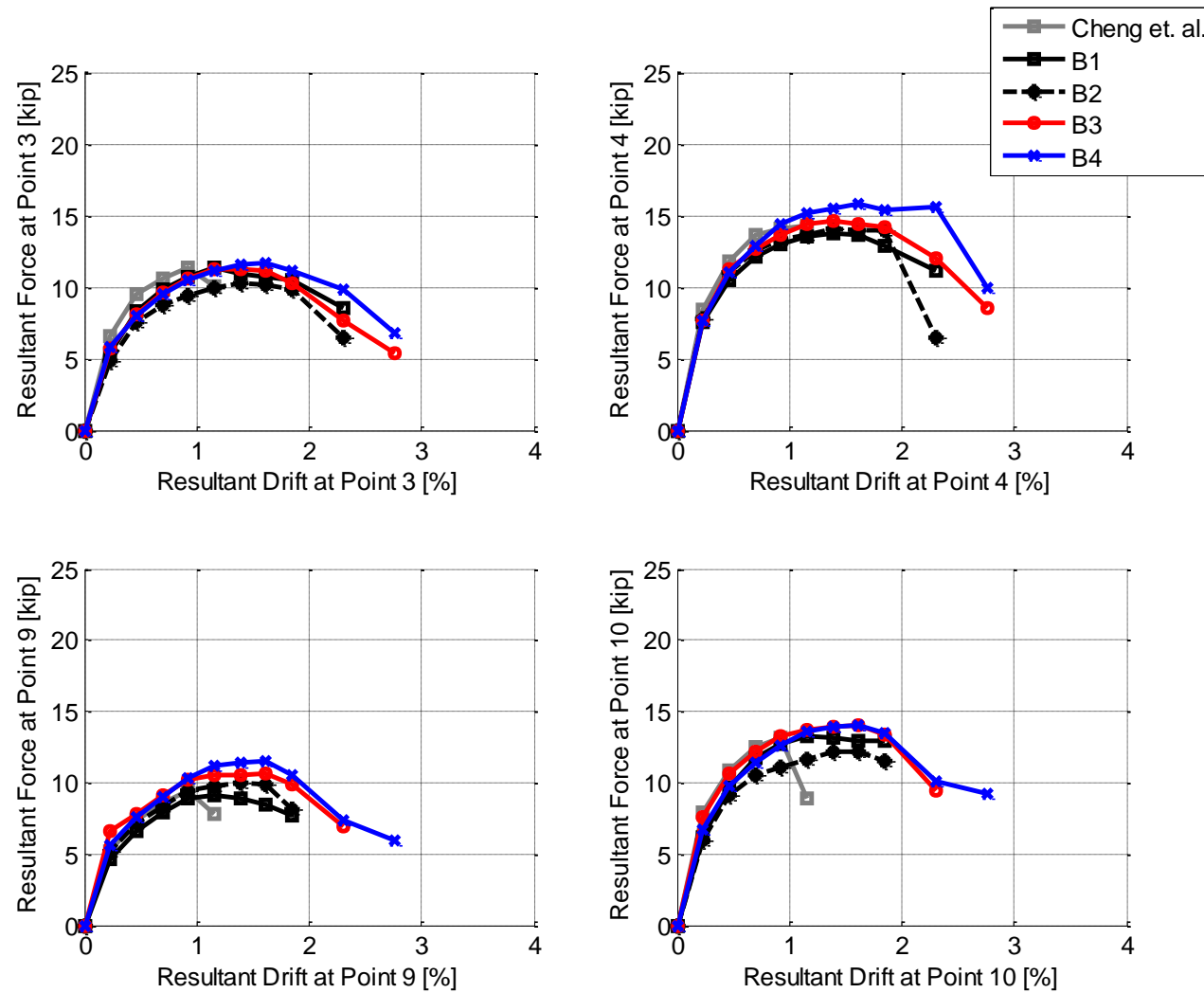
Figure 3-45: Resultant Lateral Load versus Resultant Drift Envelopes in X-Directions on Cloverleaf Cycle (Drift was Not Corrected For Base Slip)
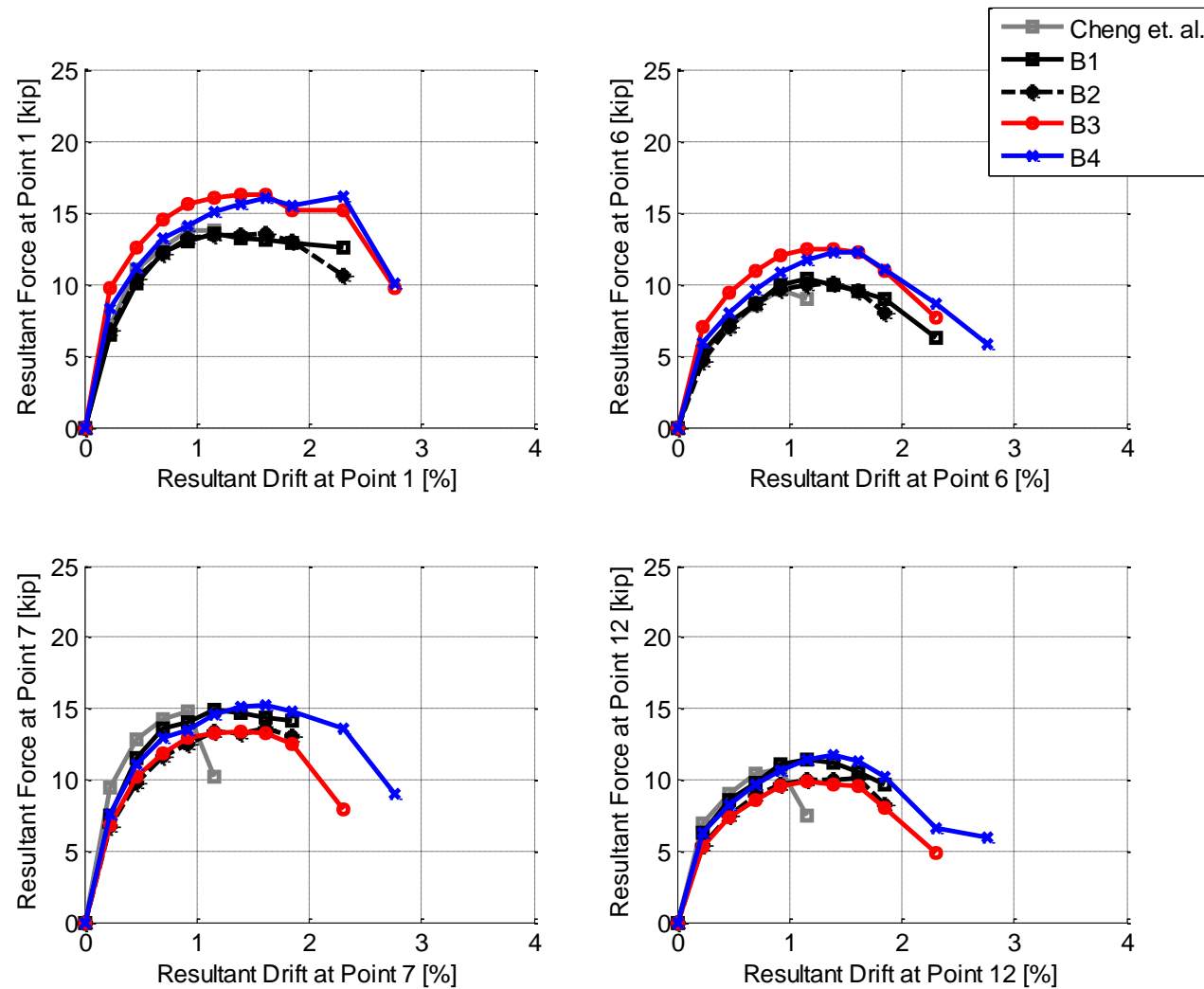
Figure 3-46: Resultant Lateral Load versus Resultant Drift Envelopes in Y-Directions on Cloverleaf Cycle (Drift was Not Corrected For Base Slip)
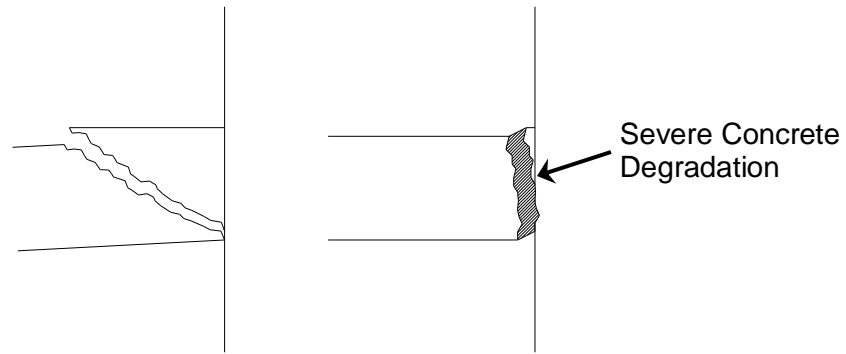
Figure 3-47: Schematic of Slab Drop Due to Diagonal Punching Shear Crack (left) and Sliding Shear (right), with Reinforcement Omitted for Clarity
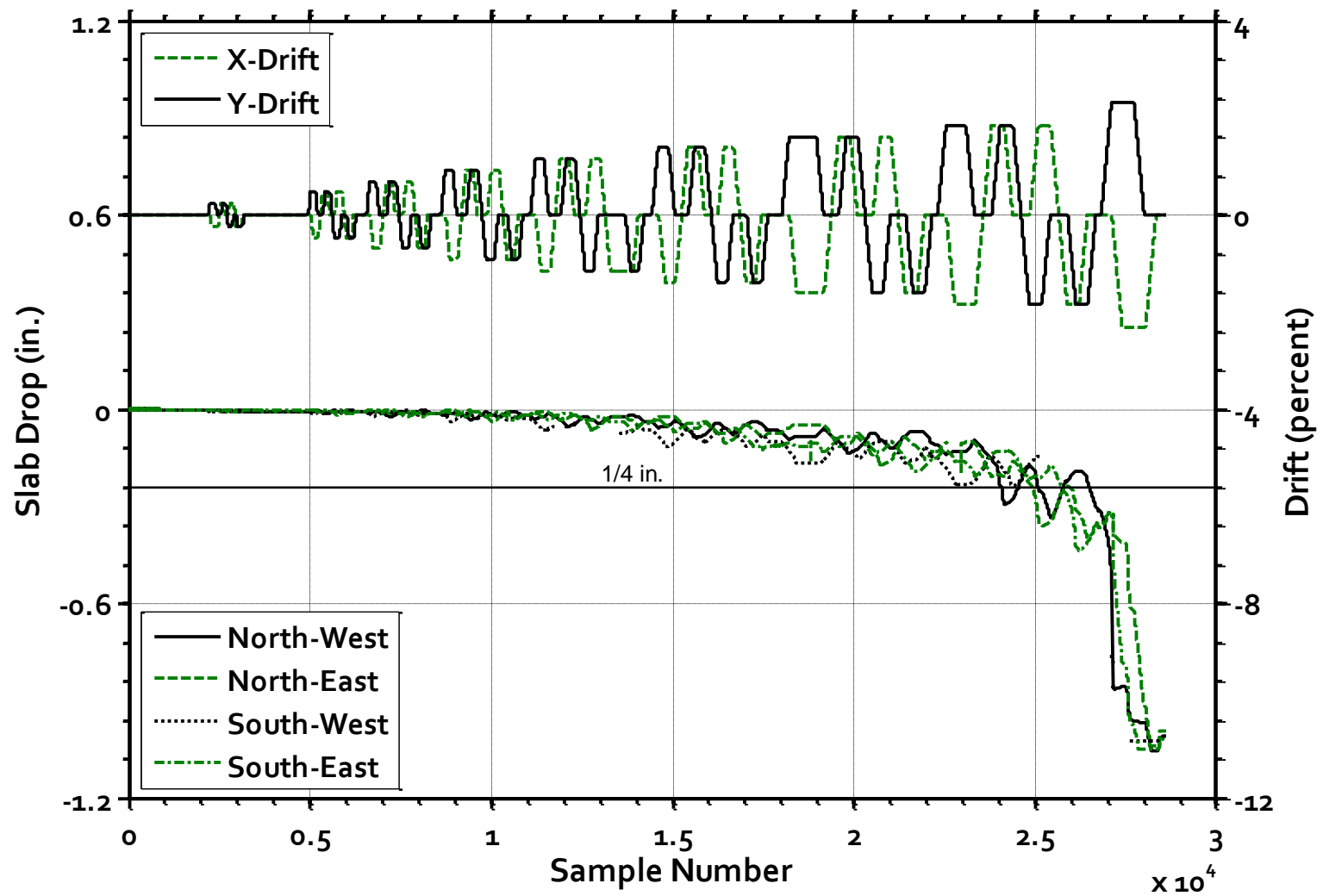
Figure 3-48: Specimen B2 – Vertical Drop of Slab Bottom Relative to the Column at Each Column Corner
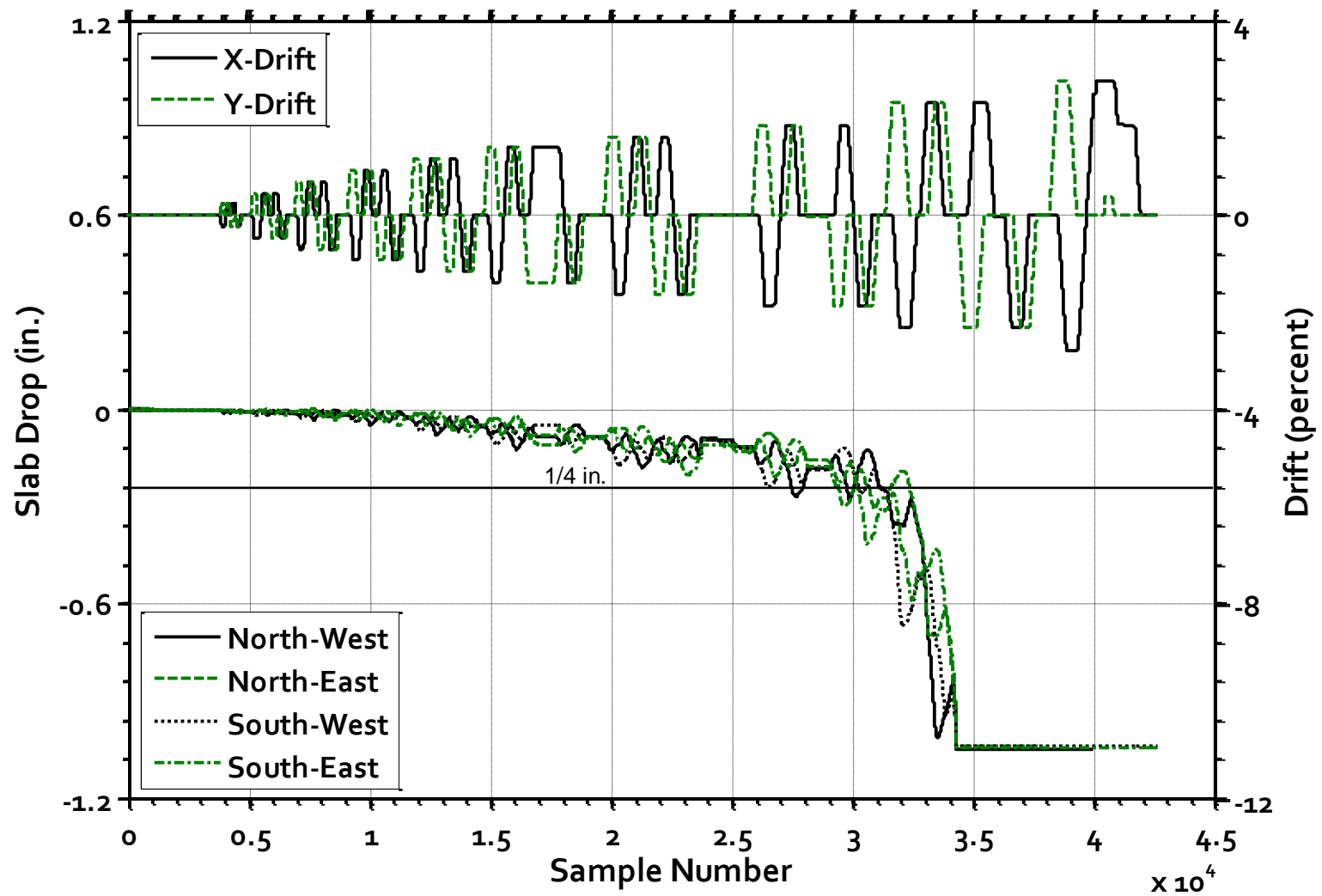
Figure 3-49: Specimen B3 – Vertical Drop of Slab Bottom Relative to the Column at Each Column Corner

174
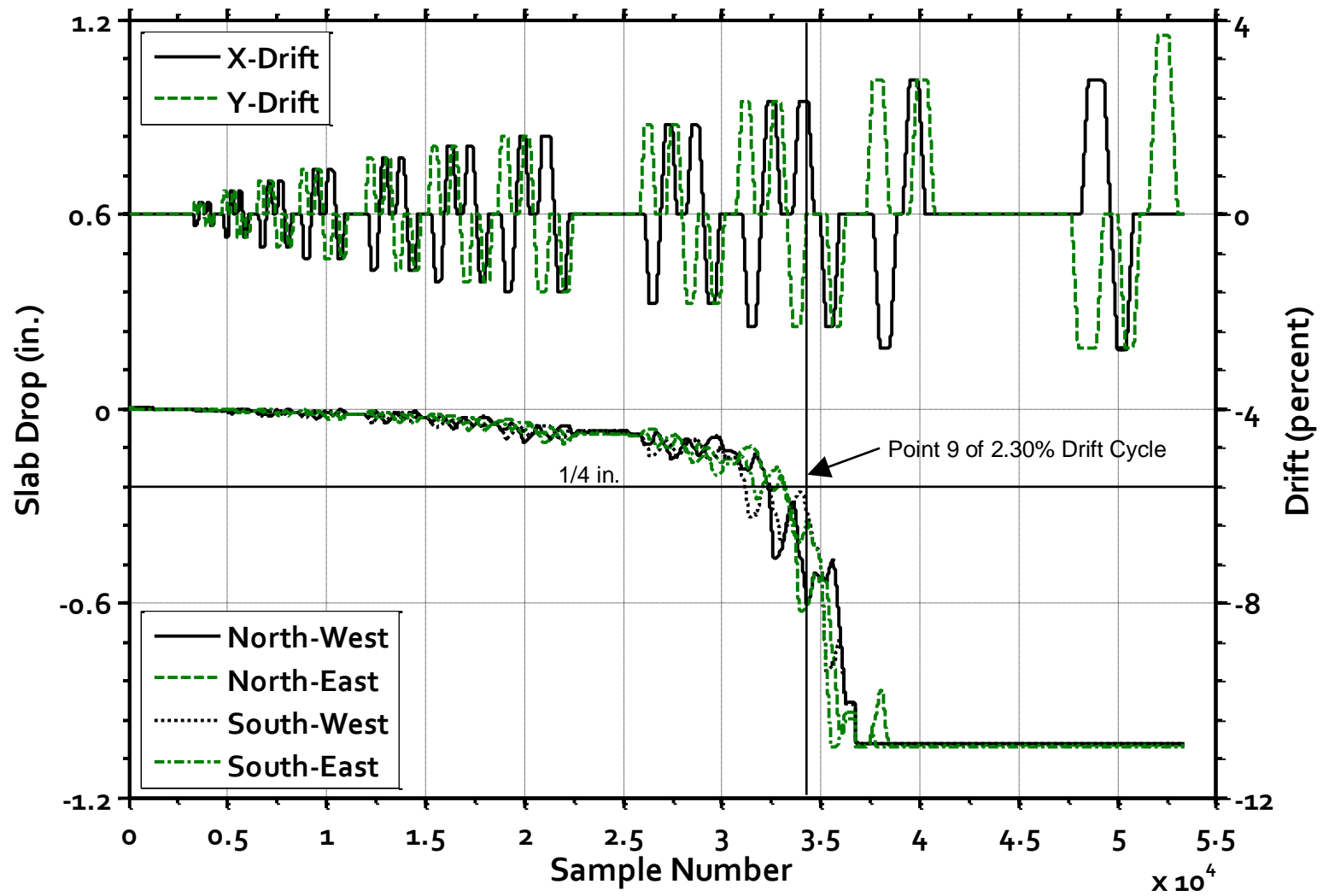
Figure 3-50: Specimen B4 – Vertical Drop of Slab Bottom Relative to the Column at Each Column Corner
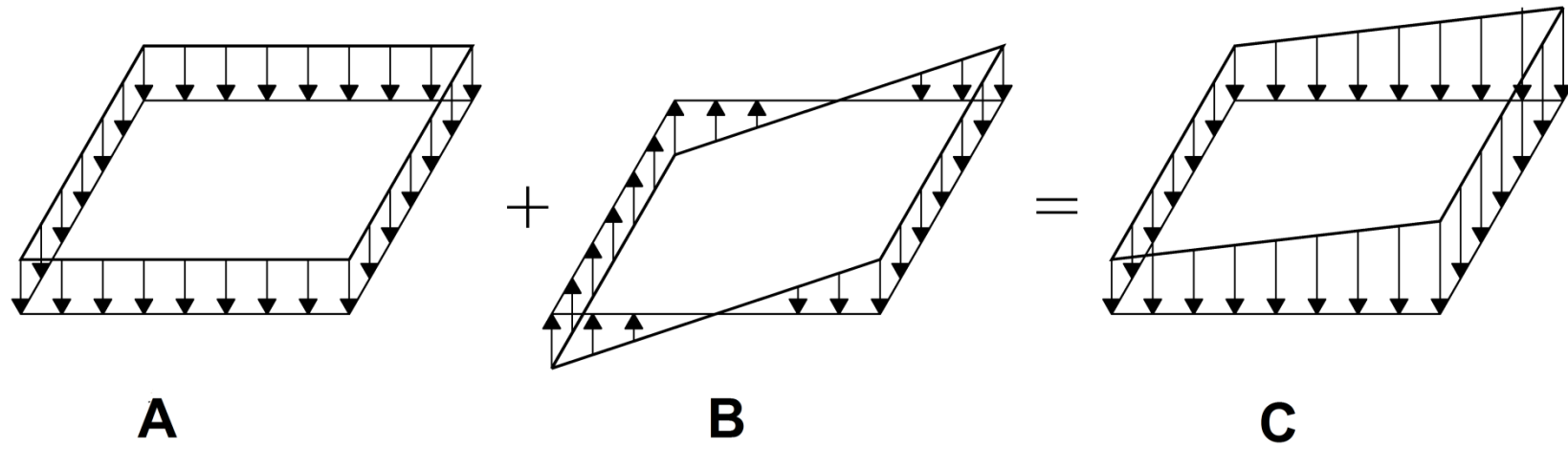
Figure 3-51: 2008 ACI Code Assumed Distribution of Shear Stresses in Square Interior Column
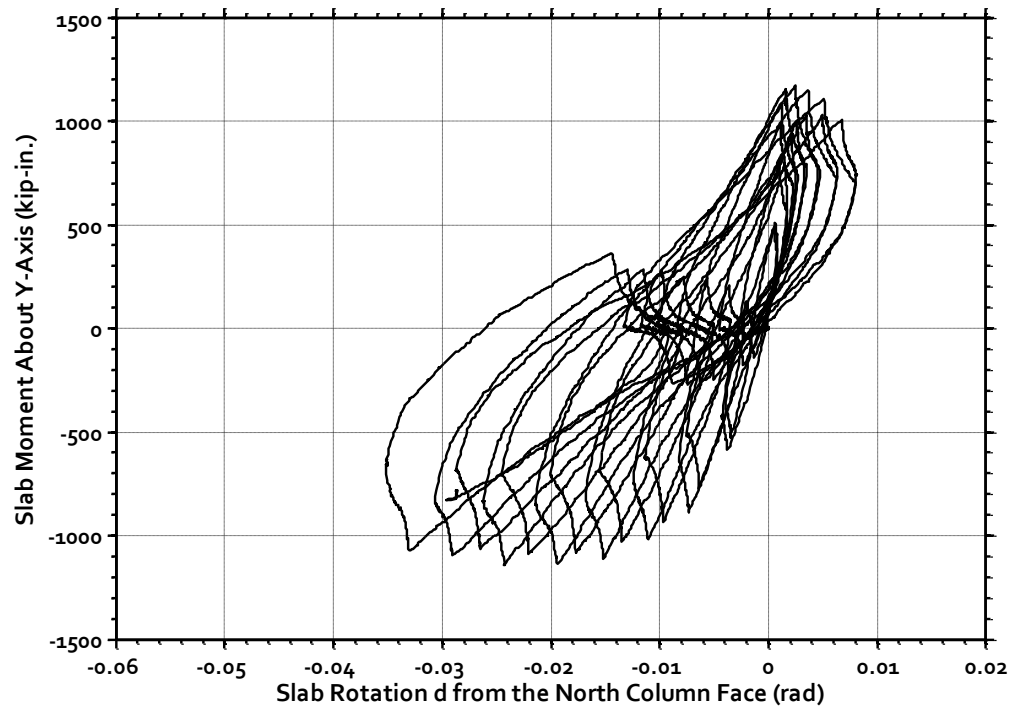
a) Slab Rotation *d* from Column Face
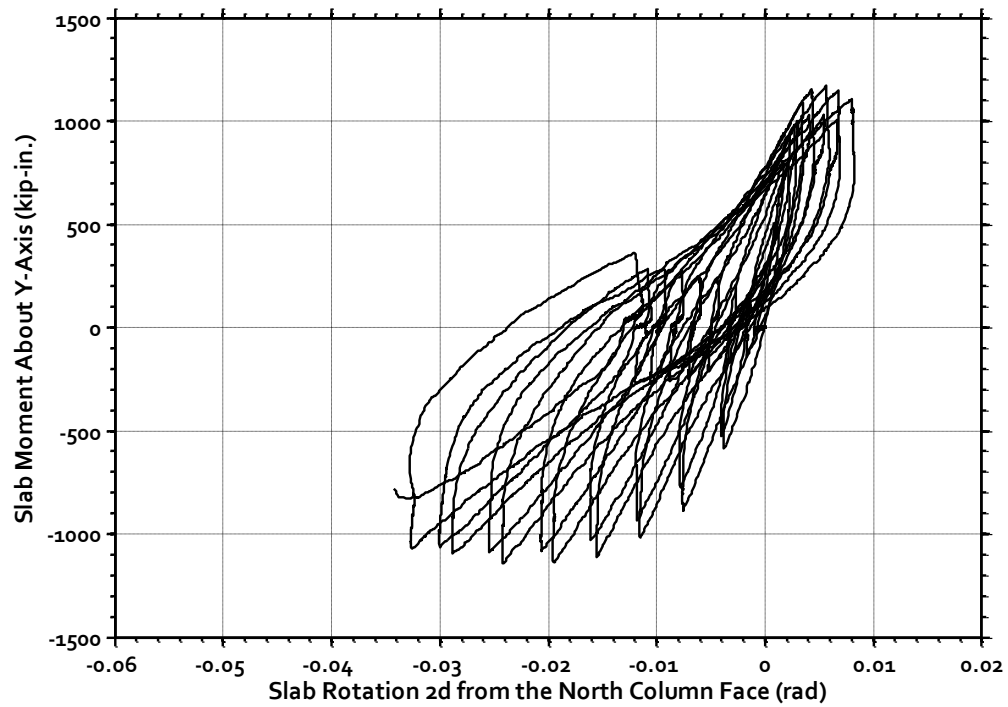
b) Slab Rotation 2*d* from Column Face

Figure 3-52: Moment Transferred to Column Versus Slab Rotation at the North Column Face of Specimen B2
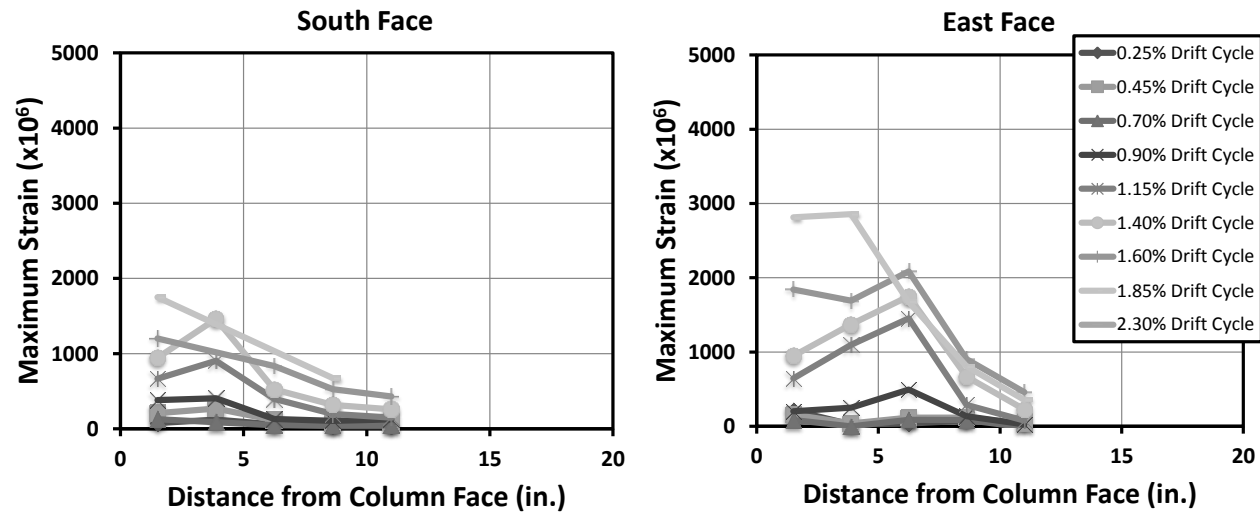
Figure 3-53: Specimen B1 – Profile of Strains in Studs on Rails Placed Orthogonal to the South and East Column Faces
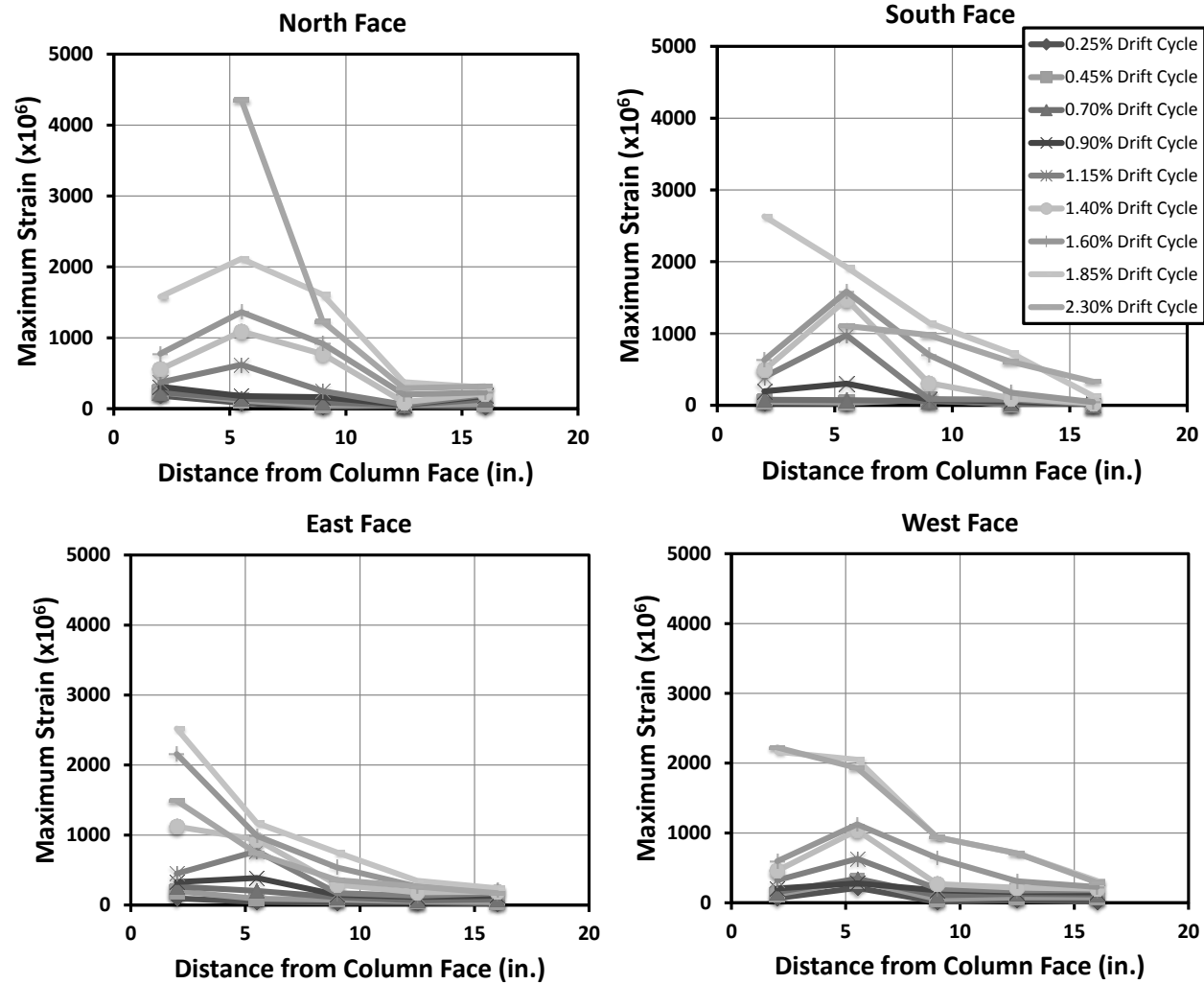
Figure 3-54: Specimen B2 – Profile of Strains in Studs on Rails Placed Orthogonal to the Column Faces
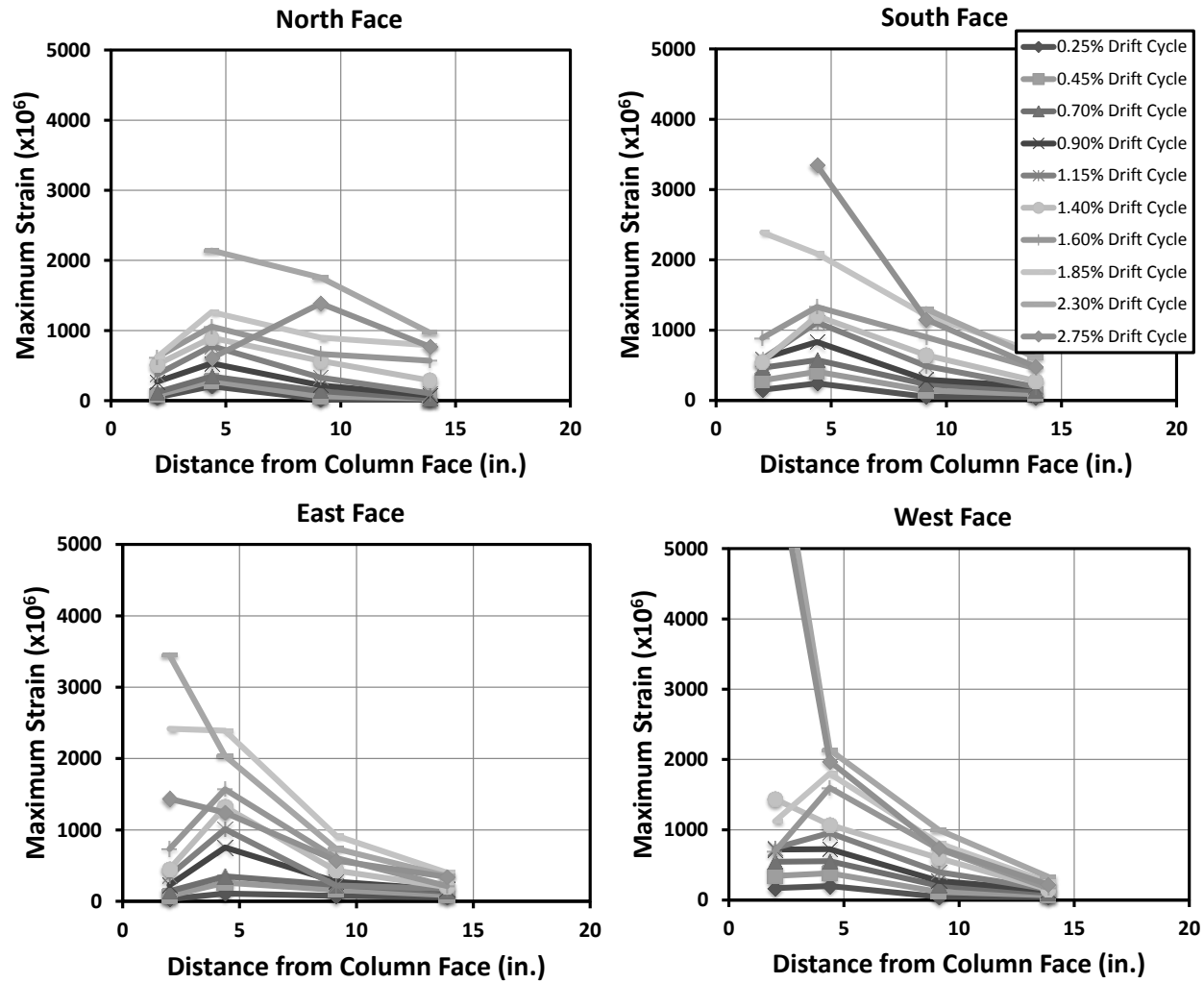
Figure 3-55: Specimen B3 – Profile of Strains in Studs on Rails Placed Orthogonal to the Column Faces
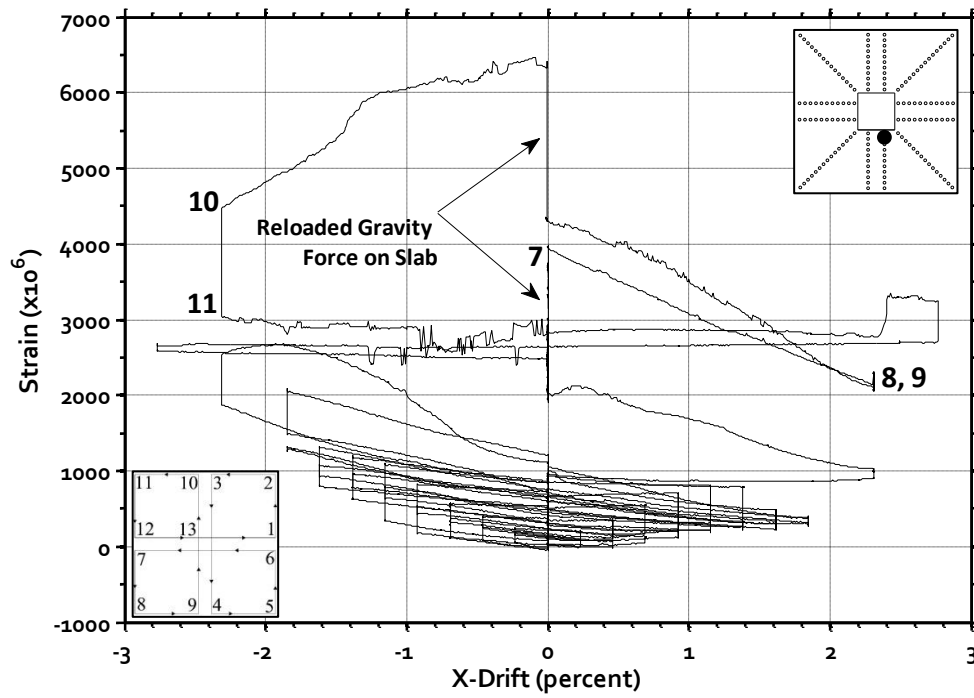
Figure 3-56: Specimen B3 – Strains Recorded in Stud RO-SE2, Showing Large Increases Before Points 7 and 10 When the Gravity Load on the Slab was Reloaded
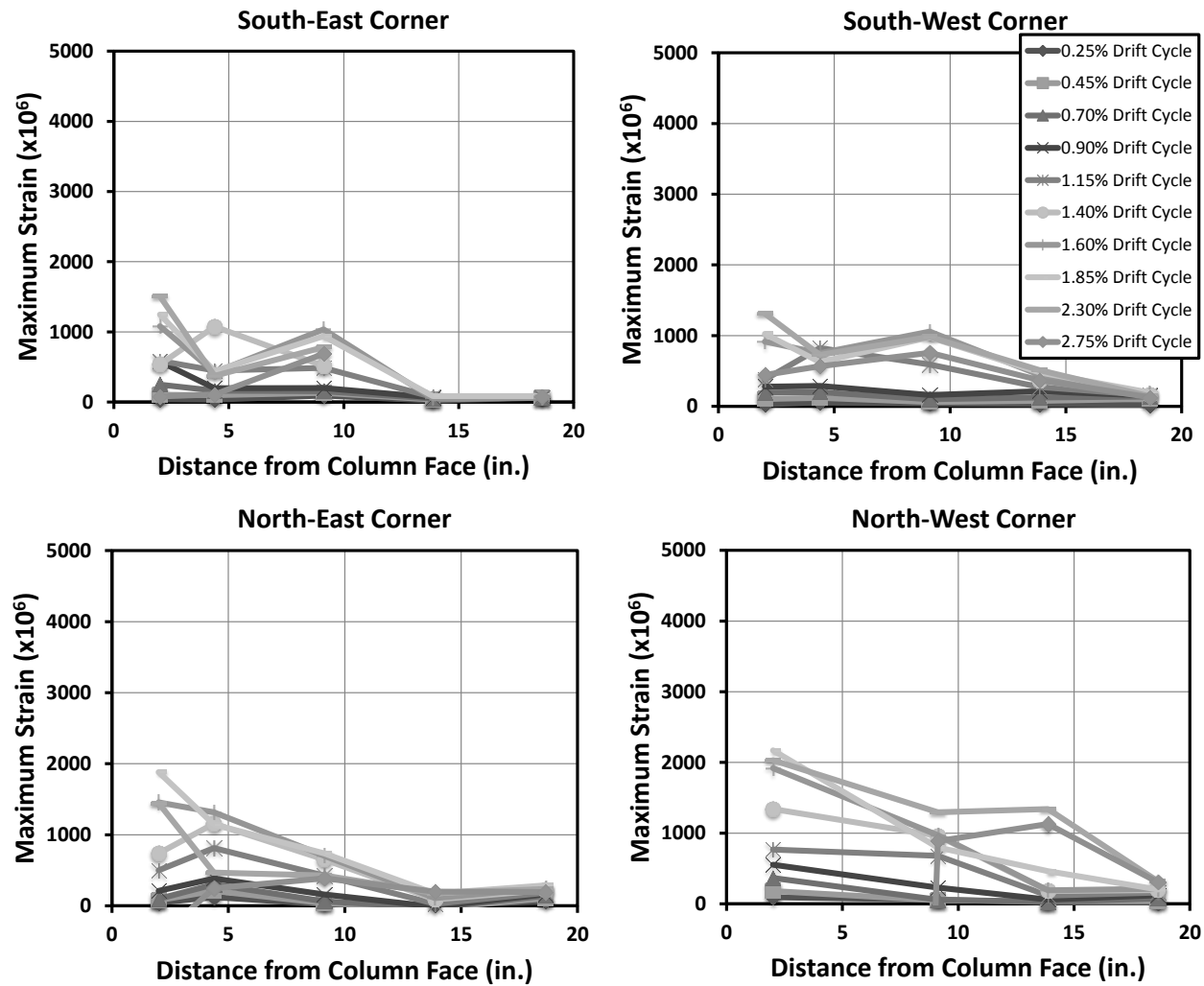
Figure 3-57: Specimen B3 – Profile of Strains in Studs on Rails Placed at 45 Degrees From Column Faces

182
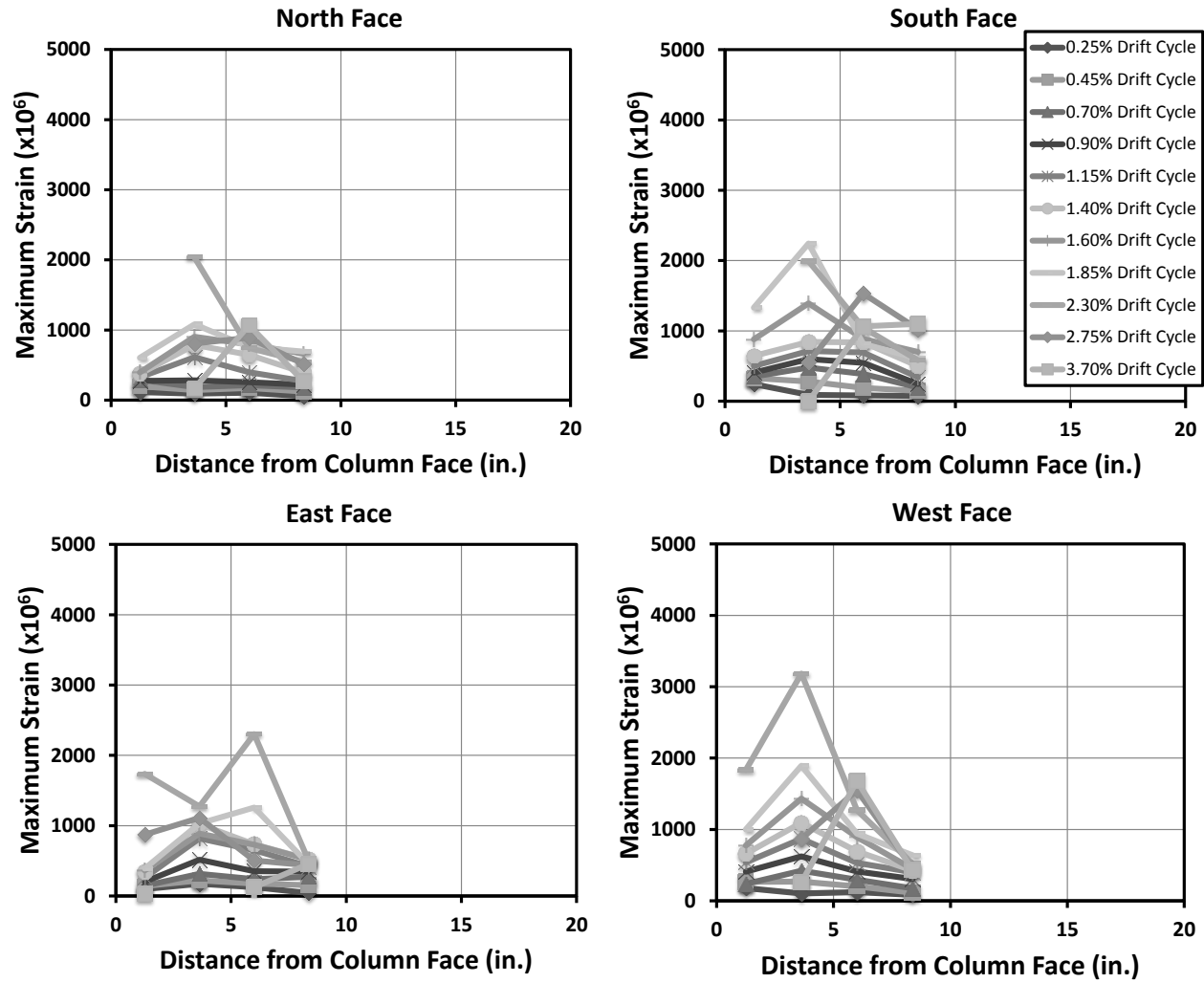
Figure 3-58: Specimen B4 – Profile of Strains in Studs on Rails Placed Orthogonal to the Column Faces Away from the Corners (Inner Orthogonal)
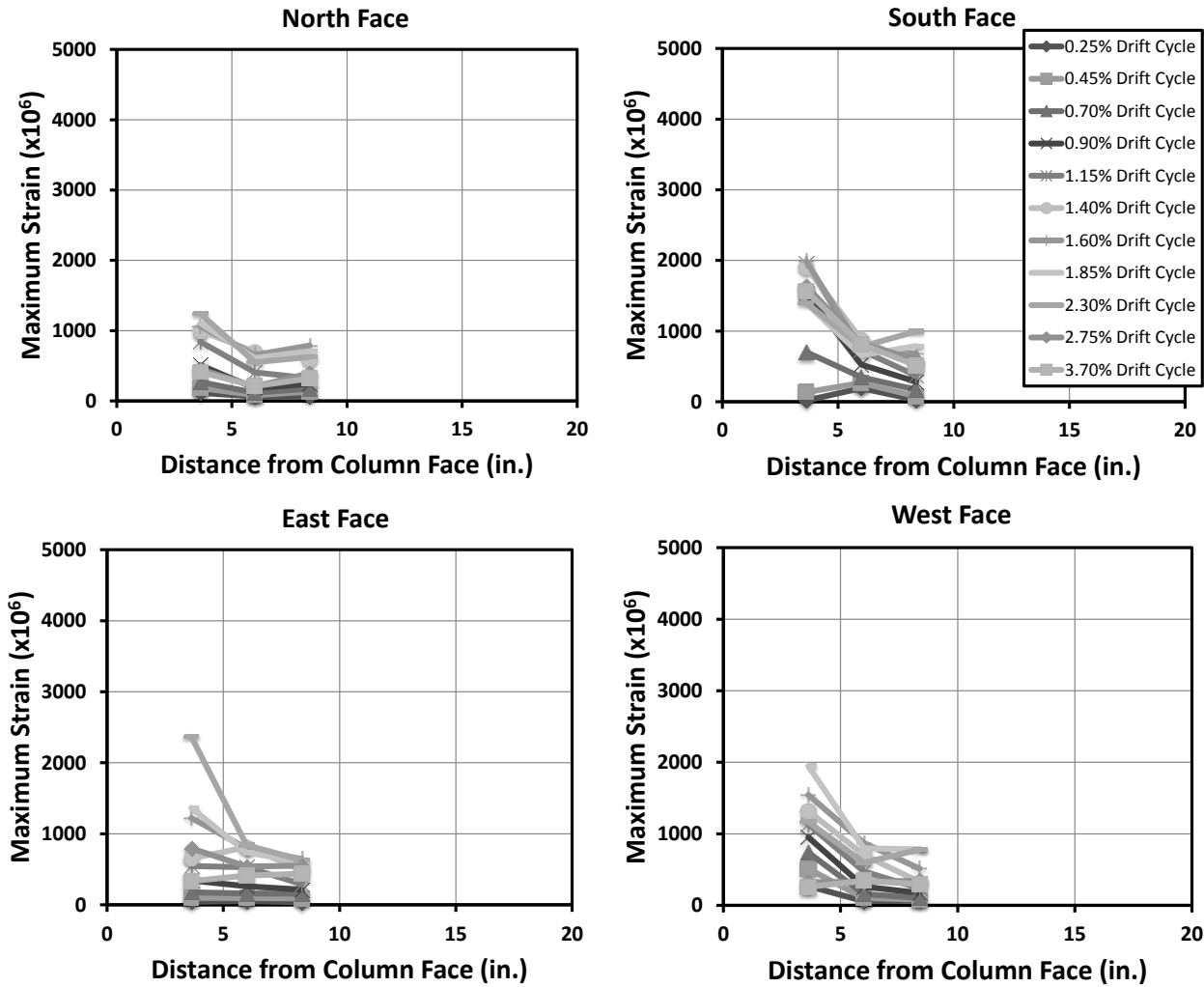
Figure 3-59: Specimen B4 – Profile of Strains in Studs on Rails Placed Orthogonal to the Column Faces Near the Corners (Outer Orthogonal)

184
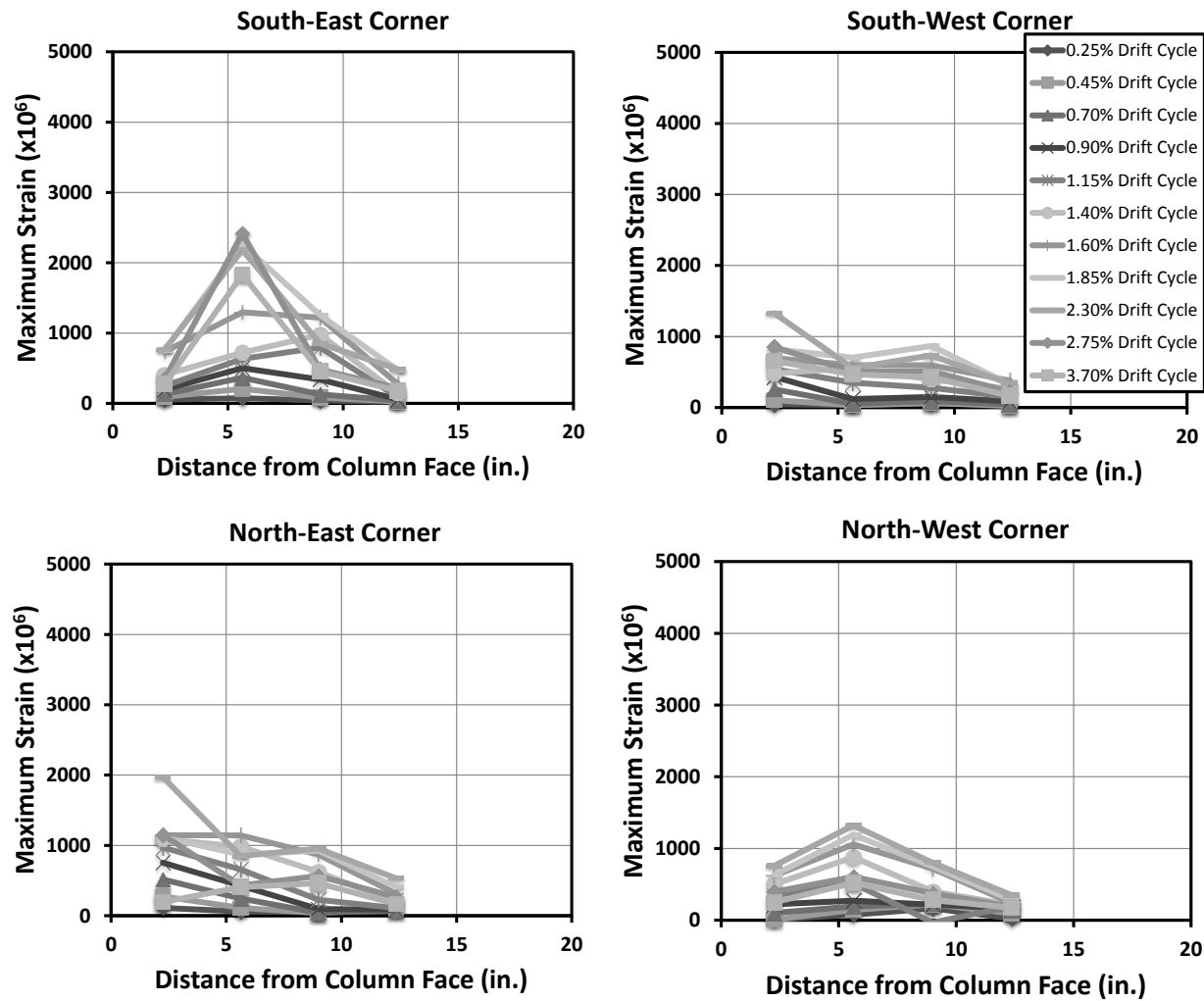
Figure 3-60: Specimen B4 – Profile of Strains in Studs on Rails Placed at 45 Degrees From Column Faces
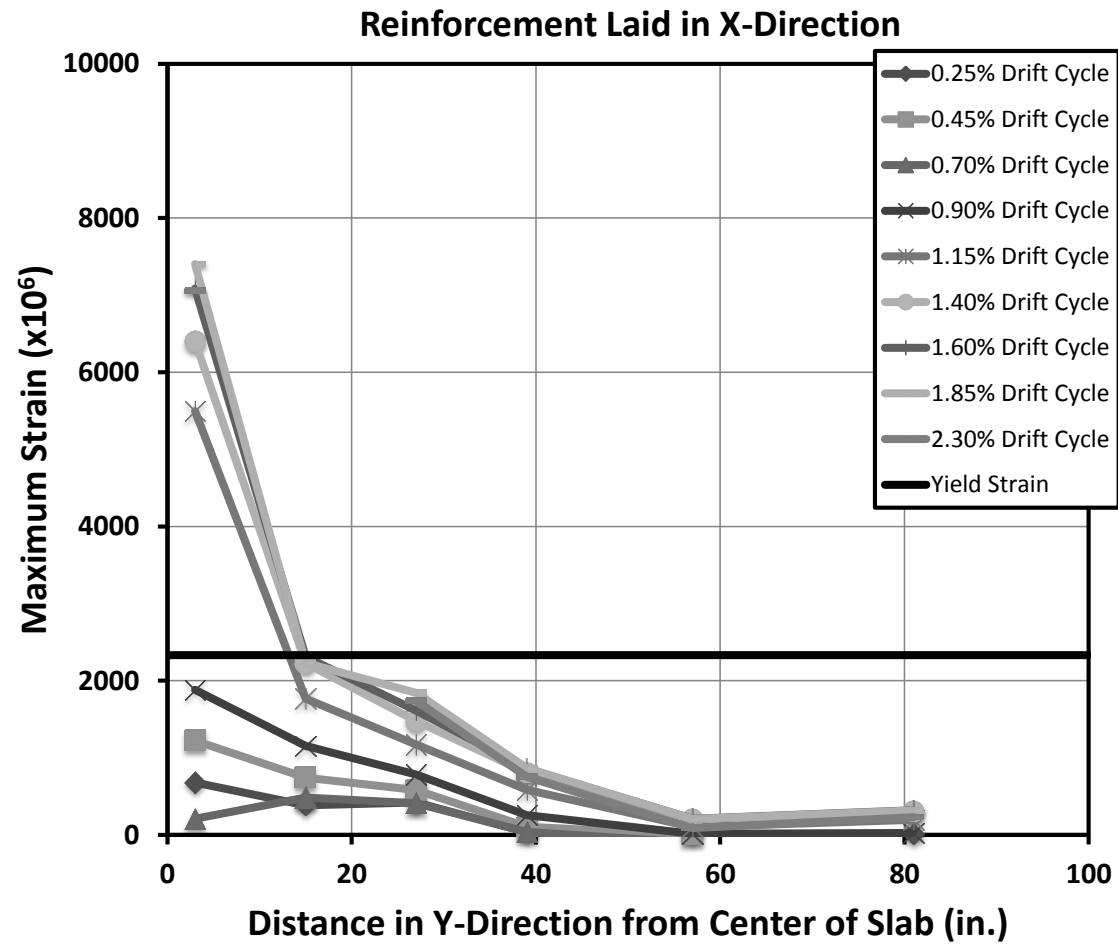
Figure 3-61: Specimen B1 – Profile of Strains in Top Mat Flexural Reinforcement Placed in the X-Direction at *d*/2 from Column Face
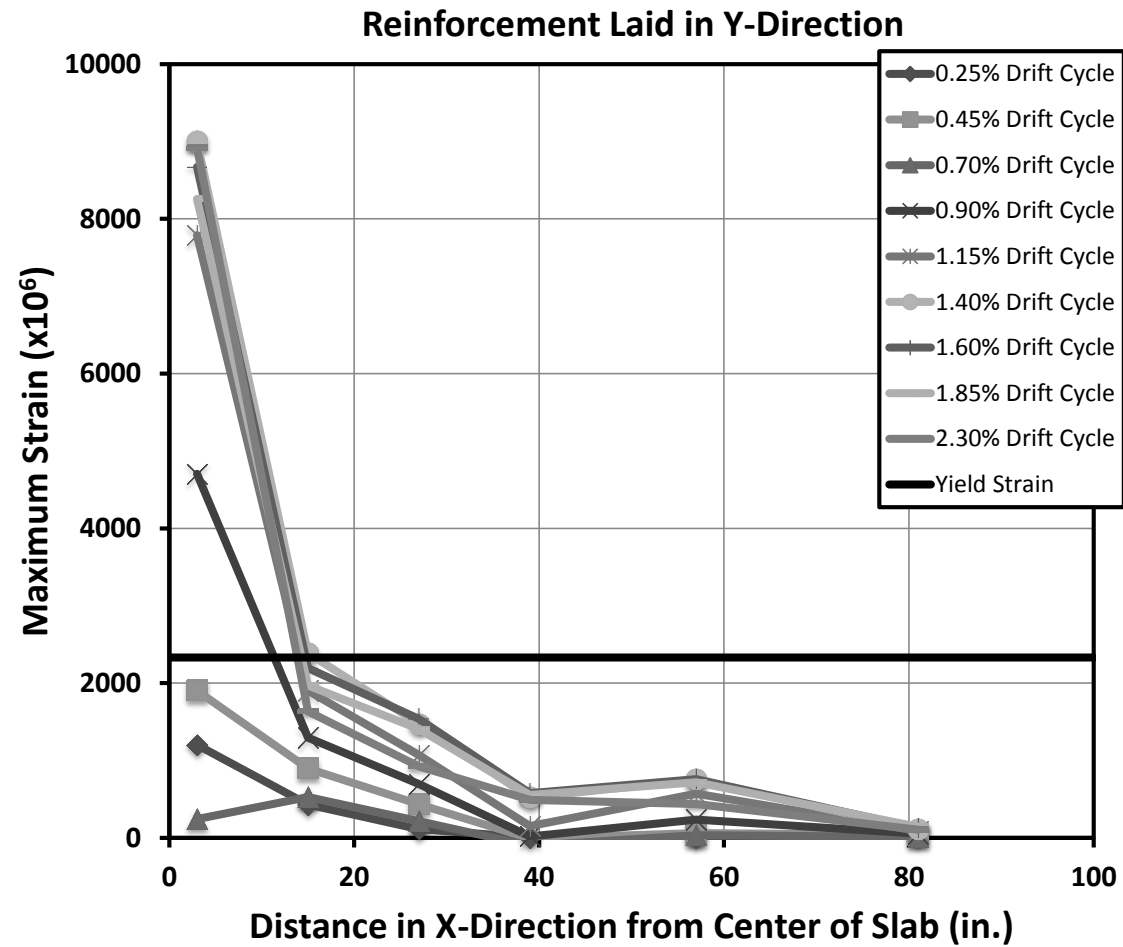
Figure 3-62: Specimen B1 – Profile of Strains in Top Mat Flexural Reinforcement Placed in the Y-Direction at *d*/2 from Column Face
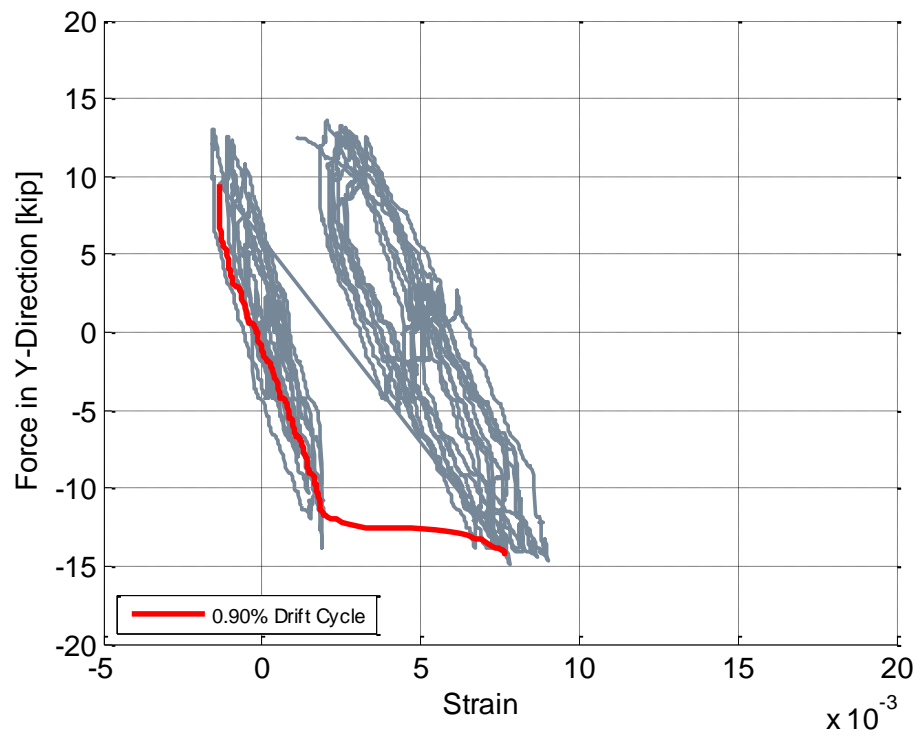
Figure 3-63: Specimen B1 – Lateral Force versus Strain in Gauge TE2
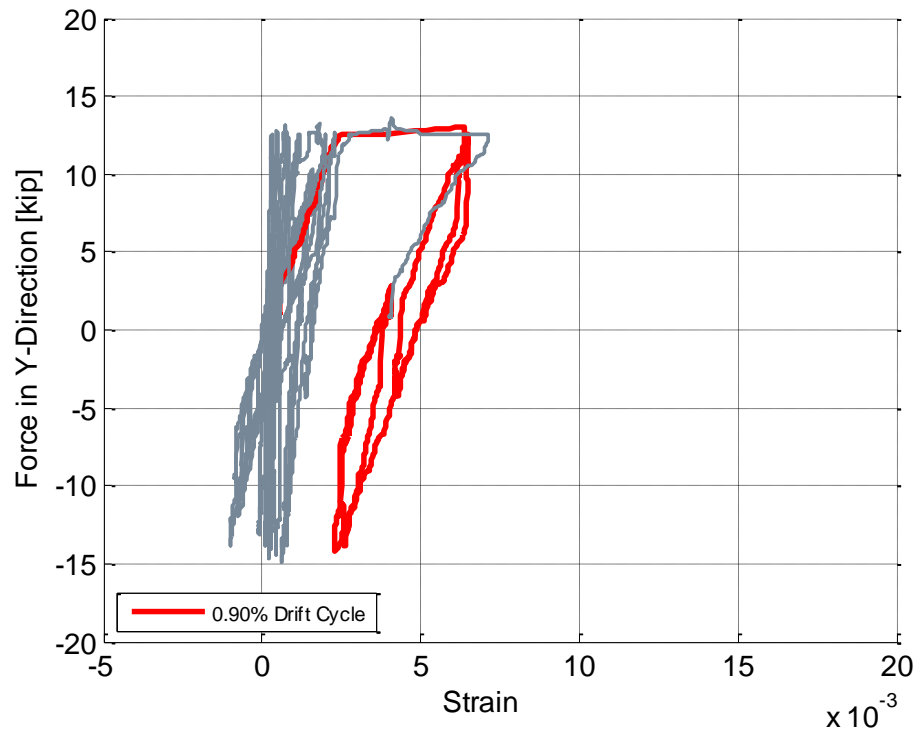
Figure 3-64: Specimen B1 – Lateral Force versus Strain in Gauge TE3
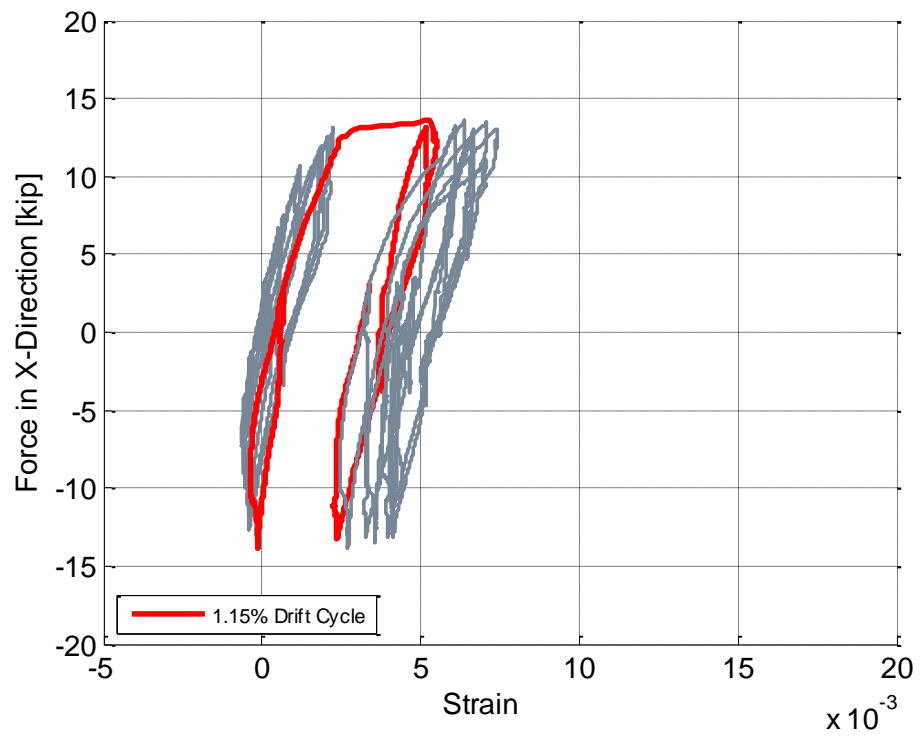
Figure 3-65: Specimen B1 – Lateral Force versus Strain in Gauge TS3
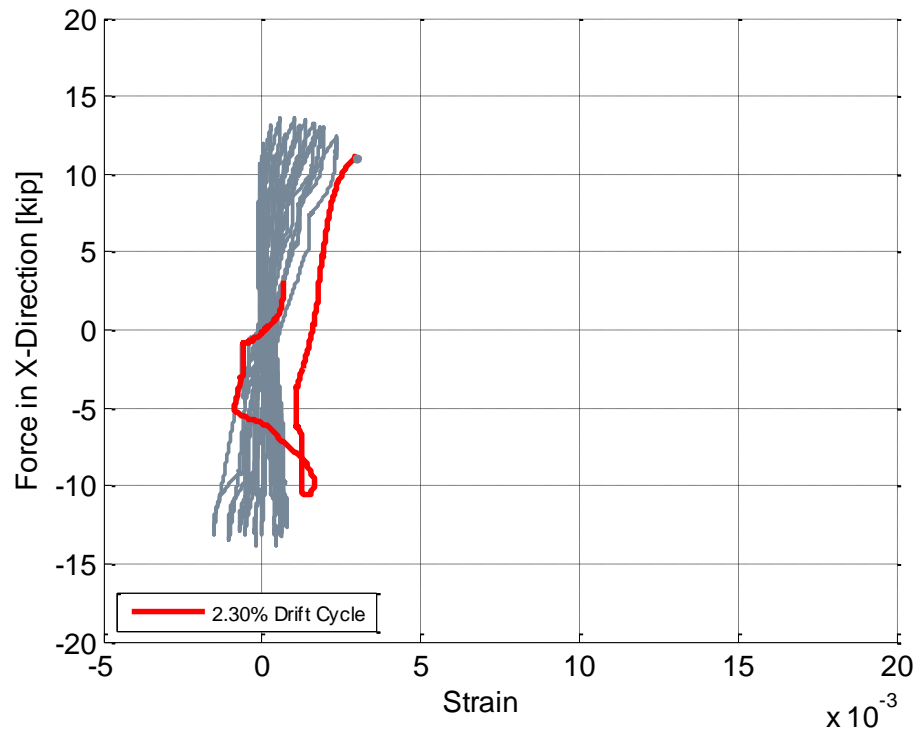
Figure 3-66: Specimen B1 – Lateral Force versus Strain in Gauge BS2
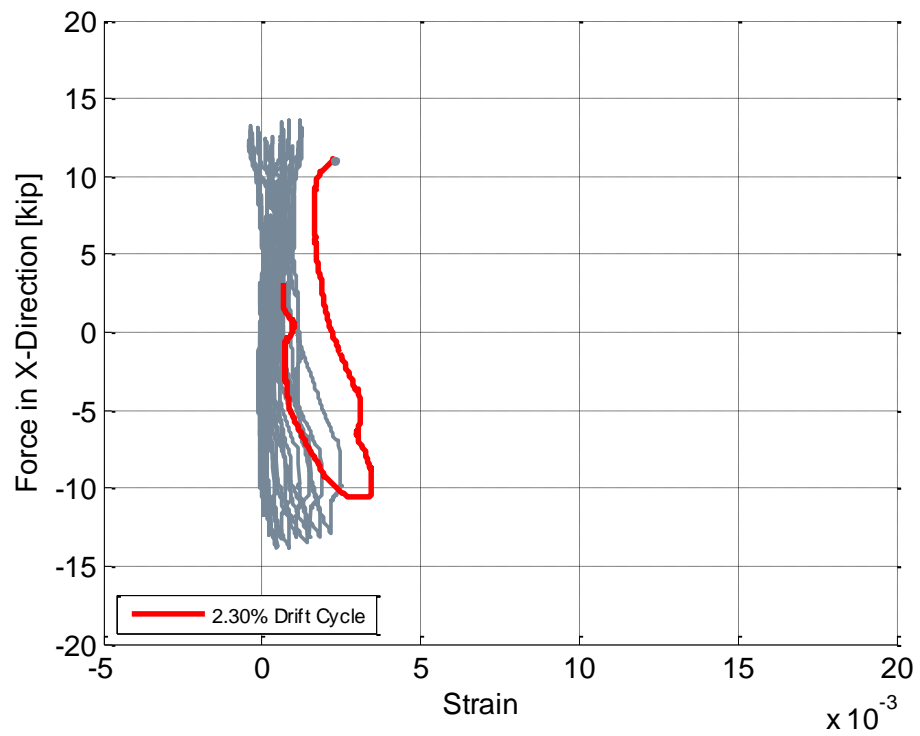
Figure 3-67: Specimen B1 – Lateral Force versus Strain in Gauge BS3
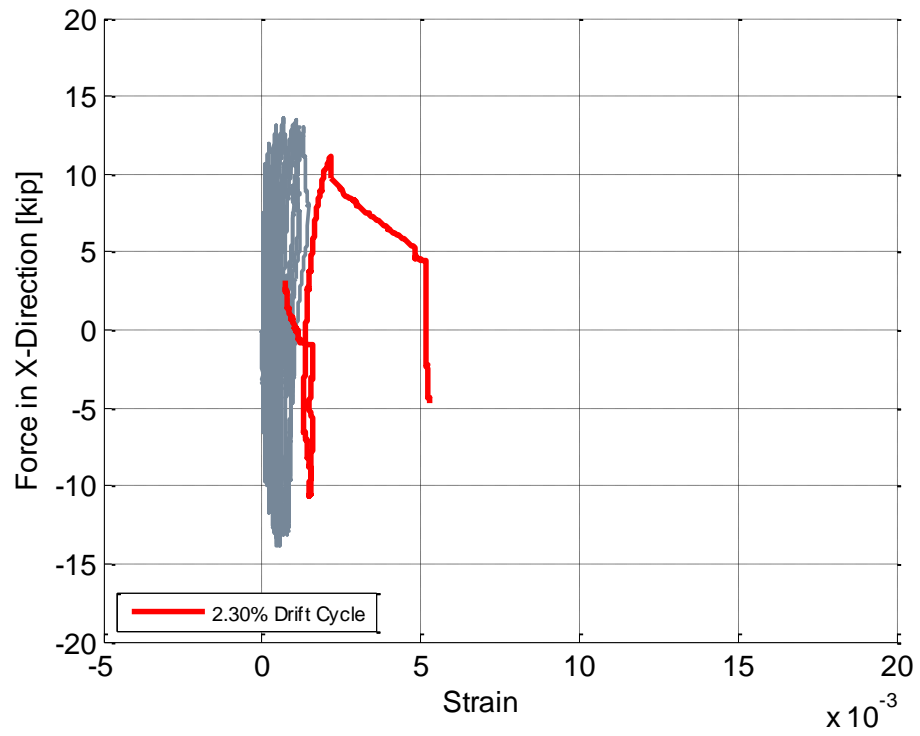
Figure 3-68: Specimen B1 – Lateral Force versus Strain in Gauge BS6

190
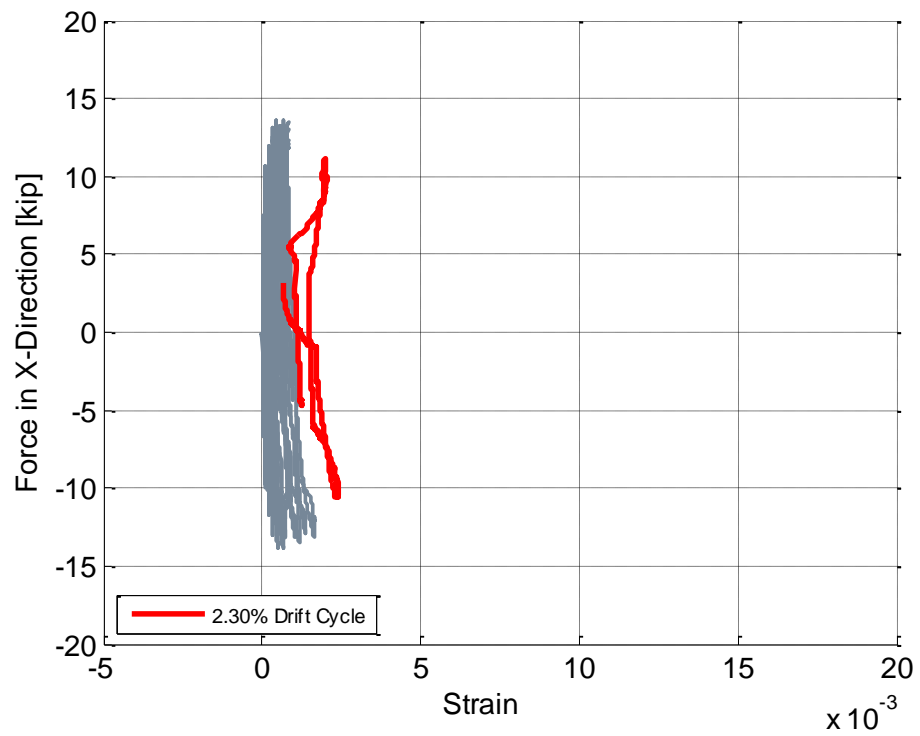
Figure 3-69: Specimen B1 – Lateral Force versus Strain in Gauge BS7
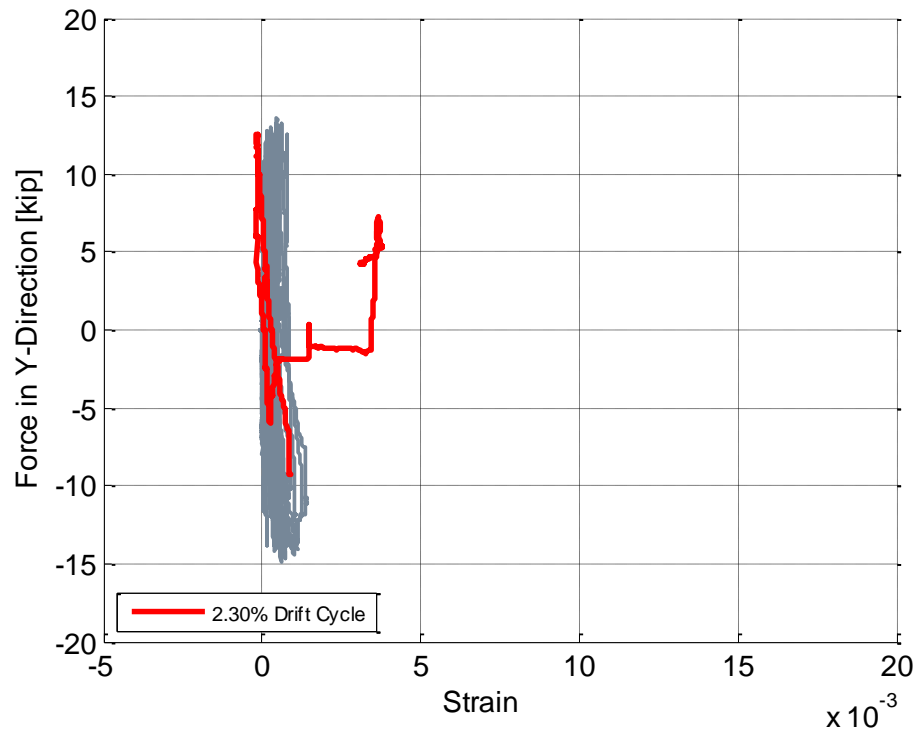
Figure 3-70: Specimen B1 – Lateral Force versus Strain in Gauge BE7
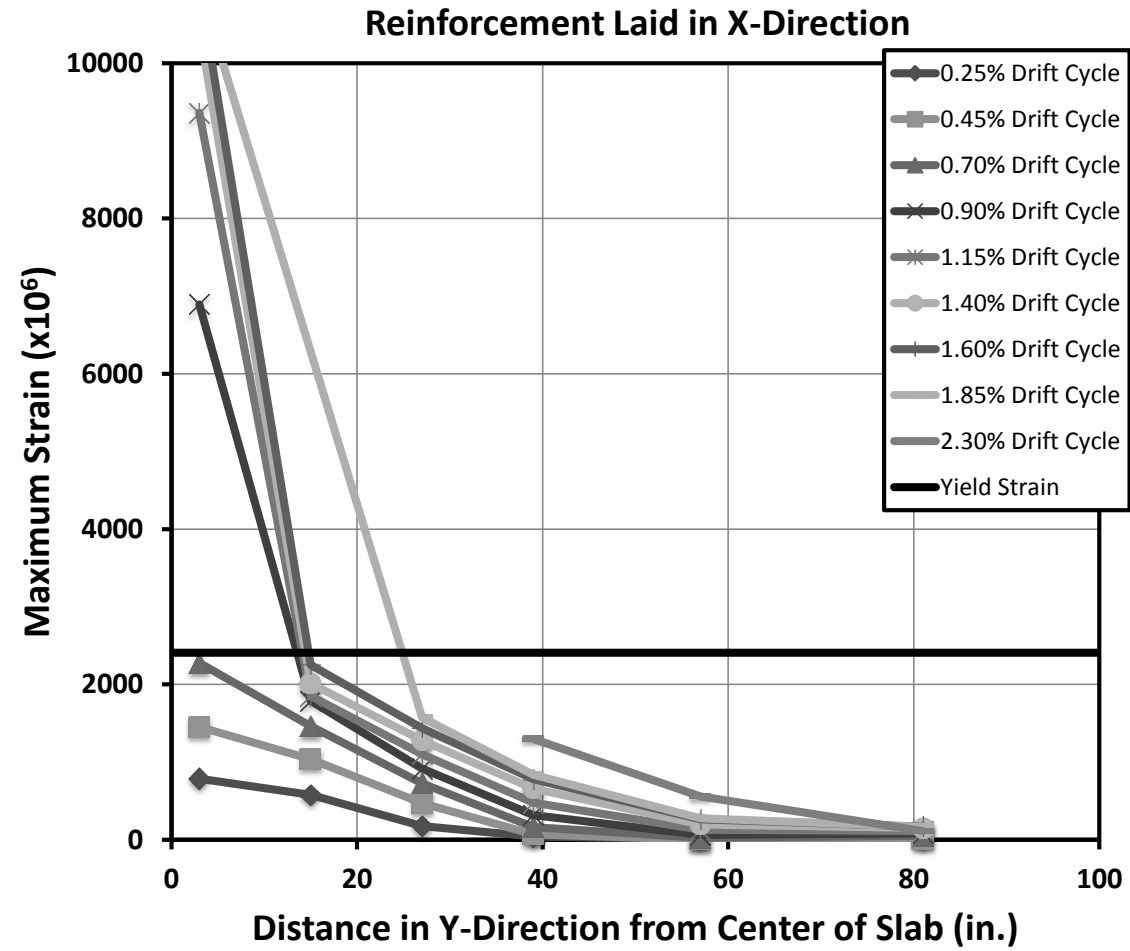
Figure 3-71: Specimen B2 – Profile of Strains in Flexural Reinforcement Placed in the X-Direction at *d*/2 from Column Face
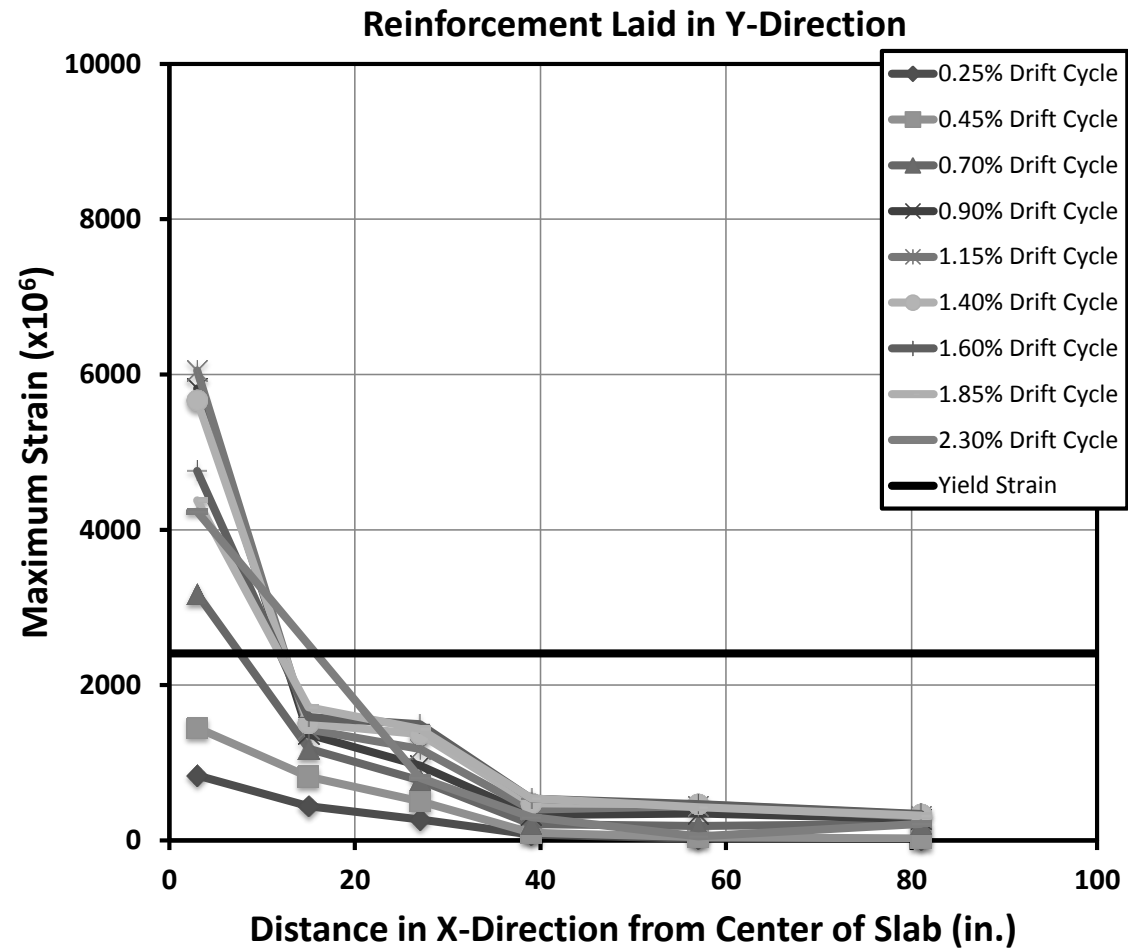
Figure 3-72: Specimen B2 – Profile of Strains in Flexural Reinforcement Placed in the Y-Direction at *d*/2 from Column Face
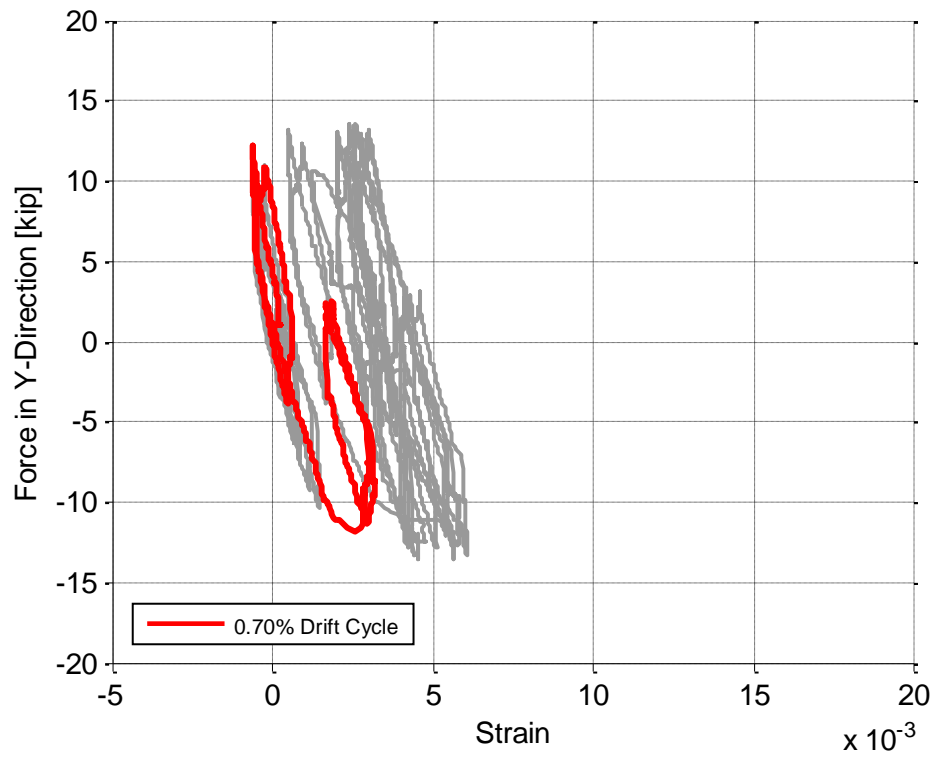
Figure 3-73: Specimen B2 – Lateral Force versus Strain in Gauge TE2
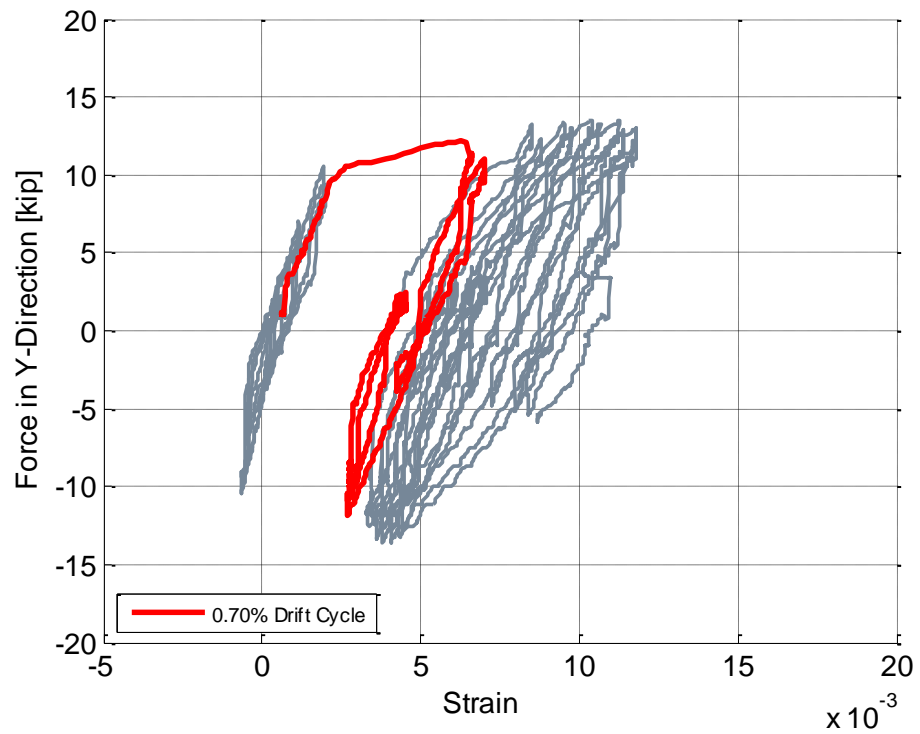
Figure 3-74: Specimen B2 – Lateral Force versus Strain in Gauge TE3
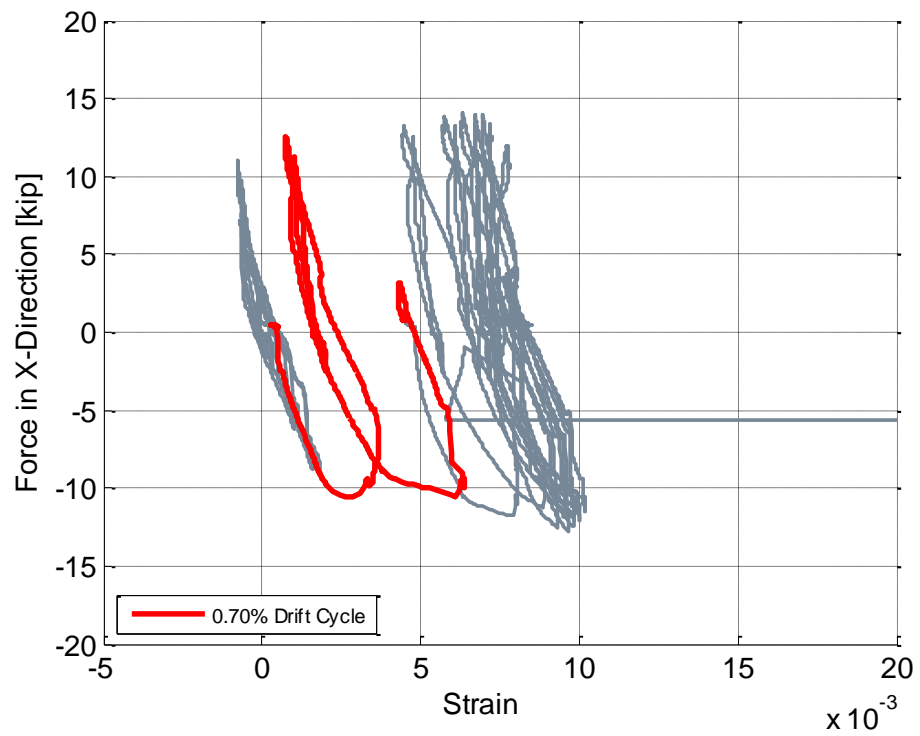
Figure 3-75: Specimen B2 – Lateral Force versus Strain in Gauge TS2
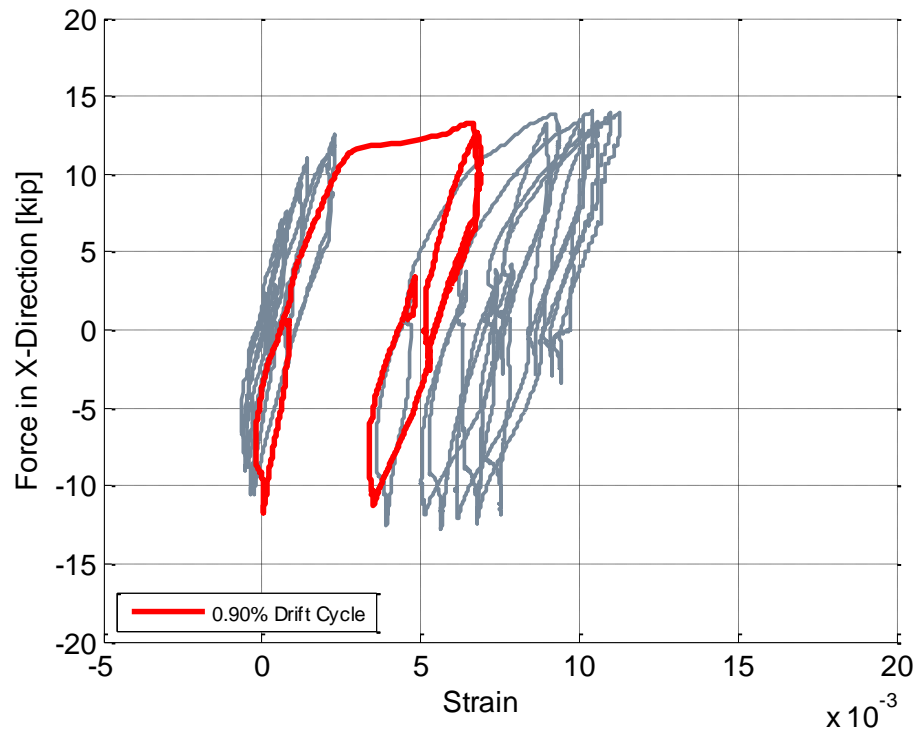
Figure 3-76: Specimen B2 – Lateral Force versus Strain in Gauge TS3

195
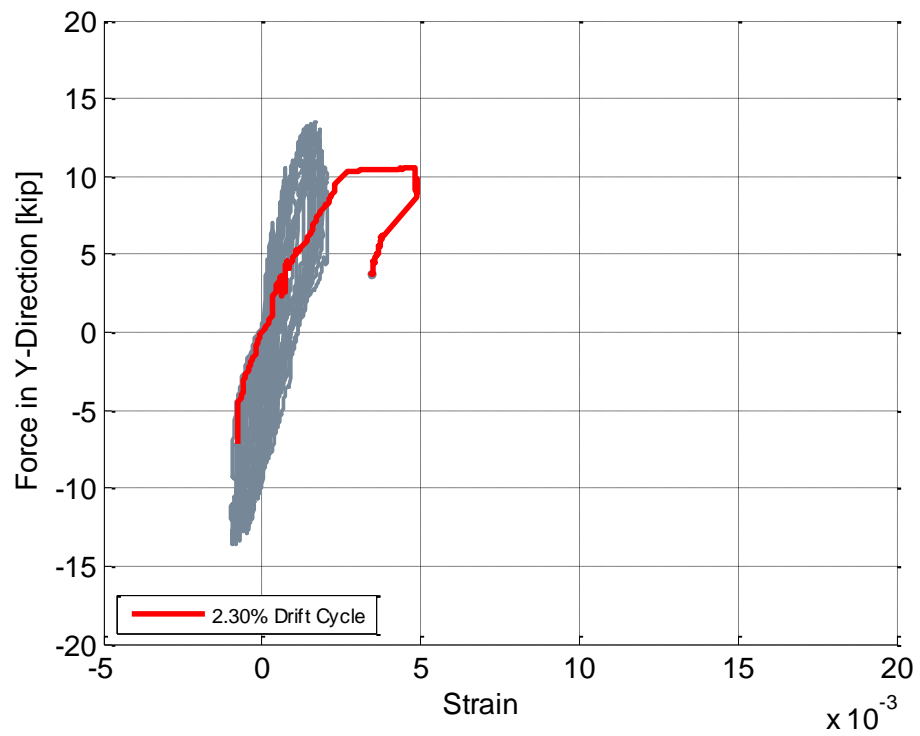
Figure 3-77: Specimen B2 – Lateral Force versus Strain in Gauge TE4
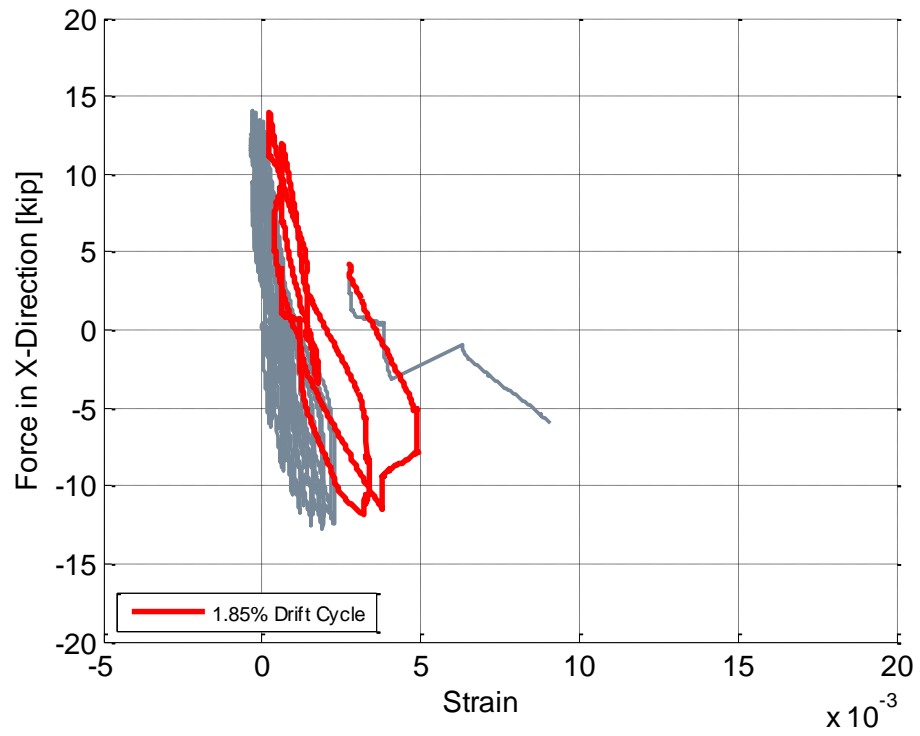
Figure 3-78: Specimen B2 – Lateral Force versus Strain in Gauge TS1
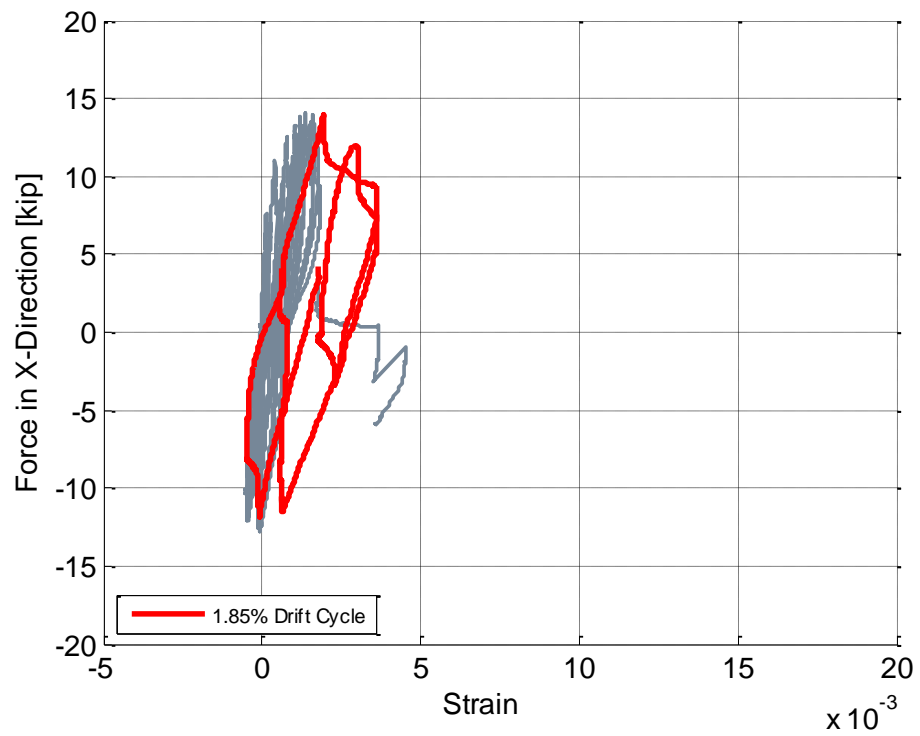
Figure 3-79: Specimen B2 – Lateral Force versus Strain in Gauge TS4
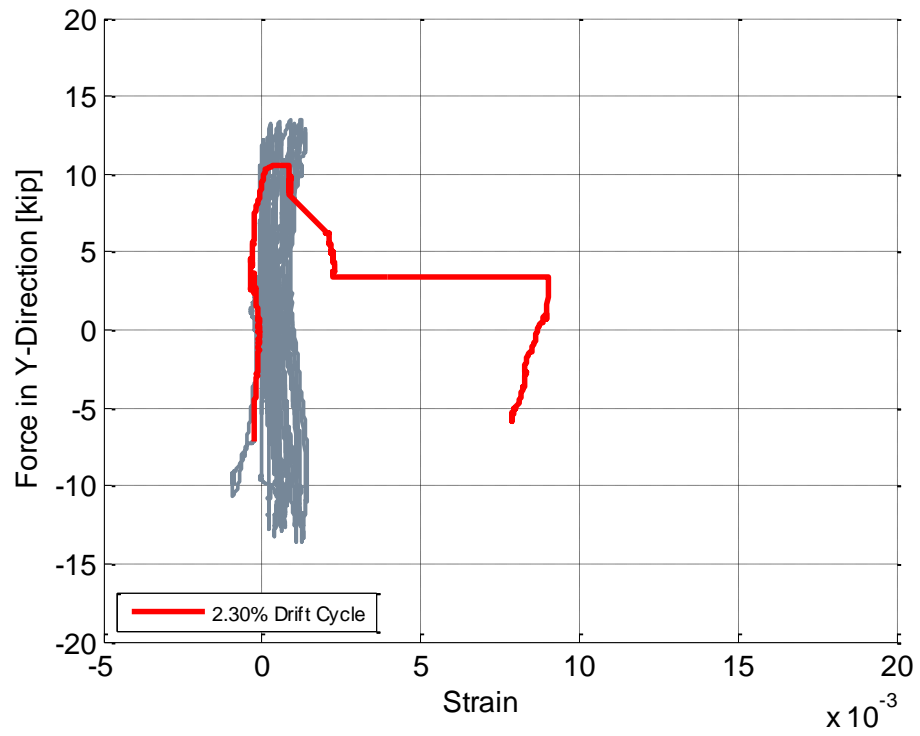
Figure 3-80: Specimen B2 – Lateral Force versus Strain in Gauge BE2
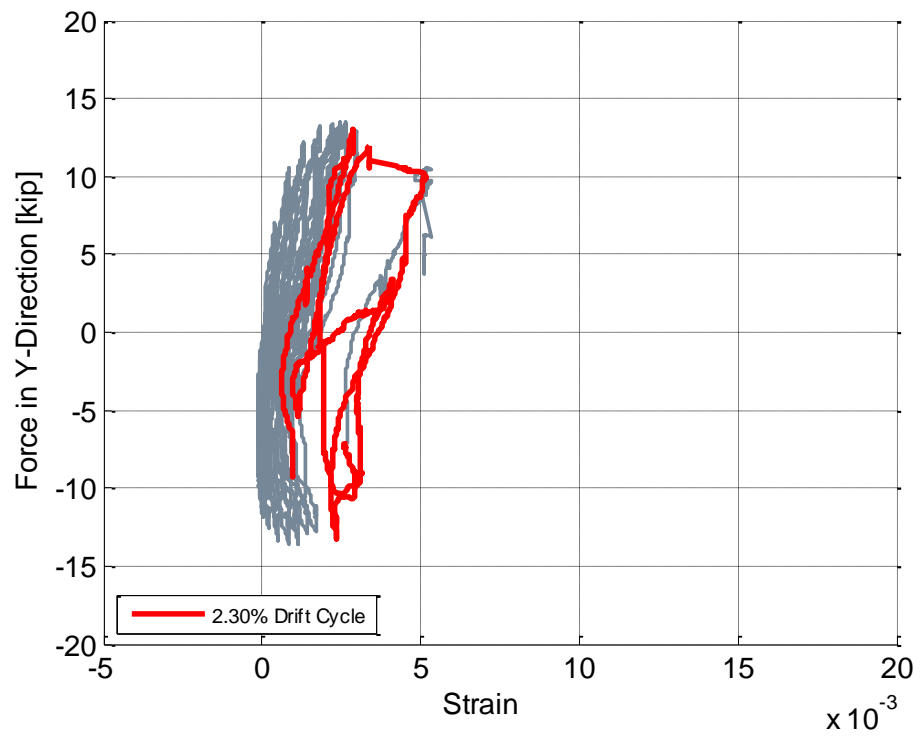
Figure 3-81: Specimen B2 – Lateral Force versus Strain in Gauge BE3
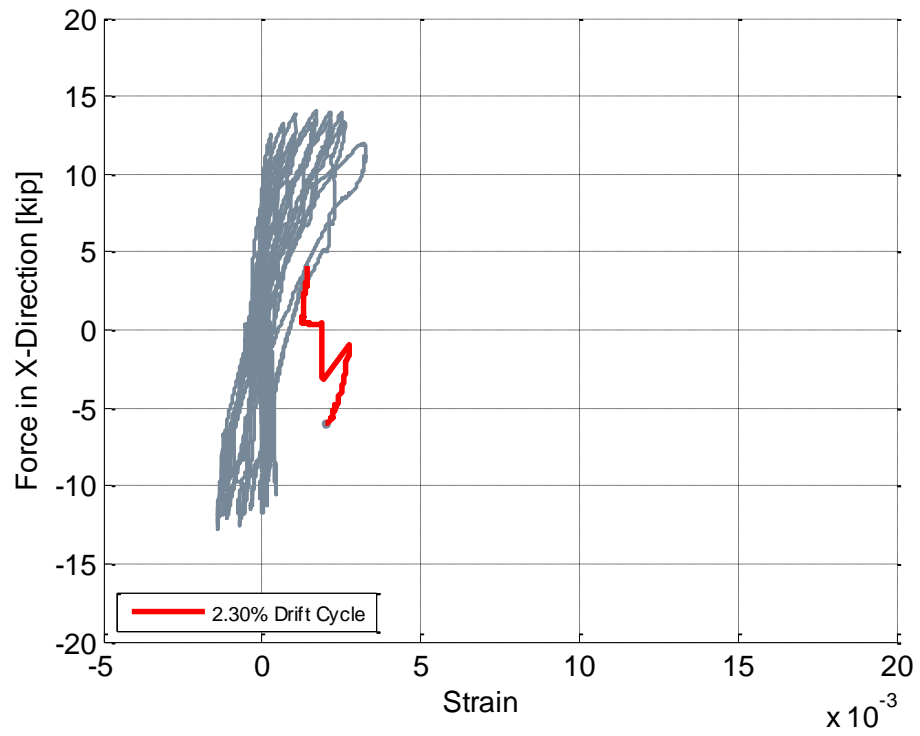
Figure 3-82: Specimen B2 – Lateral Force versus Strain in Gauge BS3
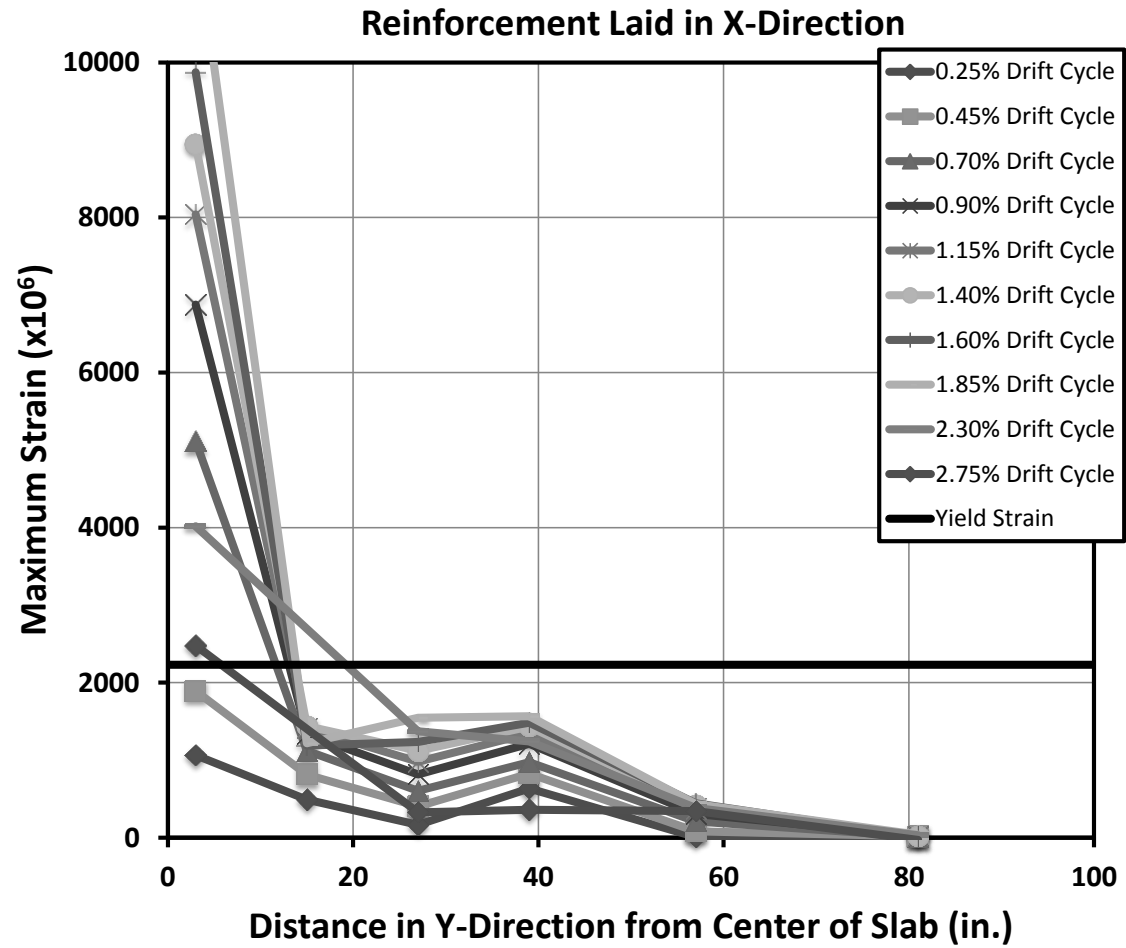
Figure 3-83: Specimen B3 – Profile of Strains in Top Mat Flexural Reinforcement Placed in the X-Direction at *d*/2 from Column Face
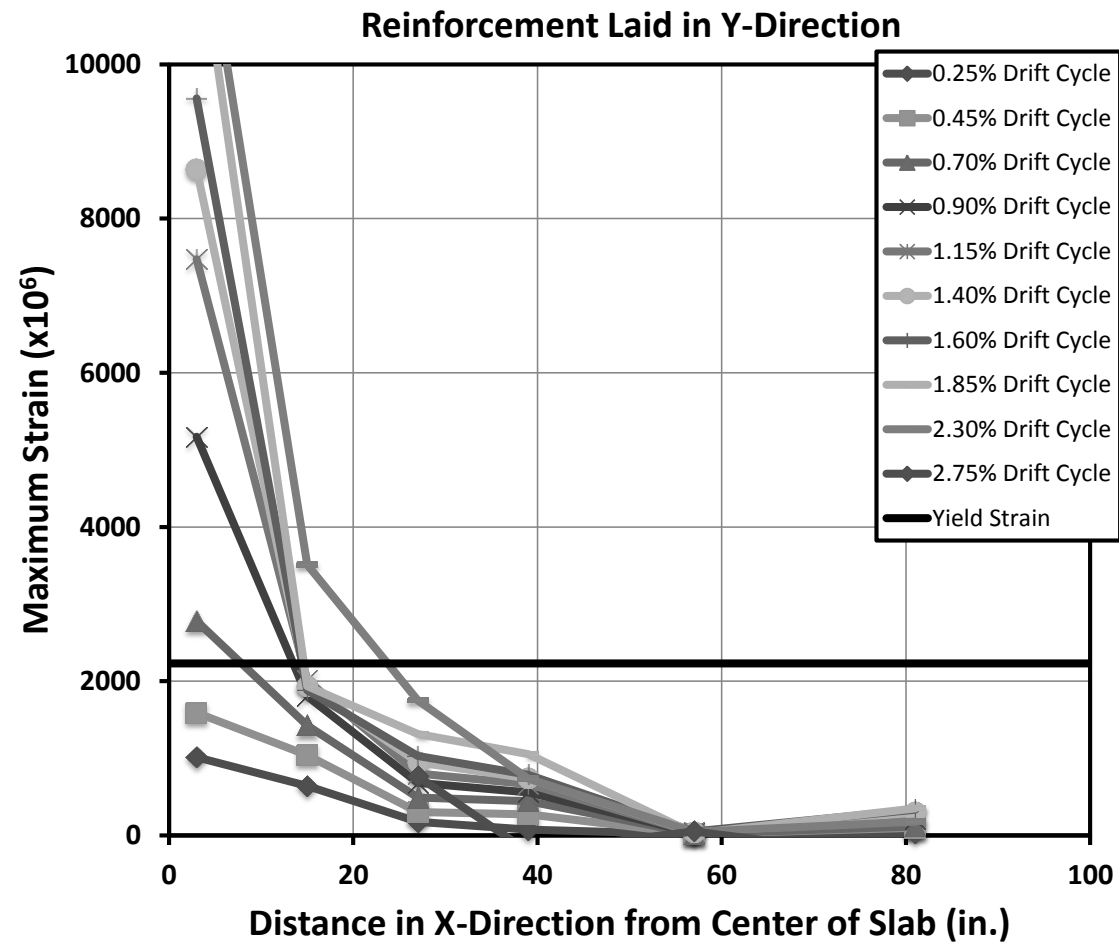
Figure 3-84: Specimen B3 – Profile of Strains in Top Mat Flexural Reinforcement Placed in the Y-Direction at *d*/2 from Column Face
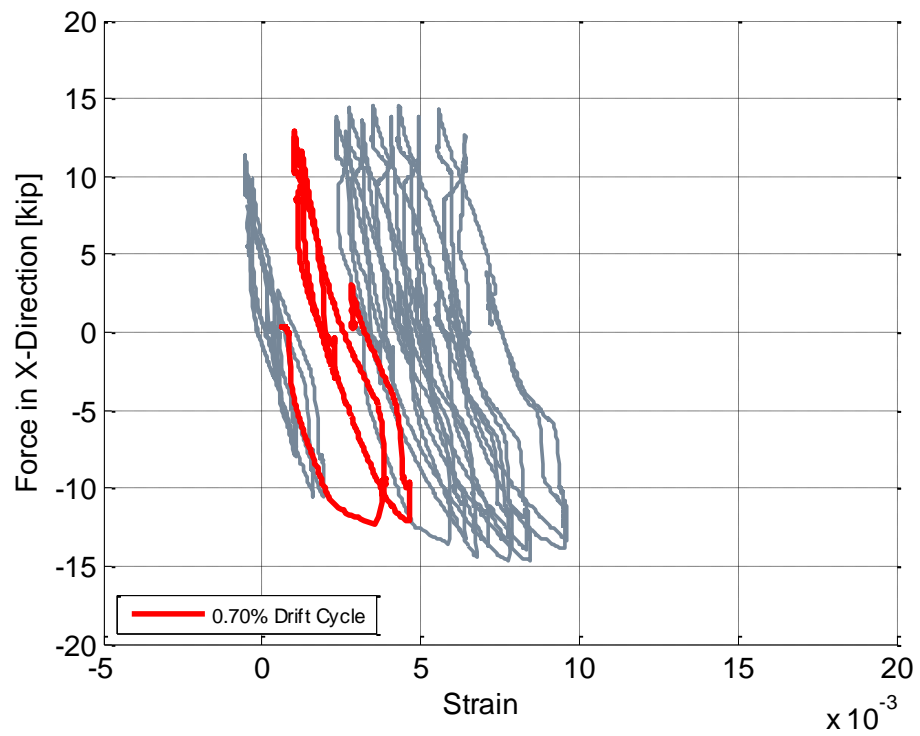
Figure 3-85: Specimen B3 – Lateral Force versus Strain in Gauge TS2
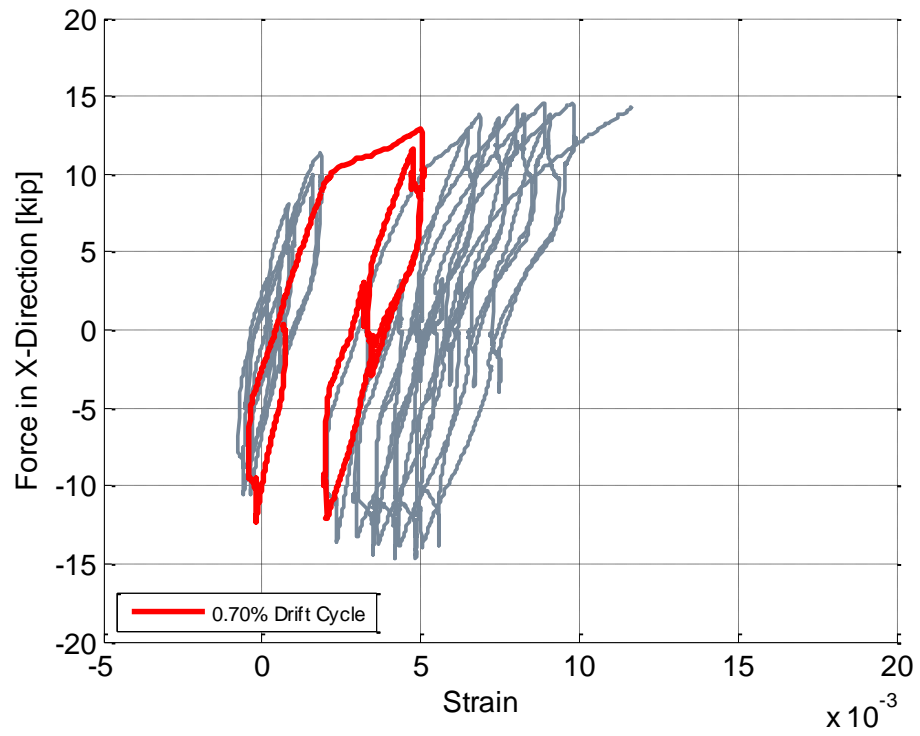
Figure 3-86: Specimen B3 – Lateral Force versus Strain in Gauge TS3
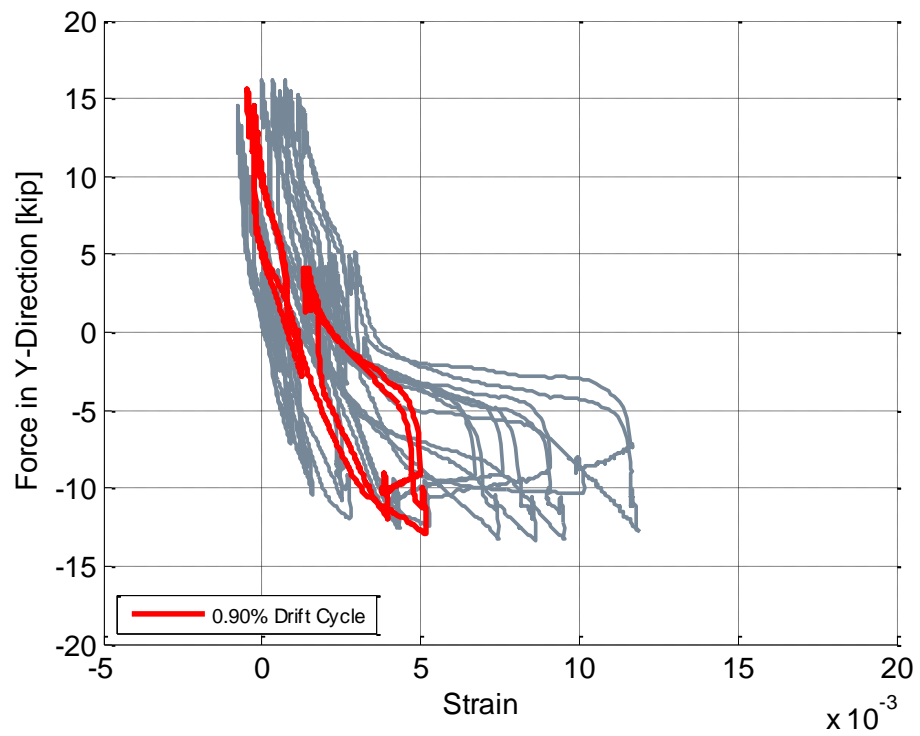
Figure 3-87: Specimen B3 – Lateral Force versus Strain in Gauge TE2
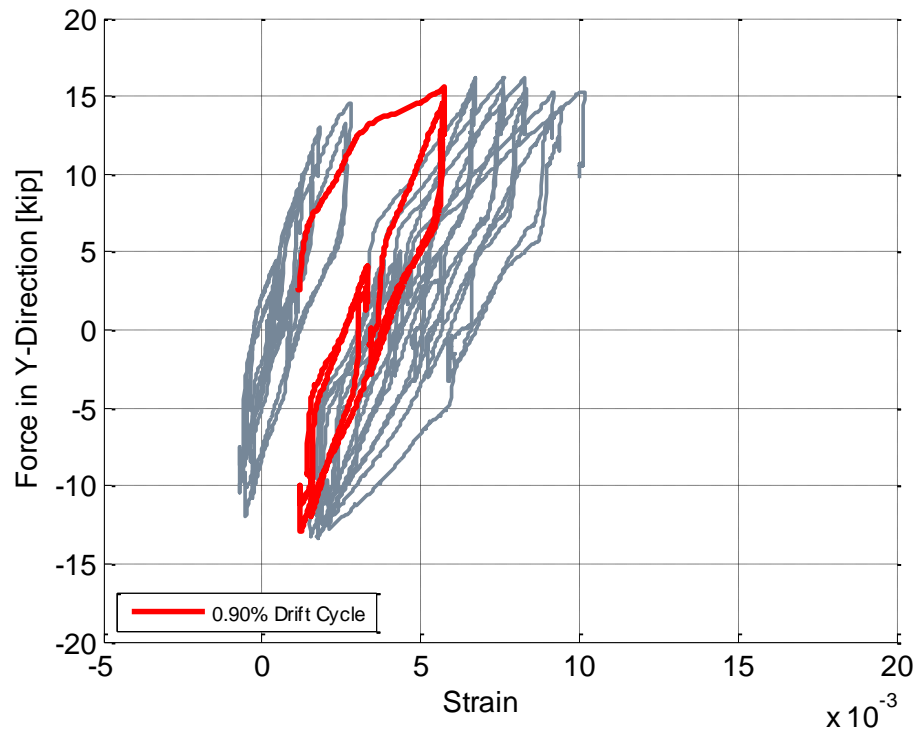
Figure 3-88: Specimen B3 – Lateral Force versus Strain in Gauge TE3
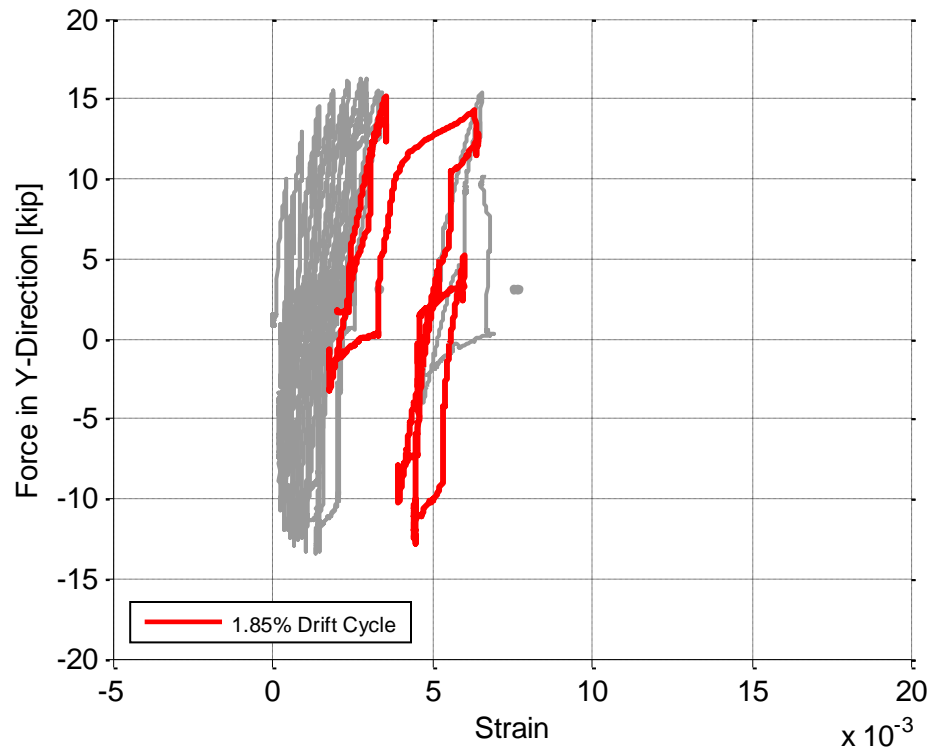
Figure 3-89: Specimen B3 – Lateral Force versus Strain in Gauge TE8
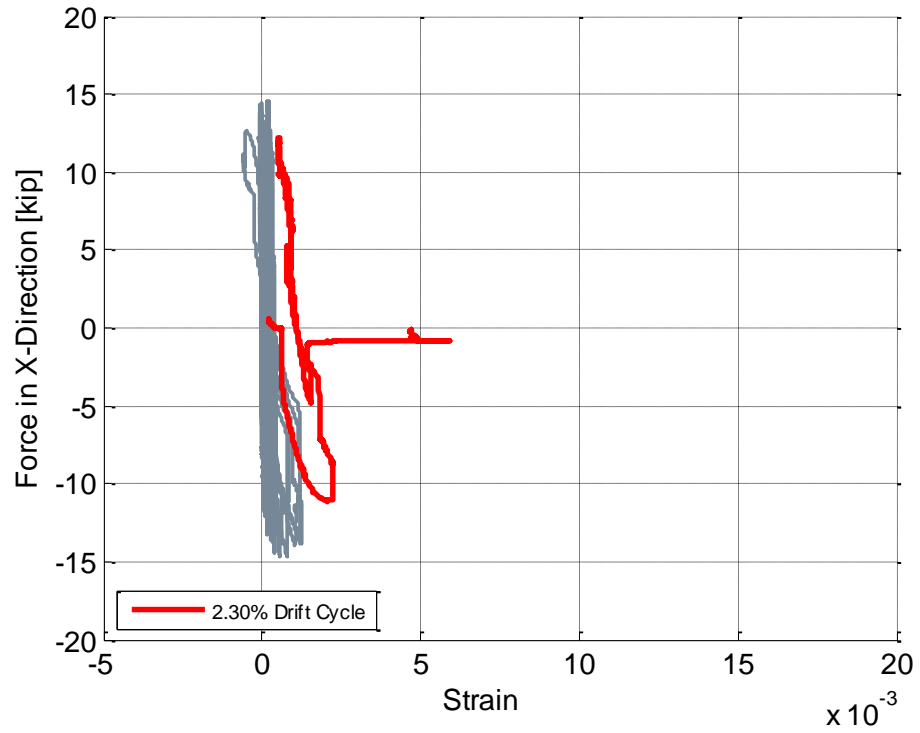
Figure 3-90: Specimen B3 – Lateral Force versus Strain in Gauge BS3

203
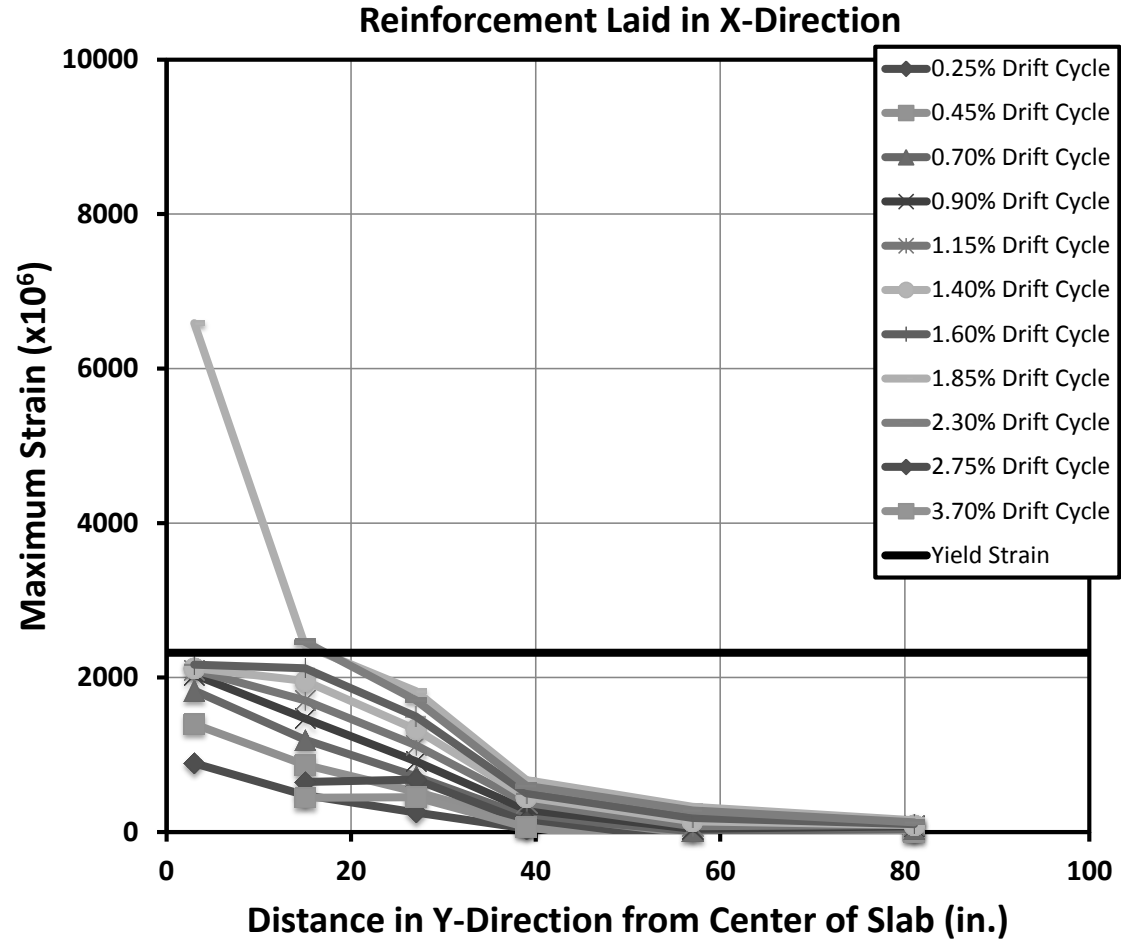
Figure 3-91: Specimen B4 – Profile of Strains in Top Mat Flexural Reinforcement Placed in the X-Direction at *d*/2 from Column Face. Gauge TS3, Located 3 in. From the Centerline of the Slab, was Damaged After the 1.85% Drift Cycle.
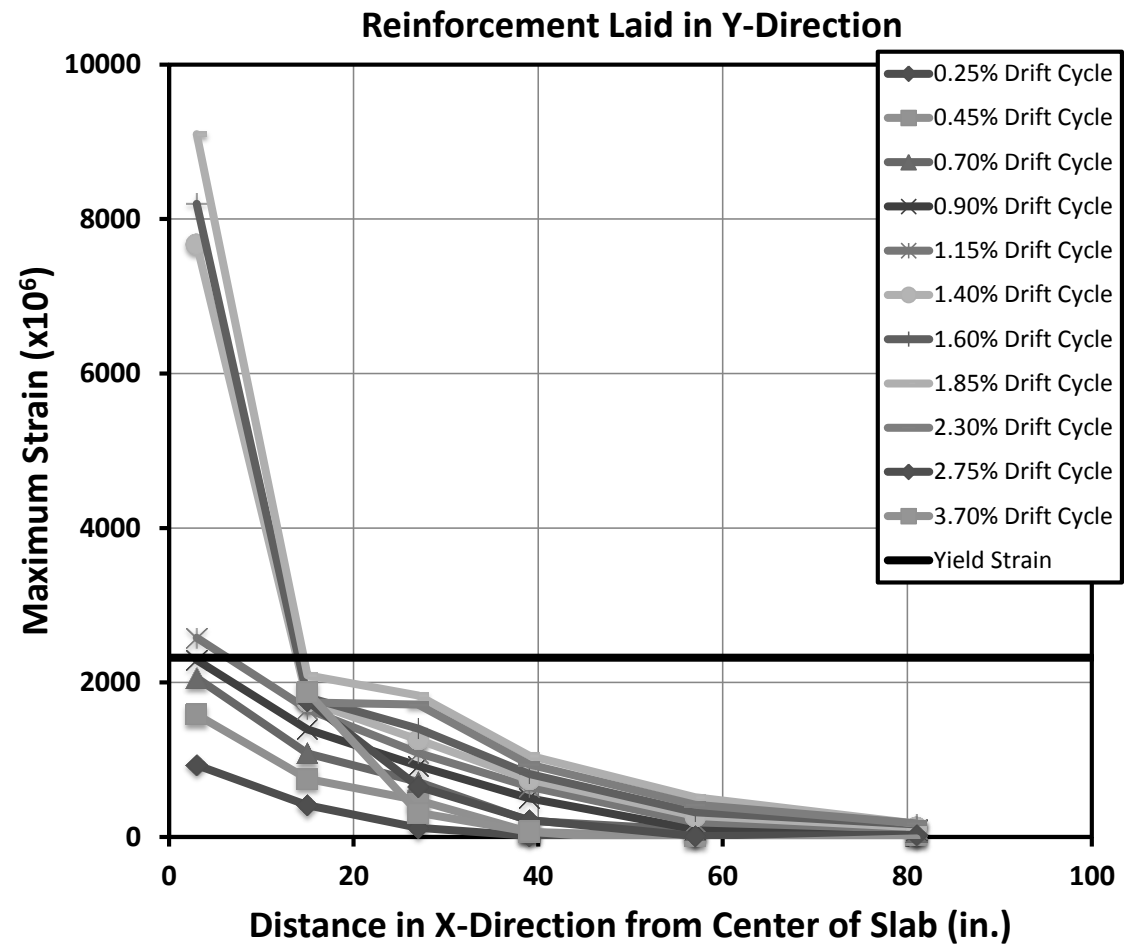
Figure 3-92: Specimen B4 – Profile of Strains in Top Mat Flexural Reinforcement Placed in the Y-Direction at *d*/2 from Column Face
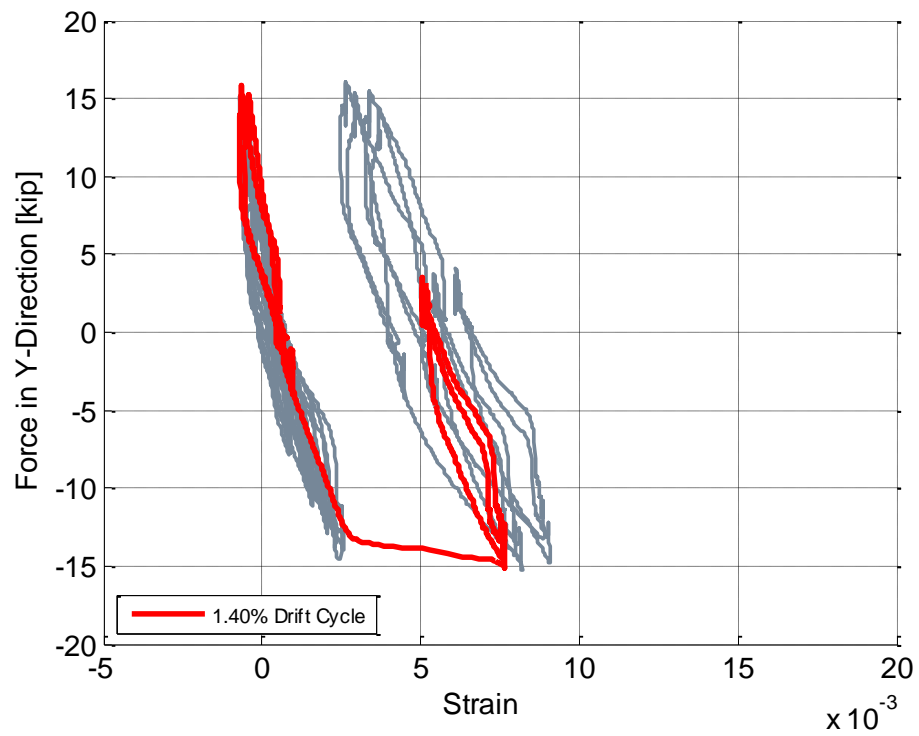
Figure 3-93: Specimen B4 – Applied Lateral Force versus Strain in Gauge TE2
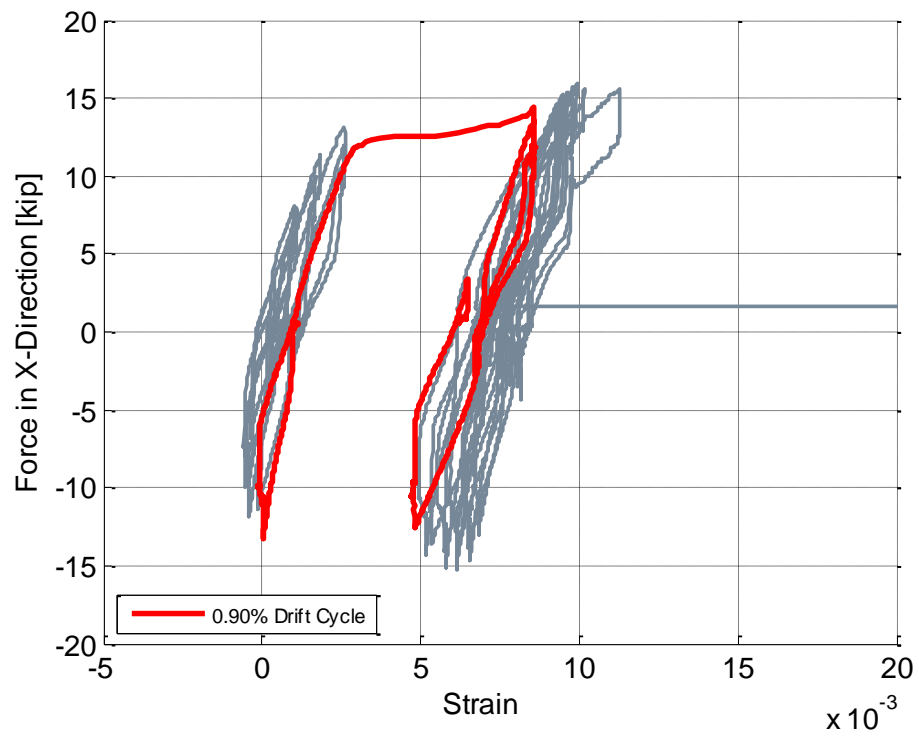
Figure 3-94: Specimen B4 – Applied Lateral Force versus Strain in Gauge TS2

206
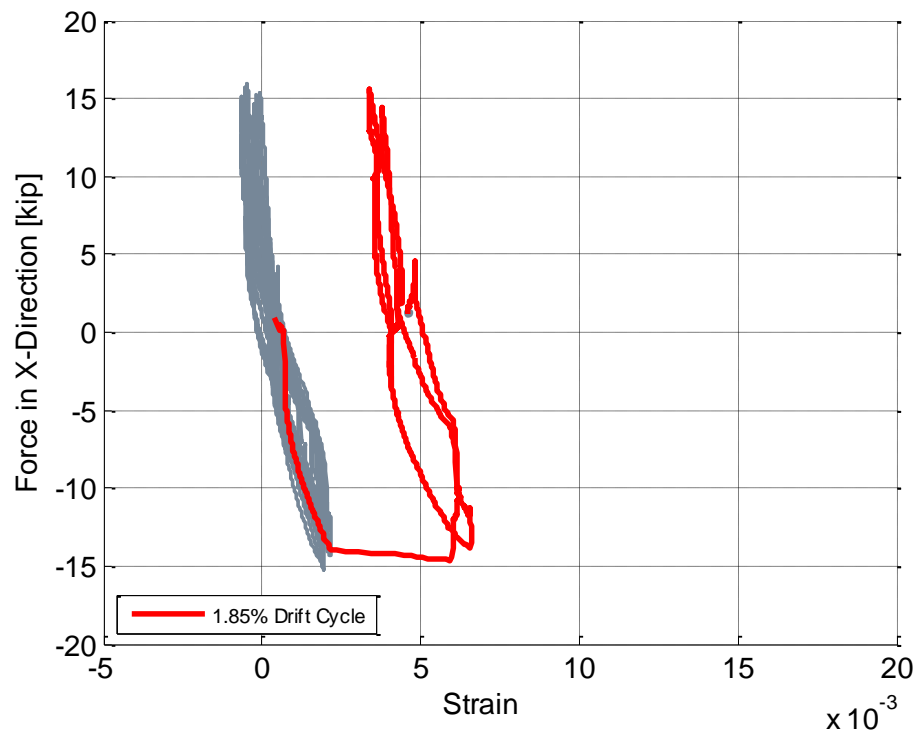
Figure 3-95: Specimen B4 – Applied Lateral Force versus Strain in Gauge TS3
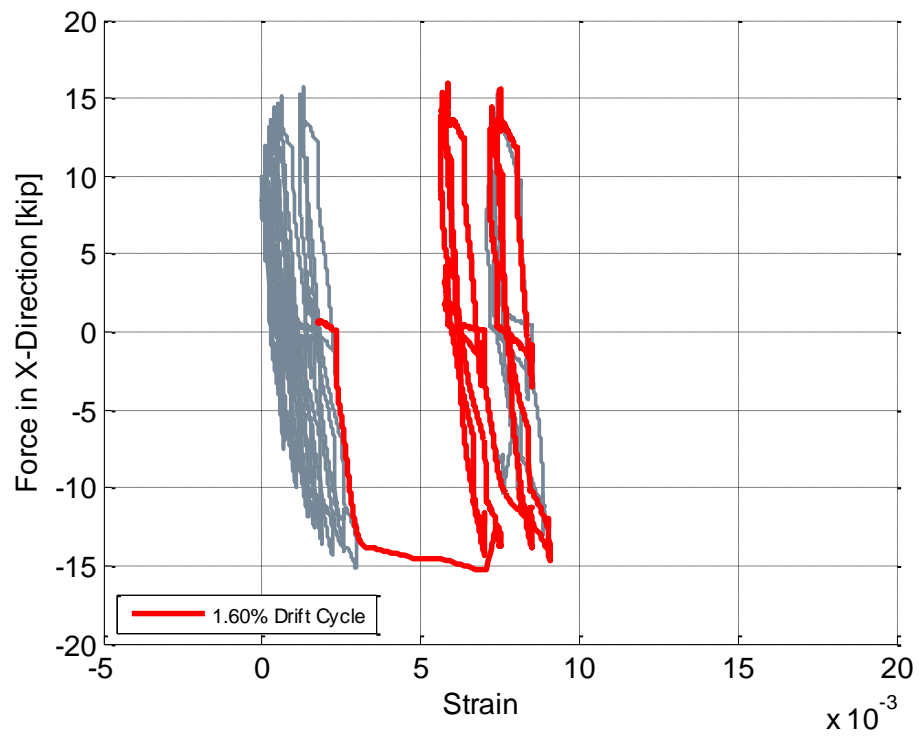
Figure 3-96: Specimen B4 – Applied Lateral Force versus Strain in Gauge TS5
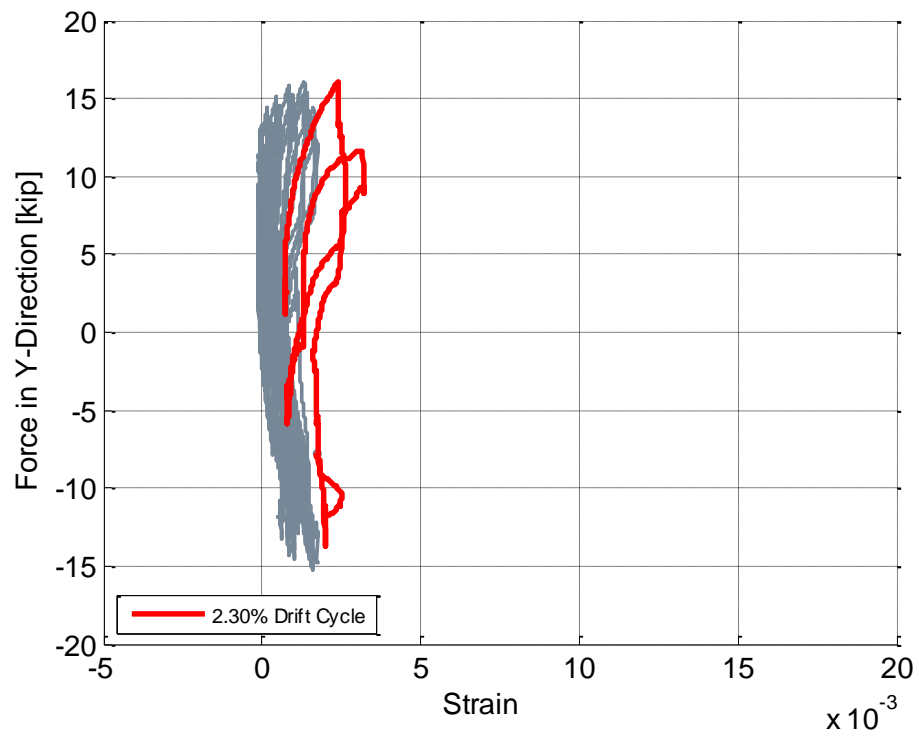
Figure 3-97: Specimen B4 – Applied Lateral Force versus Strain in Gauge BE2
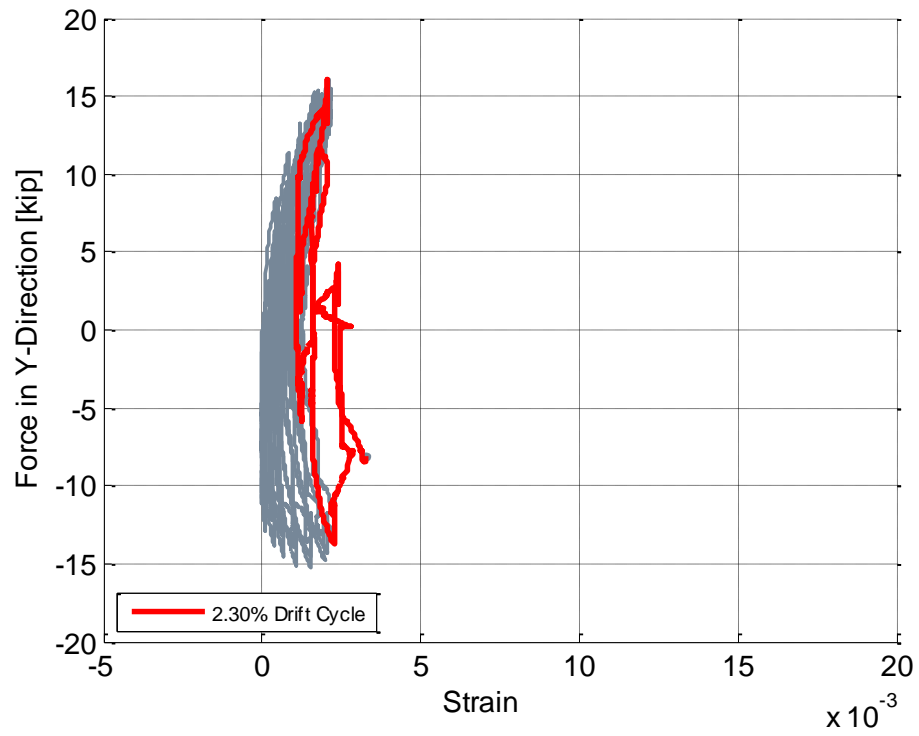
Figure 3-98: Specimen B4 – Applied Lateral Force versus Strain in Gauge BE3
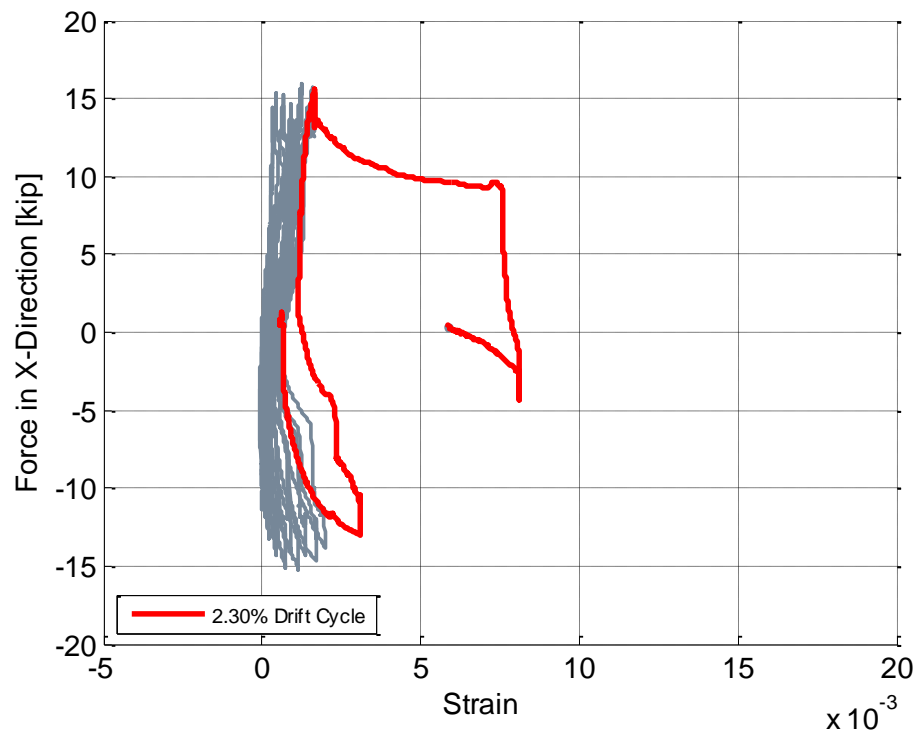
Figure 3-99: Specimen B4 – Applied Lateral Force versus Strain in Gauge BS3
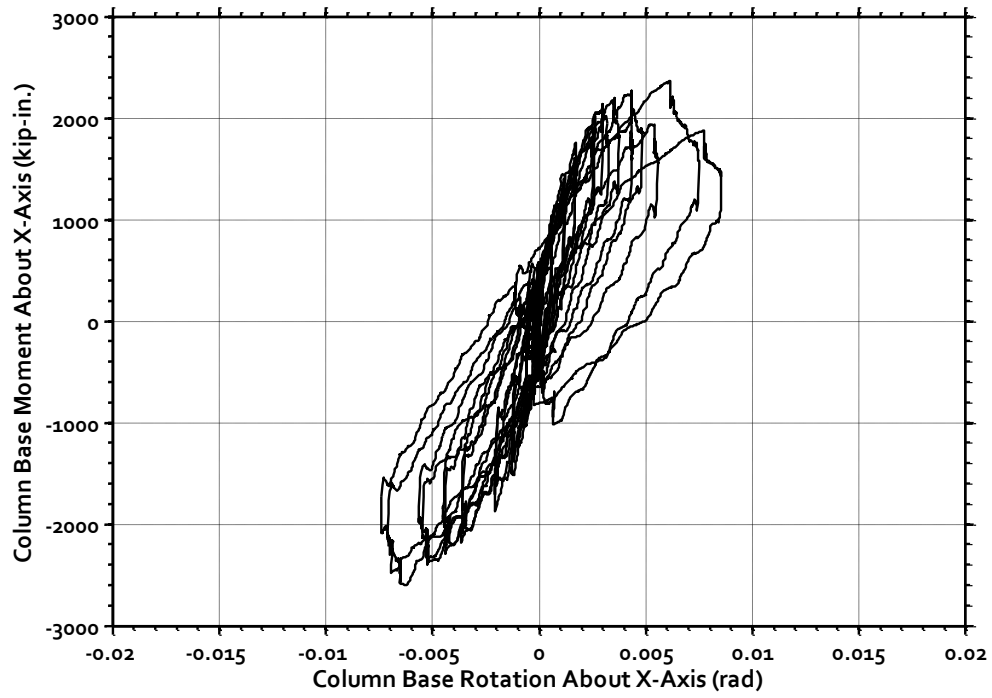
Figure 3-100: Specimen B1 – Column Base Moment versus Rotation (About X-Axis)
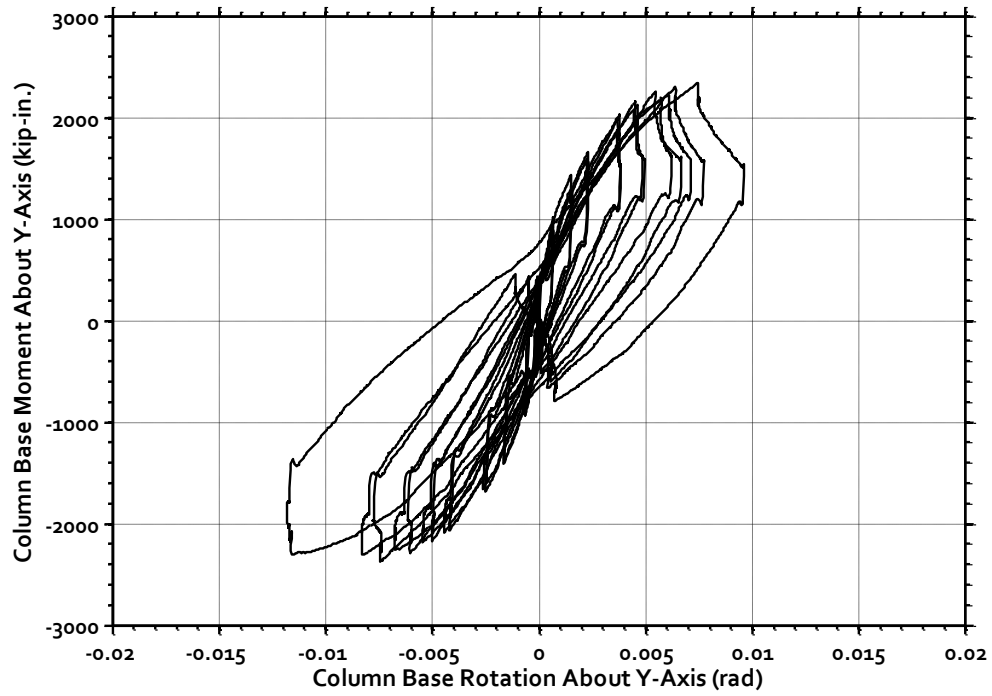
Figure 3-101: Specimen B1 – Column Base Moment versus Rotation (About Y-Axis)
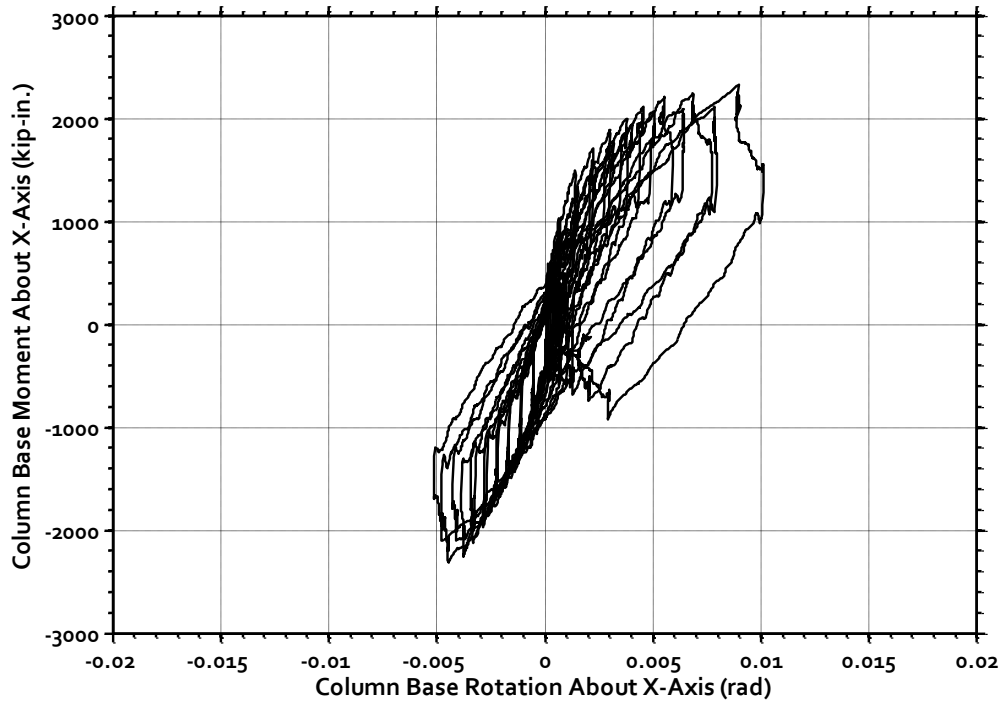
Figure 3-102: Specimen B2 – Column Base Moment versus Rotation (About X-Axis)
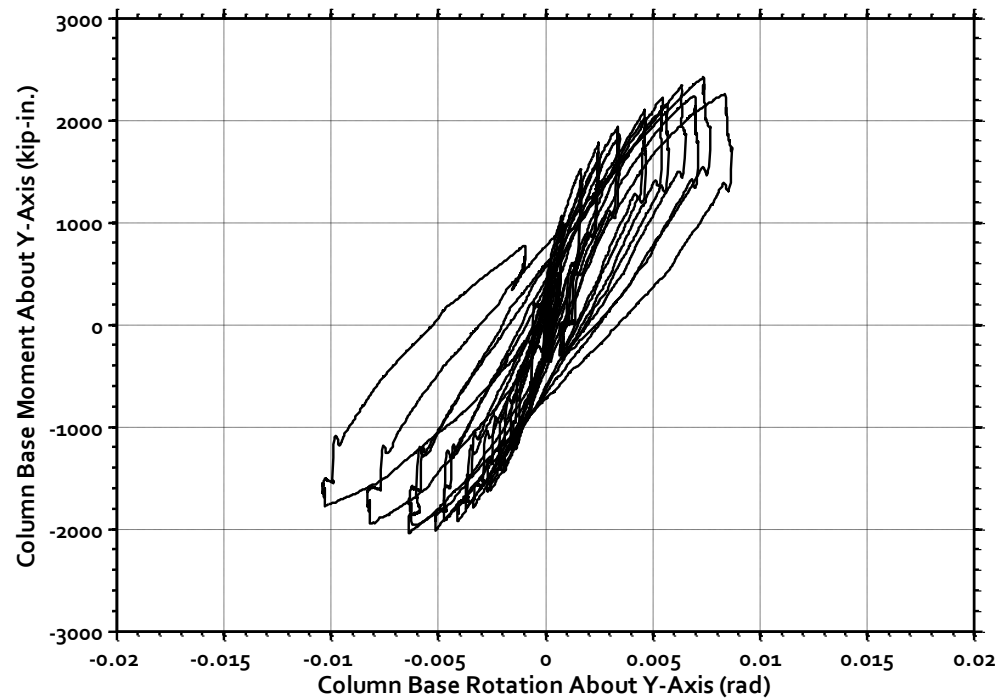
Figure 3-103: Specimen B2 – Column Base Moment versus Rotation (About Y-Axis)
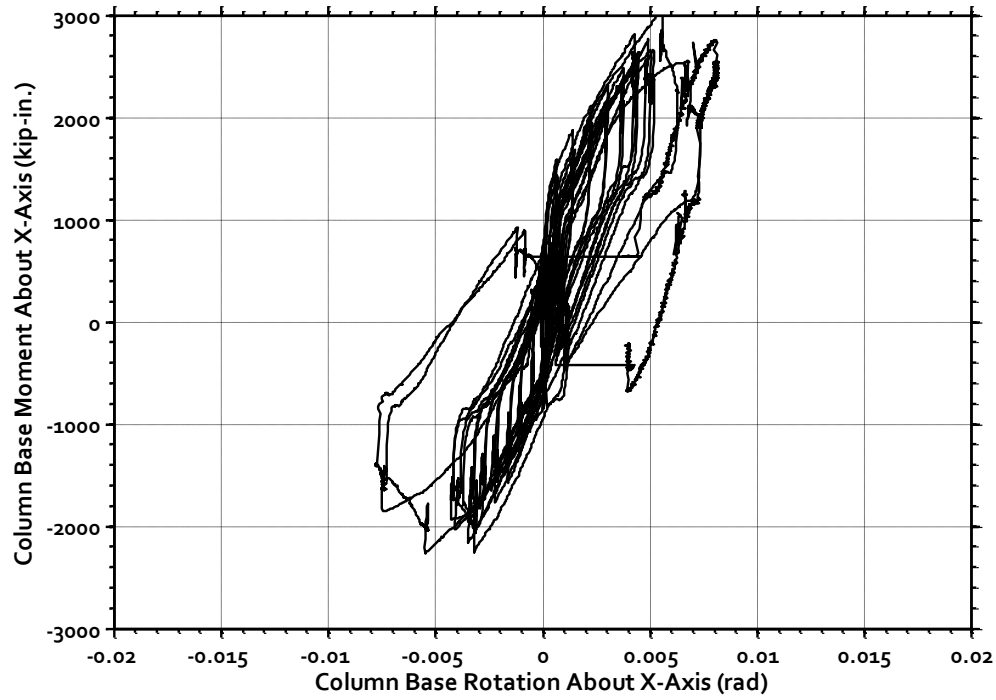
Figure 3-104: Specimen B3 – Column Base Moment versus Rotation (About X-Axis)
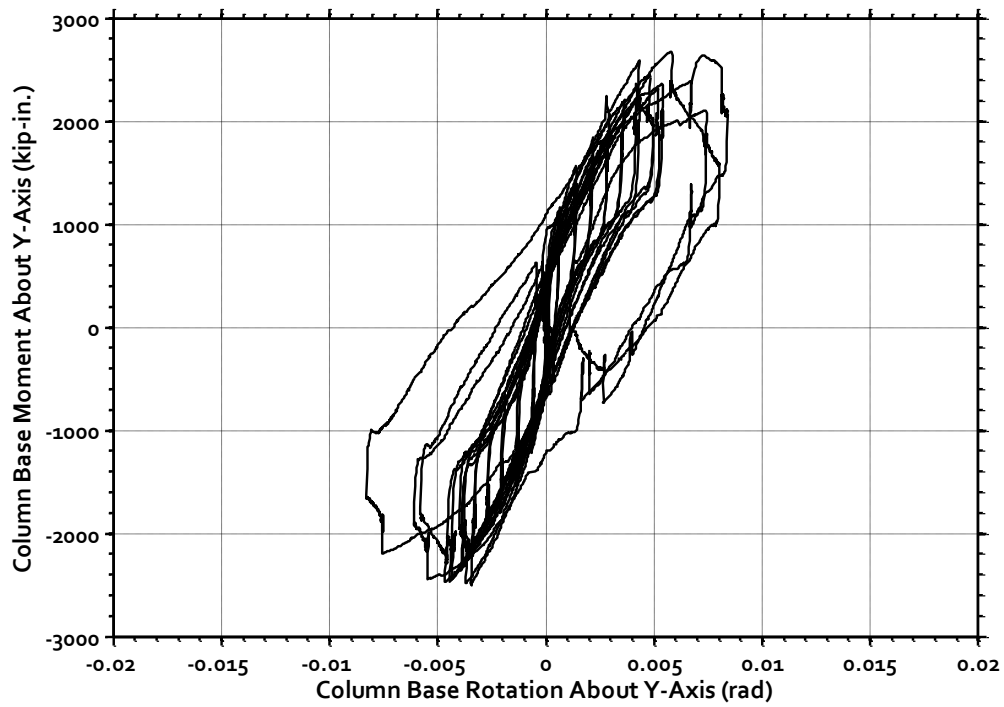
Figure 3-105: Specimen B3 – Column Base Moment versus Rotation (About Y-Axis)

212
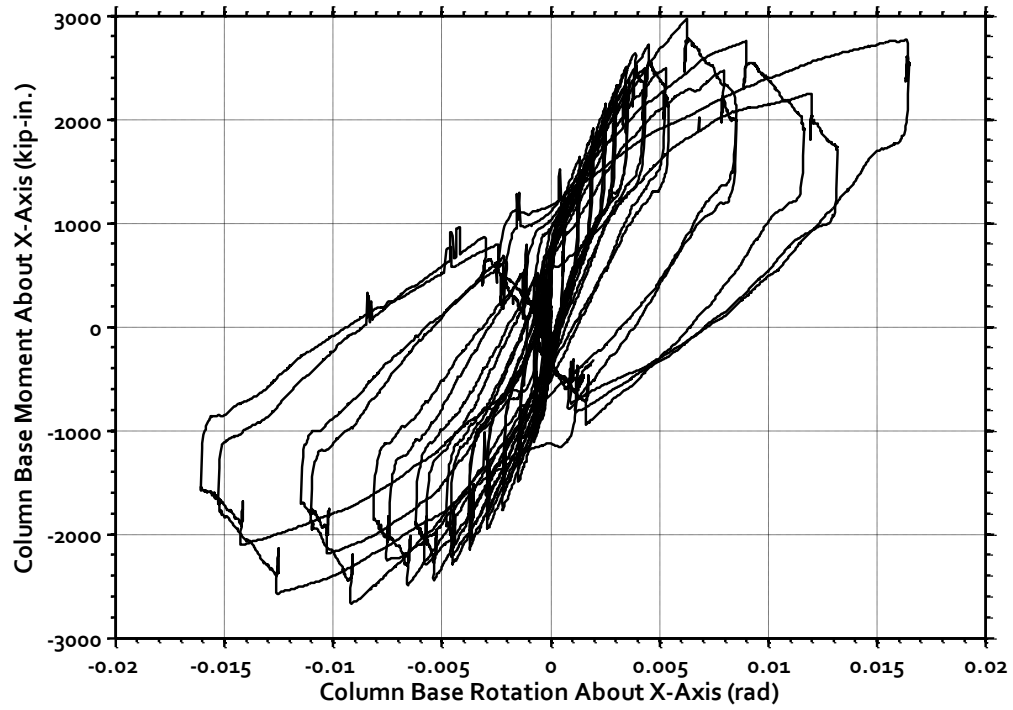
Figure 3-106: Specimen B4 – Column Base Moment versus Rotation (About X-Axis)
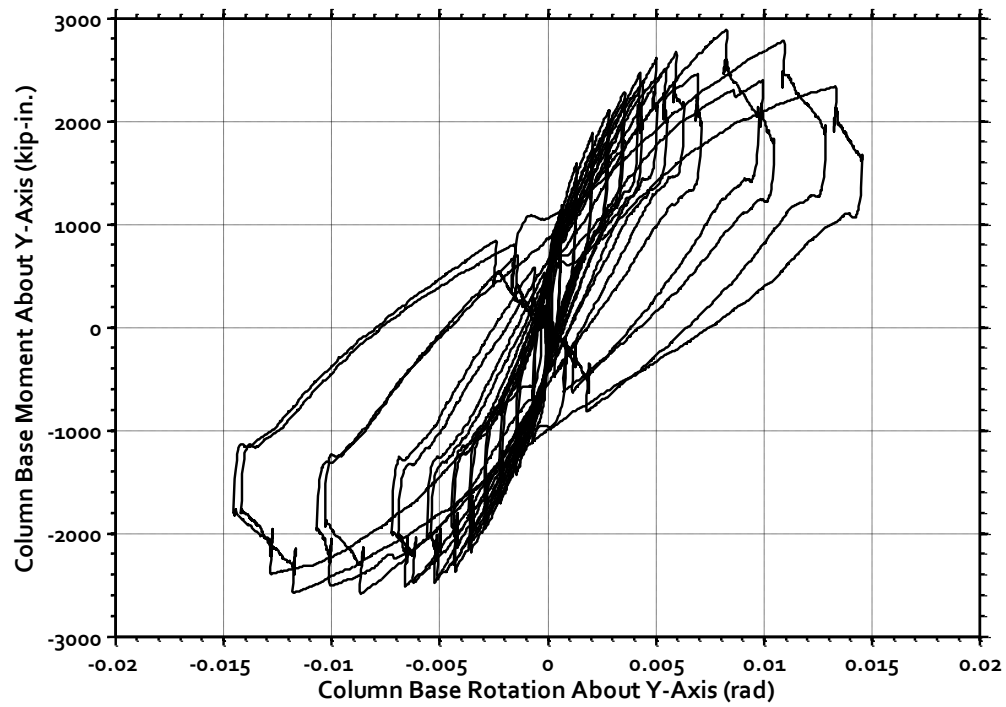
Figure 3-107: Specimen B4 – Column Base Moment versus Rotation (About Y-Axis)

213
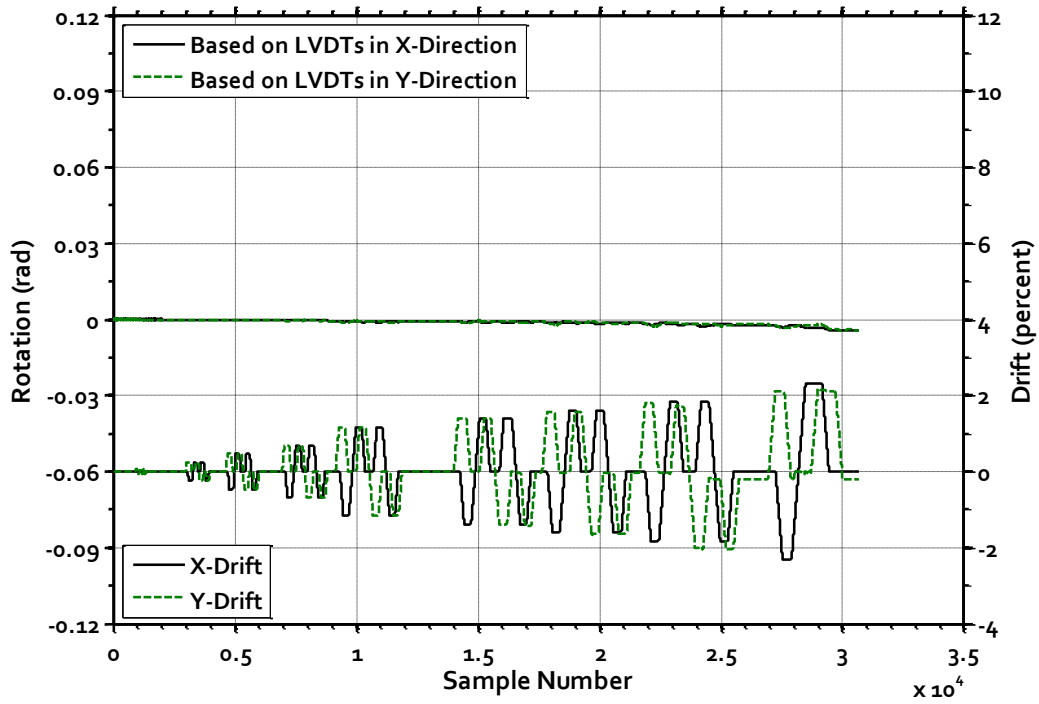
Figure 3-108: Specimen B1 – Rotation About Vertical Z-Axis
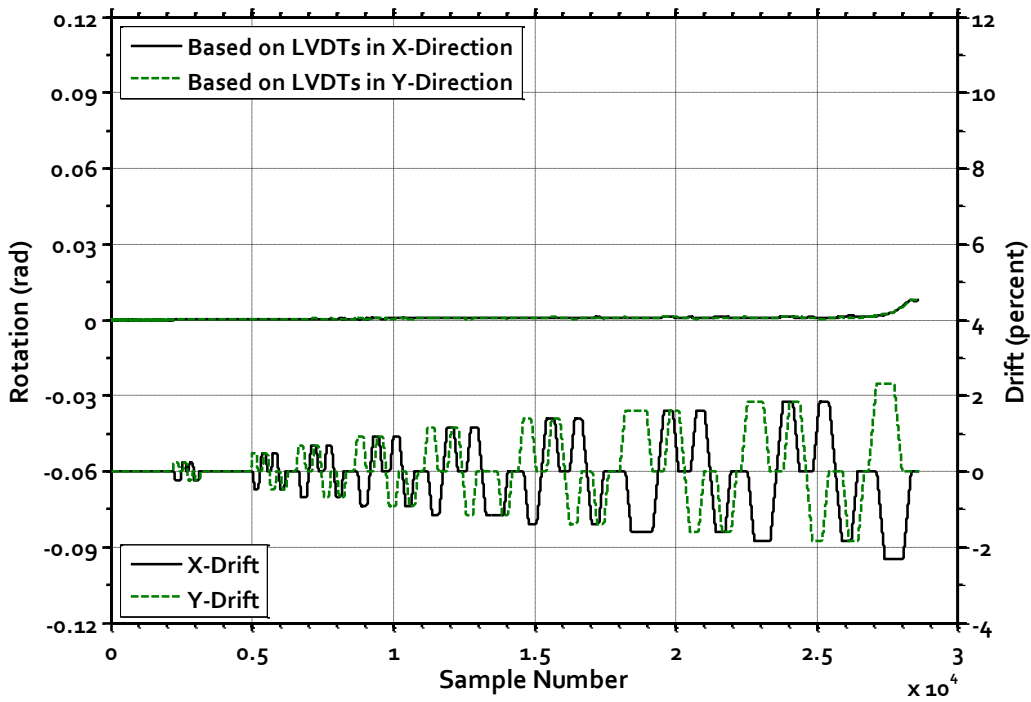
Figure 3-109: Specimen B2 – Rotation About Vertical Z-Axis
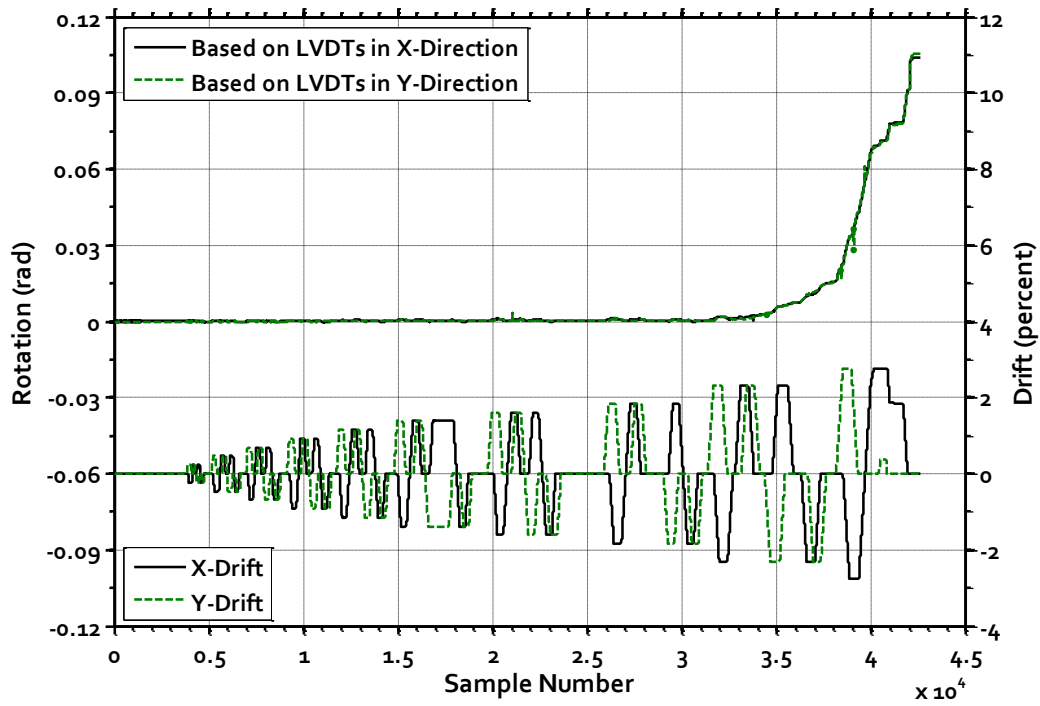
Figure 3-110: Specimen B3 – Rotation About Vertical Z-Axis
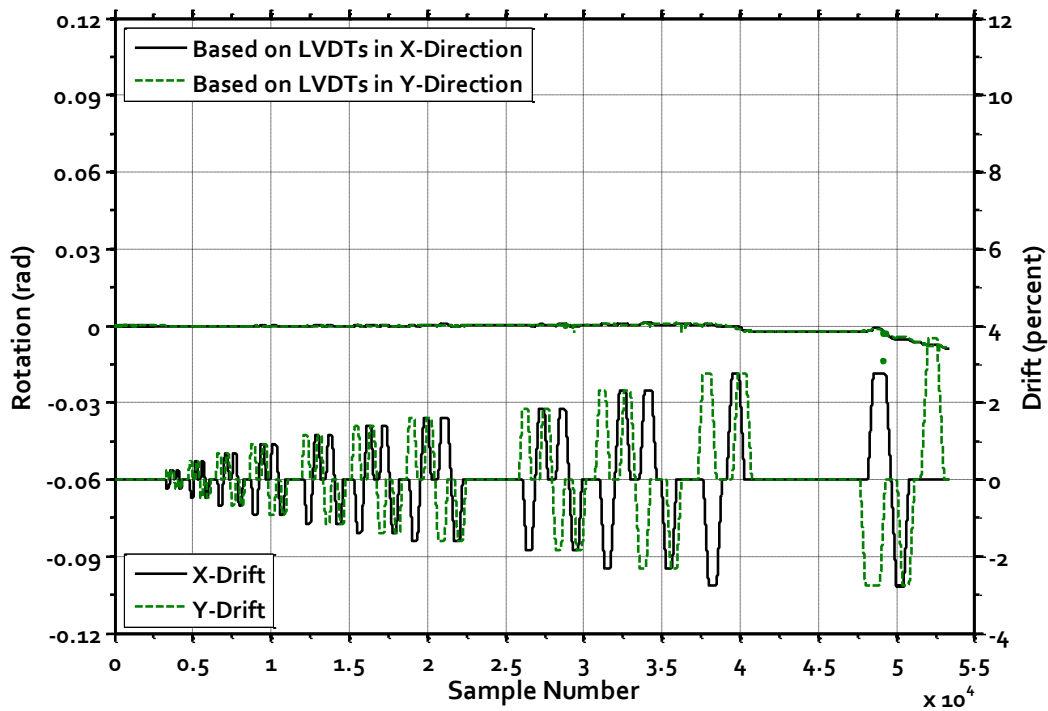
Figure 3-111: Specimen B4 – Rotation About Vertical Z-Axis

215
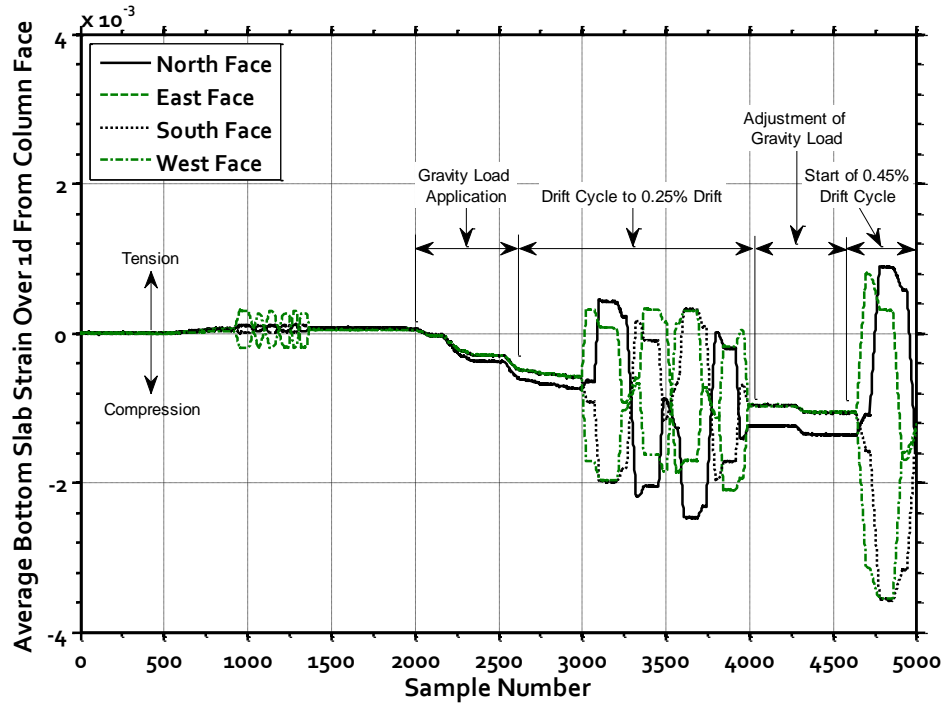
Figure 4-1: Average Strain in the Bottom Face of the Slab of Specimen B1, Measured Within One Effective Slab Depth of the Column Face
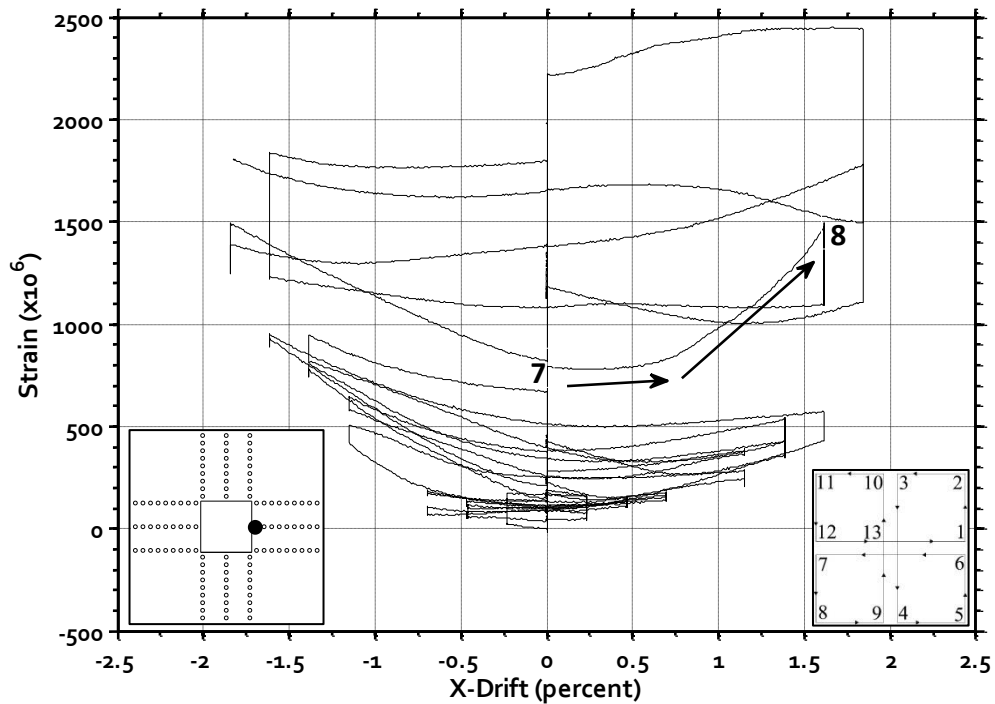
Figure 4-2: Specimen B1 – Strain from Gauge R-E1, Showing a Change in Slope and Large Increase In Strain While Loading to Point 8 of 1.60% Drift Cycle
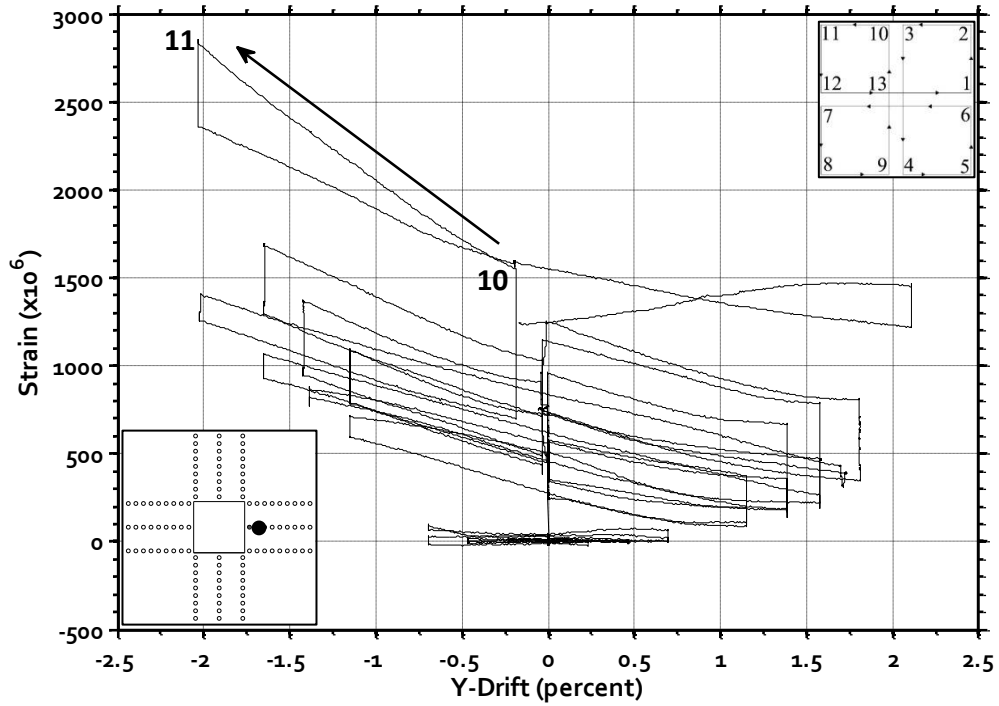
Figure 4-3: Specimen B1 – Strain from Gauge R-E2, Indicating a Large Increase in Strain Beyond Yield While Loading to Point 11 of 1.85% Drift Cycle
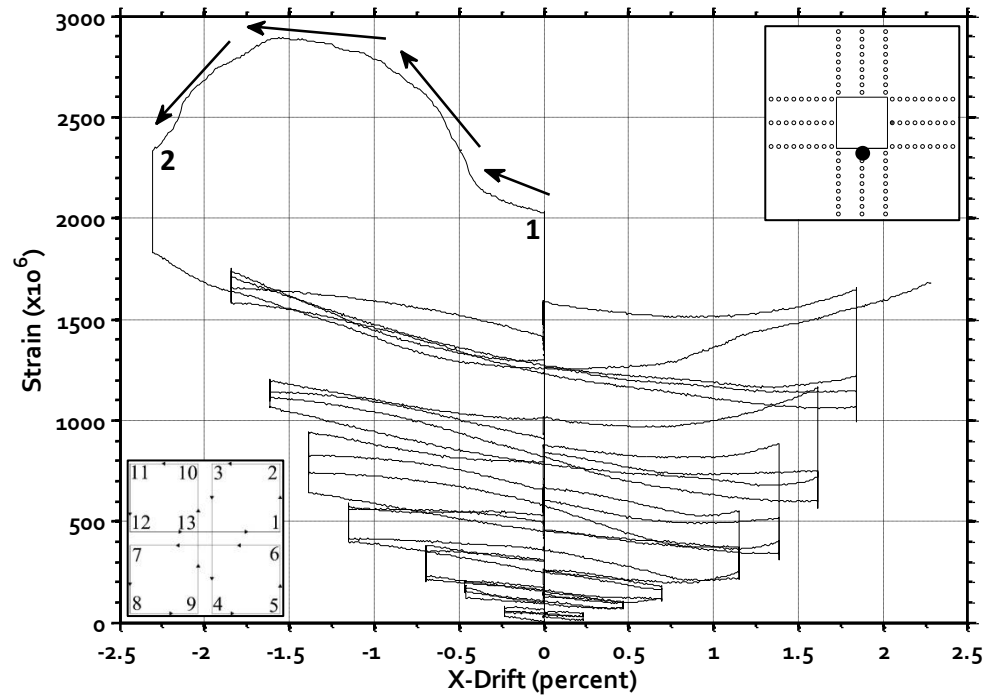
Figure 4-4: Specimen B1 – Strain from Gauge R-S1, Indicating a Large Increase in Strain Beyond Yield Followed by a Decrease in Strain While Loading to Point 2 of 2.30% Drift Cycle

217
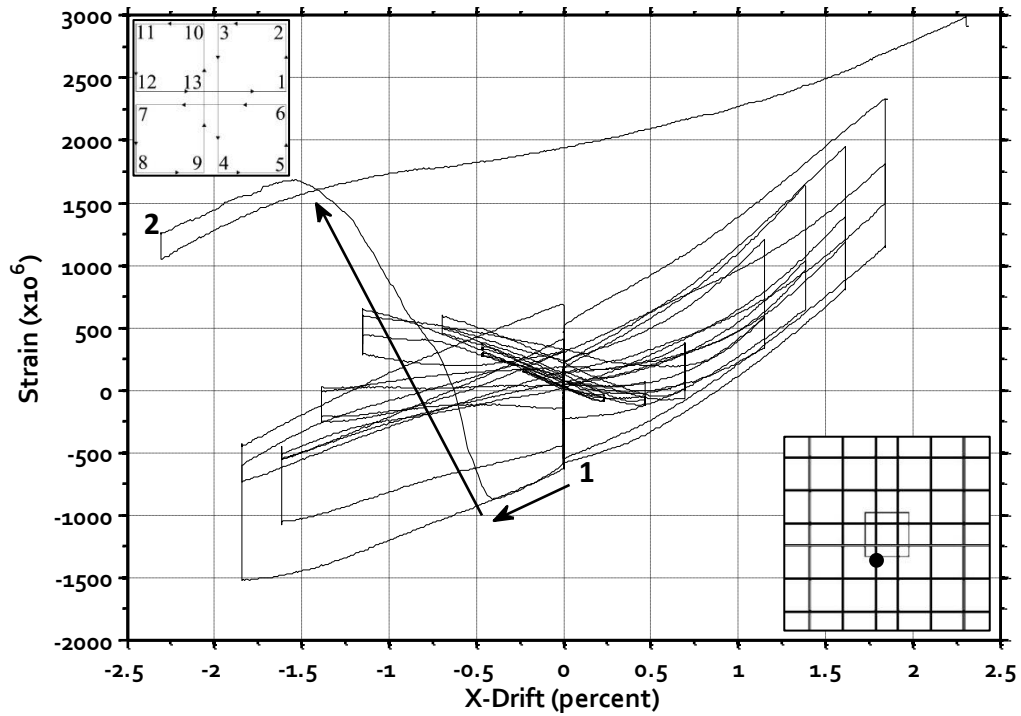
Figure 4-5: Specimen B1 – Strain from Gauge BS-S2, Indicating a Shift from Compression to Tension Strains While Loading to Point 2 of 2.30% Drift Cycle
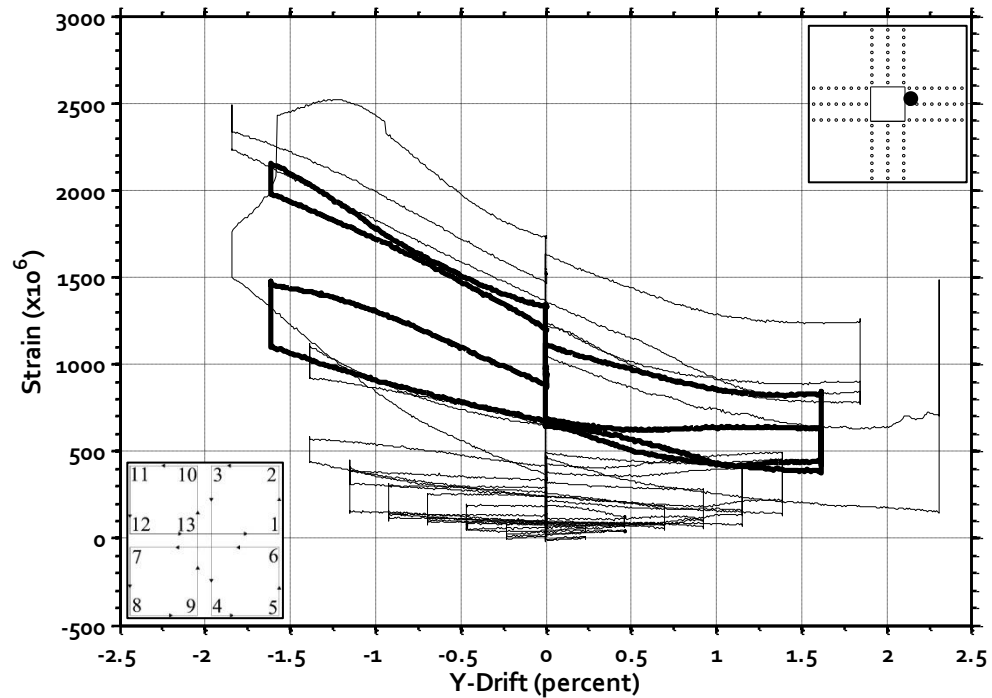
Figure 4-6: Specimen B2 – Strain from Gauge R-E1, the Only Instrumented Stud to Exhibit Strains Exceeding 0.0015 Prior to the Cycle to 1.85% Drift (1.60% Drift Cycle is Bold)
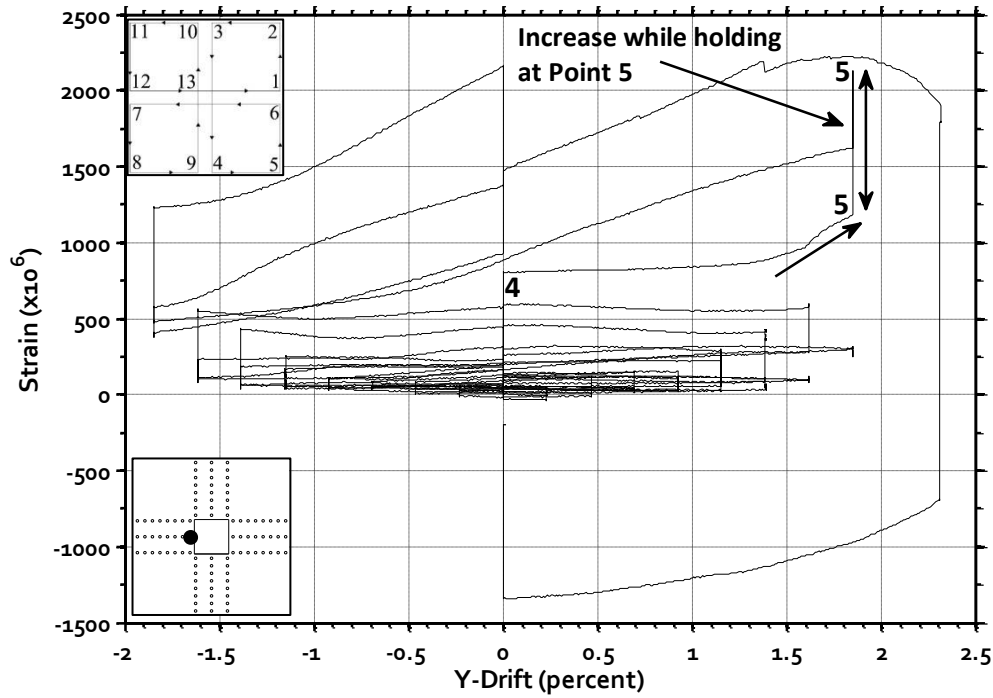
Figure 4-7: Specimen B2 – Strain from Gauge R-W1, Showing a Large Increase in Strain During the 1.85% Drift Cycle as the Specimen Reached Point 5
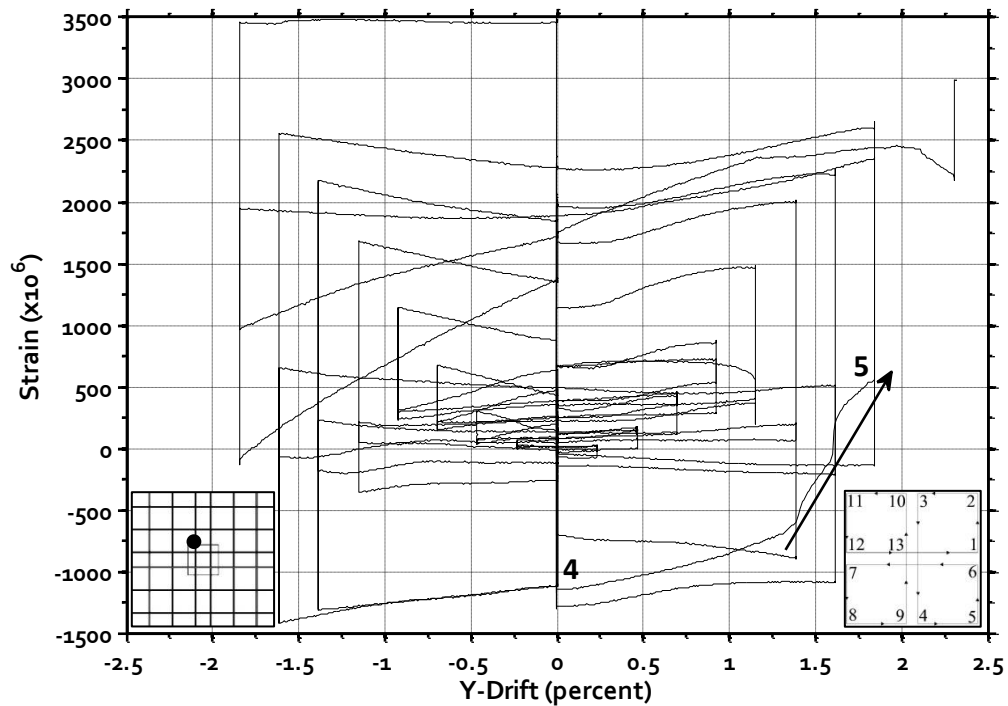
Figure 4-8: Specimen B2 – Strain from Gauge BS-S3, Showing a Shift from Flexural Compression to Integrity Reinforcement-Type Tension During the 1.85% Drift Cycle
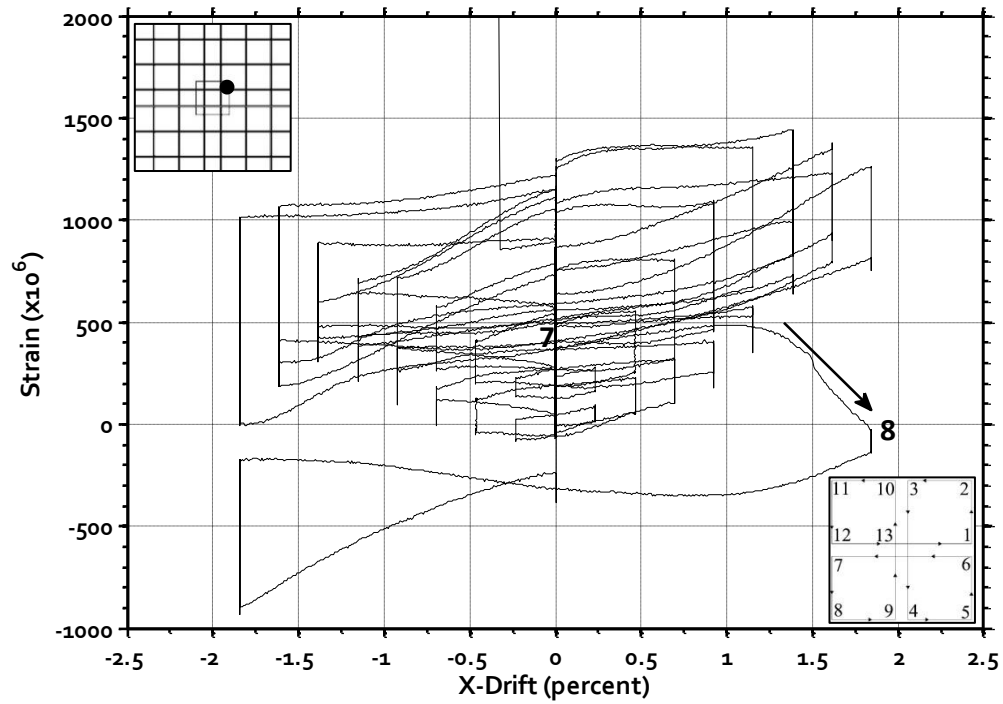
Figure 4-9: Specimen B2 – Strain from Gauge BS-E2, Showing a Decrease in Strain of 0.0006
While Loading to Point 8 of 1.85% Drift Cycle
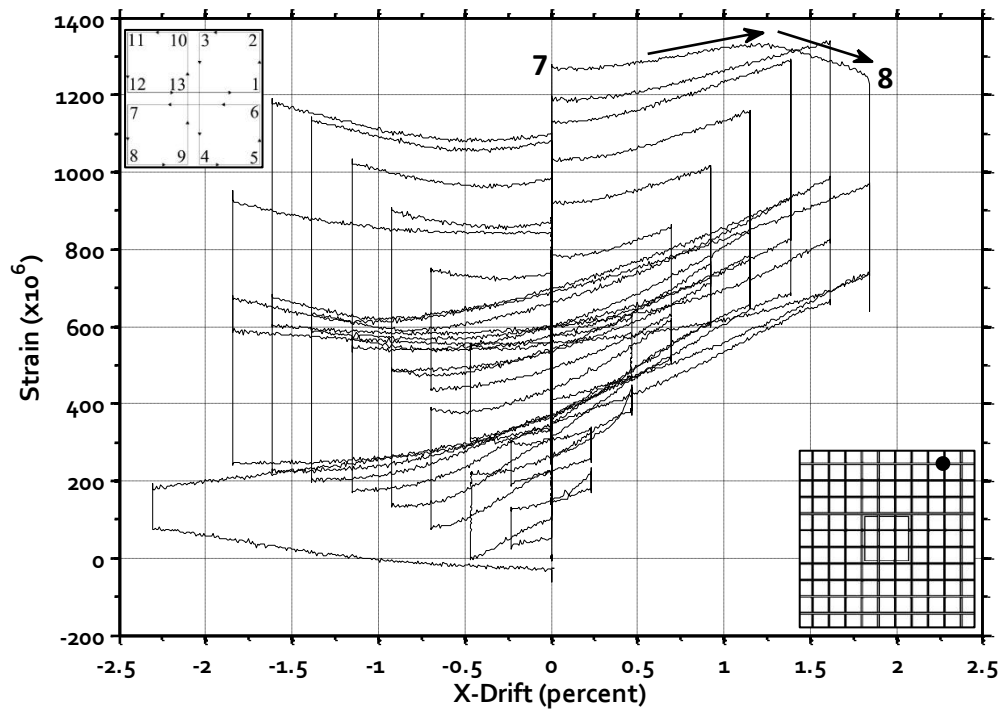
Figure 4-10: Specimen B2 – Strain from Gauge TS-E9, Showing a Change in Slope While
Loading to Point 8 of 1.85% Drift Cycle

220
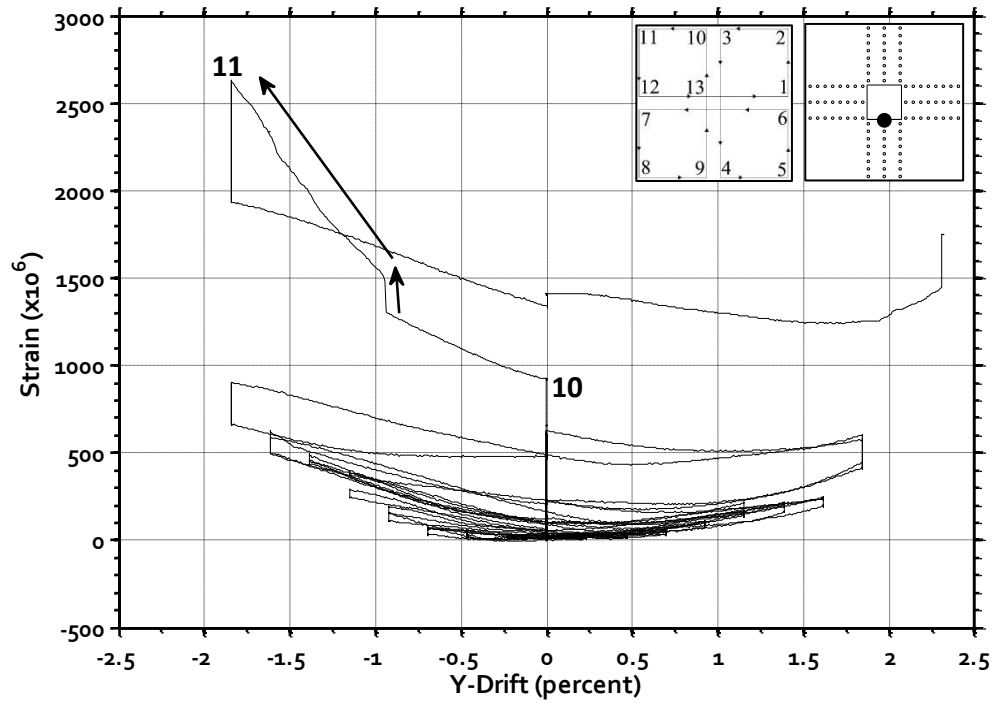
Figure 4-11: Specimen B2 – Strain from Gauge R-S1, Showing a Jump in Strain and Increase
Beyond Yield While Loading to Point 11 of 1.85% Drift Cycle
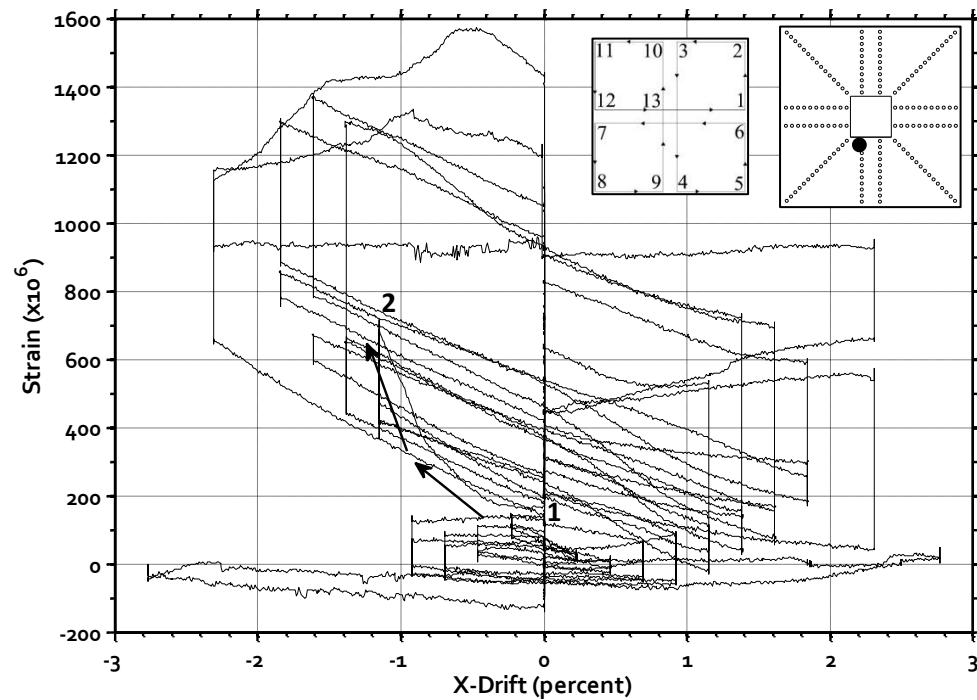
Figure 4-12: Specimen B3 – Strain from Gauge RO-SW2, Showing a Marked Increase in Strain
While Loading to Point 2 of 1.15% Drift Cycle

221
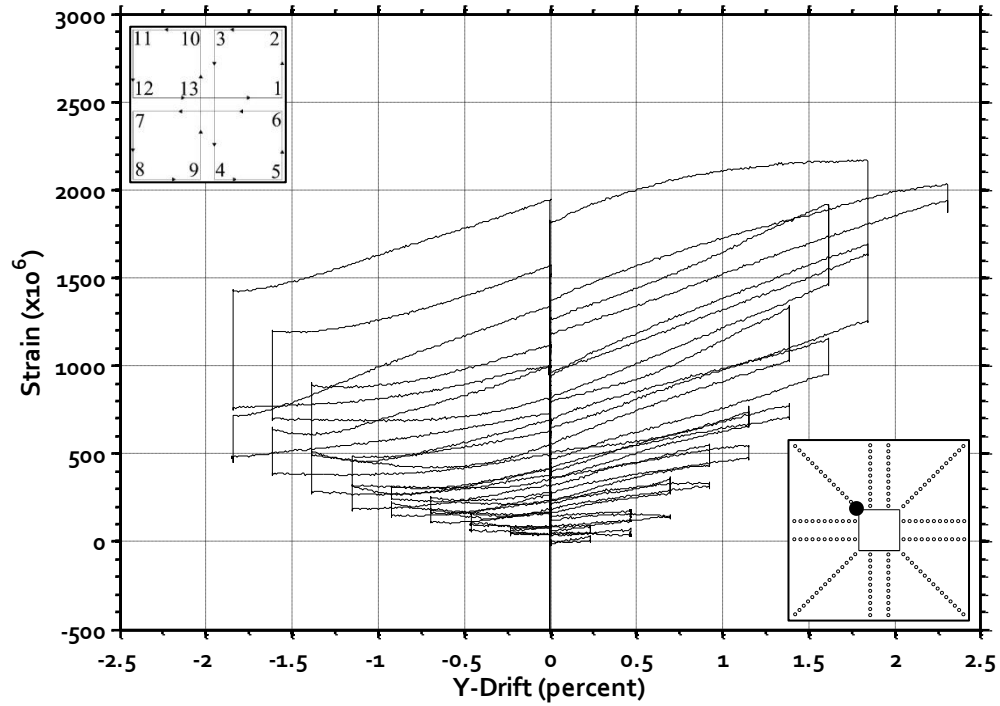
Figure 4-13: Specimen B3 – Strain from Gauge RR-NW1, Showing Large Strains But No Clear
Initiation of Cracking (Response versus X-Drift is Similar)
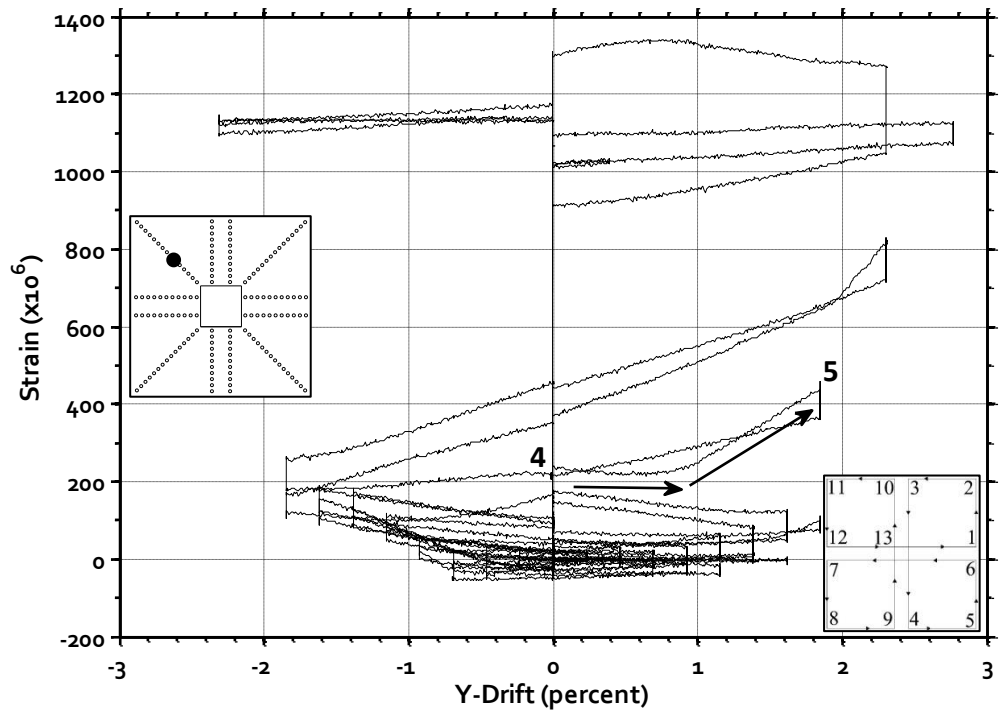
Figure 4-14: Specimen B3 – Strain from Gauge RR-NW6, Showing a Change in Slope and
Increase in Strain While Loading to Point 5 of 1.85% Drift

222
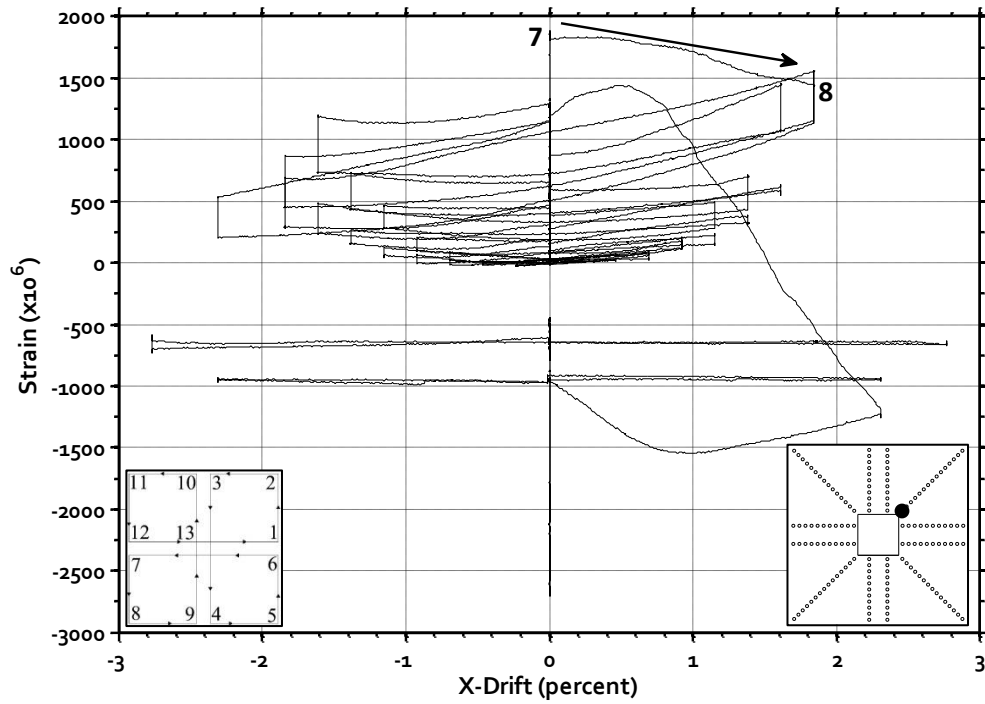
Figure 4-15: Specimen B3 – Strain from Gauge RR-NE1, Showing an Uncharacteristic Negative Slope While Loading to 8 of 1.85% Drift
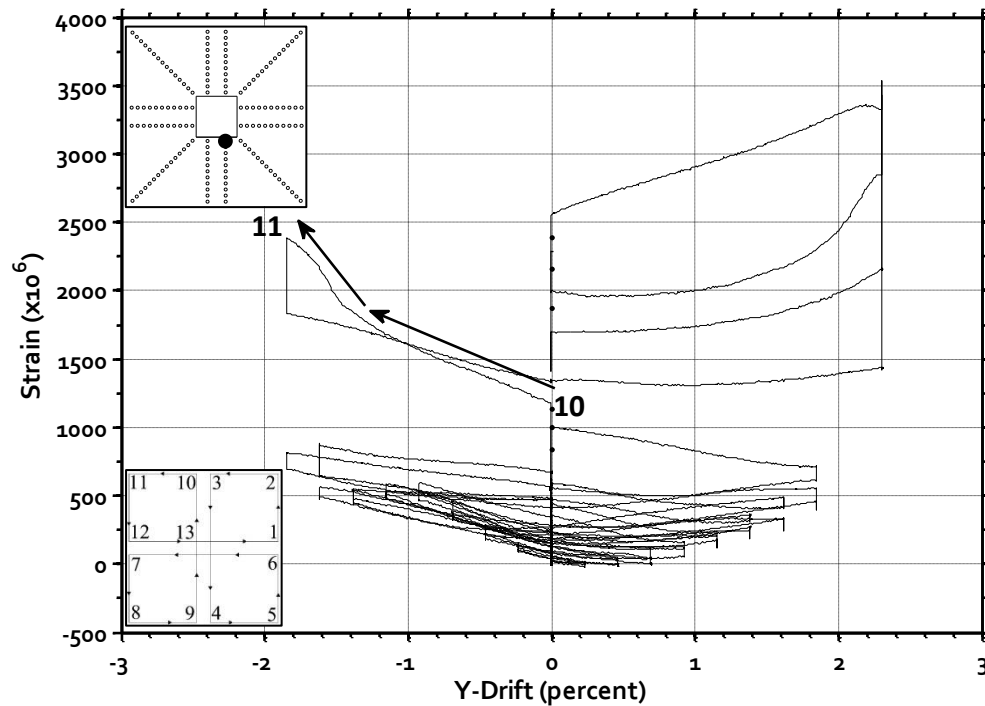
Figure 4-16: Specimen B3 – Strain from Gauge RO-SE1, Showing a Large Increase in Strain While Loading to Point 11 of 1.85% Drift

223
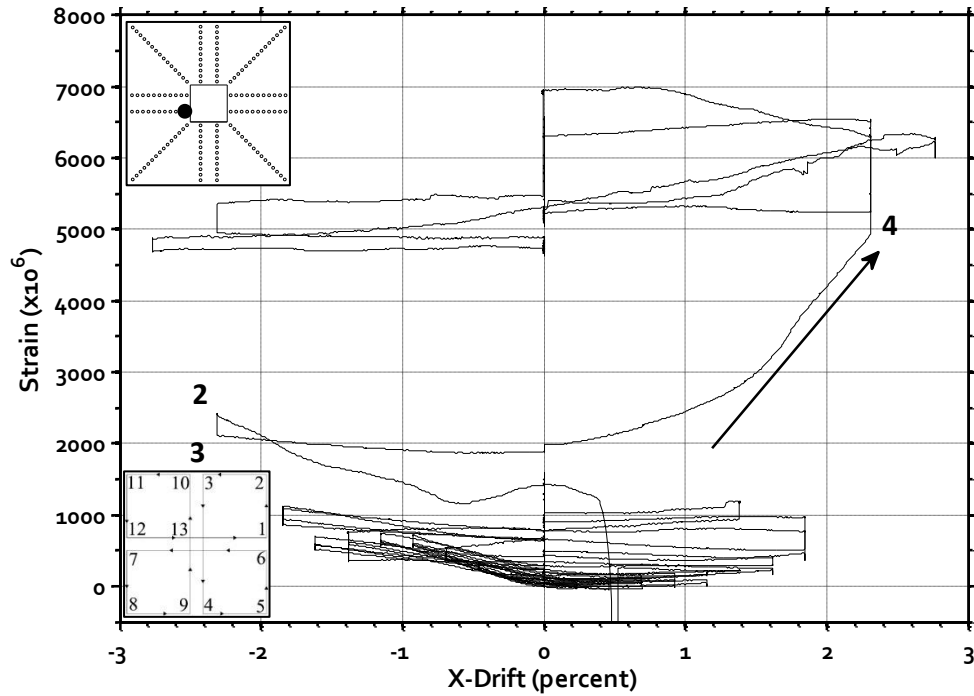
Figure 4-17: Specimen B3 – Strain from Gauge RO-WS1, Showing Yielding and a Large Increase in Strain While Loading to Point 4 of 2.30% Drift Cycle
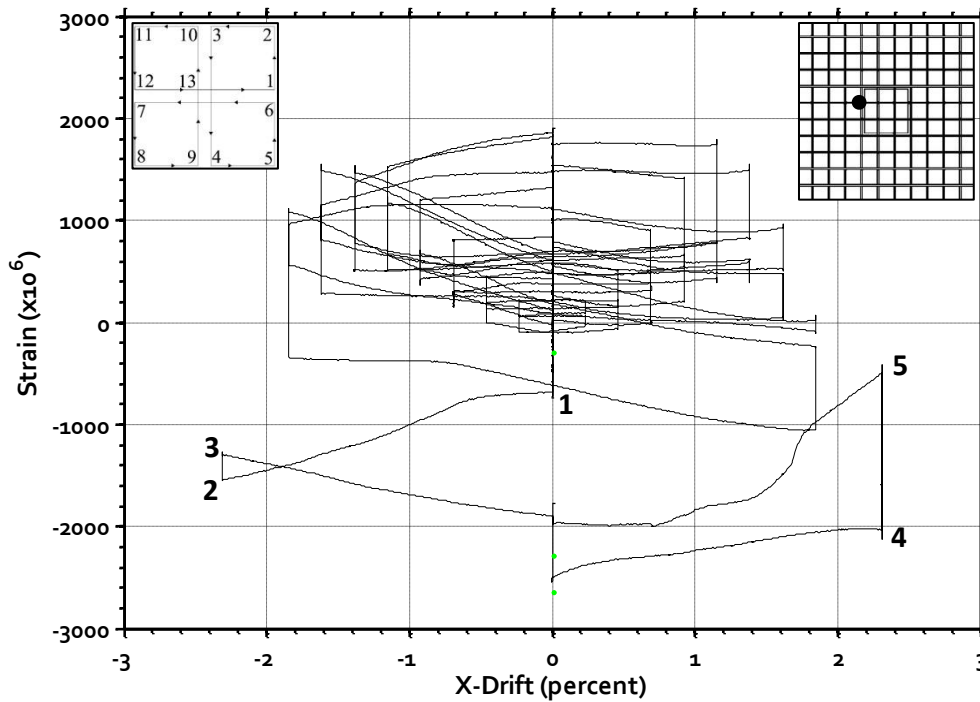
Figure 4-18: Specimen B3 – Strain from Gauge BS-E3, Showing Compressive Strains Late in the 1.85% Drift Cycle and Throughout the 2.30% Drift Cycle
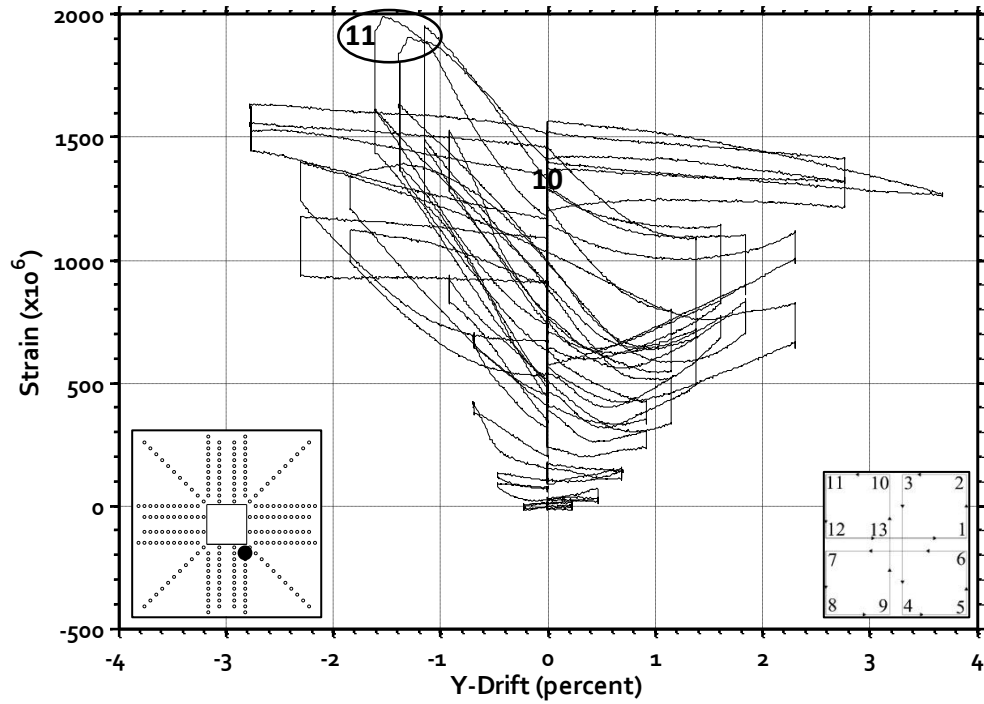
Figure 4-19: Specimen B4 – Strain from Gauge OO-SE2, Showing an Uncharacteristic Decline in Strain While Loading to Point 11 of the 1.40% and 1.60% Drift Cycles
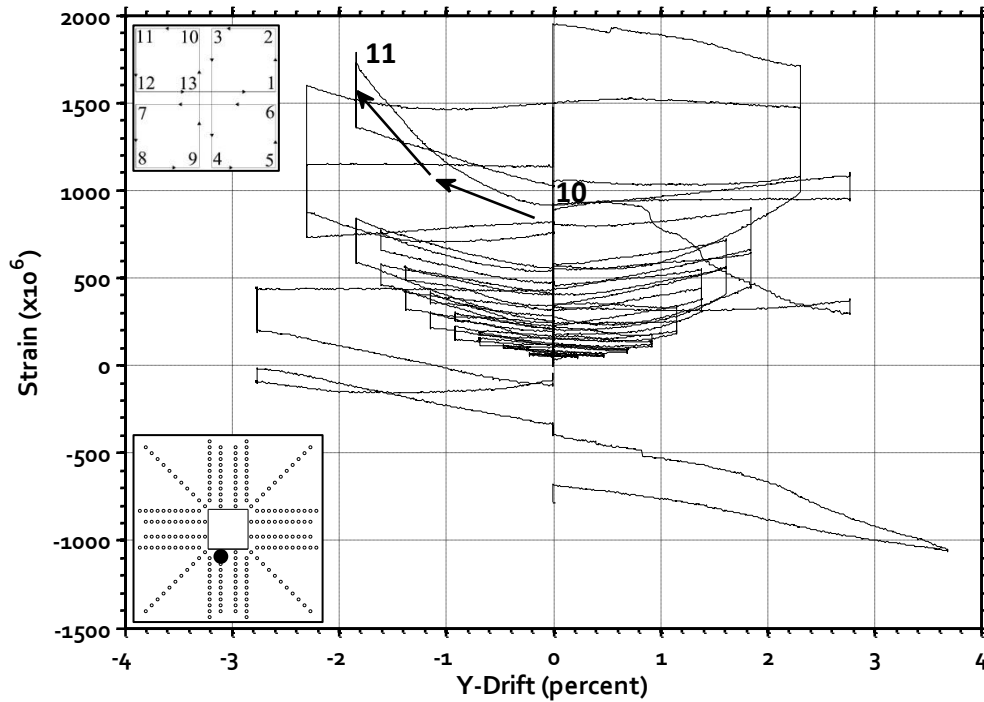
Figure 4-20: Specimen B4 – Strain from Gauge OI-SW2, Showing a Steep Increase in Strain While Loading to Point 11 of the 1.85% Drift Cycle
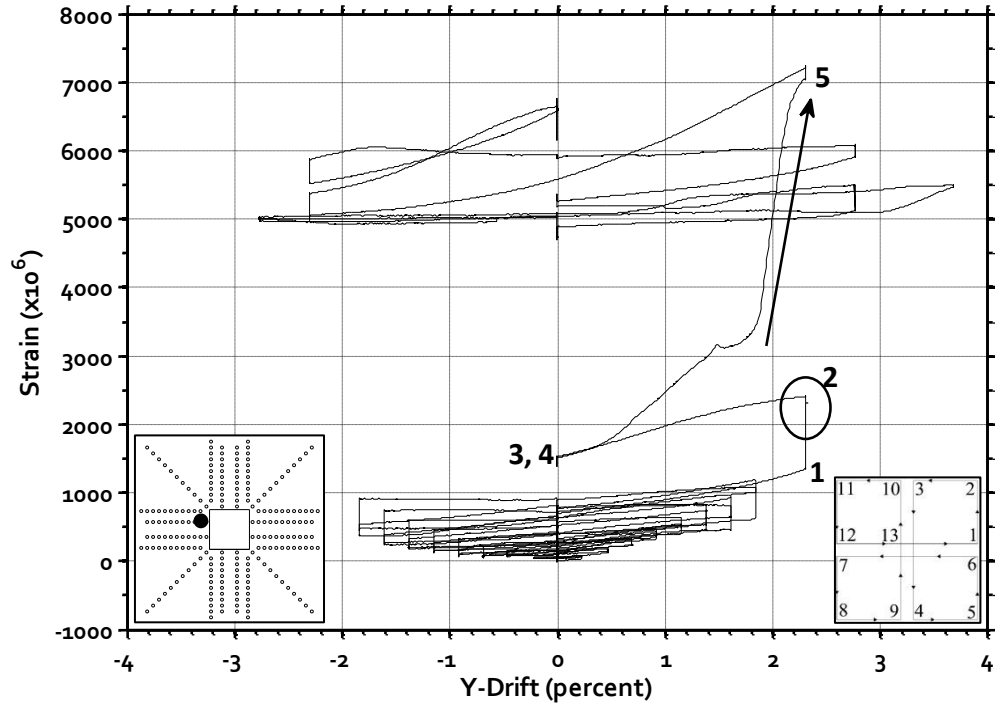
Figure 4-21: Specimen B4 – Strain from Gauge OI-WN2, Showing Strains Near Yield (Circled) Followed by a Large Increase in Strain While Loading to Points 2 and 5 of the 2.30% Drift Cycle
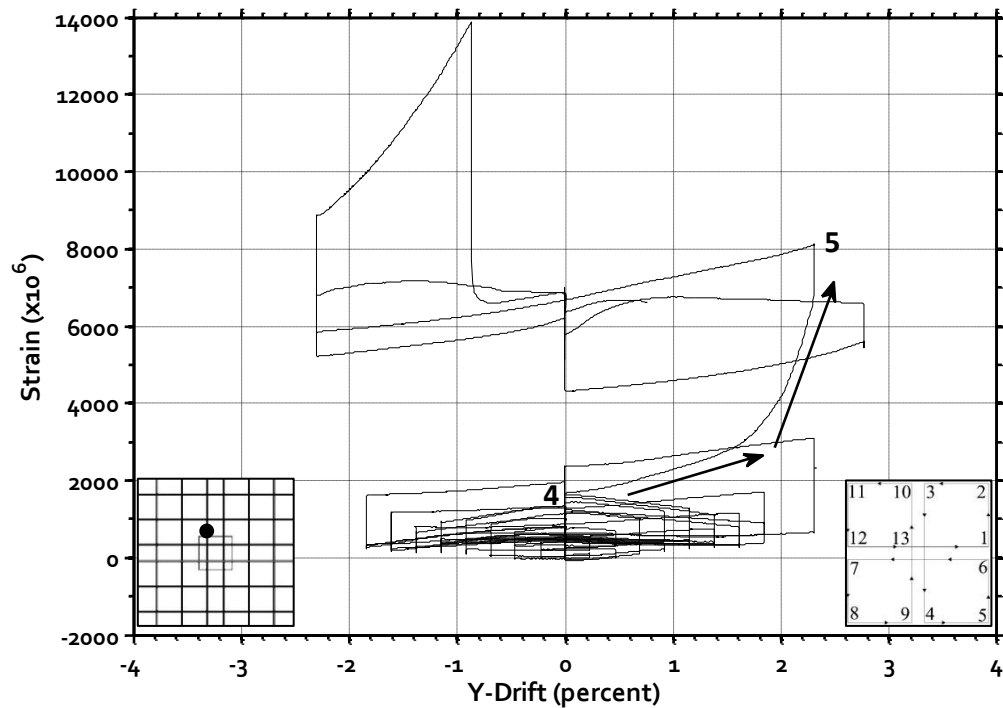
Figure 4-22: Specimen B4 – Strain from Gauge BS-S3, Showing a Very Large Increase in Strain While Loading to Point 5 of the 2.30% Drift Cycle

Figure 4-23: Specimen B2 – Connection Region where Damaged Concrete was Removed by Hand

Figure 4-24: Specimen B3 – Void in Connection Region after Loose Concrete was Removed

Figure 4-25: Specimen B4 – Gravel-Like Concrete within Connection Region

Figure 4-26: Specimen B4 – Void between Slab and Column after Loose Concrete Had Been Removed
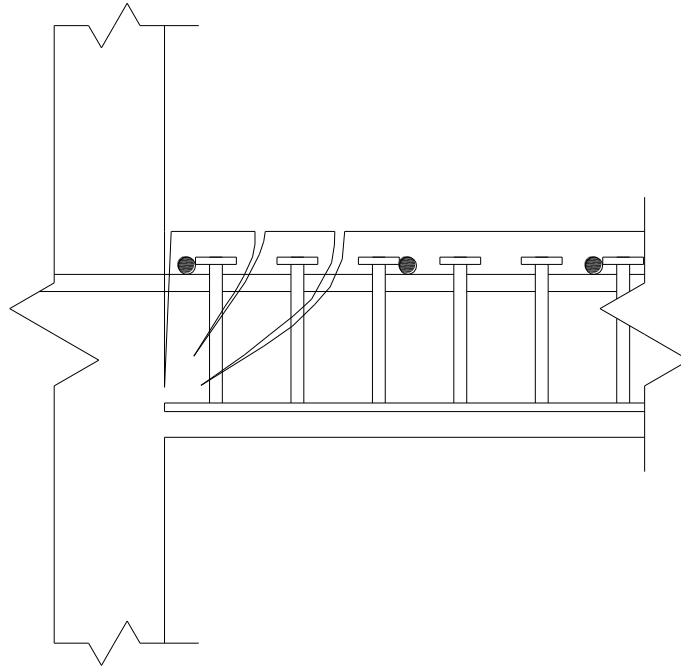
Figure 4-27: Schematic of Traditional Shear Failure Mechanism Governed by Diagonal Shear
Cracking Bridged by Shear Stud Reinforcement
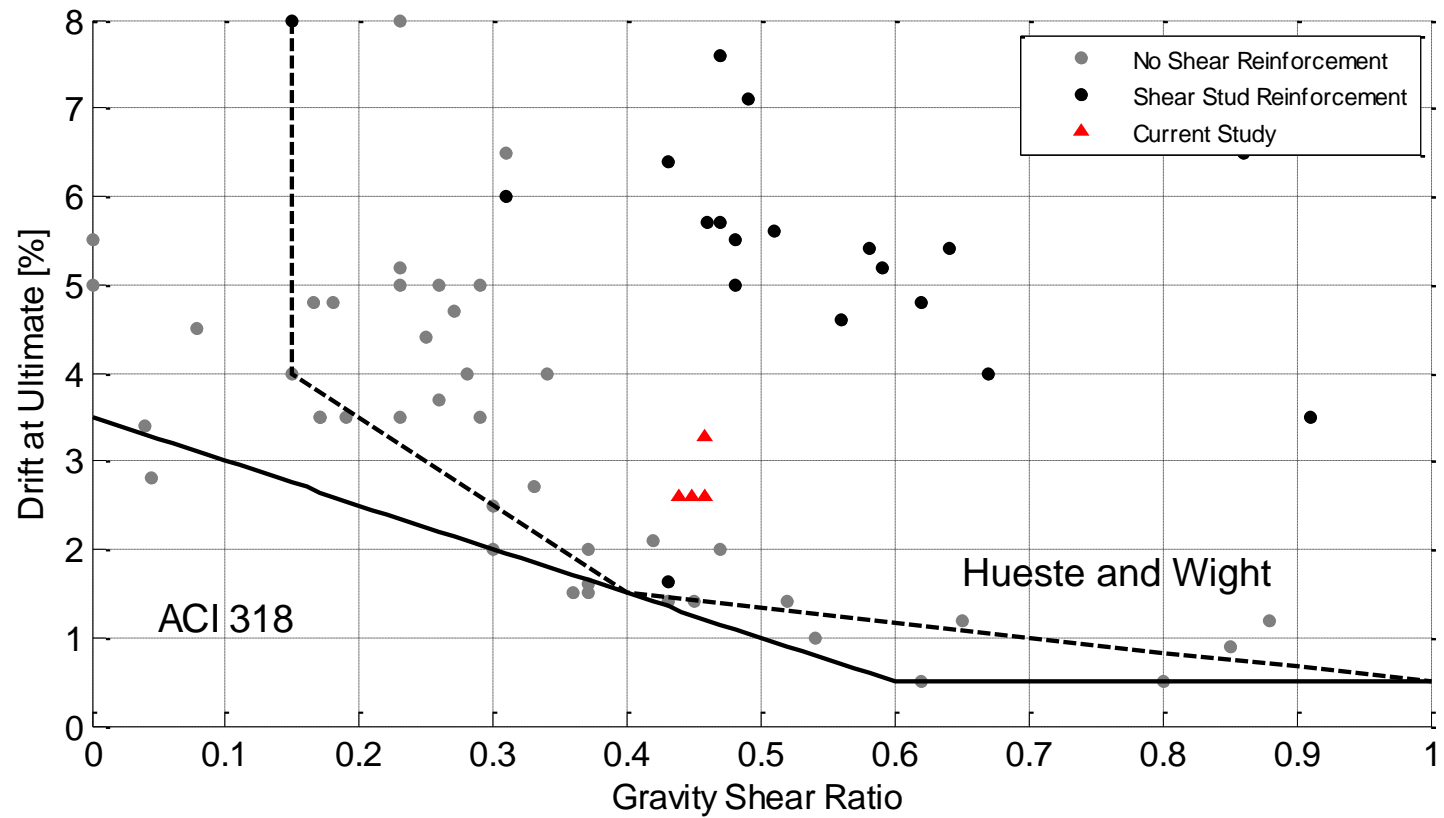
Figure 4-28: Drift Capacity versus Gravity Shear Ratio from Various Researchers

A. SHEAR STUD REINFORCEMENT DESIGN

This appendix reports the design calculations used for detailing the shear reinforcement for Specimens B1 and B2. Specimen B3 was provided with an identical amount of shear reinforcement as Specimen B1. Specimen B4 was provided with a greater amount of shear reinforcement than Specimens B1, B2, and B3.

<u>Specimen B1:</u>

<u>Critical Section properties</u>

$$b_0 = 4(16in + 4.75in) = 83in$$

$$A_0 = b_o \cdot d = 4.75in \cdot 83in = 394in^2$$

$$J_c = \frac{d(l_1 + d)^3}{6} + \frac{d^3(l_1 + d)}{6} + \frac{d(l_2 + d)(l_1 + d)^2}{2} = 28662in^4$$

<u>Design Forces</u>

The design for this specimen was based on the approach outlined in ACI 318-08 Section 21.13.6(a). The assumed strength of the concrete was 5000 psi. Based on mill certs provided by VSL Post-Tensioning, the shear stud strength was conservatively taken as 55 ksi. The design shear force, V_u, was calculated based on a 50% gravity shear ratio.

$$V_u = 2\sqrt{f_c'}A_o = 2\sqrt{5000} \cdot 394.25in = 55.76kip$$

An unbalanced moment of 1400 kip-in was assumed based on test results from a previously tested shear stud reinforced specimen (Cheng et al. 2009). Using the eccentric shear model, the maximum shear stress was calculated as

$$v_u = \frac{V_u}{A_o} + \frac{M_u \cdot c \cdot \gamma_v}{J_c} = \frac{55kip}{394.25in} + \frac{1400kip \cdot in \cdot 10.375in \cdot 0.4}{28662in^4} = 344psi$$

$$c = \frac{l+d}{2} = \frac{16in + 4.75in}{2} = 10.375in$$

$$\gamma_v = 1 - \frac{1}{1 + \frac{2}{3}}$$

Design of Shear Studs

Design shear stress = 344 psi

According to Section 11.11.5.2 of the ACI Building Code, if $v_u < 5\sqrt{f_c'}$, then a maximum spacing of 0.75d is allowed spacing is allowed. For Specimen B1, a spacing of 0.5d, or 2.375 in., was used to increase the capacity due to the design assumption that $v_c=0$

Using Eqn. 11-15: $V_s = \frac{A_v f_y d}{s}$

$$\Rightarrow \frac{A_v}{s} \geq \frac{V_s}{f_y d} = \frac{v_s b_0}{f_y} = \frac{344\,psi \cdot 83in}{55000\,psi} = 0.519$$

$$\Rightarrow A_v = 1.23in^2$$

If 3/8 in. diameter rods are selected, A_s (per rod) = $0.11in^2$.

12 rods are provided in each peripheral row of reinforcement

Per ACI 318-08 Section 11.11.5.1:

$$v_s = \frac{A_v f_y}{b_o s} = \frac{1.32in^2 \cdot 55000\,psi}{83in \cdot 2.375in} = 368\,psi > 2\sqrt{5000} = 141\,psi$$

$$v_s + v_c \geq v_u$$
$$368\,psi + 0\,psi \geq 344\,psi$$

Height of Shear Stud Assemblies per Section 11.11.5

a – concrete cover on the top flexural reinforcement 0.75 in

b – concrete cover on the base rail 0.75 in.

c – one-half of the bar diameter of the tension flexural reinforcement = 0.25 in.

$$h_{SSR} \geq h - a - b - c$$
$$h_{SSR} \geq 6in - 0.75in - 0.75in - 0.25in = 4.25in$$

Total height of assembly shall be 4.25in

Layout of Shear Stud Reinforcement

The layout of the shear stud assemblies is shown in Figure A-1. Three stud rails were placed perpendicular to each face of the column. The spacing between rails was $7.375in \leq g_{max} = 2d = 9.5in$. The first peripheral row of studs was located a perpendicular distance from the column equal to $1.5in \leq s_{o\,max} = d/2 \leq 2.375in$.

<u>Shear Check Outside of Critical Section</u>

$$c = \frac{61.75}{2} = 30.875"$$

$$b_o = 4(16.72in + 31.84in) = 192.96in$$

$$J = d\sum \frac{l}{3}(y_i^2 + y_i y_j + y_j)$$

$$= 4.75 \left\{ \begin{array}{l} \frac{16.72}{3}\left(8.63^2 - 8.63^2 + 8.63^2\right) \times 2 + \\ \frac{29.88}{3}\left(30.88^2 + 30.88 \cdot 8.36 + 8.36^2\right) \times 4 + \frac{16.72}{3}\left(3 \cdot 30.88^2\right) \times 2 \end{array} \right\}$$

$$= 397943in^4$$

Per Section 11.11.7.2:

$$v_u = \frac{55kip}{194.24in \cdot 4.75in} + \frac{1400kip \cdot in \cdot 30.875in \cdot 0.4}{397943in^4} = 103.06\,psi \leq 2\sqrt{5000\,psi} = 141.42\,psi$$
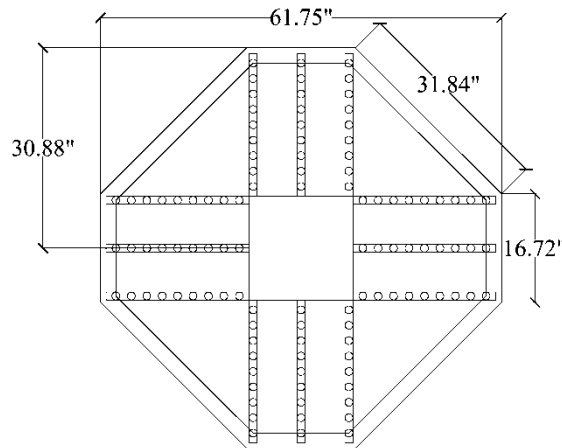
Figure A-1: Shear Reinforcement Layout for Specimen B1

Specimen B2:

The same sectional and material properties were used for the design of Specimens B1 and B2.

Concept:

The design for this specimen was based on the minimum shear reinforcement required by ACI 318-08 Section 21.13.6 where neither a stress or drift capacity check is performed.

$$V_c \geq 3.5\sqrt{f_c'}b_o d = 3.5\sqrt{5000psi} \cdot 83in. \cdot 4.75in. = 97.57kip$$

If 3/8 in. diameter rods are selected, A_s *(per rod)* $= 0.11in^2$.

12 rods are provided in each peripheral row of reinforcement

Using Eqn. 11-15: $V_s = \dfrac{A_v f_y d}{s}$

$$\Rightarrow s \leq \frac{f_y d A_v}{V_s} = \frac{55000psi \cdot 4.75in \cdot 1.32}{97500lb} = 3.54in \leq 0.75d = 3.56in$$

The resulting design is shown in Figure A-2. The first stud is positioned a perpendicular distance of 2 in. from the column face on each stud rail with a subsequent stud spacing be equal to 3.5 in. Eight rows of reinforcement are provided such that the last row of studs is located 26.5 in. from the column face, which is greater than 4h, or 24 in.
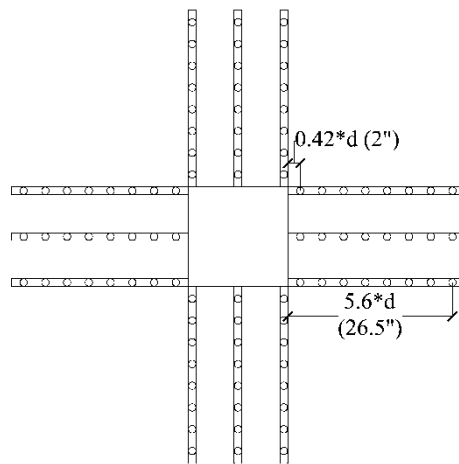
Figure A-2: Shear Reinforcement Layout for Specimen B2

234

B. SLAB-COLUMN ROTATIONS

Shown below in Figure B-1 to Figure B-8 are plots of moment transferred into the column versus slab rotation at each column face in the four specimens tested. LVDTs were mounted to the slab surface; therefore, as the slab began to drop as punching initiated, the data collected became unreliable. Using photographic data indicating when the slab began to exhibit punching damage, a point was chosen for each specimen to signify when LVDT data became unreliable. Punching initiated in each specimen during the 1.85% drift cycle; accordingly, only data collected prior to loading to Points 8, 8, 5, and 11 in the 1.85% drift cycle for Specimen B1, B2, B3, and B4 respectively were plotted.
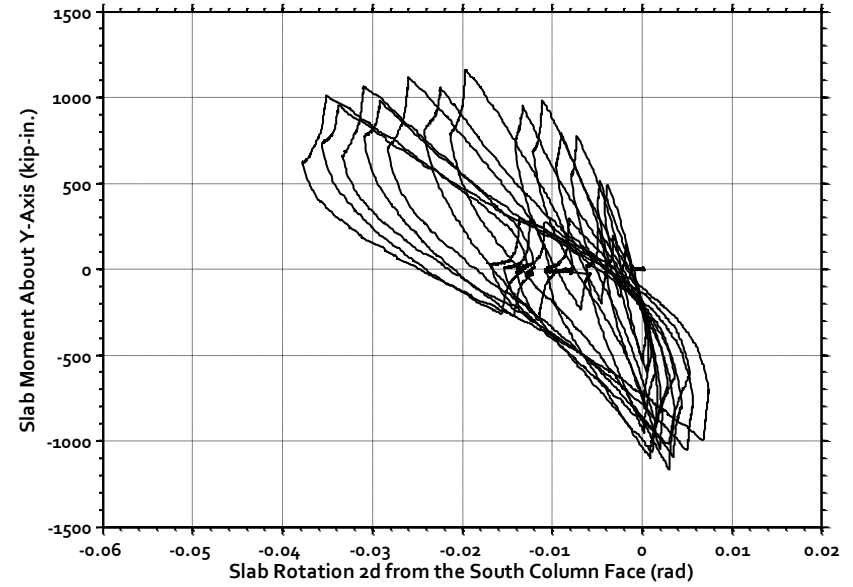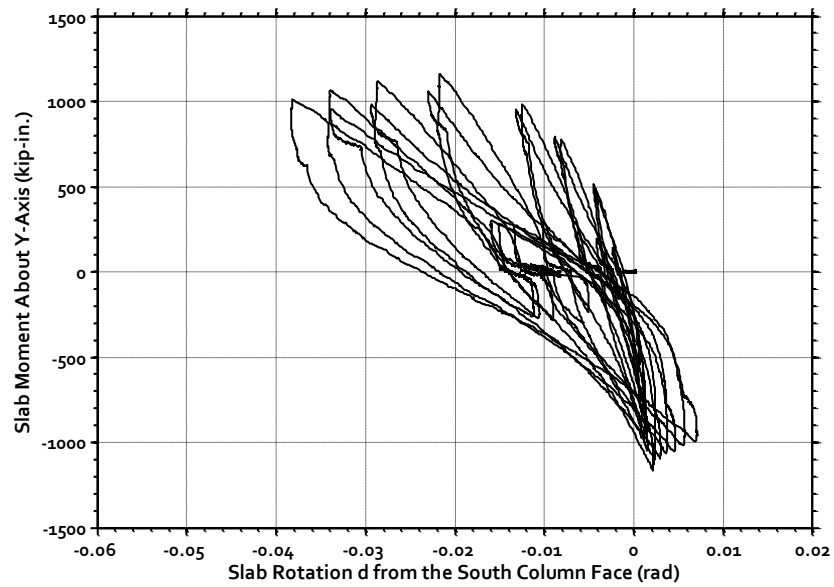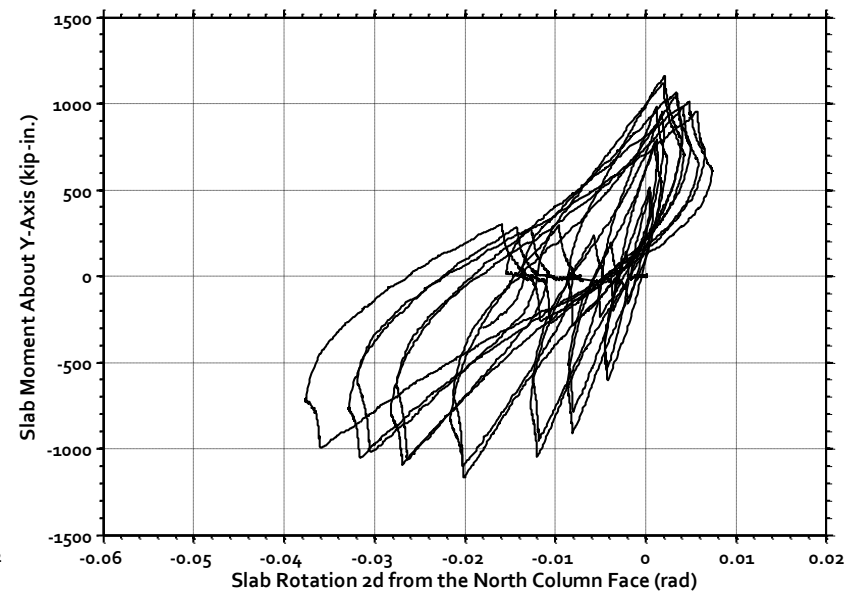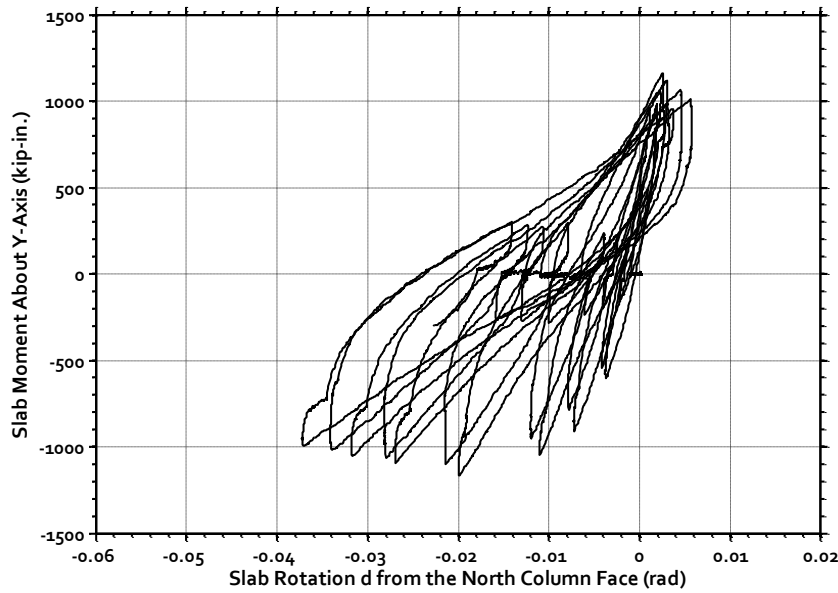
Figure B-1: Specimen B1 – Slab-Column Rotations in X-Direction
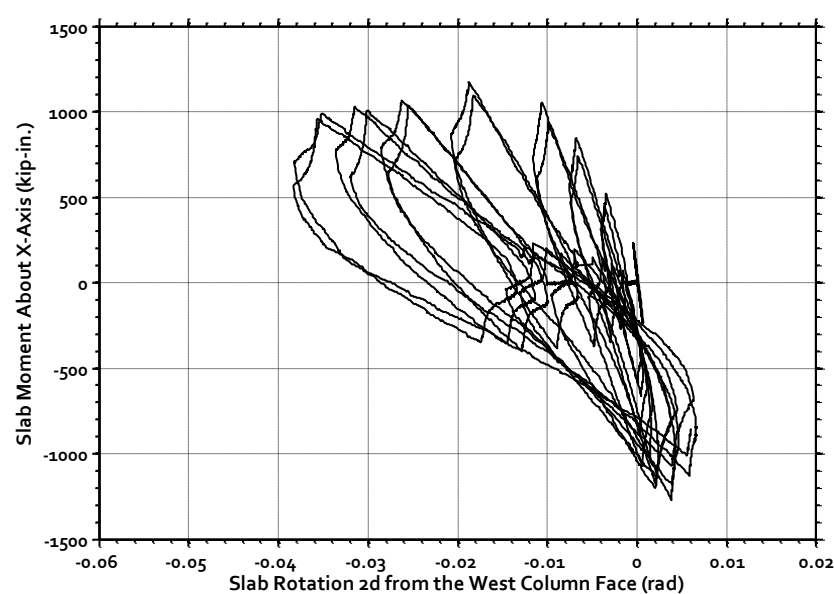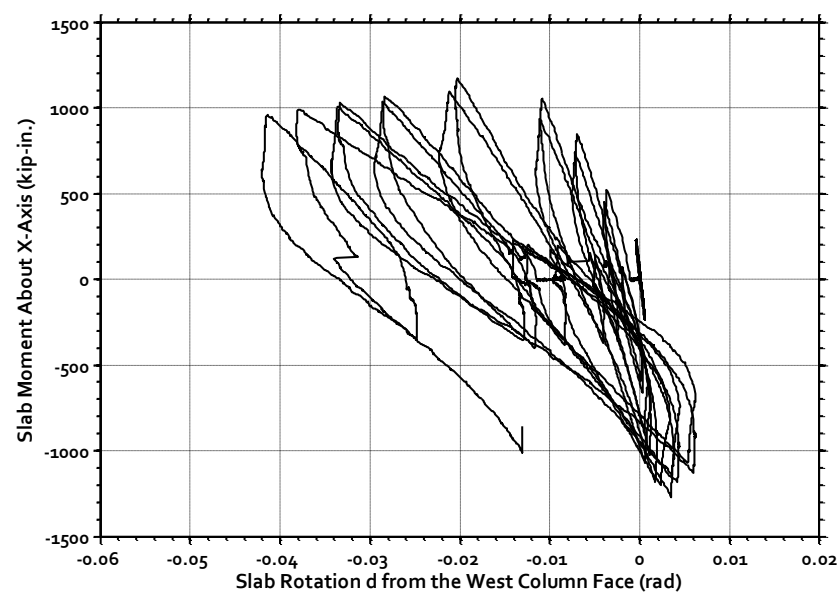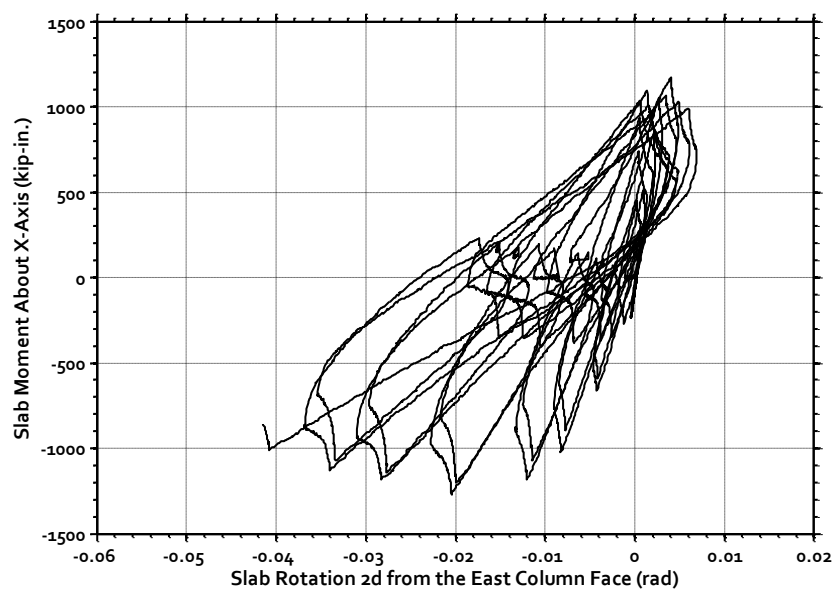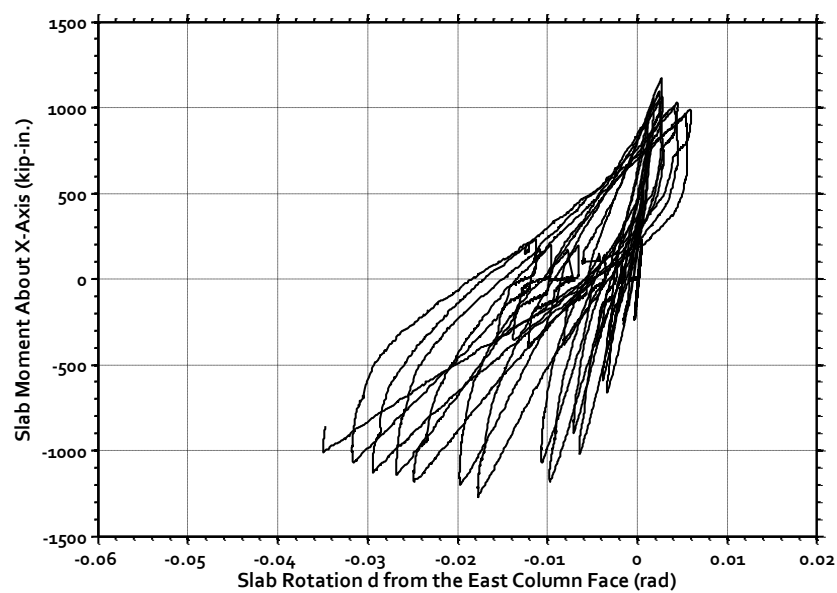
Figure B-2: Specimen B1 – Slab-Column Rotations in Y-Direction

237
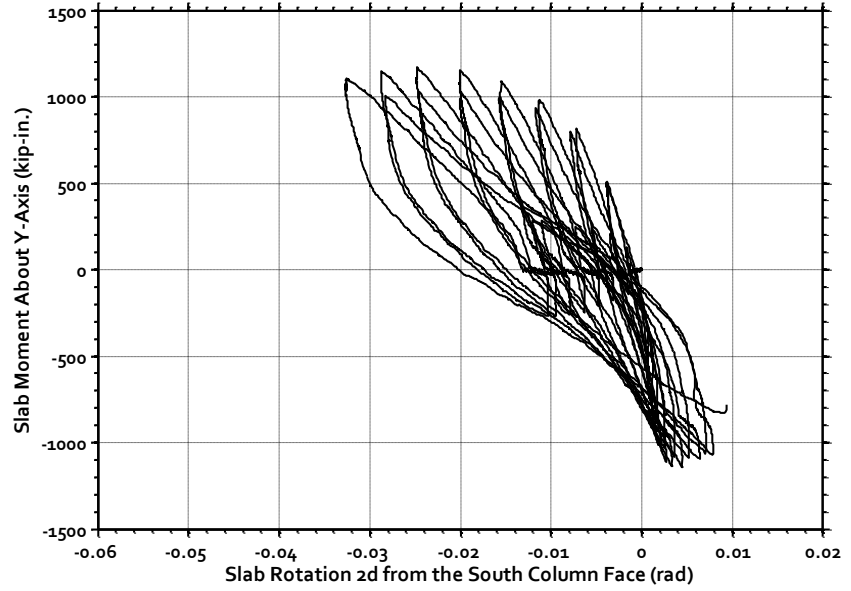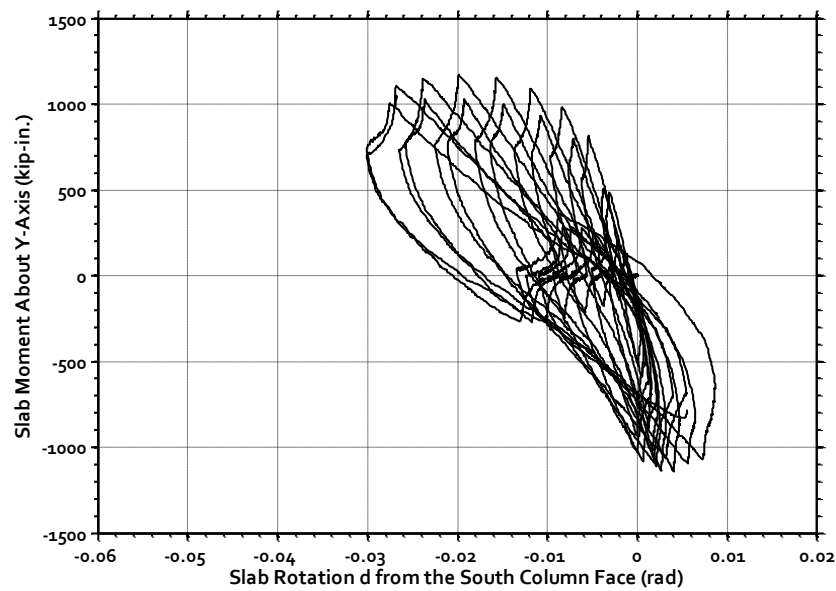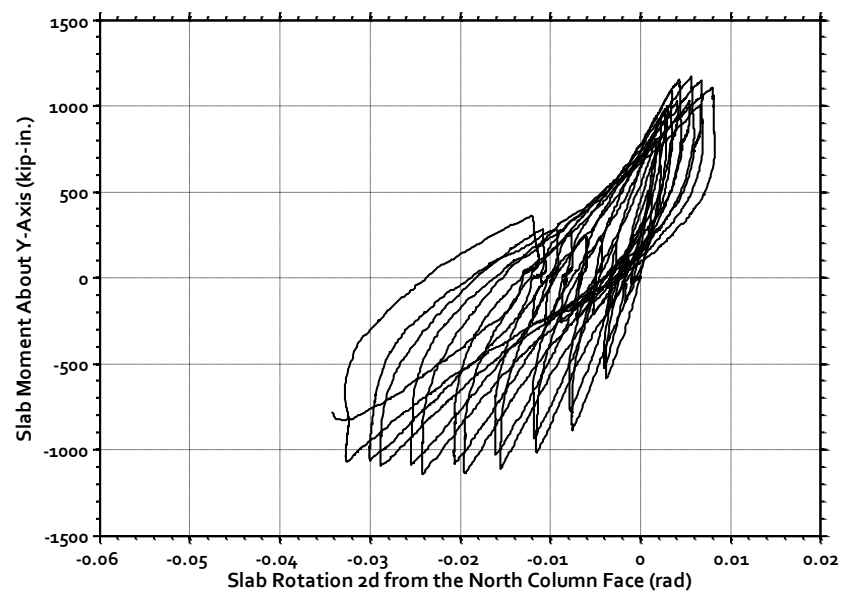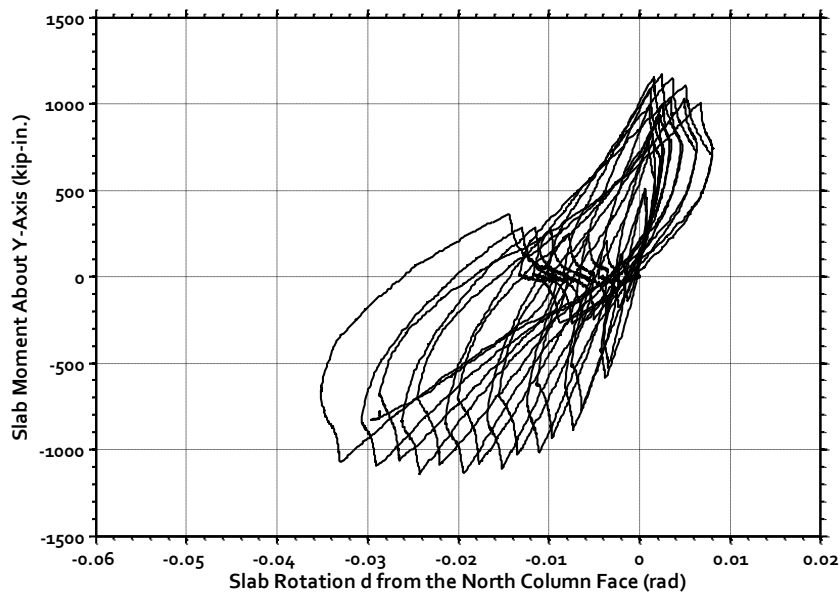
Figure B-3: Specimen B2 – Slab-Column Rotations in X-Direction

238
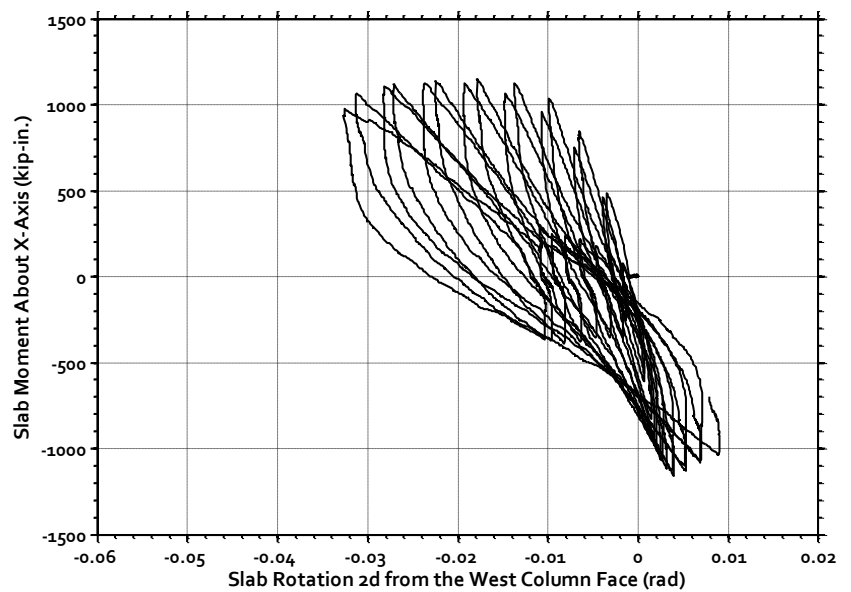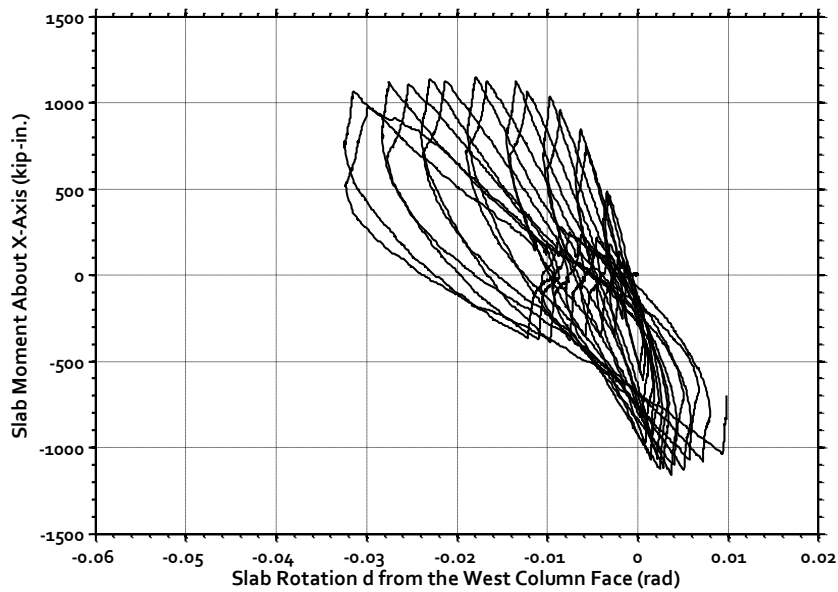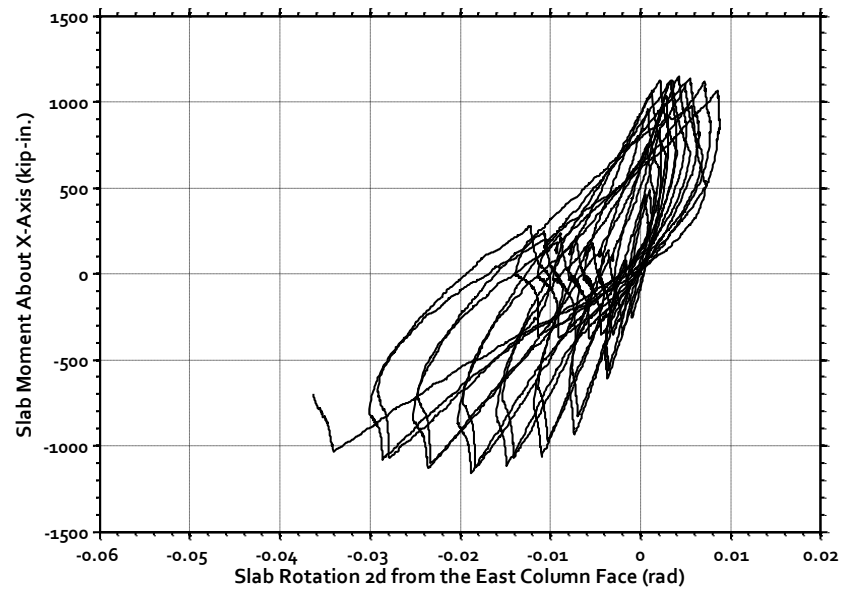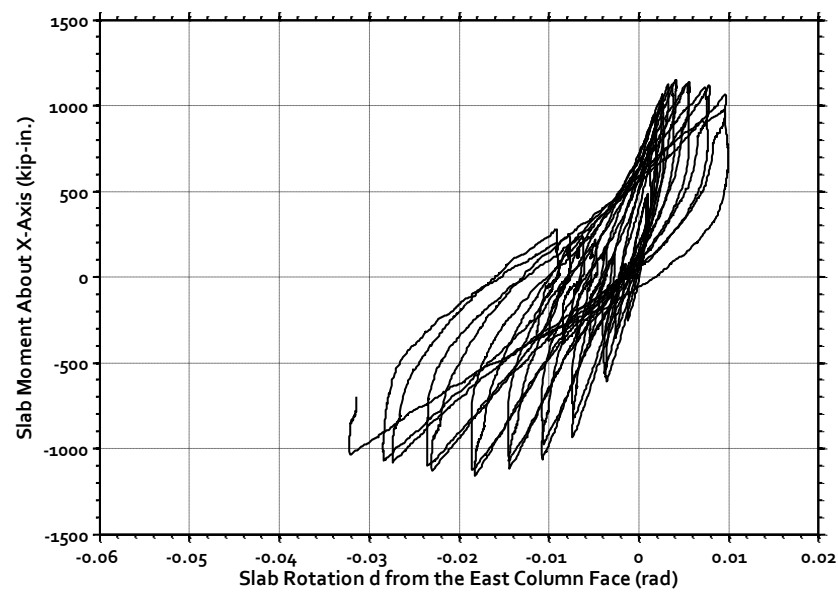
Figure B-4: Specimen B2 – Slab-Column Rotations in Y-Direction

239
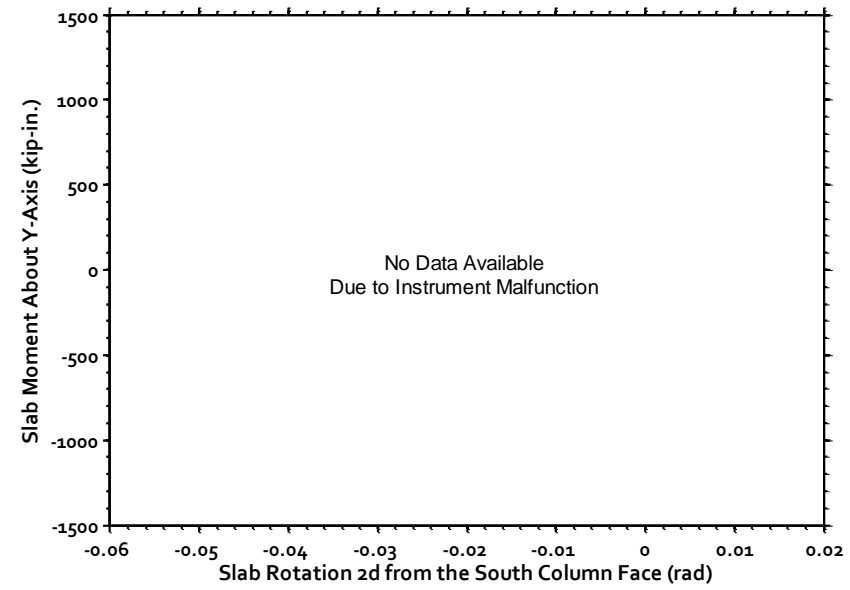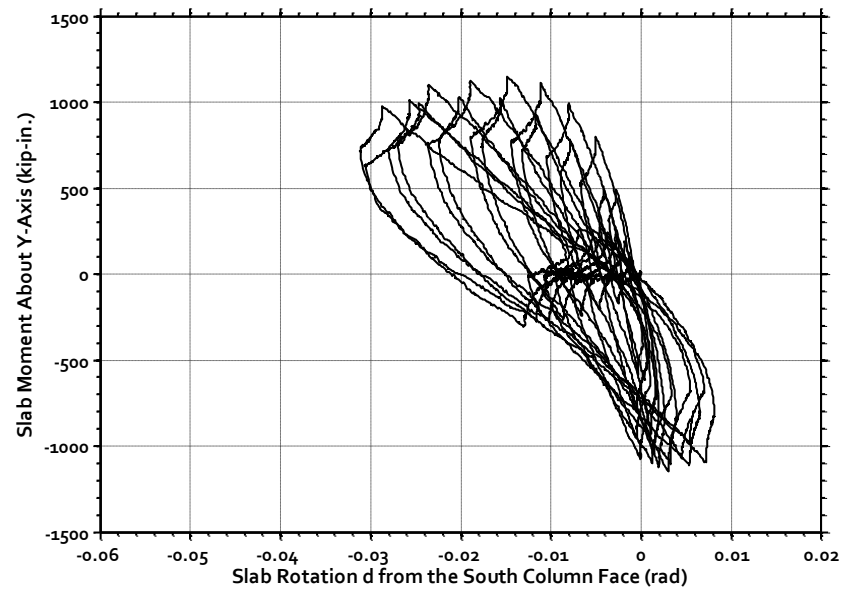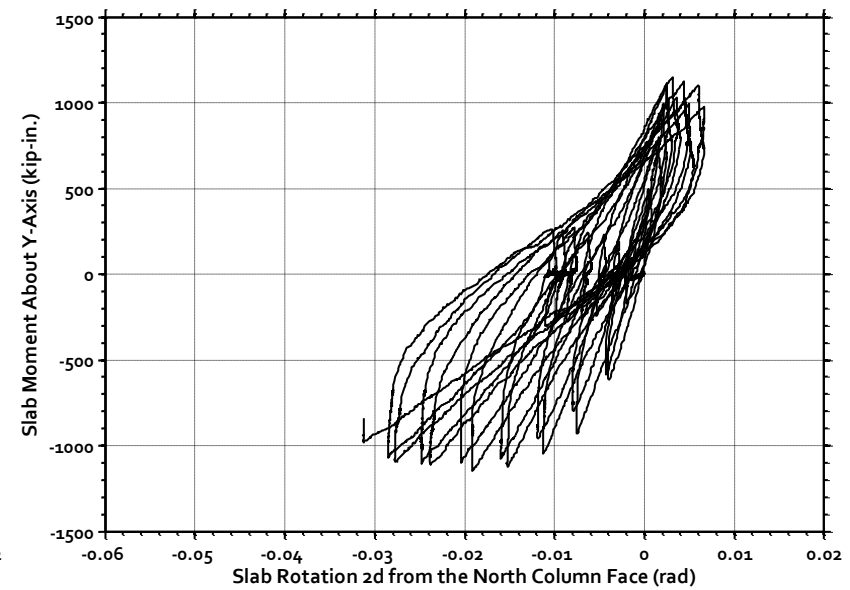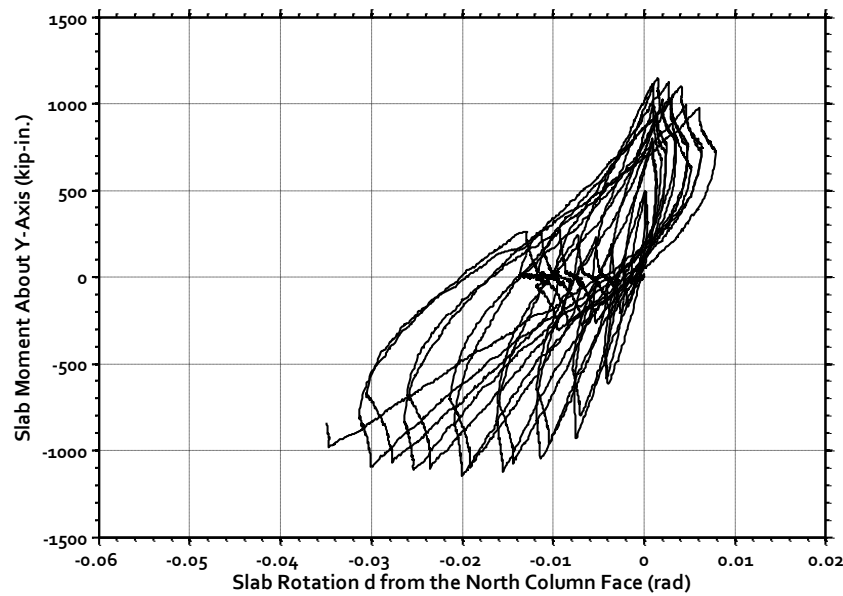
Figure B-5: Specimen B3 – Slab-Column Rotations in X-Direction
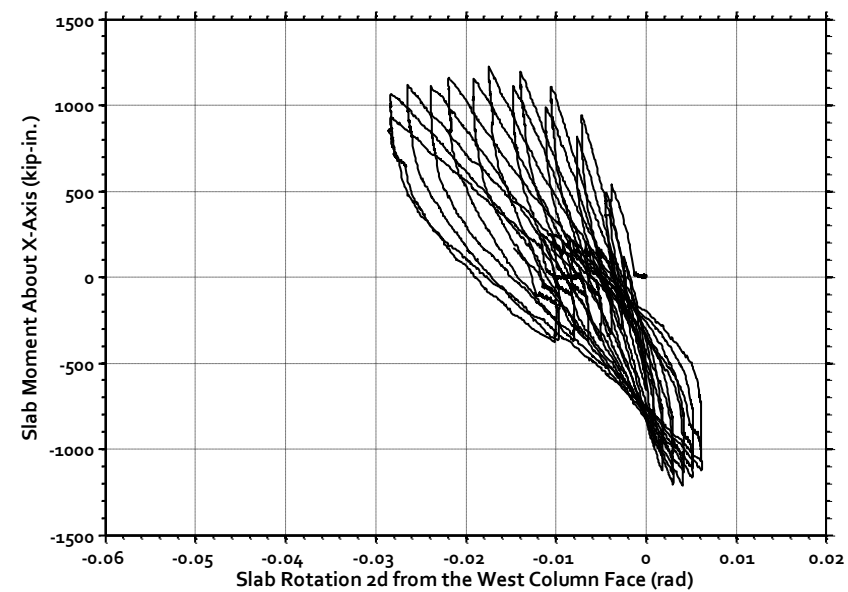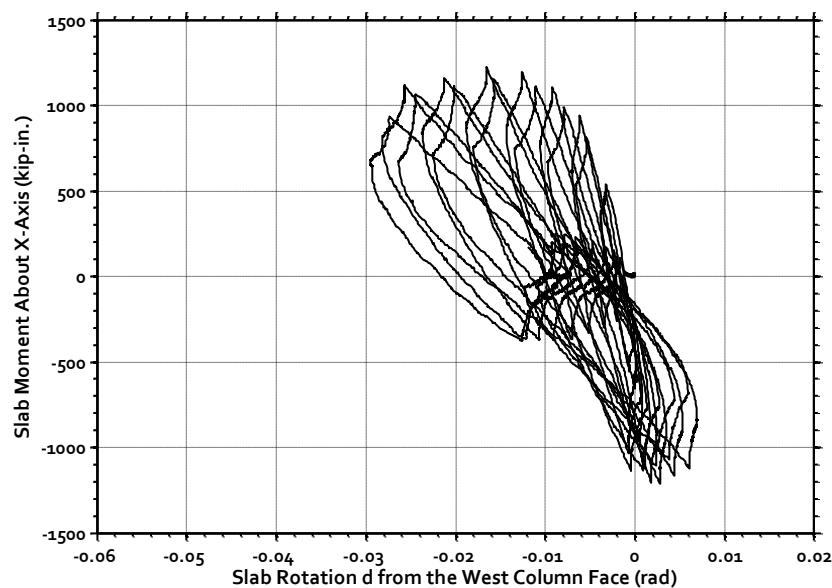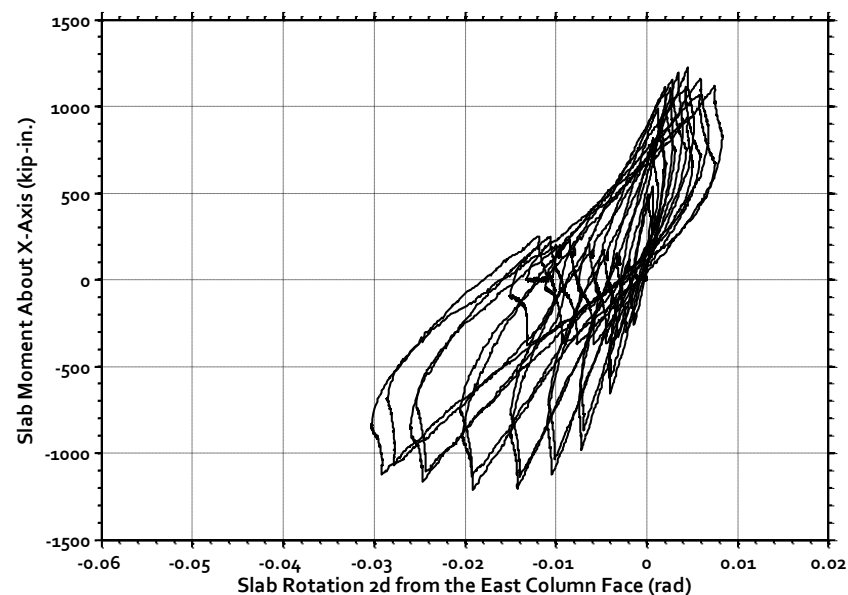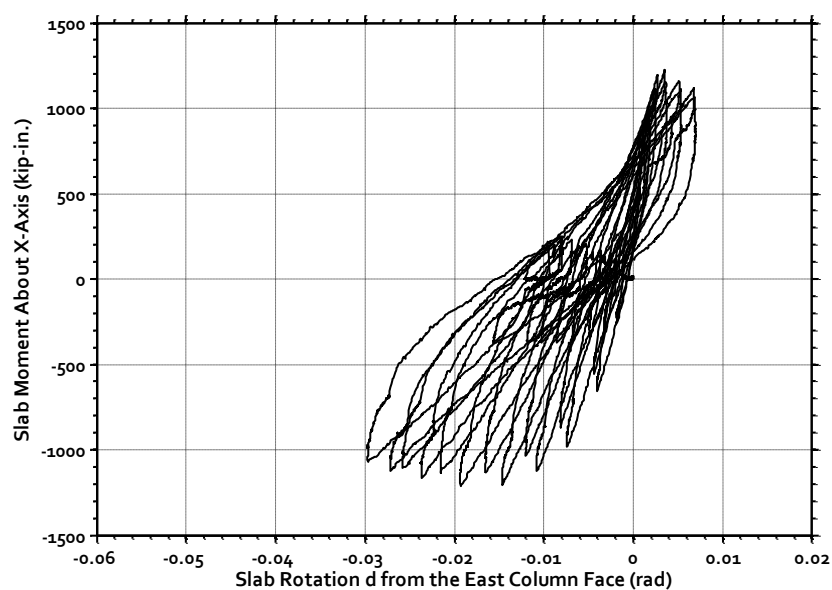
Figure B-6: Specimen B3 – Slab-Column Rotations in Y-Direction

241
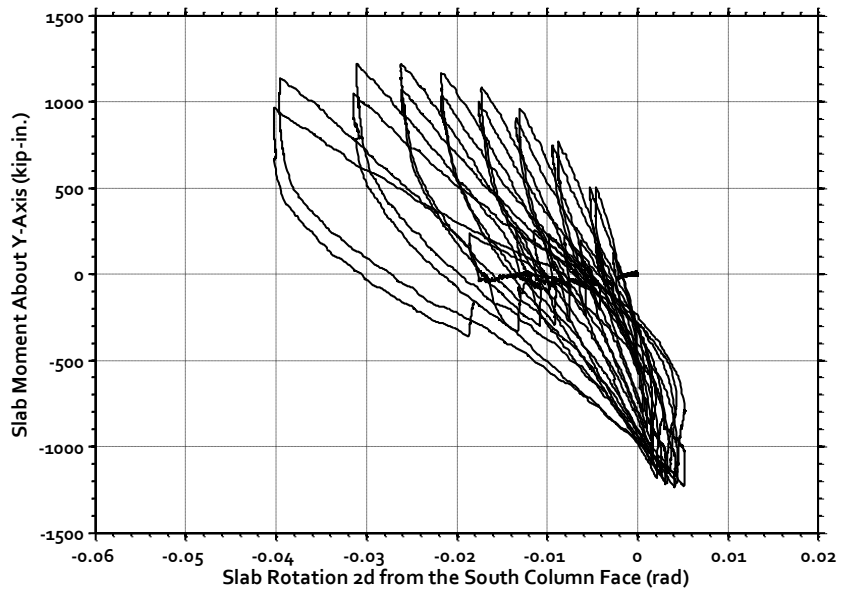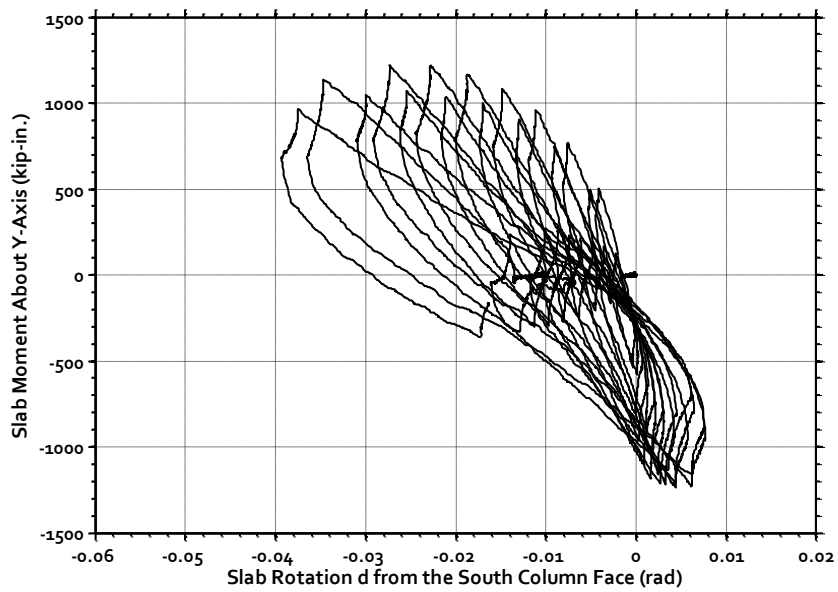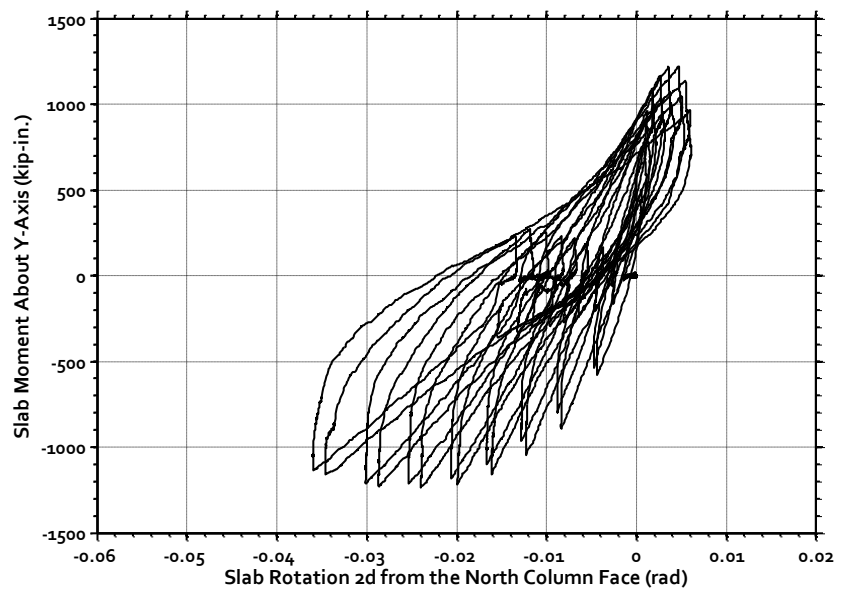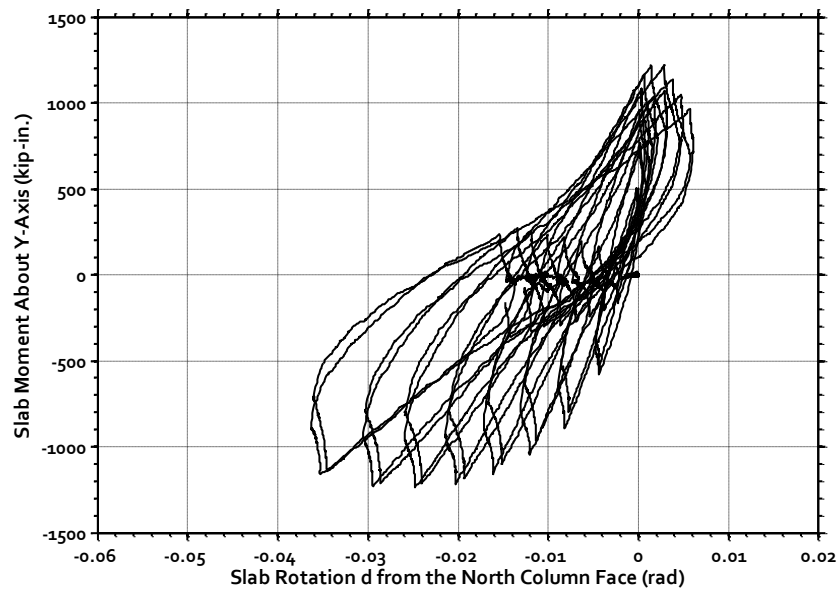
Figure B-7: Specimen B4 – Slab-Column Rotations in X-Direction
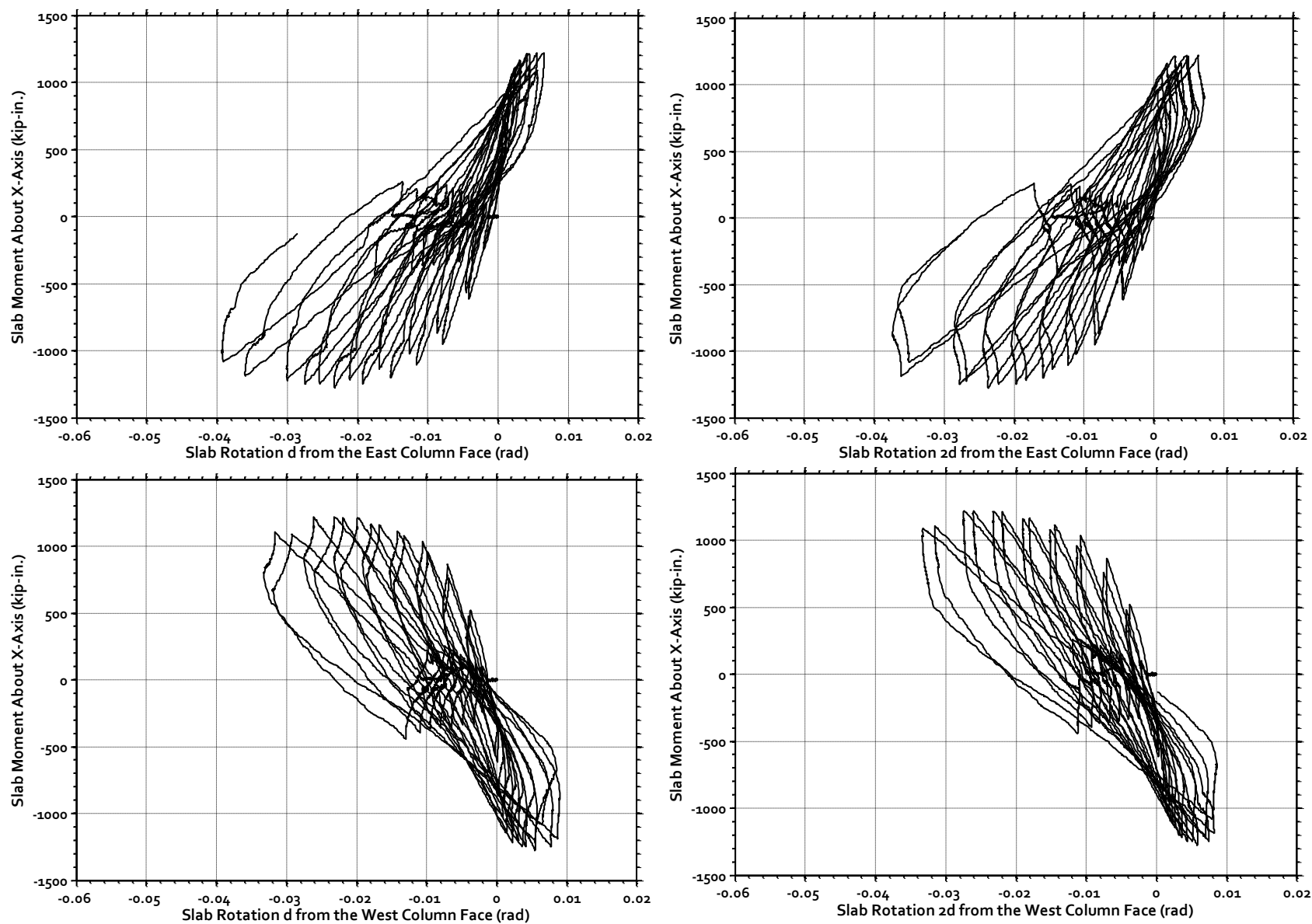
Figure B-8: Specimen B4 – Slab-Column Rotations in X-Direction

243

C. BOTTOM STORY AND SECOND HALF-STORY DRIFT RATIOS

Story drift ratio is defined as the relative lateral displacement of floor slabs in consecutive stories in a building as a percentage of the height of the respective story. Most of the analyses discussed herein were performed using the drift of the entire 1.5 stories of the specimen as it was believed to be more representative than either the first story or the second half-story drift. However, measurements were also taken that allow calculation of the drift of the first story and second half-story of the specimen. Hysteresis plots using drifts calculated over the bottom story and top half-story are included in this section. The calculation of the top half-story drift, δ_2, and bottom story drift, δ_B, can be found in Eqns. (2.2) and (2.3) respectively.

Hysteresis plots for loading in the X and Y directions for Specimens B1, B2, B3, and B4 are shown in order in Figure C-1 to Figure C-16. Also, in Figure C-17 through Figure C-24, the first story, second half-story, and full specimen drifts are plotted for each of the four specimens. Second half-story drifts were larger than first story drifts throughout the tests by approximately 40 to 60%.
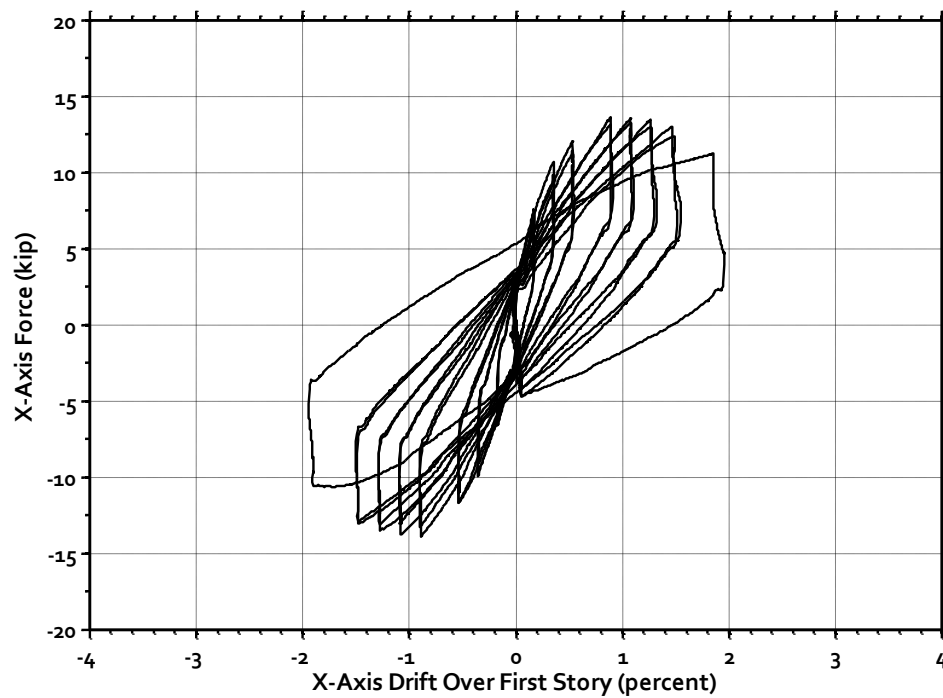
Figure C-1: Specimen B1 – Load versus First Story Drift in X-Direction
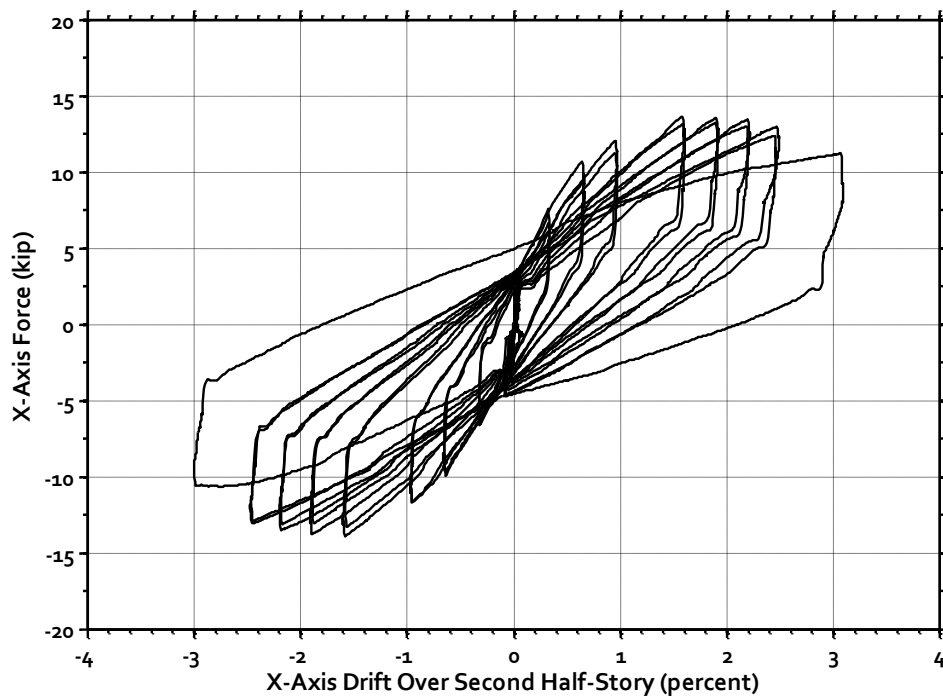
Figure C-2: Specimen B1 – Load versus Second Half-Story Drift in X-Direction
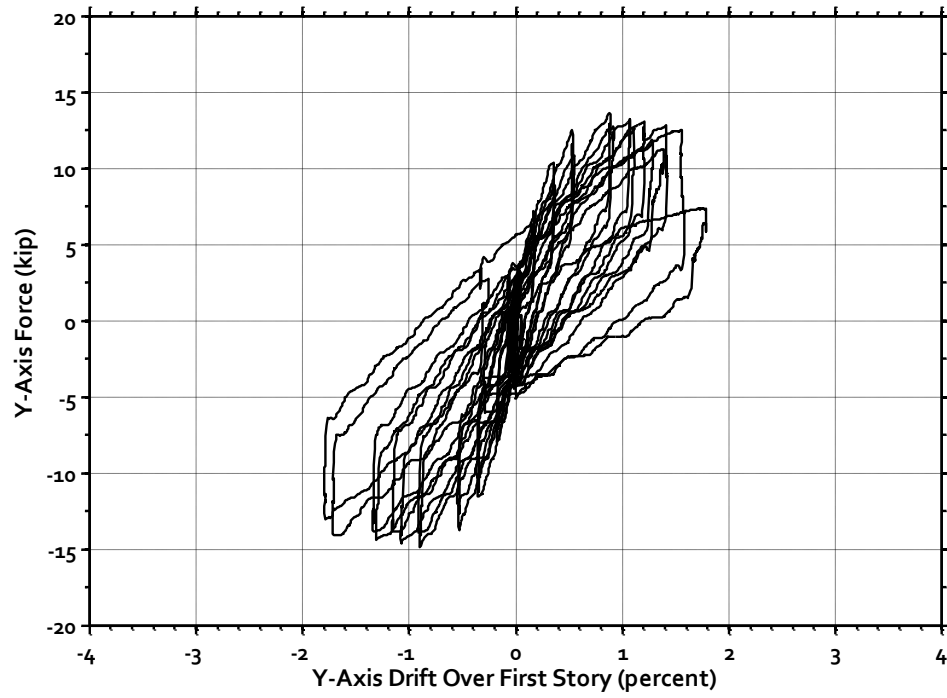
Figure C-3: Specimen B1 – Load versus First Story Drift in Y-Direction

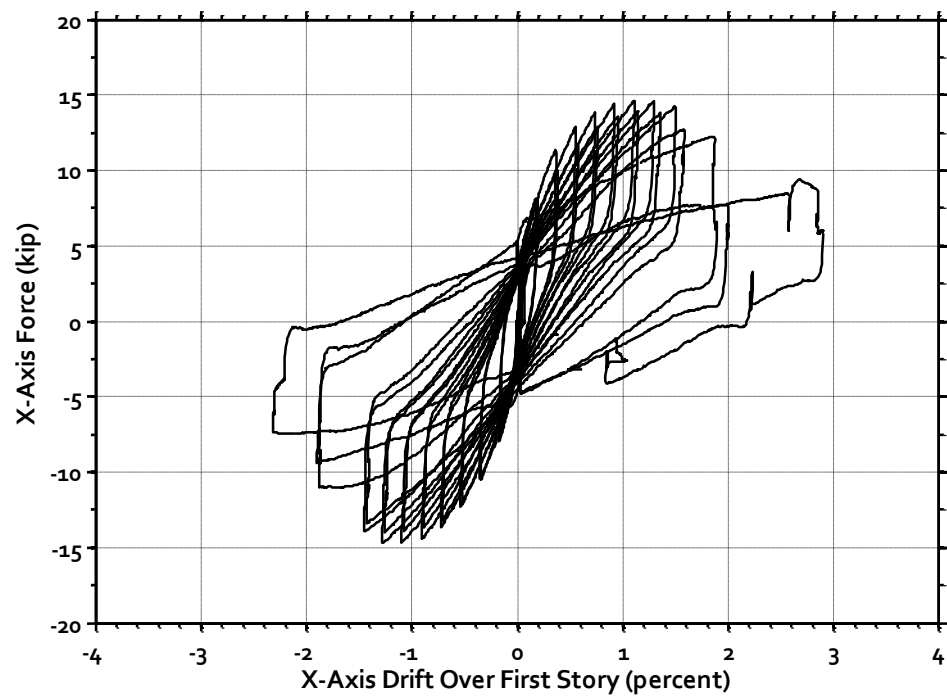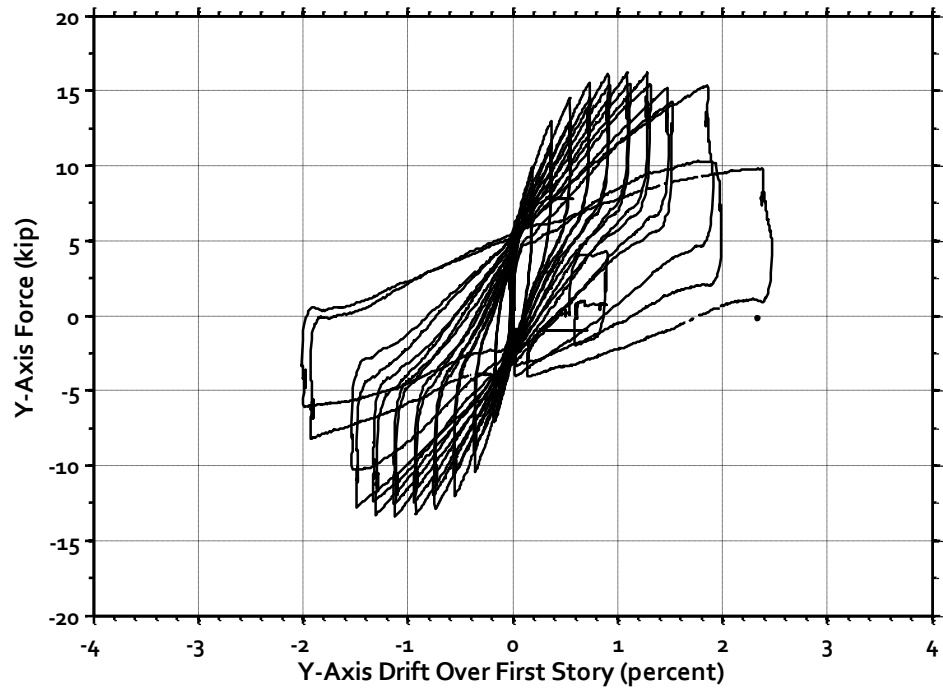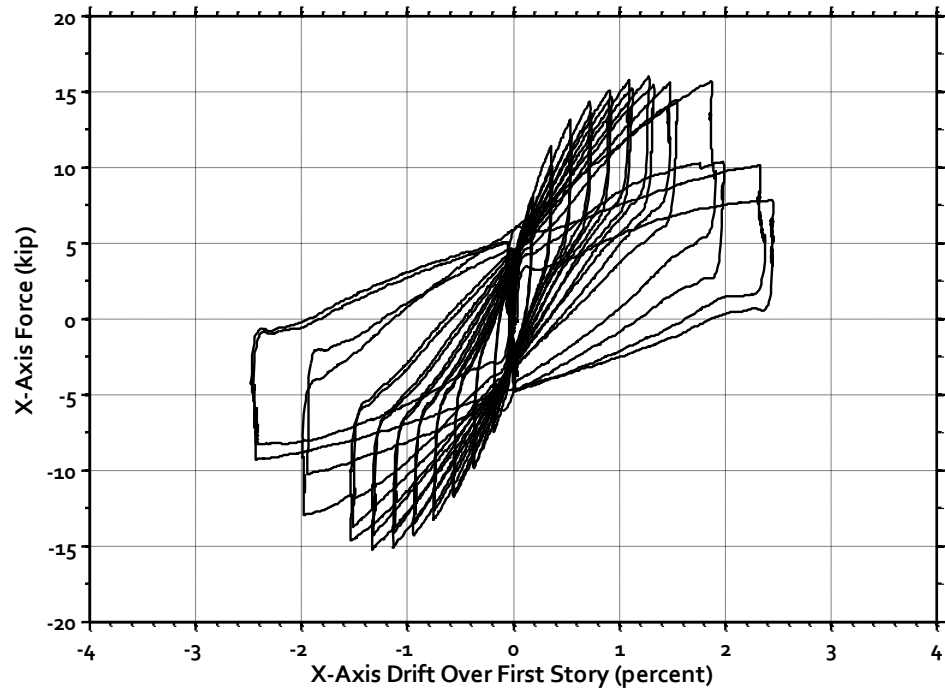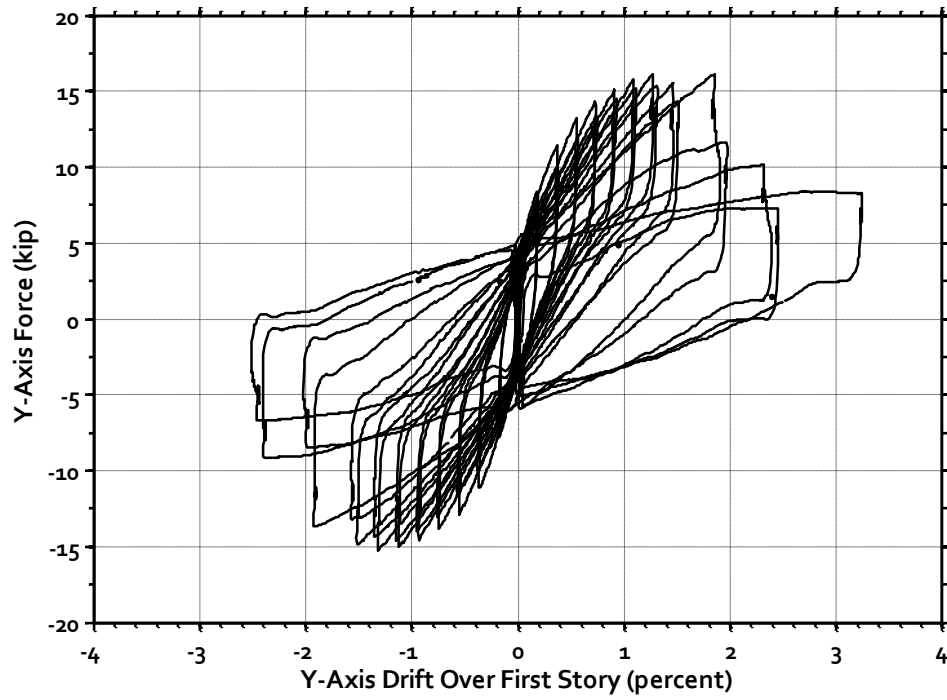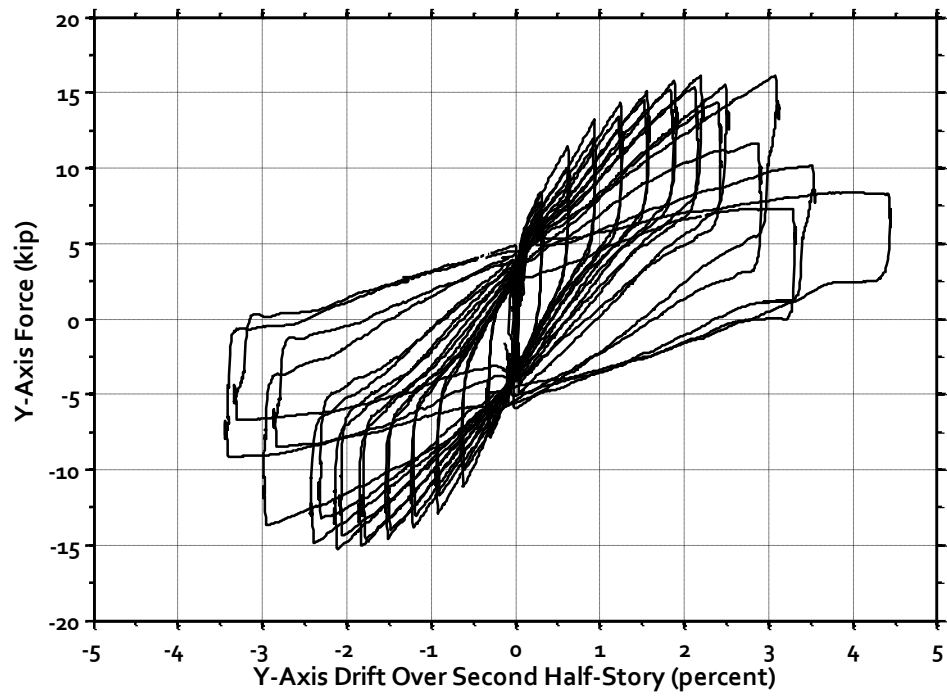Figure C-4: Specimen B1 – Load versus Second Half-Story Drift in Y-Direction

246
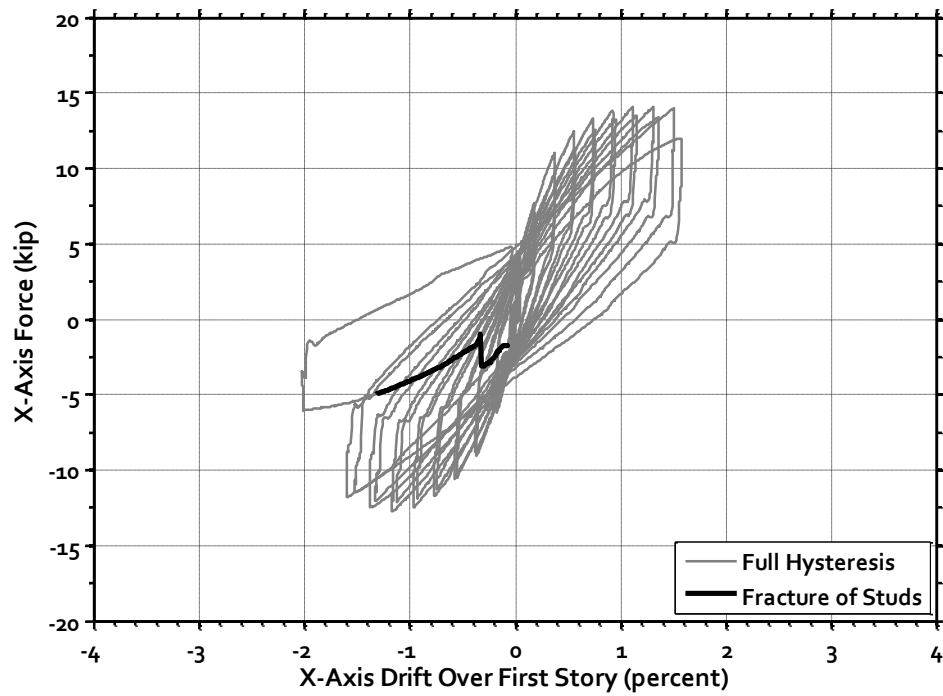
Figure C-5: Specimen B2 – Load versus First Story Drift in X-Direction
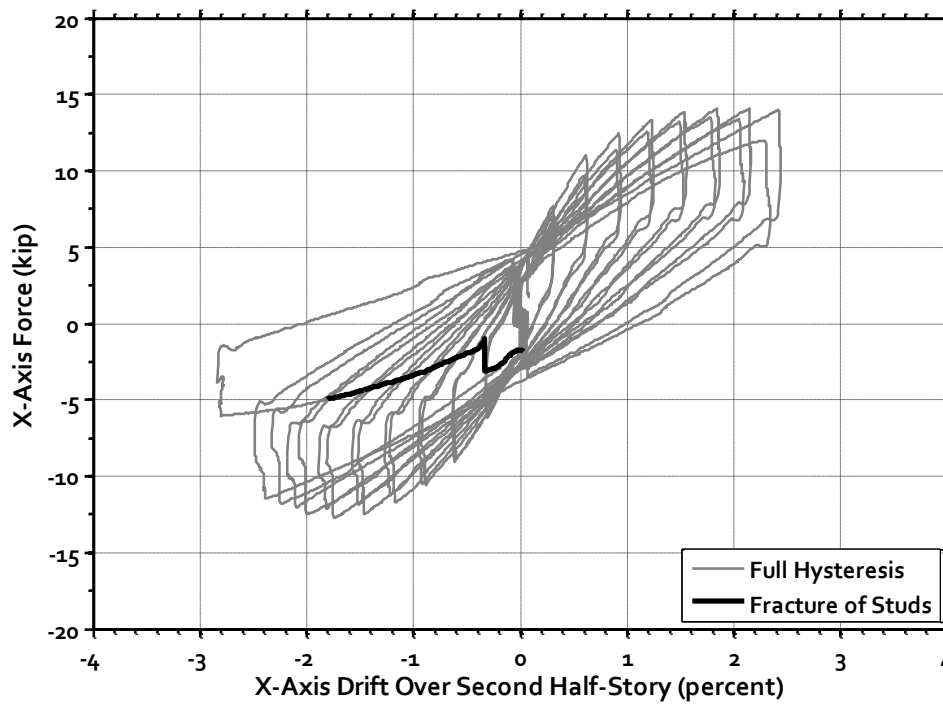
Figure C-6: Specimen B2 – Load versus Second Half-Story Drift in X-Direction

247
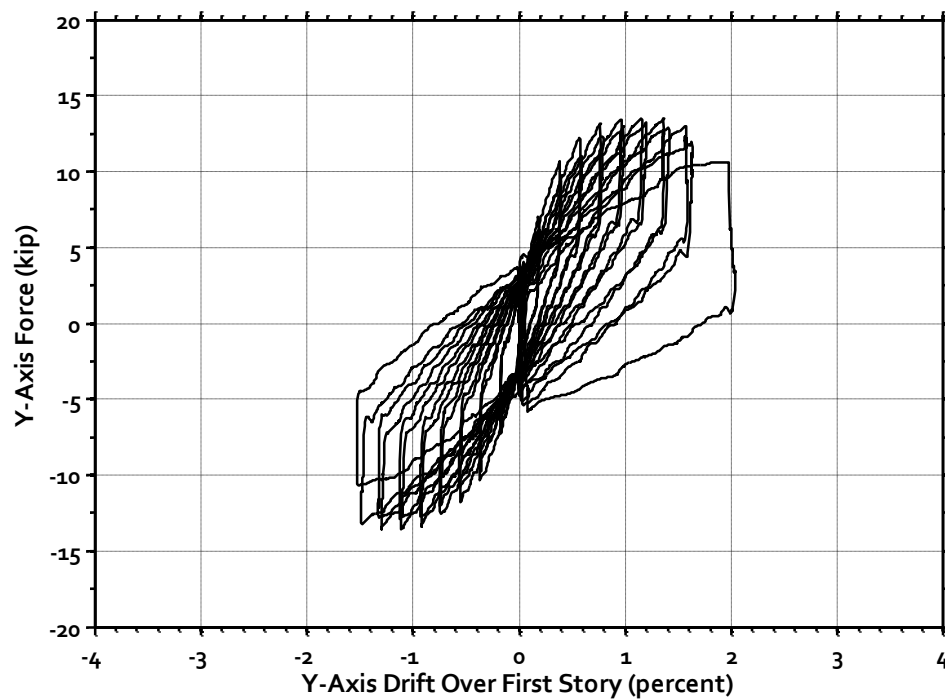
Figure C-7: Specimen B2 – Load versus First Story Drift in Y-Direction

Figure C-8: Specimen B2 – Load versus Second Half-Story Drift in Y-Direction

248

Figure C-9: Specimen B3 – Load versus First Story Drift in X-Direction

Figure C-10: Specimen B3 – Load versus Second Half-Story Drift in X-Direction

Figure C-11: Specimen B3 – Load versus First Story Drift in Y-Direction

Figure C-12: Specimen B3 – Load versus Second Half-Story Drift in Y-Direction

250

Figure C-13: Specimen B4 – Load versus First Story Drift in X-Direction

Figure C-14: Specimen B4 – Load versus Second Half-Story Drift in X-Direction

Figure C-15: Specimen B4 – Load versus First Story Drift in Y-Direction

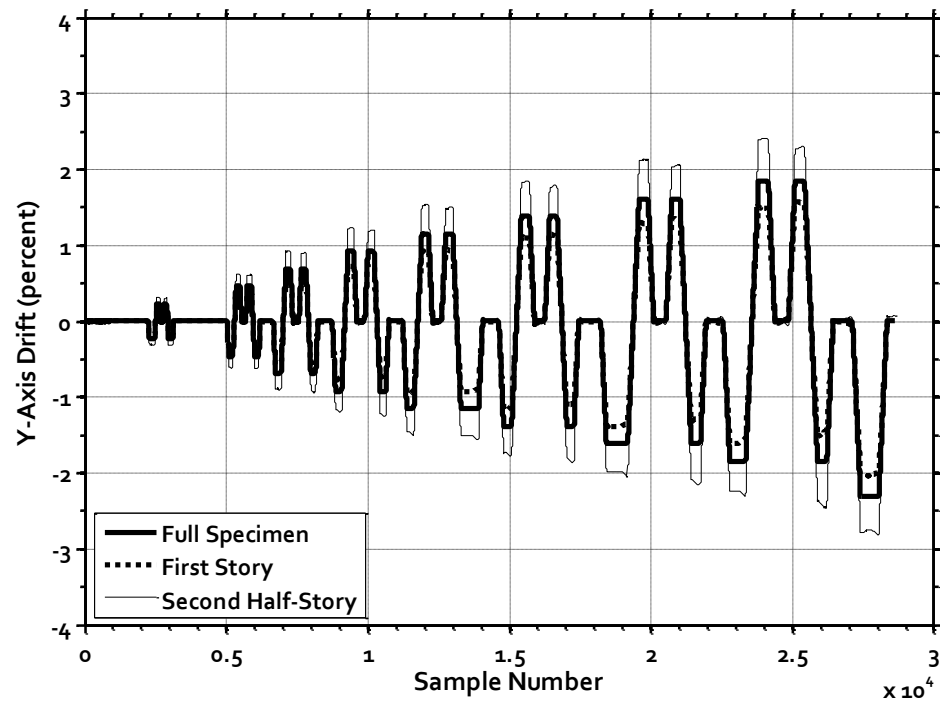Figure C-16: Specimen B4 – Load versus Second Half-Story Drift in Y-Direction

252
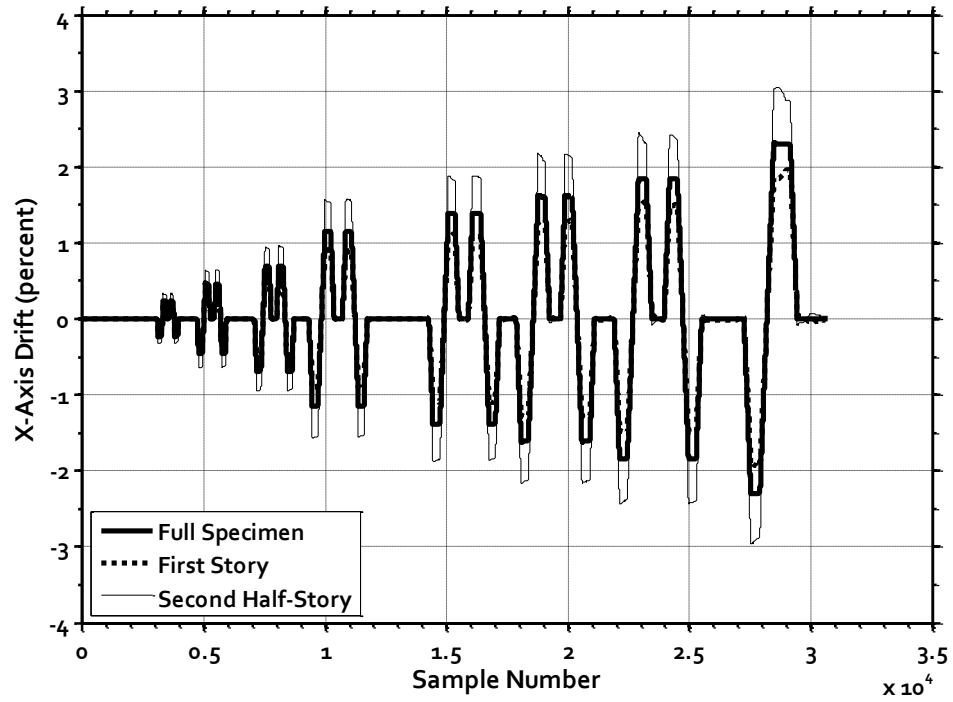
Figure C-17: Specimen B1 – First Story, Second Half-Story, and Full Specimen X-Axis Drift
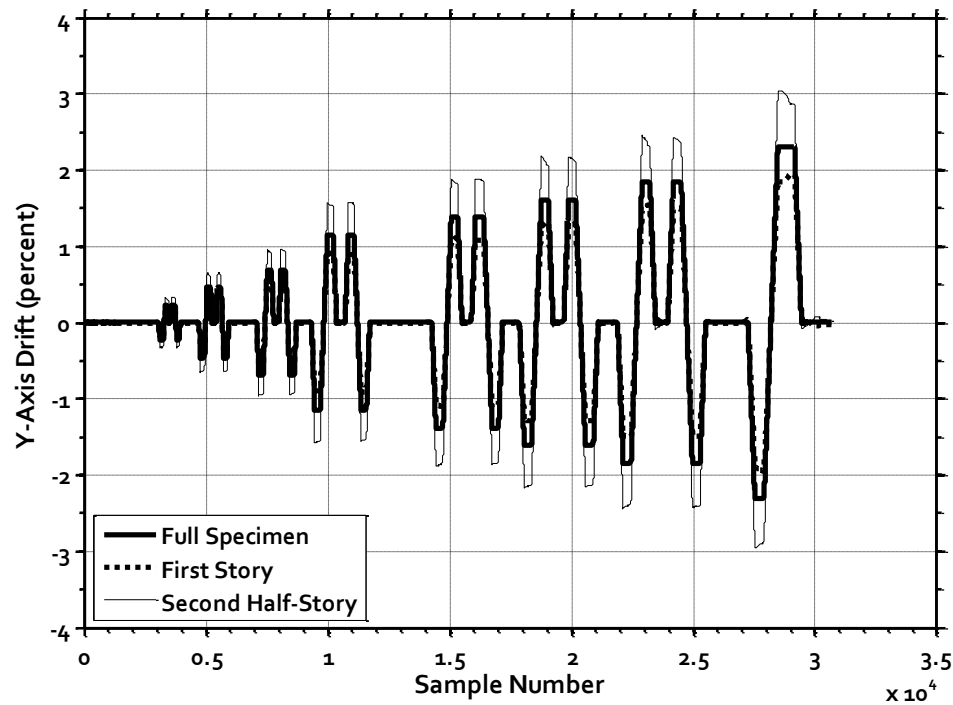
Figure C-18: Specimen B1 – First Story, Second Half-Story, and Full Specimen Y-Axis Drift

253
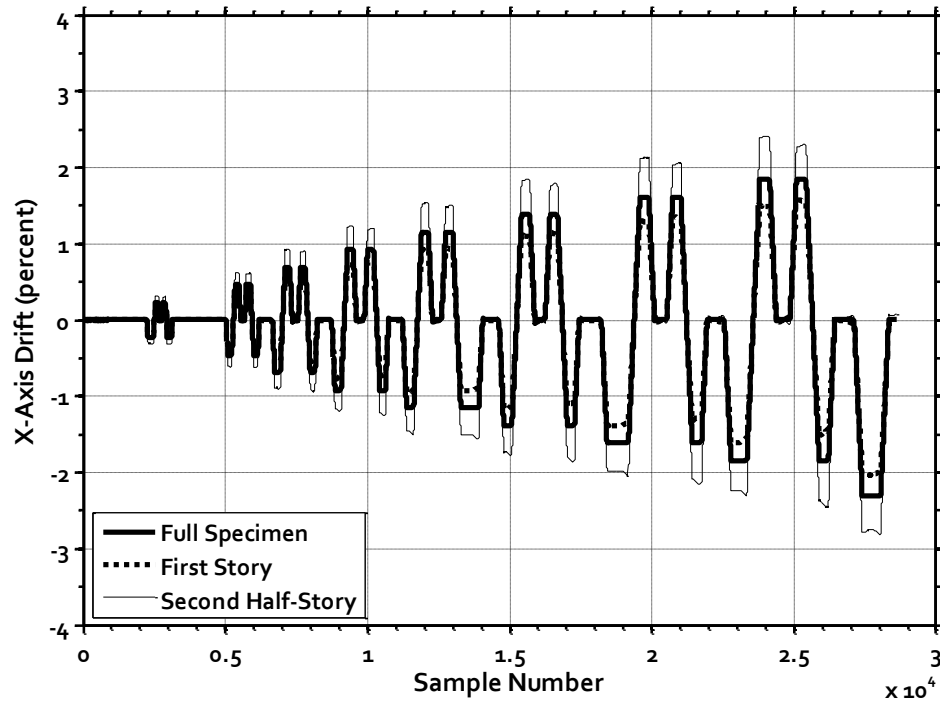
Figure C-19: Specimen B2 – First Story, Second Half-Story, and Full Specimen X-Axis Drift

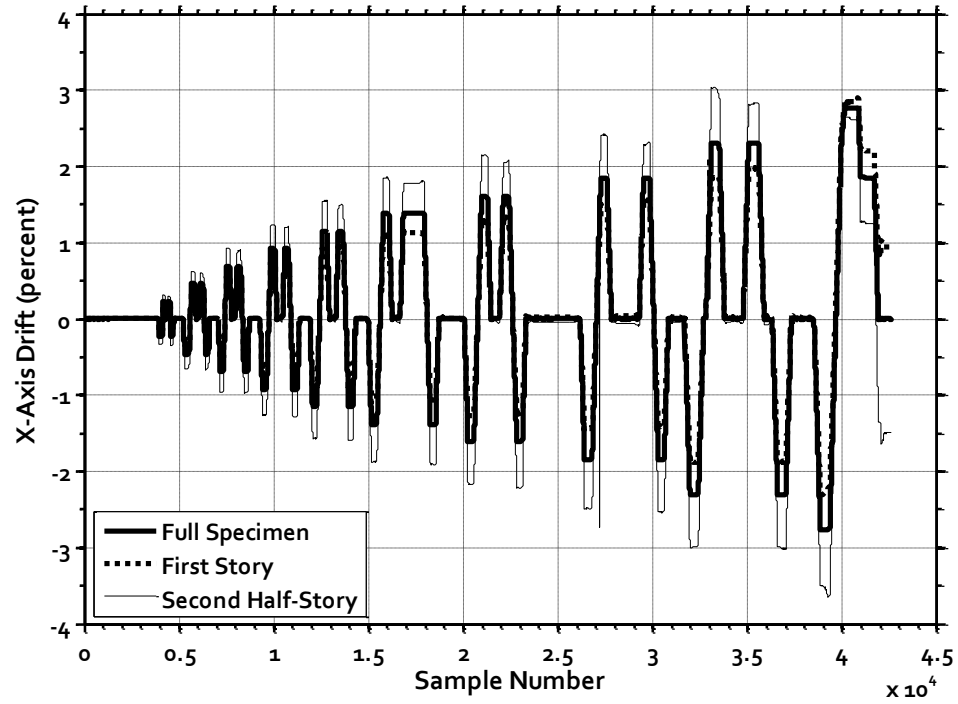Figure C-20: Specimen B2 – First Story, Second Half-Story, and Full Specimen Y-Axis Drift
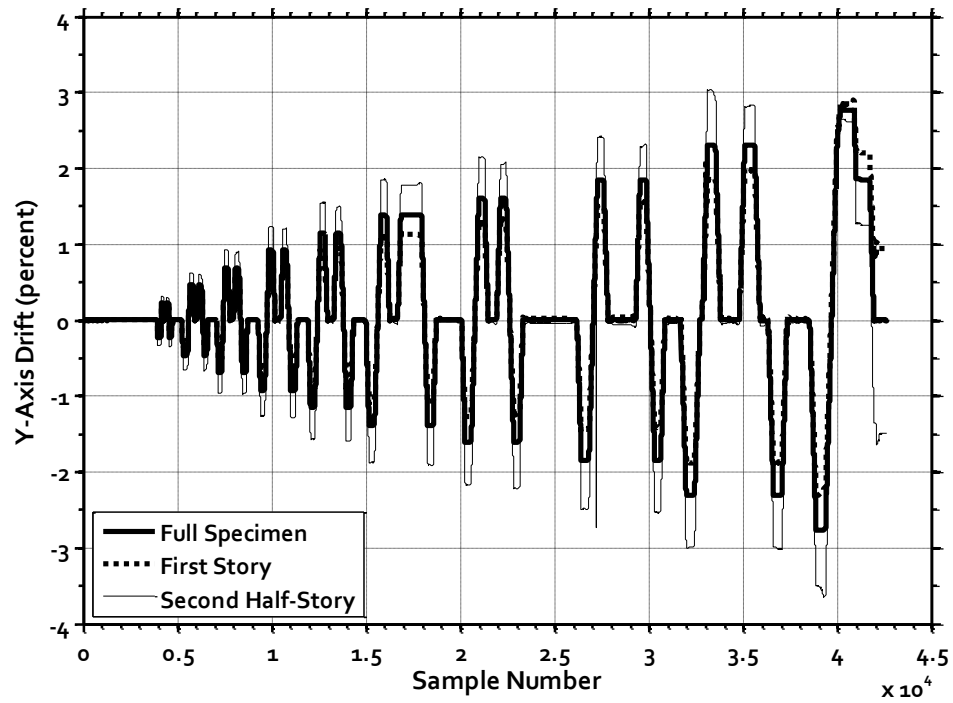
254

Figure C-21: Specimen B3 – First Story, Second Half-Story, and Full Specimen X-Axis Drift

Figure C-22: Specimen B3 – First Story, Second Half-Story, and Full Specimen Y-Axis Drift
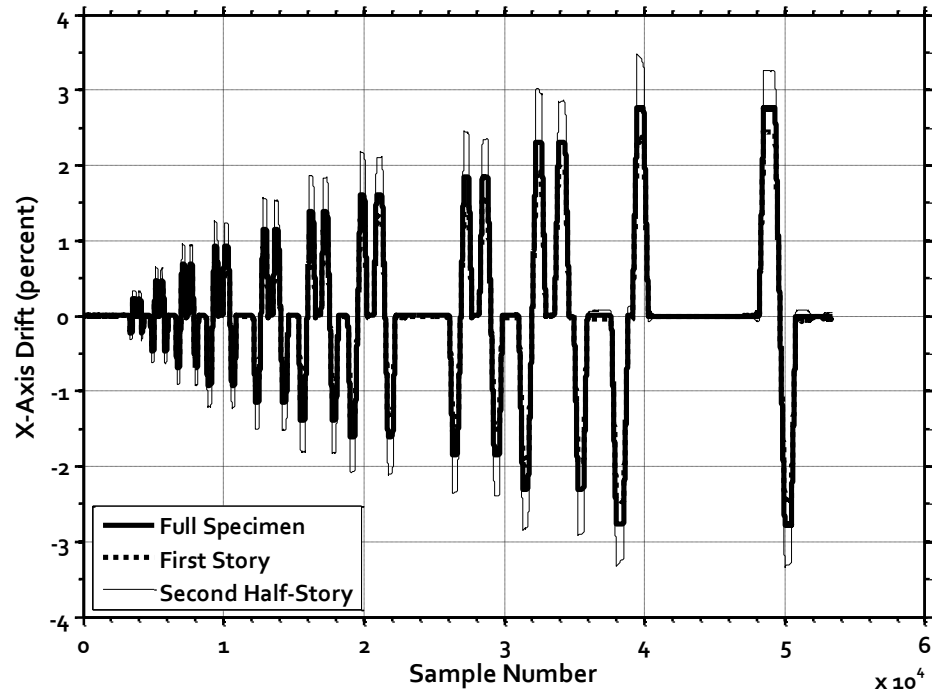
255

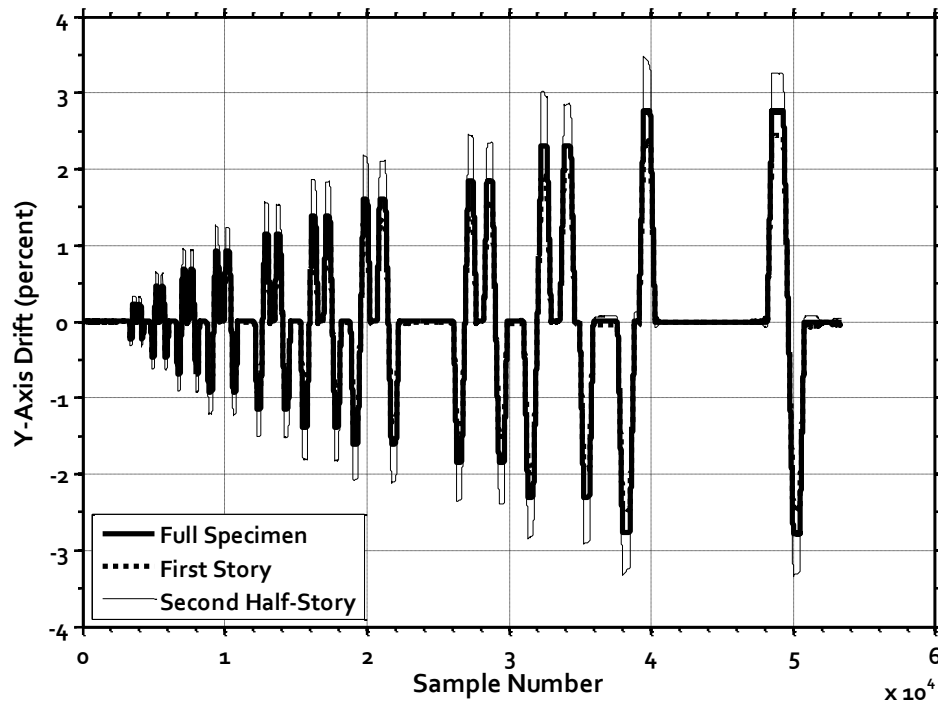Figure C-23: Specimen B4 – First Story, Second Half-Story, and Full Specimen X-Axis Drift

Figure C-24: Specimen B4 – First Story, Second Half-Story, and Full Specimen Y-Axis Drift

256